VERSATILE INGREDIENTS FROM RAPESEEDS FOR STRUCTURING PLANT-BASED SOFT MATERIALS

ELENI NTONE

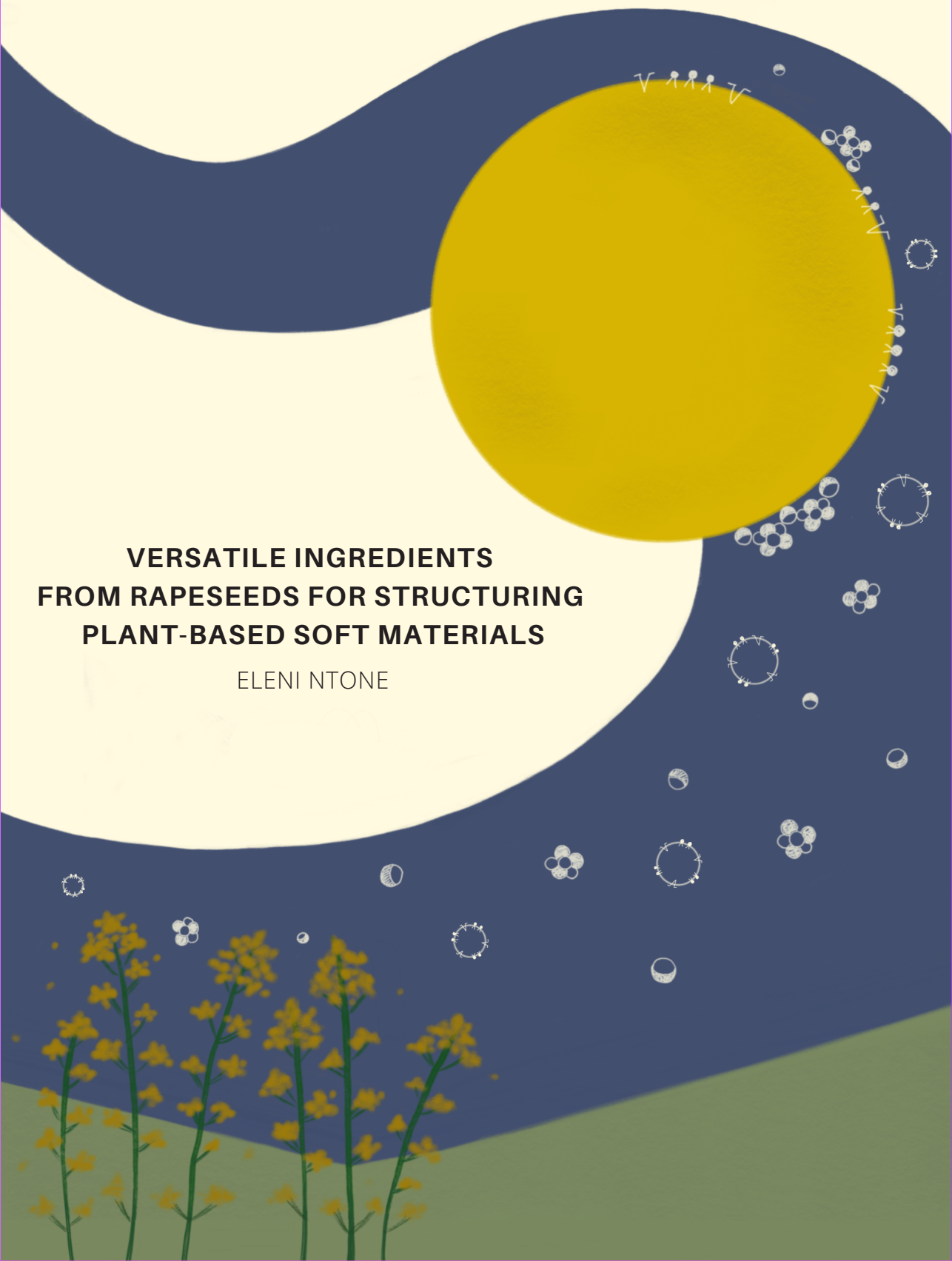

Propositions

1. Oilseed protein and oleosome extracts could be used as versatile ingredients in food applications.
   (this thesis)

2. A mechanistic understanding of the functional properties of plant protein extracts is necessary to assess the necessity of purification.
   (this thesis)

3. The perception of academia as the Eden of intellectual freedom does not align with the interests of the closely collaborating industry.

4. The academic life is a daily tightrope walking above self-criticism.

5. Plant-based foods address the tasting palette of people that can afford a western-pattern diet.

6. Gender-based discrimination and violence emerges from deeply rooted gender stereotypes.

Propositions belonging to the thesis, entitled
Versatile ingredients from rapeseeds for structuring plant-based soft materials
Eleni Ntone
Wageningen, 15 December 2021

Versatile ingredients from rapeseeds for structuring plant-based soft materials

Eleni Ntone

Thesis committee

Promotor

Prof. Dr J.H. Bitter

Professor of Biobased Chemistry and Technology

Wageningen University & Research

Co-promotors

Dr K. Nikiforidis

Associate professor, Biobased Chemistry and Technology

Wageningen University & Research

Dr L.M.C. Sagis

Associate professor, Physics and Physical Chemistry of Foods

Wageningen University & Research

Other members

Prof. Dr V. Fogliano, Wageningen University & Research

Prof. Dr J. Van der Gucht, Wageningen University & Research

Prof. B. Wolf, University of Birmingham, UK

Dr E. Goossens, Cargill R&D Centre Europe, Niel, Belgium

This research was conducted under the auspices of Graduate School VLAG

(Advanced Studies in Food Technology, Agrobiotechnology, Nutrition and Health Sciences).

Versatile ingredients from rapeseeds for structuring plant-based soft materials

Eleni Ntone

Thesis

submitted in fulfilment of the requirements for the degree of doctor
at Wageningen University
by the authority of the Rector Magnificus,
Prof. Dr A.P.J. Mol,
in the presence of the
Thesis Committee appointed by the Academic Board
to be defended in public
on Wednesday 15 December 2021
at 11 a.m. in the Aula.

Eleni Ntone
Versatile ingredients from rapeseeds for structuring plant-based soft materials
194 Pages

PhD thesis, Wageningen University, Wageningen, the Netherlands (2021)
With references, with summary in English

ISBN: 978-94-6395-776-2
DOI: https://doi.org/10.18174/554792

Πάντα στον νού σου να χεις την Ιθάκη.

Κ. Καβάφης

Contents

Chapter 1

General introduction

1.1 The need for transition from animal- to plant-based ingredients in foods

The current food supply chain, from production practices to consumption patterns, contributes to climate change by producing more than 25% of all anthropogenic green-house gas (GHG) emissions[1]. From the whole food supply chain, livestock production utilizes more than 80% of the global agricultural land and 70% of freshwater resources. Moreover, it degrades the ecosystem via deforestation and overapplication of fertilizers for crop cultivation intended for livestock feed[1–4].

Several studies have suggested that the reduction of the environmental impact of foods is generally proportional to the reduction in production/consumption of animal-based foods[3]. The most effective measure to reduce the environmental impact of foods is a change in consumers' dietary patterns towards more plant-based (or flexitarian) diets[1,2,5]. Moving towards animal-free diets can reduce GHG emissions by almost 50%, land use by 76%, freshwater use by 19% and changes in the ecosystem by almost 50%[1]. Therefore, in the last decades, food science aims to address how to substitute animal-based products by plant-based products with less environmental impact.

For this reason, different plants are being exploited as potential sources of food ingredients, such as proteins and lipids, essential structuring and nutritional ingredients in foods[6,7]. The first challenge in using plant-based ingredients in foods is their extraction from the plant matrix. In plant matrices proteins and lipids are enclosed in the cell and coexist with other molecules, such as carbohydrates and phenolic compounds. Due to this complexity, the extraction of plant-based ingredients is a cumbersome process, as it requires multiple extraction and purification steps and high amounts of water and energy to obtain highly purified ingredients[8]. In addition, the existing methods often result in losses of ingredients and low yields[9] and can negatively affect the functionality of the extracts. Therefore, the current extraction process of plant-based ingredients might not be suitable to outcompete the environmental footprint of the production of animal-based ingredients[8].

It is therefore necessary to develop or improve the extraction processing technologies to produce plant-based ingredients which can assure an environmental gain. A solution can be offered from the reduction of the number of applied processing steps in order to reduce the energy and water expenditure[10] and to minimize ingredient losses[9]. However, reducing the processing steps will result in less purified plant-based ingredients instead of highly purified ingredients, with potentially different functionality in food systems.

Therefore, one of the focuses of the current research is to determine to which extent less purified plant-based ingredients can provide similar functionality to the highly purified ones. Hence, efforts are being made to assess different plant protein sources and extraction processing methods to establish the relation between processing and functionality of the plant extracts.

In recent years, from the different available plants, various oilseeds have been increasingly exploited as protein sources for food purposes. One of the functional applications of proteins in foods is to stabilize free oil in aqueous food systems, forming oil-in-water emulsions. Stabilization of oil droplets in foods is necessary to provide structure and desirable sensory attributes in the system[11]. Oilseeds containing both oil (40-50%) and proteins (20-30%) are promising ingredient sources for oil-in-water emulsion applications. So far, oilseeds are mainly used to provide the oil that is used as raw material to produce emulsion-type foods[7]. However, due to the high amounts of proteins, oilseeds can also provide the proteins needed for stabilizing the emulsions.

The main oilseed proteins currently been exploited as emulsifiers derive from soybeans[11,12]. Among other oilseeds, rapeseeds (*Brassica napus*), being the second most important oilseed crop globally after soybeans[7,13] and containing high amounts of proteins (20 wt%)[13], is a rising source of sustainable proteins.

To examine the potential of rapeseed proteins as emulsifiers in food systems, in this thesis we aimed to establish the relation between the extraction process and the emulsifying properties of rapeseed proteins. This knowledge would allow us to determine the optimal processing conditions based on the desired functionality, and allow for a more accurate assessment of the sustainability aspects of rapeseed protein extracts.

1.2 Understanding the oilseed structure before the extraction

The first factors to be considered for the extraction process of oilseed proteins is 1) the structural organization of the molecules inside the cells and 2) the structure of each molecule. The reason behind this consideration is that, the cell architecture and the high interconnection between cell components, as well as the biochemical differences between oilseed sources, such as the type of proteins present, and the presence of lipids, can determine the extraction steps, the extraction yields and the functionality of the protein extracts[14]. Moreover, oilseeds contain phenolic compounds which should also be considered for the decision of the extraction process. Phenolic compounds are known to create irreversible complexes with proteins during extraction, lowering the functionality of plant extracts[15].

Inside the oilseed cell matrix, proteins are stored in protein storage vacuoles[16,17] and lipids are organized in spherical structures named oleosomes or lipid droplets[18]. A cryo-SEM image of

rapeseed cells, showing the structural organization of proteins and lipids is illustrated in Figure 1.1.

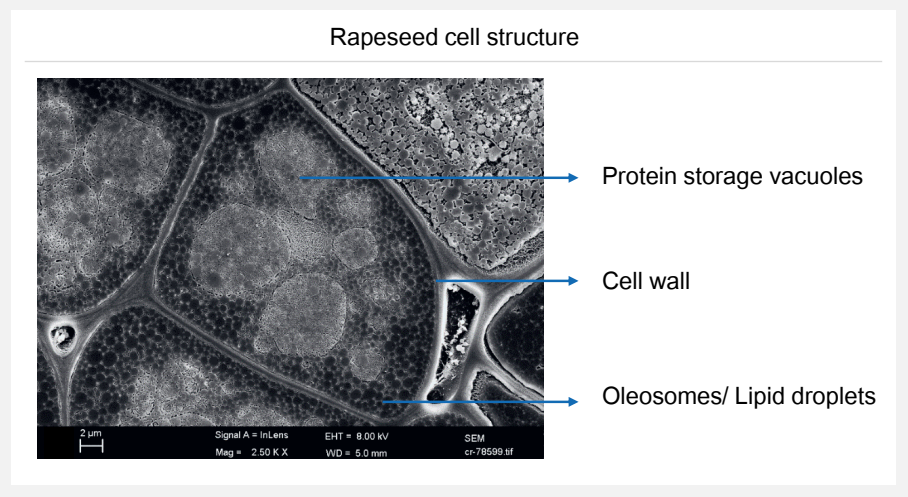

Figure 1.1 Cryo-scanning electron microscopy image of rapeseed cells after hydration of the seeds for 24h

1.2.1 Structure of lipids

Rapeseeds typically contain 40-50 wt% lipids. The structure of lipids inside the cell, is in the form of spherical emulsified oil droplets, called oleosomes or lipid droplets[19]. In this thesis to refer to the natural structure of lipids the term oleosomes will be used.

In these organelles the triacylglycerols are enclosed in a monolayer of phospholipids and structural proteins, as illustrated in Figure 1.2. The phospholipid monolayer composes about 2 wt% of the total mass of the oleosomes[20]. The enclosure of lipids into these structures has been developed by nature during evolution to store energy and provide triacylglycerols with extreme physical and chemical stability[20]. Moreover, oleosomes in cells do not only serve as hubs of energy storage but their role expands to several dynamic functions that contribute to cell homeostasis[19]. The main contribution is to absorb, accumulate and channel lipids and proteins inside the cells, realizing molecular trafficking.

The size of oleosomes is in the micron or submicron-range and is determined by the number and type of phospholipids and proteins that oleosomes acquire in their monolayer during their biogenesis from the endoplasmic reticulum[19,21]. Rapeseed oleosomes have a size of 0.2-5.0 µm and are constructed by mainly oleic acid in their lipid core[16,22,23] which is surrounded by phosphatidylcholine (PC) and phosphatidylserine (PS) and structural proteins named oleosins, caleosins and stereoleosins[24]. Oleosins are the most abundant oleosome related proteins[24] with a

molecular weight of 15-20 kDa and a hairpin-like structure with a very extended hydrophobic domain, which provides them high interfacial activity[25,26].

Considering the structural properties of oleosomes, it important to understand that the storage of lipids into these robust and relatively small structures can determine the extraction conditions, extraction yields and purity of the oil extracts.

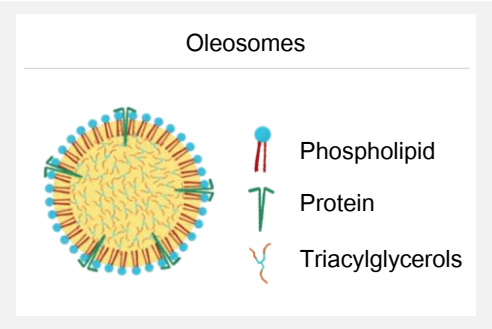

Figure 1.2 Schematic representation of the oleosome/lipid droplet structure and structural components

1.2.2 Structure of proteins

Oilseeds typically contain two types of storage proteins stored in the protein vacuoles. Storage proteins are solely used by the seed for germination[27]. The main storage proteins are classified by the Osborne method into water-soluble albumins and salt-soluble globulins, and have different structural and physicochemical properties[27]. Hence, it is vital to realize that the selected extraction process can impact the type of extracted proteins and subsequently the functionality of the protein extracts.

In rapeseeds, two main storage proteins -napins and cruciferins- can be found. In European varieties the two proteins appear in a ratio from 0.6 to 2.0[28]. Napins are low molecular weight albumins (12-17 kDa) and consist of a small and a large polypeptide chain linked together by two inter-chain disulfide bonds[16,29]. Forty-five percent (45%) of the amino acids of the peptide chain of napins are hydrophobic and concentrated mostly on one exposed side of the protein. This distribution results in a structure that resembles amphiphilic Janus particles[30]. Cruciferins are high molecular weight (300 kDa) globulins and have a hexameric structure that consists of two trimers. Cruciferins have a wide distribution of the hydrophobic domains over their surface and also buried in the inner face of the trimers[29,31,32]. Napins are less susceptible to pH changes and soluble in a wide pH range[29,33]. In contrast, the hexameric structure of cruciferins is more susceptible to pH and temperature changes[29,34]. The structure and distribution of hydrophobic and hydrophilic domains of napins and cruciferins is given in Figure 1.3.

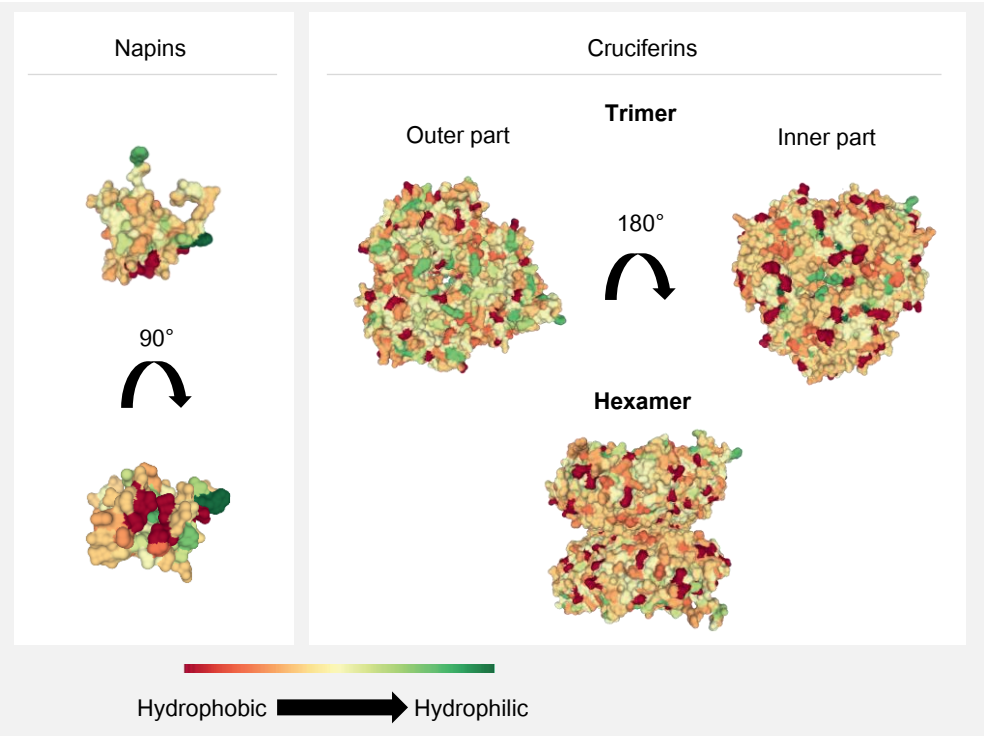

Figure 1.3 Sketch of napins and cruciferins (trimer and hexamer) structure represented as molecular surface, showing the distribution of hydrophobic (red) and hydrophilic (green) domains (Images retrieved from the RCSB PDB[35,36]).

1.2.3 Structure of phenolic compounds

Phenolic compounds are secondary metabolites found in plants and their chemical structure includes a hydroxyl group bonded to an aromatic ring[37]. Depending on the extraction conditions, for instance the extraction pH, phenolic compounds can form complexes with proteins resulting in changes in the structural, functional and nutritional properties of both compounds[37].

Rapeseeds contain around 1-3% phenolic compounds, mainly in the form of sinapic acid[38,39]. The chemical structure of sinapic acid is given in Figure 1.4. During the extraction, at pH values above 9.5 ionic bonding between proteins and sinapine (the choline ester of sinapic acid) can occur, leading to co-extraction of phenolic compounds[40]. In addition, at pH values above pH 10, oxidation of sinapic acid to thomasidioic acid and further to quinones accelerates. The latter can interact with proteins, and bind to them covalently[41,42]. Therefore, the extraction conditions like pH, can

affect the coextraction of phenolic compounds and the interactions between proteins and phenolic compounds.

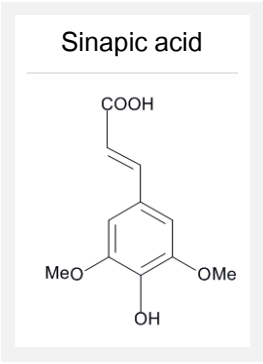

Figure 1.4. Chemical structure of sinapic acid

1.3 The current extraction process of oilseeds

Due to the high amounts of lipids stored in oilseeds, the most common extraction process of oilseeds focuses on maximizing the lipid extraction yields. During this process, the seeds are first flaked to rupture the seed coat and the cells. The seed flakes are heated (77°-100°C) to reduce moisture, inactivate enzymes, decrease oil viscosity, increase oil droplet coalescence, and facilitate solvent diffusion. Thereafter, the seed flakes are pressed to extract most of the lipids (60 -70%), resulting in large cake fragments. The remaining oil in the pressed cake is further extracted with solvent (i.e. with hexane) to maximize the oil yield. The residual cake after the lipid extraction, also referred as meal, is further processed in a de-solventizer/toaster with steam (100°-130°C) to remove the solvent and to improve the nutritional quality by removing volatile glucosinolates[43,44]. The resulting protein-rich meal contains around 35-40 wt% proteins on dry matter[45] and 1-2 wt% oil[46]. As the natural lipid structure is disrupted during the oil extraction, fragments of the oleosome monolayer containing the structural components (i.e. phospholipids and proteins) are also present in the protein-rich meal.

The first pitfall in the commonly applied extraction process of oilseeds is that is an energy intensive process as it requires multiple steps, and includes the use of organic solvents, with impact on the sustainability of plant-based ingredients. The second drawback concerns the proteins; due to the heating and solvent-removal steps applied on the seeds and the meal, proteins denature, which impacts the physicochemical and functional properties[44]. The heating during the de-solventizing step is also responsible for Maillard reactions and protein-crosslinking, with negative impact on protein solubility[46]. As a result, lower protein extraction yields are achieved and dark-colored protein extracts with low functionality are obtained. To optimize the protein extraction yields from

the residual cake, high alkaline (pH 11-12) or saline solutions are usually applied. The alkaline extraction of proteins is followed by acid precipitation to further separate the different protein species (i.e. albumins and globulins) and obtain highly purified protein ingredients[28,47].

Although these extraction conditions might improve the protein extraction yields and purity of the protein extracts, there is a lurking risk of further implications on protein structure and functionality. The functional properties of rapeseed proteins have been shown to be highly affected by the applied extraction and processing conditions[44,47]. During the extraction of proteins from the meal under high alkaline pH conditions, phenolic compounds (i.e. sinapic acid in rapeseeds) are co-extracted and interact with the proteins through covalent bonds[37,48,49]. As a result of these interactions, the structural properties of the proteins are altered[37]. The structural changes of proteins in turn affect protein functionality, for instance by decreasing the capability of proteins to adsorb at an interface and decrease the surface tension[15,37]. These interactions of proteins with phenols under alkaline conditions are also responsible for the dark color of the obtained protein extracts[44]. Additionally, as different types of proteins (i.e. albumins and globulins) with different physicochemical properties are present, the use of high alkaline/saline conditions followed by precipitation leads to 1) selective extraction of proteins and loss of proteins in the non-precipitated fraction 2) partially irreversible aggregation of precipitated proteins with impact on their functionality. For example, protein aggregation has shown to reduce the emulsion stability against coalescence upon large deformations compared to non-aggregated proteins[50]. As a consequence of all the above processing conditions, the use of many oilseed residual protein meals such as rapeseed is currently limited to livestock feed[28,43].

1.4 Reconsidering the current extraction process of oilseeds

Due to all the above implications of the conventional processing of oilseeds, alternative extraction processes should be exploited, with fewer processing steps, lower amount of energy, water and losses during extraction, and more focus on the functionality potential of the extracts.

In the alternative extraction process the de-oiling, heating and organic solvent steps can be omitted and proteins and lipids can be simultaneously extracted in water at low alkaline pH conditions (pH<10). After the extraction, proteins from lipids can be further separated by centrifugation. Additionally, removal of the seed hulls prior to the extraction, where phenolic compounds are mainly concentrated, can be included to limit the amounts of co-extracted phenols in the extracts. Dehulling of oilseeds has been previously reported to enhance the quality of the residual meal[51]. In the case of rapeseeds, maintaining the pH below pH 10 during extraction also prevents the complexation between the co-extracted phenols and proteins, resulting only in free phenols in the protein extracts which can be simply removed by a diafiltration step. This process leads to less

purified protein-rich extracts, containing both storage proteins and to oleosome-rich extracts containing intact oleosomes. In both extracts, proteins, oleosomes and free phenols can co-exist at different ratios.

The advantage of this method is that fewer processing steps are required, while at the same time both protein and lipid natural structures and their carried functionalities are preserved. Another benefit of such a method is that, since different molecules with varied functionalities coexist in mixtures, they can potentially have a synergy, which can result in ingredients with versatile functionalities. Moreover, the retained nativity of the molecules allows a better evaluation of their physicochemical properties and of their functionality potential for food applications. A schematic overview of all the extraction processing routes of proteins and lipids from rapeseeds is given in Figure 1.5.

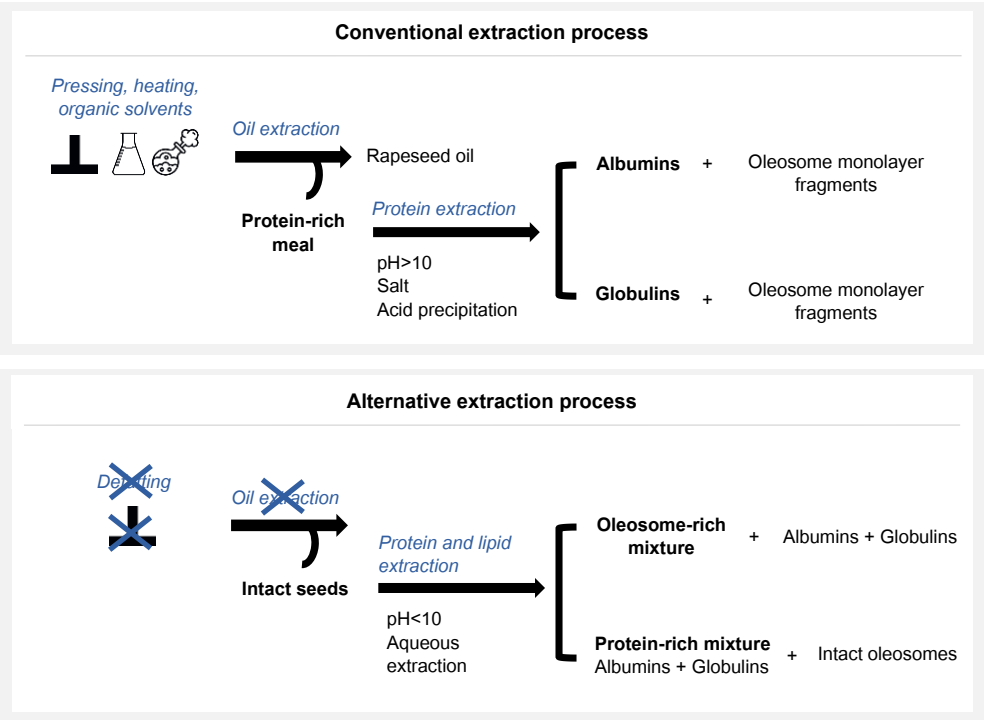

Figure 1.5 Extraction processing routes of rapeseed proteins and lipids

1.5 Assessing the functional properties of less purified oilseed extracts

When it comes to the functionality of the less purified protein-rich extracts, where albumins and globulins co-exist, and free phenols and oleosomes can be also present, a synergistic or antagonistic effect between the different molecules can occur. Therefore, a mechanistic understanding on the relation between the physicochemical properties with the functional properties of each molecule present in these extracts is necessary. Such understanding will allow to determine the optimal level of purification needed for the desired functionality, and it is thoroughly discussed in this thesis.

Rapeseed proteins have promising functional properties, such as emulsifying, foaming and gelling properties[30,34,52–55]. As the molecular structure of cruciferins and napins differs, they also exhibit distinct functional properties[28]; Napins, due to their small size and distribution of the hydrophobic and hydrophilic domains, are more surface active than cruciferins[30,56]. Differently, cruciferins can form firmer gels (at equal protein concentration) than napins upon heat-induced gelation[55,57,58]. When co-existing in mixtures, depending on the application, the two proteins can cooperate or compete.

Regarding the functionality potential of oleosomes, using aqueous extraction processes oleosomes are obtained intact from the seed matrix[59–61], which results in a natural oil-in-water emulsion. This natural emulsion provides lipid stability against physical and chemical stresses. Therefore, intact oleosomes are promising natural replacers of engineered oil droplets, which are currently used in emulsion type food applications[20]. In addition, the ability of oleosomes to traffic lipids and other hydrophobic molecules paves the way to exploit oleosomes as emulsifiers or carriers of hydrophobic molecules, such as flavors, colors, and nutraceuticals. Understanding the physicochemical properties of oleosomes is essential, not only to unlock the functionality potential of these organelles, but also to evaluate their effect when present in oilseed protein extracts, intact or as fragments of their monolayer.

1.6 Thesis aim and outline

The research described in this thesis had three main objectives: the **first** research objective was to understand the effect of the **extraction process** on the **physicochemical properties of rapeseed proteins and oleosomes**. The **second** research objective was to investigate the **functional properties** of **rapeseed proteins** when present in mixtures with other non-protein molecules. The **third** research objective was to characterize the **interfacial properties** of **rapeseed oleosomes** and investigate their **functionality** potential. By combining the insights of all chapters, we aim to provide new design rules for the use of rapeseed protein ingredients in food systems. These research topics are described in the following chapters.

In **Chapter 2** the effect of the **extraction method** was investigated, where defatting of the seeds is omitted, on the **physicochemical properties** of **rapeseed proteins and oleosomes**. The chapter describes the extraction method and the reasoning behind the selected extraction conditions, the resulting extraction yields and the physicochemical characterization of the obtained less purified protein and oleosome extracts.

In **Chapters 3, 4 and 5,** the **functional properties** of the less purified **rapeseed protein extracts** obtained as described in Chapter 2 are reported. In **Chapter 3** the interfacial stabilization mechanism of less purified rapeseed protein extracts at oil/water interfaces was investigated at neutral pH conditions (pH 7). The aim of this research was to identify the role of each protein species (i.e. napins and cruciferins) and of the coexisting non-protein molecules present on droplet formation and stabilization. In **Chapter 4** the effect of purification on the emulsifying and interfacial properties of rapeseed extracts of different protein purities at acidic pH (pH 3.8) was evaluated. The outcome about the role of each protein species on the interfacial stabilization mechanism found in **Chapters 3** and **4** guided the research described in **Chapter 5** where the different functionalities of each protein species present in the less purified rapeseed protein extract were combined to create emulsion-filled gels. The protein extract was used to stabilize both the emulsion droplets and the protein matrix. The effect of pH and oil concentration on the structural and rheological properties of the emulsion-filled gels were investigated.

In **Chapter 6** the **oleosome monolayer properties** and the potential **functional properties of oleosomes** are discussed. As described in **Chapter 6**, by combining light scattering techniques, dilatational interfacial rheology and advanced microscopy techniques with molecular dynamic simulations, we evaluated the effect of oleosome monolayer density (number of molecules per area), lateral interactions and dilatability on the ability of oleosomes to absorb and release lipids.

In **Chapter 7** an overview of the main findings and conclusions from the previous chapters is provided. In this chapter the emerging changes in the current extraction processes are discussed, providing general guidelines for the extraction of functional food ingredients from oilseeds and an outlook and future perspective.

Chapter 2

Extraction process and physicochemical properties of rapeseed proteins and oleosomes

This chapter has been published as: Ntone, E., Bitter, J. H., & Nikiforidis, C. V. (2020). Not sequentially but simultaneously: Facile extraction of proteins and oleosomes from oilseeds. *Food Hydrocolloids*, 102, 105598. https://doi.org/10.1016/j.foodhyd.2019.105598

Abstract

Oilseeds represent a sustainable source of oils and proteins that can replace those of animal origin. However, the extraction of oil and proteins from oilseeds currently requires multiple steps and is plagued by undesired reactions occurring during the extraction, which limits valorization. In this paper, we describe a successful method for the simple simultaneous extraction of proteins and oil (as intact oleosomes). Non-defatted dehulled rapeseeds served as oilseed model. First, an aqueous extraction step at pH 9.0 was performed resulting in a protein-oleosome extract, with extraction yields of 78.8 ± 0.2 wt% and 82.8 ± 0.4 wt% of proteins and oleosomes, respectively. Further separation resulted in a protein-rich and an oleosome-rich mixture. The oleosomes were recovered as high oil volume oil-in-water emulsion, while simple filtration of the protein-rich mixture led to a highly soluble (81.4 ± 1.9 wt%) protein concentrate. Following this extraction method, complexation between proteins and phenolic compounds was prevented, a clear advantage over the existing methods. These findings emphasize the importance of designing new processes for the extraction of oilseed proteins and oleosomes that could initiate their use in food systems.

2.1 Introduction

In view of the environmental issues and moral dilemmas associated with the production of animal-derived foods, replacing them with plant-based foods is in the spotlight, as producing the latter is less problematic[1]. Oilseeds, such as soybeans, sunflower seeds, and rapeseeds, are among the most promising plant-based food sources since they contain oil and proteins, both of which are essential food-structuring ingredients and nutrients[6]. Their valorization is therefore essential for a sustainable future.

A commonly used approach in oilseed valorization is an oil extraction process that involves pressing and use of organic solvents to maximize the oil yield. However, different problems arise when using these extraction processes. This type of oil extraction disrupts the oil carriers in the seed (oleosomes), thereby wasting a valuable resource. When extracted intact, oleosomes can serve as a dispersed oil phase (natural emulsion) with high physicochemical stability compared to engineered emulsions[62,63]. Moreover, due to their high physicochemical stability, they can also serve as carriers of sensitive molecules or diagnostics[20]. Besides losing the functionality of oleosomes, the defatting process has a negative impact on the physicochemical properties of the remaining proteins. Heating during pressing and the use of organic solvents promote undesired reactions among proteins as well as between proteins and phenols[40]. This has a negative impact on protein extraction yields[64] and on properties like solubility[65], interfacial tension and emulsifying ability[37,66]. As a result, the extraction of plant proteins remains challenging, which is one of the main causes of the present underutilization of the proteins in oilseeds[13,67].

Some researchers have proposed the extraction of proteins after defatting under highly alkaline (pH 11-12) or saline conditions[29,64,68,69]. Neither of these proposed approaches eliminates the defatting step. In fact, the use of highly alkaline conditions promotes even more protein-phenol complexation, with an increasingly negative effect on the physicochemical properties of the proteins, including solubility[37,70]. The use of saline conditions to improve protein extraction requires extra processing steps to remove salts from the end product and results in a saline wastewater stream with a high environmental impact.

Hence, there is a need for an alternative approach to oil and protein extraction from oilseeds[71]. In this research, by skipping the defatting step we aimed for the simultaneous extraction of oleosomes and proteins in one fraction under mild conditions (water, low temperature, near-neutral pH), followed by a separation step to obtain an oleosome-rich and a protein-rich fraction. In this paper, we report on an exploration of this alternative extraction approach, using rapeseeds as a typical oil- and protein-containing resource. The same approach could likely be applied to other oilseeds.

Rapeseeds were chosen as a potential oleosome and protein source as they contain about 40 wt% oil and 21 wt% protein[72]. The main storage proteins of rapeseeds are 11S globulins called cruciferins and 2S albumins called napins[13,67], which differ in structure, isoelectric point, and solubility[29,33]. These proteins are located in membrane-bound and highly specialized compartments called protein bodies[13].

Rapeseed proteins have superior functional properties compared with soybean proteins and similar functional properties as dairy proteins[73]. Still, the use of rapeseed proteins in foods is limited by the presence of undesirable compounds like glucosinolates, phytates, and phenols, which have a negative impact on the functional properties of proteins[37,70]. Although many studies have reported on the effects of phenolic compounds on protein properties[37,40,70,74], only a few looked at their elimination during protein extraction[40,75], in order to increase the usability of these proteins[76].

2.2 Materials and methods

2.2.1 Materials

We used untreated Alizze rapeseeds. All chemicals were of analytical grade and were purchased from Sigma Aldrich (St Louis, MO, USA).

2.2.2 Extraction process

A pin mill (DLFM, Bühler GmbH, Braunschweig, Germany) was used to break the seeds in half of their size (~ 3 mm) and facilitate the removal of hulls. The hulls were eliminated with the use of a fluid bed dryer (Retsch GmbH, Haan, Germany) connected to a vacuum cleaner (Turbo XL, BÜFA Cleaning Systems GmbH & Co, Oldenburg, Germany). After dehulling, 150 g of rapeseed particles were dispersed in deionized water at a ratio of 1:8 (w/w) and kept at room temperature for 4 h under continuous head stirring (EUROSTAR 60 digital, IKA, Staufen, Germany). The pH of the dispersion was maintained at 9.0 by the addition of a few drops of NaOH (0.5 M). The dispersion was subsequently blended for 2 min at maximum speed with a kitchen blender (HR2093, Philips, Netherlands). The slurry was filtered with a twin-screw press (Angelia 7500, Angel Juicer, Naarden, The Netherlands). The obtained liquid phase was adjusted to pH 9.0 and centrifuged (10000 g, 30 min, 4°C) (Sorvall Legend XFR, ThermoFisher Scientific, Waltham, MA, USA). The obtained cream layer (oleosome-rich), serum (protein-rich mixture (RPM)) and pellet (fiber-rich) were collected separately. The RPM was further concentrated by ultrafiltration and then diluted 1:1 with NaCl (0.08 M) to avoid protein precipitation. The mixture was pumped through two coupled diafiltration cassettes (cut-off 5 kDa; membrane area 0.2 m^2) (Hydrosart, Sartorius, Göttingen, Germany) for 6 cycles until a transparent filtrate was obtained. In the last cycle only, deionized water was used to remove any remaining salt. The retentate constituted the rapeseed protein

concentrate (RPC). Finally, the protein samples (RPM and RPC) were freeze-dried (Alpha 2-4 LD plus, Martin Christ Gefriertrocknungsanlagen GmbH, Osterode am Harz, Germany).

We calculated the weight-based extraction yields of proteins and oleosomes in the protein-oleosome extract from the remaining protein content and oil content in the solid residue after screw pressing by using:

$$protein\ yield\ (wt\%) = 100 - 100 * \left(\frac{g\ of\ proteins\ in\ the\ solid\ residue}{g\ of proteins\ initially\ in\ the\ seed}\right)^{*} \quad (2.1)$$

**The same equation was applied for the oleosome yields, with "oleosomes" instead of "proteins".*

We calculated the yields in the other fractions (i.e. oleosome-rich, protein-rich and protein concentrate) on dry-matter weight by using:

$$protein\ yield\ (wt\%) = 100 * \left(\frac{g\ of\ proteins\ in\ protein\ mixture}{g\ of proteins\ initially\ in\ the\ seed}\right)^{*} \quad (2.2)$$

**The same equation, with "oleosomes" instead of "proteins", was applied for the oleosome yields in the oleosome-rich mixture.*

All the experiments and subsequent analyses were performed in triplicates.

2.2.3 Physicochemical characterization of rapeseed extracts

Composition analysis

We determined the protein content of the seeds and of the different protein fractions obtained with the Dumas method (FlashEA 1112 Series, Thermo Scientific, Waltham, Massachusetts, US). Samples of known mass were combusted at a high temperature in the range of 800-900°C in the presence of oxygen. D-methionine (≥ 98%, Sigma Aldrich, Darmstadt, Germany) was used as a standard for the calibration curve and as control. Cellulose (Sigma Aldrich, Darmstadt, Germany) served as blank. A nitrogen–protein conversion factor of 5.7 was used to calculate the protein content by using:

$$PC\ (wt\%) = 100 \times \left(\frac{NC \times 5.7}{M}\right) \quad (2.3)$$

Here PC is the protein content, NC is the nitrogen content, and M is the mass of the dry sample.

We determined the oil content (OC) of the seeds and of the mixtures on a dry-matter weight basis. The oil was extracted for 7 h, by Soxhlet extraction with petroleum ether as a solvent. We used 1 g of dried material and calculated the oil content after extraction by using:

$$OC\ (wt\%) = 100 \times \left(\frac{M_0}{M}\right) \tag{2.4}$$

where M_o [g] is the mass of the extracted oil and M [g] the initial sample mass.

The moisture content of the samples was determined by drying a sample (1 g) at 60°C in an oven (Memmert, Memmert GmbH & Co.KG, Schwabach, Germany) until stable weight (24 h). We defined the moisture content as g of water per g of wet material.

The concentration of phenolic compounds was determined with the aid of the Folin-Ciocalteu reagent. The reduction (at alkaline pH) by the phenolic compounds of phosphomolybdate and phosphotungstate present in the reagent resulted in a color change. The concentration of blue-green reaction product was determined based on the absorbance of the solution at 725 nm. We used a tannin solution (0.0-0.1 mg/mL in water) to obtain a calibration curve.

Protein solubility

The solubility of the protein mixture (RPM) and the concentrate (RPC) was measured at a range of pH (pH 3-11). Dispersions standardized at 0.5 wt% protein content were prepared in deionized water; the pH was adjusted using 0.5 M NaOH or HCl and the dispersions were stirred at room temperature for 4 h with a magnetic stirrer at 300 rpm (2mag magnetic e motion, 2mag AG, Munich, Germany). After that, the dispersions were centrifuged at 10000 g for 30 mins at 20°C (Sorvall Legend XFR, ThermoFisher Scientific, Waltham, MA, USA) and we obtained a pellet, a clear serum and a tiny layer of oleosomes at the surface. We reported as soluble, the fractions that were present at the clear serum. We calculated the protein solubility as g of proteins present in the serum per g of proteins present in the initial dispersion.

Electrophoresis (SDS-PAGE)

The protein profile of the seeds and the molecular mixtures was determined with sodium dodecyl sulphate–polyacrylamide gel electrophoresis (SDS-PAGE) under reducing and non-reducing conditions. Each sample was mixed with a buffer (NuPAGE® LDS, ThermoFisher, Landsmeer, the Netherlands) to achieve a protein concentration of 1.0 mg/mL. For reducing conditions, dethiothreitol (DTT) was used as a reducing agent (NuPAGE® Sample Reducing Agent, ThermoFisher, Landsmeer, the Netherlands). 10.0 µL of protein marker (PageRuler™ Prestained

Protein Ladder, 10 to 180 kDa, ThermoFisher, Landsmeer, the Netherlands) and 20 µL of the sample were loaded onto the gel (NuPAGE® Novex® 4-12% Bis-Tris Gel, ThermoFisher, Landsmeer, the Netherlands). MES running buffer (NuPAGE® MES SDS Running Buffer, ThermoFisher, Landsmeer, the Netherlands) was added to the buffer chamber. The gel was washed with water and stained (Coomassie Brilliant Blue R-250 Staining Solution, Bio-Rad Laboratories B.V., Lunteren, the Netherlands) overnight under gentle shaking.

Gel permeation size exclusion chromatography

Protein profile analysis of the rapeseed protein concentrate was undertaken before and after diafiltration by using gel permeation size exclusion chromatography (SEC) (AKTA FPLC System, Amersham Biosciences, Little Chalfont, UK). The system was connected to a Superdex 200 10/300 GL column and a UV detector (λ = 280 nm). The sample was dissolved in a mixture of Tris/HCl (20 mM) at pH 8 and NaCl (0.2 M) for 30 min and centrifuged at 16000 g. The supernatant was filtered through a membrane with a pore size of 0.22 µm; the flow was 0.4 mL/min.

Protein secondary structure

Far-UV circular dichroism (CD) (185-265 nm) was used to determine the secondary structure of the proteins present in the rapeseed protein mixture and concentrate (J815 CD spectrometer, JASCO Benelux B.V.) Cruciferins and napins were recovered from the Superdex 200 10/300 GL column and diluted in 10 mM phosphate buffer at pH 7.5 to a protein concentration of 0.1 mg/mL and analyzed in a 1.0 mm cuvette. The recorded spectra for each sample were calculated after subtraction of the buffer spectrum. We calculated the percentages (%) of each structure by using online CD structure prediction software as described elsewhere[77].

ζ-potential measurements

To measure the charge of the proteins present in rapeseed protein mixture under different pH conditions, titration was performed by using a ZS Nanosizer (Malvern Instruments, Ltd, Worcestershire, U.K.). The sample was prepared by dispersing the protein mixture (RPM) or protein concentrate (RPC) in deionized water to a final protein concentration of 0.03 wt%. The equilibration time was set to 120 s and the temperature to 25°C. The ζ-potential of the sample was measured at a pH ranging from 2 to 12, by adjusting it with HCl (0.5 M) or NaOH (0.1 or 0.5 M).

Particle size distribution

The particle size distribution of the oleosomes was determined by laser diffraction (Malvern Instruments, Ltd, Worcestershire, UK) after dilution of the oleosome-rich mixture with deionized

water at a ratio of 1:100. To investigate the presence of aggregated oleosomes and determine their actual size, we added 1.0 wt% sodium dodecyl sulfate (SDS) to the sample in a ratio of 1:1. The used refractive index was 1.47. Measurements are reported as the surface ($d_{3,2} = \Sigma n_i d_i^3 / \Sigma n_i d_i^2$) and volume ($d_{4,3} = \Sigma n_i d_i^4 / \Sigma n_i d_i^3$) mean diameter where n_i is the number of droplets with a diameter of d_i. Besides, to determine the effect of storage proteins on the particle size of oleosomes, two washing steps were applied to the oleosome-rich mixture by diluting with deionized water in a ratio 1:5 (w/w) and centrifuging at 10000 g for 30 min. The process was repeated two times and the final sample was diluted as described above for particle size measurements.

The particle size of the protein dispersions (RPM, RPC) at different pH values (3-11) was measured with dynamic light scattering (DLS) using a Nano sizer ZS (Malvern Instruments, Ltd, Worcestershire, U.K). The protein content was standardized to 0.001 wt% into deionized water, the pH was adjusted and the dispersions were stirred for 4 h at 20°C with a magnetic stirrer at 300 rpm (2mag magnetic e motion, 2mag AG, Munich, Germany) before measurement. A refractive index of 1.45 was chosen for the proteins. The results were given as mean number particle size diameter (nm).

2.2.4 Microscopy

Light microscopy (LM)

Light microcopy (Leica DMi8, Leica Microsystems, Wetzlar, Germany) was used to visualize the oleosomes after extraction. The samples were diluted at 1:100 in deionized water. Images were taken at 40x magnification, with an oil immersion objective.

Cryo-scanning electron microscopy (cryo-SEM)

Cryo-SEM was used for imaging of solids after screw pressing, of oleosome-rich mixtures, and of the protein concentrate. The samples were frozen by placing a tiny volume of each sample (one droplet / one seed) on top of a rivet and plunge-freezing in melting ethane. The sample was cryo-planed (at -110°C) with a cryo-ultramicrotome (Leica Ultracut UCT EM FC7) to obtain a freshly prepared cross-section. The sections were made at decreasing thicknesses down to 20 nm, and down to a speed of 1 mm/sec. The rivet was mounted onto the SEM holder and transferred into a Gatan Alto2500 preparation chamber. To reveal the microstructures under the planed surface, the temperature of the sample was increased to -90°C to remove a thin layer of ice by sublimation. The sample was sputter-coated with platinum (30 sec) for a better SEM contrast and to prevent charging by the electron beam, then imaged in a Zeiss Auriga field-emission SEM at -125°C and an accelerating voltage of 3 kV. We used two secondary electron detectors. The Everhart-Thornley

detector in the microscope chamber provides images with high topographical contrast. The in-lens detector provides high edge contrast, which in the case of our study produced a quasi-compositional contrast (oil and other non-aqueous structures: black; other materials: white and grey).

Transmission electron microscopy (TEM)

Cu grids (400 mesh, with carbon support film) were first cleaned with a glow discharger for 20 seconds (10-1 Tor). 10 µl of sample diluted in deionized water (1:100) was put on the Cu grids. The grids were dried by blotting with filter paper. The samples were then stained with 10 µl of 2.0 % phosphotungstic acid (PTA) (Sigma Aldrich, St Louis, MO, USA). We dried the grids again by blotting with filter paper and imaged them with a JEOL JEM 1400 plus TEM (Jeol USA, Peabody, MA, USA), operating at 120 kV.

2.3 Results and discussion

2.3.1 Release of proteins and oleosomes from rapeseed cells

Figure 2.1 illustrates the proposed extraction method, in which proteins and oleosomes are first extracted as one protein-oleosome fraction (Figure 2.1A) and then further separated into an oleosome-rich (Figure 2.1B) and a protein-rich mixture (Figure 2.1C).

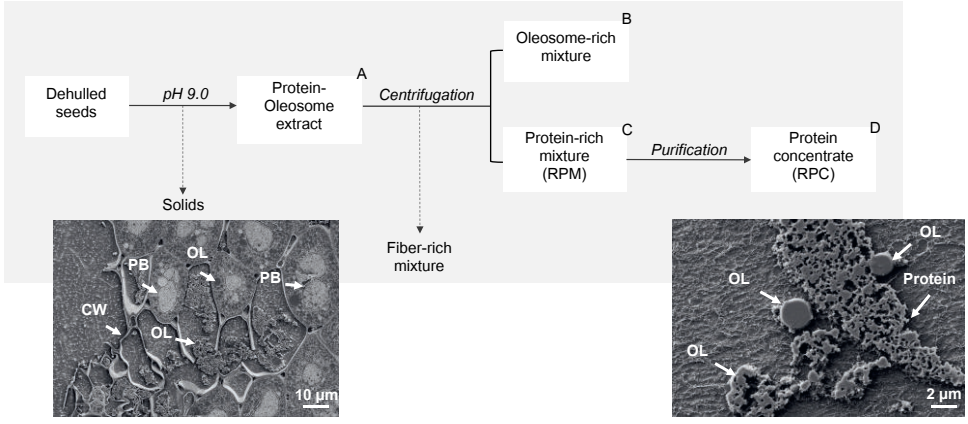

Figure 2.1 Extraction process of rapeseed protein-rich mixture (RPM), rapeseed protein concentrate (RPC) and oleosome-rich mixture. Images of cryo-SEM of solids after extraction (left) and of RPC in deionized water (right). CW: cell wall, OL: oleosomes, PB: protein bodies. Scale bar: 10 µm and 2 µm respectively.

To avoid contamination of the samples with phenols originating from the hulls[40], the rapeseeds were dehulled before any further processing. The protein and oil content of the obtained rapeseed particles was 18.7±0.6 wt% and 41.9 ± 0.9 wt%, respectively, which is similar to values reported in literature[78].

The dehulled seeds were first soaked in aqueous media to allow the softening of the cells and ease further diffusion of proteins and oleosomes from the seed cells into the solvent after disruption of the cells[60,69,79]. To facilitate this, electrostatic repulsion between the molecules should be induced[71]. This can be achieved by adjusting the pH of the solvent far from the isoelectric points (IEP) of the proteins and oleosomes. The IEP of oleosomes occurs around pH 5[80], and the IEPs of rapeseeds proteins are pH 7 for cruciferins and pH 11 for napins[13]. As we intended to extract all proteins and oleosomes simultaneously at near-neutral pH values, we adjusted the pH of the solvent to 9.0.

Previous studies on rapeseed protein extraction have used pH values above 10[47,65,68,79]. However, such highly alkaline environments induce oxidation of phenols to aldehydes, ketones and carboxylic acids, which can subsequently polymerize or covalently bind to proteins[40]. The pH values that promote these interactions depend on the type of phenols present. For example, in sunflower seeds, chlorogenic acid is present, which oxidizes and covalently binds to proteins at pH 9.0[81]. Oxidation of sinapic acid in rapeseeds to thomasidioic acid and further to quinones accelerates at pH values above 10[41,42]. In addition, ionic bonding between proteins and sinapine (the choline ester of sinapic acid) occurs at pH values above 9.5, leading to co-extraction of phenolic compounds[40].

Another parameter that influences the extraction yields of proteins and oleosomes is the solid-to-solvent ratio, with higher amounts of solvent leading to higher extraction yields[68,69,79]. A ratio of 1:18 (5.0 w/v% solids) is commonly used[65,73,82]. However, to make the extraction more environmentally sustainable, it is important to use the minimum amount of solvent that leads to sufficient extraction yields. On the basis of previously published reports on oleosome[83] and protein extraction[68] as well as of preliminary internal data, a solid: solvent ratio of 1:8 was used.

This extraction procedure resulted in a protein-oleosome extract (Figure 2.1A) that contained 78.8 ± 0.2 wt% of the proteins and 82.8 ± 0.4 wt% of the oleosomes initially present in the dehulled seeds. The extraction yield of proteins was higher than values reported in other studies (28-50%)[47,65,68,73]. We ascribe the difference to the fact that in the other studies, proteins were extracted from defatted rapeseeds and at highly alkaline pH conditions (pH > 10), which stresses the negative impact that defatting processes have on protein solubility and subsequent extraction yields[13,46,65]. The oleosome extraction yield reported here was the same or higher compared to what was reported in comparable studies on oleosome extraction from other oilseeds. For example, oleosomes from soybeans have been extracted at a yield of 65-70 wt%[71], while the oleosome extraction yield from maize germs was around 78 wt%[84].

Cryo-SEM analysis was employed to explore the rupture of the cell walls during the extraction. The cryo-SEM image in Figure 2.1 (solids) shows the solids remaining after the extraction process. Broken, deformed and empty cells were visible. Intact cells were also identified. It is important to mention at this point that a 2D image is not representative image of the general status of the seed cells after pressing. It is only a cut of the seed and the image is giving information only regarding the status of the cells in this surface without knowing what the status is above or under this surface. At most of the parts of the cells we analyzed, we mostly identified ruptured cells. However, the reason that this image was chosen amongst all the images we had, was to show that despite the blending and pressing, some cells seemed to be still intact. The fact that around 80 % yield was achieved means that apparently around 20 % of the mass of the cells was not extracted and remained in the cells.

2.3.2 Separation of proteins and oleosomes from the protein-oleosome extract

Next, we carried out centrifugation of the protein-oleosome extract (Figure 2.1A). This led to separation into three phases, namely an oleosome-rich mixture (Figure 2.1B) as a concentrated cream at the top, a protein-rich mixture (Figure 2.1C, rapeseed protein mixture or RPM) as a serum phase and a fiber-rich mixture as a pellet. The protein-rich mixture was diafiltrated, resulting in a protein concentrate (Figure 2.1D, RPC).

Table 2.1 summarizes the recovery yields and compositions of the obtained mixtures after centrifugation and diafiltration. The rapeseed protein mixture (RPM) contained 37.0 ± 1.3 wt% of the proteins initially present in the seeds (Figure 2.1C). The composition of its dry mass was 39.5 ± 0.8 wt% proteins, 11.9 ± 0.5 wt% oil and 6.3 ± 0.1 wt% phenolic compounds.

Table 2.1 Recovery yields and compositions of obtained mixtures after centrifugation and diafiltration as percentage (wt%) of total dry matter.

	Recovery yield wt%	Composition wt%		
		Protein	Phenolic compounds	Oil
Rapeseed protein mixture (RPM)	37.7 ± 1.3	39.5 ± 0.8	6.3 ± 0.1	11.9 ± 0.5
Rapeseed protein concentrate (RPC)	31.2 ± 1.2	65.1 ± 1.9	2.7 ± 0.1	15.1 ± 0.9
Oleosomes	63.3 ± 0.3	7.8 ± 0.2	-	81.8 ± 0.3

Diafiltration of RPM (Figure 2.1C) was applied to remove low-molecular-weight compounds, such as free phenolic compounds, inorganic material, and monosaccharides. This step resulted in a

rapeseed protein concentrate (RPC) (Figure 2.1D) with 65.1 ± 1.9 wt% and 15.1 ± 0.9 wt% protein and oil content respectively, while the phenolic compound content was reduced to 2.7 ± 0.1 wt% (Table 2.1).

After diafiltration, the protein yield in the RPC was 31.2 ± 1.2 wt% of the proteins present in the initial seeds (Table 2.1). This value was higher than what has been accomplished in other studies, in which defatted meal was used as starting material (15-28%)[46,47,65]. In most of these studies, isoelectric point precipitation was applied[65,72,82,85]. This probably leads to the selective separation of rapeseed proteins due to their different isoelectric points and solubility. In addition, defatting of oilseeds prior to protein extraction and isoelectric precipitation can lead to extensive protein-protein or protein-phenol complexation[42], which impacts protein structure and extraction yields.

To investigate whether the oil present in RPC was in the form of oleosomes or free oil, we performed cryo-SEM. The cryo-SEM image in Figure 2.1 reveals intact oleosomes present in the concentrate (RPC) rather than free oil. Previous research has shown that oil present in protein mixtures in the form of oleosomes does not influence the functional and physicochemical properties of the proteins[86]. Therefore, the obtained protein extract (RPC) can be considered as a protein concentrate.

The oleosome-rich mixture obtained after centrifugation (Figure 2.1B) contained 63.3 ± 0.3 wt% of the initial oil in the seed. The mixture had 81.8 ± 0.3 wt% oil and 7.8 ± 0.2 wt% protein content expressed on dry matter; see Table 2.1. The recovery yields were similar to those reported for maize germ oleosomes recovered at pH 9.0 (64.1%)[61] and for oleosomes recovered from different oilseeds (60%)[87]. A similar recovery yield (65%) of soybean oleosomes was obtained in a different study, but only after three subsequent extractions of the residues after one-stage extraction[88]; after one-stage extraction the reported oil yields of soybean oleosomes varied between 29-59%[89]. In our study, rapeseed oleosomes were recovered by using only one extraction and centrifugation step, minimizing the required processing steps.

2.3.3 Physicochemical characterization of rapeseed proteins

To gain insight into the physicochemical properties of RPM and RPC, we determined the ζ-potential, the solubility, and the protein particle size under a range of pH values (pH 3-11). Besides these, the protein profile, the protein composition, and changes at the secondary structure were investigated as well.

Figure 2.2A displays the ζ-potential of the RPM and RPC as a function of pH. The results show that at pH values higher than 5 the protein fractions were negatively charged in both cases. A similar curve has been previously reported for rapeseed protein extracts[68]. This indicates that the

ζ-potential of the protein mixture and concentrate is dictated by the protein molecules. Furthermore, as it was recently published, the effect of the pH on the surface charge of oleosomes was expected to follow a similar pattern[60,90].

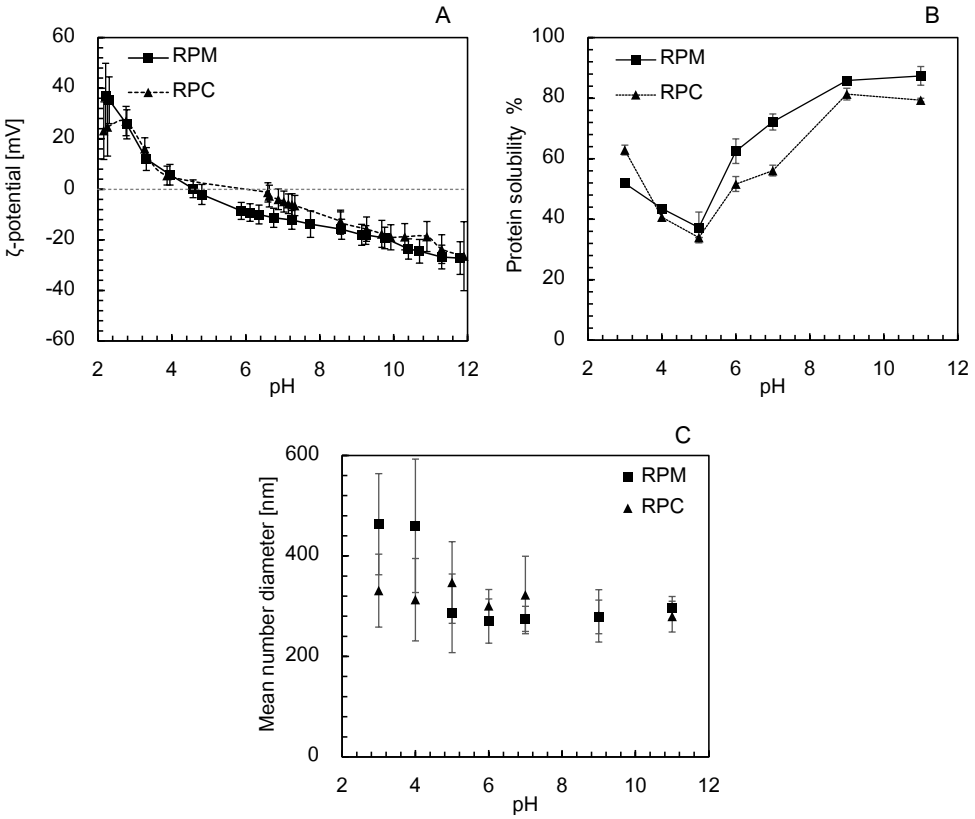

Figure 2.2 Influence of pH on A) ζ-potential, B) solubility and C) protein particle size of the rapeseed protein mixture (RPM) and protein concentrate (RPC).

Solubility is an essential functional property of the proteins. Figure 2.2B shows that the proteins in RPM and RPC have similar solubility patterns at different pH conditions. The solubility of the proteins at the extraction conditions (pH 9) was 85.8 ± 0.8 and 81.4 ± 1.9 wt% for RPM and RPC respectively. The similar solubility of the RPM and RPC indicated that phenolic compounds present in the RPM didn't interact with proteins and subsequently didn't significantly affect the solubility of the RPM. The slightly higher solubility of RPM in comparison to RPC can be attributed to the removal of salts that takes place during diafiltration. The lowest solubility values of both RPM and RPC were observed at pH 5 (37 and 34 wt% respectively), where the surface charge reached the lowest value and apparently weak electrostatic repulsive forces occurred and aggregates were formed (Figure 2.2C). At pH values above 6, the size of the aggregates was constantly at about

300 nm. However, at pH values lower than 6, aggregates with a wide size distribution were formed for both RPM and RPC (300-600 nm). The formation of relatively bigger aggregates at pH values below 6 can be linked with the lower solubility observed in this pH region.

In most previously published studies, significantly lower protein solubility at pH 9.0 (50-60%) has been reported[43,46,91,92]. This considerable difference is most likely related to the defatting process that was applied, inducing extensive protein-protein and protein-phenol interactions that decrease protein solubility[43,44,46,93,94]. Indeed, in a different study on the effect of defatting on protein extraction yields, proteins extracted from cold-pressed rapeseed meal had a solubility of 65% at pH 9.0, which reduced to 15% when the meal was pre-pressed and toasted in the defatting procedure[46]. These observations highlight the high negative effect of conventional defatting processes on protein quality[46,95] and explain why other researchers have resorted to the use of a high extraction pH or addition of salts to solubilize and extract the proteins[64].

To investigate the protein composition of RPM and RPC, SDS-PAGE analysis was carried out (Figure 2.3A). In RPM, under non-reducing conditions (RPM, lane-), cruciferins showed distinct dissociation characteristics with six subunits appearing as bands of 20-70 kDa while napins appeared as a single band around 17 kDa. Both cruciferins and napins are composed of chains linked by disulphide bonds[96,97]. Under reducing conditions (RPM, lane+), new bands showed at 20-40 kDa and 5-11 kDa related to cruciferins and napins, respectively, indicating the breaking of the disulphide bonds. Oleosins (~15-19 kDa) were also present in the protein mixture. The analysis confirmed the successful extraction of both families of storage proteins, by only using a pH far enough from their isoelectric points (pH 9.0). No changes in protein composition were reported after diafiltration as the protein profile was identical in RPM and RPC (Figure 2.3A).

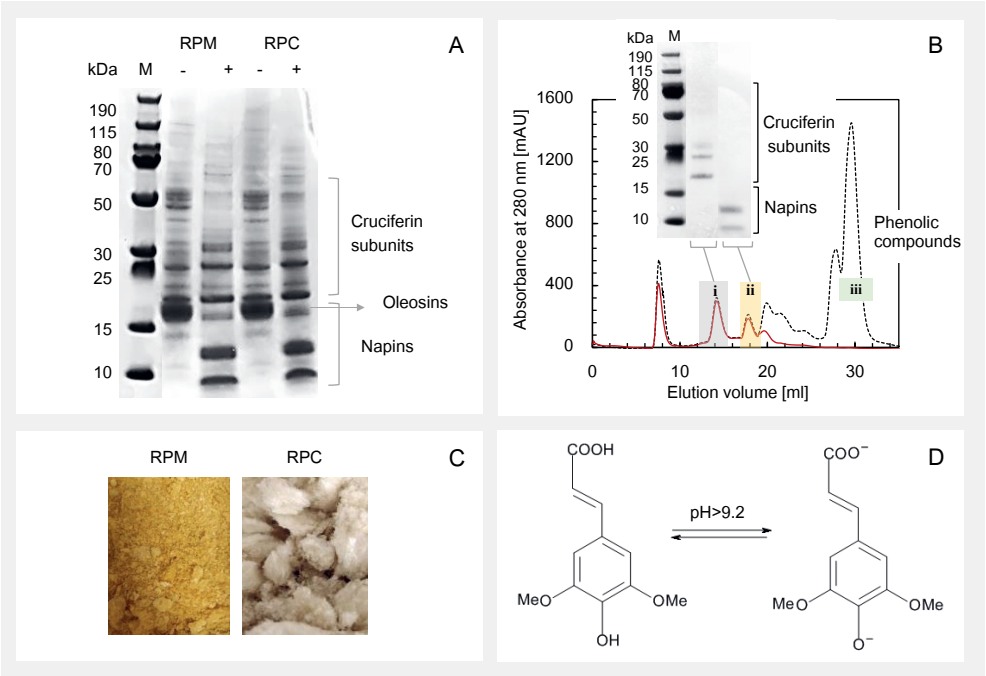

Figure 2.3 A) Electrophoregram (SDS-PAGE) of RPM and RPC under non-reducing (−) and reducing (+) conditions. M: protein molecular weight marker, B) Gel permeation size exclusion chromatogram of RPM (black dashed line) and RPC (red continuous line), measured at 280 nm, showing cruciferins (i), napins (ii) and free phenolic compounds (iii). Inset picture: Electrophoregram (SDS-PAGE) of the proteins under reducing conditions, C) Pictures of freeze-dried RPM (left) and RPC (right), D) Chemical structure of sinapic acid (left) and its ionized form (right).

To further explore the composition of RPM and RPC, we carried out gel-permeation size-exclusion chromatography. Figure 2.3B displays the chromatogram of RPM and RPC. Their higher molecular weight (~300 kDa) caused cruciferins (peak i) to be eluted first, followed by napins (~17 kDa) (peak ii). The protein profile of the identified peaks was similar for RPM and RPC and also confirmed by SDS-PAGE analysis (Figure 2.3B, inset). Phenolic compounds (peak iii) were eluted last. The chromatogram shows that the peak assigned to phenolic compounds in RPM disappeared after diafiltration, which confirmed that no protein-phenol covalent bonding occurred during the extraction process. It is known that when phenolic compounds are covalently bound to proteins, their removal can take place through alkaline hydrolysis and /or the use of solvents such as urea[40]. The fact that in our case the protein-phenol complexation was prevented, and efficient removal of the phenolic compounds took place with diafiltration is a clear advantage over the previously proposed methods.

It is important to mention at this point that in most earlier studies of rapeseed proteins, the researchers obtained dark-colored concentrates, probably due to phenol oxidation and

complexation with proteins[40,41,72]. In this study, as Figure 2.3C shows, RPM had a yellow color. As Figure 2.3D shows, both the carboxylic and hydroxyl groups of sinapic acid are ionized at pH > 9.2, resulting in a yellow color during absorption[41]. This could explain the yellow color observed in RPM since the pH was kept at 9.0 during extraction. However, after diafiltration, the intensity of the yellow color was remarkably decreased in RPC (Figure 2.3C) as the phenolic compounds were removed. This indicates that during the extraction time (4 h), sinapic acid was still in its monomeric form and had not been oxidized[41], preventing complexation with the proteins. Alkali-induced oxidation of sinapic acid to tomasidioic acid and further to quinones are known to require more than 10 h of incubation in a highly alkaline environment (pH > 10)[41].

Interactions between proteins and phenolic compounds alter the intramolecular forces responsible for maintaining protein structure, leading to changes in secondary structure[81,98]. For example, covalent bonding of oxidized chlorogenic acid with sunflower proteins led to significant changes in the protein secondary structure[81]. Such changes can affect surface properties, making proteins less or more hydrophilic[37]. Therefore, to get an insight into possible conformational changes in the secondary protein structure during the applied processing, far-UV circular dichroism (CD) spectra were obtained (Figure 2.4).

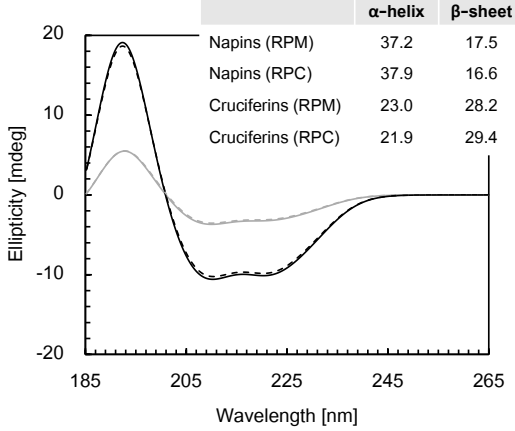

	α-helix	β-sheet	β-turn	Others
Napins (RPM)	37.2	17.5	12.8	32.5
Napins (RPC)	37.9	16.6	12.8	32.7
Cruciferins (RPM)	23.0	28.2	10.1	38.7
Cruciferins (RPC)	21.9	29.4	9.9	38.8

Figure 2.4 Changes in far-UV CD spectra of napins (black) and cruciferins (grey) in RPM (continuous line) and in RPC (dashed line). The inset table shows the secondary structure composition (%) for napins and cruciferins in RPM and in RPC.

The spectra of napins in RPM showed two main peaks at around 208 and 222 nm and a positive peak at 193 nm. The presence of the two main peaks corresponds to a predominant α-helix structure[99]. Cruciferins in RPM had less intense peaks at these spectra.

The inset table (Figure 2.4) shows the compositional analysis (based on UV CD), which found a principal α-helix structure for napins in RPM (37.2%) with no significant difference for napins in

RPC (37.9%). Cruciferins in RPM had a high percentage of the β-sheet structure (28.2%), but also a high percentage of other structures (38.7%), including other types of helix, β-strand, bends and unordered or invisible structures. After diafiltration, the composition of cruciferins in RPC also remained similar (i.e. 29.4% β-sheet and 38.8% others). This confirmed that no structural changes occurred to both proteins during diafiltration and that no complexation between proteins and phenolic compounds took place.

2.3.4 Physicochemical characterization of oleosomes

Extracting oleosomes in their native form is of high importance since they can then be used as a naturally emulsified phase. Thus, aiming to assess the impact of the extraction process on the physicochemical properties of the oleosomes, the particle size, the protein profile and the structure of the oleosomes were determined.

Particle size is one of the main parameters that reflect the effect of the extraction process on the structural properties of oleosomes. In our experiments, the obtained oleosomes showed a bimodal particle size distribution with two peaks of around 0.7 and 25.0 μm (Figure 2.5A, dashed line). The oleosomes had a volume mean diameter, $d_{4,3,}$ of 23.3 ± 2.4 μm and a surface area mean diameter, $d_{3,2}$ of 3.0 ± 0.1 μm. These values were higher than what was found ($d_{4,3}$~5 μm) in another study[60].

We attribute this difference to the relatively high amount of proteins present (Table 2.1), as we did not further purify the obtained oleosomes. Storage proteins can interact with the oleosomes' interfacial proteins through electrostatic and hydrophobic forces and act as molecular bridges that lead to aggregation (bridging flocculation)[100]. The presence of oleosome aggregates explains the second peak of 25.0 μm observed in Figure 2.5A (dashed line). The protein profile analysis of the oleosome-rich mixture (Figure 2.5C) revealed a band at ~19 kDa assigned to oleosins but also some bands related to cruciferins and napins. Other researchers have also observed the presence of storage proteins in research that used a single washing step of oleosomes[80,87].

Therefore, SDS was added to determine the size of individual oleosomes. SDS is a low molecular weight surfactant, which breaks protein hydrophobic interactions[101] and, in this case, prevents bridging flocculation. The results after the addition of SDS, (Figure 2.5A, continuous line) showed a monomodal particle size distribution with a volume mean diameter, $d_{4,3}$ of 0.7 ± 0.1 μm and a surface area mean diameter $d_{3,2}$ of 0.4 ± 0.1 μm which corresponds to the actual size of the oleosomes in the seed structure. This result verifies that the proposed extraction process had no impact on the physicochemical properties of oleosomes. Light microscopy (LM) initially showed oleosome aggregates, but individual droplets after the addition of SDS (Figure 2.5A).

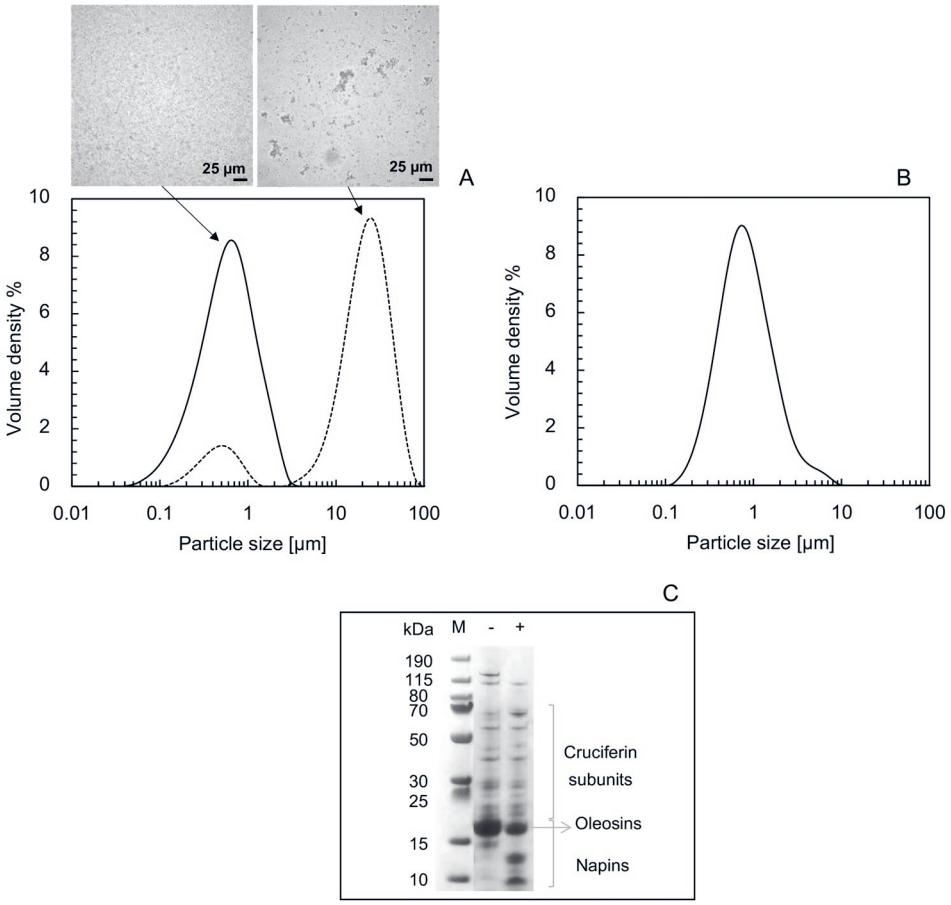

Figure 2.5 A) Particle size distribution as a percentage of volume density of rapeseed oleosomes before (dashed line) and after addition of 1.0 wt% SDS (continuous line). Scale bar in light microscopy images: 25 µm, B) Particle size distribution as a percentage of volume density of rapeseed oleosomes after two additional washing steps, C) Electrophoregram (SDS-PAGE) of oleosome-rich mixture under non-reducing (−) and reducing (+) conditions. M: protein molecular weight marker.

In addition, to examine the effect of storage proteins on the aggregation of oleosomes, we applied two additional washing steps to remove the proteins. The particle size analysis of the washed oleosomes showed a monomodal particle size distribution with a volume mean diameter ($d_{4,3}$) of 0.9 ± 0.2 (Figure 2.5B). This outcome also confirmed that the aggregates formed after the first centrifugation step were a result of the presence of storage proteins, as after their removal we obtained oleosomes in their natural size.

Finally, to further investigate the presence and conformation of storage proteins, electron microscopy analysis was carried out (Figure 2.6). Cryo-SEM analysis (Figure 2.6A) revealed that proteinaceous material was present in the oleosome-rich mixture, causing bridging between the oleosome droplets. The presence of extrinsic proteins is beneficial for the structural integrity of oleosomes during processing, as they form protective layers that envelop the oleosomes[80]. We also used transmission electron microscopy (TEM) (Figure 2.6B-C). A contrast stain with affinity to proteins was added and we clearly observed dark rings around oleosomes, confirming the high local concentration of storage proteins.

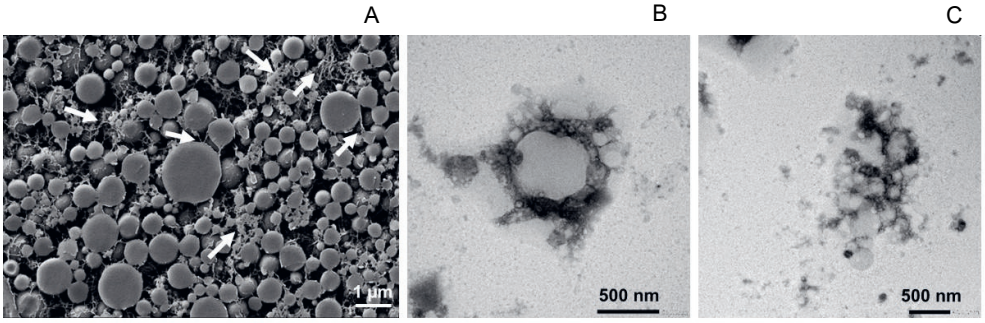

Figure 2.6 A) Cryo-SEM of extracted oleosome-rich mixture. White arrows indicate proteinaceous material surrounding the oleosomes. Scale bar: 1 µm, B–C) TEM of extracted oleosomes surrounded by storage proteins stained with contrast agent (indicated in black). Scale bar: 500 nm.

2.4 Conclusions

We have successfully tested the simultaneous extraction of proteins and oleosomes from rapeseeds in few processing steps, as an alternative to the currently used extraction process. Without defatting and by following a simple procedure under mild conditions (no organic solvents, low temperature, near-neutral pH), we simultaneously extracted storage proteins and intact oleosomes in one protein-oleosome extract, with high yields. Further separation of the extract resulted in a protein-rich and an oleosome-rich mixture. Diafiltration of the protein-rich mixture resulted in the efficient removal of co-extracted phenolic compounds leading to a light-colored protein concentrate where all storage proteins were present. Our approach avoided covalent interactions between proteins and phenolic compounds that could have altered the secondary structure and lowered protein functionality, resulting in a protein concentrate with high solubility. Oleosomes were recovered as a naturally dispersed oil phase in their natural structure and size proving that the proposed extraction process had no negative impact on either proteins or oleosomes. These findings highlight the need for designing alternative processes for the extraction of high-quality plant-derived ingredients that will introduce their use in food systems.

Chapter 3

Interfacial stabilization mechanism of less purified rapeseed protein extracts at neutral pH conditions (pH 7)

This chapter has been published as: Ntone, E., van Wesel, T., Sagis, L. M. C., Meinders, M., Bitter, J. H., & Nikiforidis, C. V. (2021). Adsorption of rapeseed proteins at oil/water interfaces. Janus-like napins dominate the interface. *Journal of Colloid and Interface Science*, 583, 459–469. https://doi.org/10.1016/j.jcis.2020.09.039

Abstract

Plants offer a vast variety of protein extracts, typically containing multiple species of proteins that can serve as building blocks of soft materials, like emulsions. However, the role of each protein species concerning the formation of emulsions and interfaces with diverse rheological properties is still unknown. Therefore, deciphering the role of the individual proteins in an extract is highly relevant, since it determines the optimal level of purification, and hence the sustainability aspects of the extract. Here, we will show that when oil/water emulsions were prepared with a rapeseed protein extract containing napins and cruciferins (in a mass ratio of 1:1), only napins adsorbed at the interface exhibiting a soft solid-like rheological behavior. The dominance of napins at the interface was ascribed to their small size (r = 1.7 nm) and its unique Janus-like structure, as 45% of the amino acids are hydrophobic and primarily located at one side of the protein. Cruciferins with a bigger size (r = 4.4 nm) and a more homogeneous distribution of the hydrophobic domains couldn't reach the interface, but they appear to just weakly interact with the adsorbed layer of napins.

3.1 Introduction

Oil-in-water emulsions are soft materials broadly used in a variety of areas, like food, pharmaceutical, cosmetic and paint industry[102]. To stabilize an interface between the two immiscible liquids, the adsorption of surface-active molecules is needed. These molecules decrease the surface tension and can impart various types of surface rheological behavior (viscous, viscoelastic fluid-like or viscoelastic solid-like behavior) to a surface[103,104]. Some of the most commonly used classes of surface-active species are low molecular weight surfactants, amphiphilic polymers, colloidal particles.

To meet the sustainability demands for a circular economy, the use of biobased surface-active molecules and preferably of plant origin is essential[11,105]. Several plant-based surfactants are currently used as emulsifiers in commercial applications, especially in food, such as polar lipids[11] and proteins, but these are mostly limited to a small number of specific sources, like soybeans and peas[12]. There are many other protein sources available in plants, that are currently being investigated for their potential to be used to design functional interfaces.

One of the reasons that plant proteins are not yet more widely exploited as emulsifiers, emerges from the high molecular complexity of plant matrices[106]. In seed cells, for example, proteins are organized in structures called protein bodies, that coexist with other structures such as oleosomes/lipid droplets, polysaccharides, and phenols. The intricacy of plant cells requires intensive treatment to extract the proteins, such as pressing, use of organic solvents, and high-alkaline conditions[68,86,106]. These extraction steps can induce extensive changes in the protein structure, leading to a decrease in the capability of proteins to adsorb at the surface and decrease the surface tension[66]. Another reason that plant proteins are not yet broadly used, is the fact that they are always present in complex mixtures of proteins with different functionalities, which are difficult to purify[12]. These bottlenecks can cast doubt on the environmental benefit of substituting synthetic and animal-based emulsifiers with purified plant proteins[107].

However, very recent studies have shown that extensive purification of plant proteins can be avoided since mildly purified plant protein mixtures are also effective in decreasing the surface tension and behave similarly to purified proteins[86,108,109]. For instance, mildly extracted sunflower protein mixtures with 50% protein content have shown similar interfacial and emulsifying properties to purified sunflower proteins[86]. In a different study, native pea flour containing only 20% protein also showed similar interfacial properties compared to concentrated pea protein systems (55 wt% in protein)[109]. Additionally, even low protein content (6.3 wt%) in a cellulosic material derived in simple steps from leaves, could reduce the surface tension and efficiently stabilize oil-in-water interfaces[110].

Even so, the exact mechanism of interface stabilization is still unknown as the protein mixtures contain different species of proteins. The adsorption at the interface of different types of plant proteins results in the formation of interfaces with diverse rheological properties[11,103] which is very relevant for the targeted applications. Thus, it is essential to decode the role of each protein species present in these extracts on the interface stabilization mechanism. This knowledge would allow us to determine the optimal level of purification based on the desired functionality, and hence the sustainability aspects of the plant extracts.

The diversity in the emulsifying and interfacial properties that plant proteins offer, in combination with the abundance of plant feedstock, makes plant protein mixtures promising emulsifiers with advanced functionalities. Furthermore, the fact that plant proteins are already interfacially active when they are present in a mildly purified mixture, allows us to investigate and exploit the properties of unique protein structures that in other cases would be difficult to purify.

Therefore, in this study we investigated the interfacial and emulsifying properties of a rapeseed protein mixture (40 wt% protein) which is mainly composed of two different types of proteins; cruciferins and napins in a mass ratio of 1:1. Napins are low molecular weight albumins of around 17 kDa with a rather unique structure, with 45% of its amino acids being hydrophobic and mainly located in one distinct domain[36]. On the other hand, cruciferins are hexamers with a molecular weight of around 300 kDa with the hydrophobic domains widely distributed amongst the protein's surface[35]. Due to their differences in physicochemical properties, these proteins can differ in their interfacial properties, while when present in mixtures, competitive adsorption can occur. So far, there are only a few studies on the differences on the interfacial properties of pure napins and cruciferins but not when present in native mixtures. Hence, we aimed to understand the mechanism of the oil/water interface stabilization when using the protein mixture, by deciphering the role of each protein on this stabilization mechanism.

3.2 Materials and methods

3.2.1 Materials

The rapeseed protein mixture was extracted from untreated Alize rapeseeds stored at -18°C. All chemicals used were of analytical grade and were purchased from Sigma Aldrich (St Louis, MO, USA).

All experiments and the subsequent analysis were performed at least in duplicates.

3.2.2 Extraction process

The protein mixture was extracted as described in our previous work[111]. Briefly, dehulled rapeseed particles were dispersed in deionized water at a ratio of 1:8 (w/w) and kept at room temperature (around 20°C) for 4 h under continuous stirring using a head stirrer (EUROSTAR 60 digital, IKA, Staufen, Germany). The pH of the dispersion was maintained at 9.0 during the soaking time using NaOH (0.5 M). Afterwards, the dispersion was blended for 2 min at maximum speed with a kitchen blender (HR2093, Philips, Netherlands). The slurry was then filtered using a twin-screw press (Angelia 7500, Angel Juicer, Naarden, The Netherlands). The filtrate was collected, the pH was adjusted to pH 9.0, and centrifuged (10000 g, 30 min, 4°C) (Sorvall Legend XFR, ThermoFisher Scientific, Waltham, MA, USA). A cream layer (oleosome-rich), a serum (protein mixture (RPM)) and a pellet (fiber-rich) were obtained which were collected separately. The protein mixture was freeze-dried (Alpha 2–4 LD plus, Martin Christ Gefriertrocknungsanlagen GmbH, Osterode am Harz, Germany) and stored at -18°C until further use.

3.2.3 Isolation of napins

For the isolation of napins, the extracted protein mixture was first diafiltrated with two coupled diafiltration cassettes of 100 kDa cut-off (Hydrosart, Sartorius, Göttingen, Germany). This step was necessary to remove the high molecular weight non-protein compounds as well as cruciferins which have a molecular weight of 300 kDa. Then, to remove the low molecular weight compounds, the filtrate containing the napins (< 100 kDa) was collected and further concentrated by ultrafiltration and then diluted 1:1 with NaCl (0.08 M) to avoid protein precipitation. The mixture was pumped through two coupled diafiltration cassettes (cut-off 5 kDa; membrane area 0.2 m^2) (Hydrosart, Sartorius, Göttingen, Germany) for 6 cycles until a transparent filtrate was obtained. In the last cycle only, deionized water was used to remove any remaining salt. The retentate which consisted of napins was freeze-dried and stored at -18°C until further use.

3.2.4 Physicochemical characterization of the protein fractions

Composition analysis

We determined the protein content (PC) of the protein mixture and the napin isolate on dry-matter weight basis using the dumas method (FlashEA 1112 Series, Thermo Scientific, Waltham, Massachusetts, US); d-methionine (≥ 98%, Sigma Aldrich, Darmstadt, Germany) was used as a standard and as a control. Cellulose (Sigma Aldrich, Darmstadt, Germany) served as blank. A nitrogen–protein conversion factor of 5.7 (based on amino acid sequence) was used and the protein content was calculated using:

$$PC\ (wt\%) = 100 \times \left(\frac{NC \times 5.7}{M}\right) \tag{3.1}$$

Here PC is the protein content, NC is the nitrogen content, and M is the mass of the dry sample.

The oil content (OC) of the mixtures was calculated on a dry-matter weight basis using Soxhlet extraction. The oil was extracted for 7 h with petroleum ether (40-60°C) as a solvent. The oil content after extraction was calculated using:

$$OC\ (wt\%) = 100 \times \left(\frac{M_o}{M}\right) \tag{3.2}$$

where M_o [g] is the mass of the extracted oil and M [g] the initial sample mass.

The concentration of phenolic compounds was determined using the Folin-Ciocalteu reagent. The reduction (at alkaline pH) by the phenolic compounds of phosphomolybdate and phosphotungstate present in the reagent resulted in a color change. A dispersion of the protein extract was prepared at a concentration of 0.5 mg/mL. The concentration of the reaction product was determined based on the absorbance of the solution at 725 nm. We used tannic acid solution (0.0–0.1 mg/mL in water) to obtain a calibration curve.

To determine the ash content 1 g of the protein extract was placed in an air oven at 550°C for 24 hrs and the weight loss during calcination was measured.

The carbohydrate content was determined by subtraction of the protein, oil, phenolic and ash content from the total dry mass of the extract.

Electrophoresis (SDS-PAGE)

The qualitative and quantitative analysis (protein profile) of the protein fractions and of the emulsion interface and continuous phase was carried out using sodium dodecyl sulphate–polyacrylamide gel electrophoresis (SDS-PAGE). Each sample was mixed with a sample buffer (NuPAGE® LDS, Thermo- Fisher, Landsmeer, the Netherlands) to achieve a final protein concentration of 1.0 mg/mL. Then, 10.0 µL of protein marker (PageRuler™ Prestained Protein Ladder, 10–180 kDa, ThermoFisher, Landsmeer, the Netherlands) and 15 µL of the sample were loaded onto the gel (NuPAGE® Novex® 4–12% Bis-Tris Gel, ThermoFisher, Landsmeer, the Netherlands). MES running buffer (NuPAGE® MES SDS Running Buffer, ThermoFisher, Landsmeer, the Netherlands) was added to the buffer chamber. The gel was washed with water and stained (Coomassie Brilliant Blue R-250 Staining Solution, Bio-Rad Laboratories B.V., Lunteren, the Netherlands) for 5 h under gentle shaking. Thereafter, the gel was washed with water and destained (destaining solution of 10% ethanol and 7.5% acetic acid in deionized water) overnight under gentle shaking.

The gels were scanned with a GS-900 Calibrated Densitometer (Bio-Rad Laboratories, California, US) and the intensity of the bands was analyzed with Image Lab software.

Particle size and ζ-potential of napin isolate

The number-based mean diameter and the ζ-potential of the napin isolate at pH 7 were determined using a ZS Nanosizer (Malvern Instruments, Ltd, Worcestershire, U.K.). The intensity-based diameter was also determined and turned out to be similar to the number-based. The napin isolate was dispersed in deionized water in a ratio of 1:100 and the pH was adjusted to 7.0 prior to the measurements. The equilibration time was set to 120 s and the temperature to 25°C.

3.2.5 Emulsion preparation

The protein mixture was used to stabilize 10.0 wt% oil-in-water emulsions. The mixture was dispersed in deionized water, standardized at different protein concentrations (0.2-1.5 wt%). The pH was adjusted to 7.0 and the dispersions were stirred for 3 h at 20° C with a magnetic stirrer at 300 rpm (2mag magnetic e motion, 2mag AG, Munich, Germany) to allow hydration and solubilization of the proteins. Subsequently, the dispersions were sheared using a disperser (Ultra-Turrax, IKA®, Staufen, Germany) at 8000 rpm for 30 s. Next, 10.0 wt% rapeseed oil was slowly added to the dispersion and sheared for 1 min at 10000 rpm. The formed coarse emulsion was further processed with high-pressure homogenizer (GEA®, Niro Soavi NS 1001 L, Parma, Italy)

5 times at 250 bars. The emulsions with napin isolate were prepared as described above using 0.35 wt% napin isolate and 10.0 wt% oil.

3.2.6 Emulsion characterization

Particle size distribution

The particle size distribution of the emulsions was determined by laser diffraction (Malvern Instruments, Ltd, Worcestershire, UK) using a refractive index of 1.47 for rapeseed oil. The emulsions were diluted with deionized water at a ratio of 1:100. To determine the individual droplet size of the emulsions, we added sodium dodecyl sulfate (SDS) (1.0 wt%) to the sample in a ratio of 1:1. The measurements were reported as the surface ($d_{3,2}$ = $\Sigma n_i d_i^3/\Sigma n_i di^2$) and volume ($d_{4,3} = \Sigma n_i d_i^4/\Sigma n_i d_i^3$) mean diameter where n_i is the number of droplets with a diameter of d_i.

ζ-potential measurements

To measure the charge of the emulsions stabilized by the protein mixture under different pH conditions, we performed titration using a ZS Nanosizer (Malvern Instruments, Ltd, Worcestershire, U.K.). The 10.0 wt% oil emulsion (at 0.7 wt% protein) were diluted with deionized water in a ratio of 1:100. The equilibration time was set to 120 s and the temperature to 25°C. The ζ-potential of the samples was measured at a pH ranging from 2 to 12.

3.2.7 Microscopy

Confocal Laser Scanning Microscopy (CLSM)

The structure of the protein mixture and of the emulsions stabilized with the protein mixture or with the napin isolate was observed using a Confocal Laser Scanning Microscope with a water immersion objective at 60x magnification (Leica SP8-SMD microscope, Leica Microsystems, Wetzlar, Germany). A 0.1 wt% protein mixture dispersion and 10.0 wt% oil emulsions with 0.7 wt% protein concentration or 0.35 wt% napin isolate were stained with fluorescent dyes in a ratio of 1:200 to visualize the structural components; Nile red was excited at 488 nm and the emission was measured between 500 and 600 nm and Fast green was excited at 633 nm and the emission was measured between 650-750 nm. The dyes were excited and emitted in a sequential mode using a white light laser.

Transmission electron microscopy (TEM)

The emulsions stabilized with 0.7 wt% protein mixture and 0.35 wt% napin were investigated with transmission electron microscopy. The emulsions stabilized with the protein mixture were washed

three times to remove the unadsorbed and non-interacting proteins by centrifugation at 10000 g (30 min, 4°C) in 15 mL tubes at pH 9.0. A cream layer (interface) and a serum phase (continuous phase) were obtained. The serum was drained by making holes in the tube. The cream was collected and resuspended (1:10 w/w) in deionized water at pH 9.0. The centrifugation step was repeated for two more times under the same conditions. After the third centrifugation the cream was collected again and analyzed.

For the sample fixation, dehydration and polymerization: The samples were mixed 1:1 in 3% LMP agarose at 40°C. Once this hardened in the fridge the sample/LMP gel was cut into approximately 1 mm by 1 mm cubes. These cubes were fixated using 2.5% glutaraldehyde (EMS) for 1 hour after which they were washed for 3 times with 0.1M phosphate/citrate buffer. The cubes were then fixated again, this time with 1% osmium tetroxide (EMS). After this step the samples were washed 3 times with deionized water. Thereafter dehydration with ethanol was applied, substituting the deionized water for 30%, 50%, 70%, 80%, 90% and 100% ethanol (10 min. for each step). Once the samples were in 100% ethanol, this was substituted by Spurr embedding liquid (EMS) in 3 steps: 2:1, 1:1, 1:2 (ethanol:Spurr, 30 min. per step). Then the sample was left in 100% Spurr for 1 h. The Spurr was refreshed once more and the sample was left overnight in Spurr. The next day one more incubation of 1 h in fresh Spurr was done after which the samples were polymerized for 8 h at 70°C to harden the Spurr and the samples in it.

For the sample sectioning and imaging: Once the samples were hardened in the Spurr, they were sectioned by first trimming the samples using a Leica EM Rapid (Leica Microsystems, Vienna, Austria), after which the sample was sectioned using the Leica Ultramicrotome UC7 Rapid (Leica Microsystems, Vienna, Austria), sectioning the sample into 70 nm thin coupes. These coupes were collected with formvar film 150 mesh copper TEM grids. The grids containing sample were loaded into the JOEL-JEM 1400 Plus-120kV TEM (JEOL, Massachusetts, USA) with an EM-11210SQCH specimen quick change holder. The samples were analyzed at spot size 1, at 120kV.

3.2.8 Interfacial protein composition

To qualitatively determine the amount of proteins adsorbed at the interface, the prepared emulsions were centrifuged at 10000 g (30 min, 4°C) in 15 mL tubes at pH 9.0 to remove any unadsrorbed proteins. A cream layer (interface) and a serum phase (continuous phase) were obtained. The serum was drained by making holes in the tube. The cream was collected and resuspended (1:10 w/w) in deionized water. The centrifugation step was repeated for two more times under the same conditions. After the third centrifugation the cream was collected again. The protein profile and the intensity of the protein bands were determined with electrophoresis (SDS-PAGE) as described in section 3.2.4.

3.2.9 Estimated radius of napins and cruciferins

We also estimated the spherical radius of napins and cruciferins $r_{p\ estiim}$ using[112] :

$$r_{p\ estim} = (3V_p/4\pi)^{\frac{1}{3}}\ [\text{nm}] \tag{3.3}$$

Where Vp is the volume of the protein, equal to $V_p = \frac{M_w}{825}$ [nm^3], and M_w [Da] equals the molecular weight of proteins (17 and 300 kDa for napins and cruciferins, respectively).

3.2.10 Interfacial properties

Interfacial tension

The ability of the protein fractions to reduce the interfacial tension of an oil/water interface was measured using an automated drop tensiometer (ADT, Tracker, Teclis-instruments, Tassin, France). An oil droplet with a surface area of 10.0 mm^2 was created at the tip of a rising-drop capillary. Stripped rapeseed oil was used. The droplet was immersed in the protein mixture dispersion standardized at 0.01 wt% protein content at pH 7.0. Since napins comprise 50% of the total protein content of the mixture, the dispersion of the napin isolate was standardized at 0.005 wt%. The interfacial tension γ was continuously monitored for 3.3 h (12000 s) at 20°C until it reached equilibrium.

Dilatational interfacial rheology

After the equilibrium state was reached (end of 3.3 h), oscillatory dilatational interfacial rheology was used to characterize the interfacial elastic (E_d') and viscous (E_d'') moduli as a function of frequency and deformation amplitude. For the frequency sweeps, the droplet was subjected to a range of oscillation frequencies ω (0.005-0.1 Hz) at constant deformation (5% amplitude). Regarding the amplitude sweeps, the droplet was subjected to sinusoidal deformations with an amplitude of 5-20% of its original surface area at a constant frequency (0.01 Hz). Each amplitude consisted of a series of 5 cycles followed by a rest period of 5 cycles. The interfacial tension and area changes were recorded during the oscillations, and the dilatational elastic (E_d') and viscous (E_d'') moduli were obtained according to:

$$E_d' = \Delta\gamma \left(\frac{A_0}{\Delta A}\right) \cos\delta \tag{3.4}$$

$$E_d'' = \Delta\gamma \left(\frac{A_0}{\Delta A}\right) \sin\delta \tag{3.5}$$

3.3 Results and Discussion

3.3.1 Composition and physicochemical properties of the coarse protein mixture

Dehulled and not-defatted rapeseeds (18.7 ± 0.6 wt% protein and 41.9 ± 0.9 wt% oil)[111] were used to extract the protein mixture. We extracted the proteins using the method that we have previously developed[111] to avoid the variability of the rapeseed cake's processing and the possible effect of the non-protein components present in the cake on the functionality of the proteins. The extracted protein mixture was composed of 39.7 ± 3.1 wt% protein and 11.5 ± 1.3 wt% oil, 6.2 ± 0.1 wt% phenolic compounds and 7.8 ± 0.3 wt% ash content. The carbohydrate content was determined by subtraction of the above components from the total mass (34.8 wt%).

To establish the composition of the protein mixture, electrophoresis (SDS-PAGE) and confocal laser scanning microscopy analysis (CLSM) were used (Figure 3.1). The protein electrophoregram (Figure 3.1A) shows the protein species present in the mixture as separated based on their molecular weight, under reducing and non-reducing conditions. Both rapeseed storage proteins, napins (~17 kDa) and cruciferins (subunits of ~20-70 kDa) were present in the protein mixture[111]. Based on the intensity of the protein bands the mass ratio of napins to cruciferins was 1:1.

Apart from a high amount of proteins, the protein mixture also contained oil, since no defatting was applied before the extraction. It has been previously reported that in mildly extracted oilseed protein extracts, the oil is present in the form of oleosomes/lipid droplets[86,111]. To confirm this, confocal microscopy was carried out. The CLSM image (Figure 3.1B) shows the dispersion of the protein mixture at pH 7.0 stained for the oil (red color) and the proteins (green color). Spherical oil droplets of 0.2-3.0 μm and protein clusters were present. The presence of oil droplets and absence of free oil confirmed our previously reported observation that oleosomes were present in the protein mixture[111]. The size of the oleosomes corresponded to the native individual size of the oleosomes in the rapeseed cell embryos[113], proving that they were not damaged during the extraction. It has been previously reported that when protein mixtures with oleosomes are extracted, storage proteins are forming a film around the oleosomes by interacting with the oleosome membrane proteins through hydrophobic and van der Waals attractive forces[114]. This film provides additional protection to the oleosomes against coalescence[80] which even withstand the drying processing step[86].

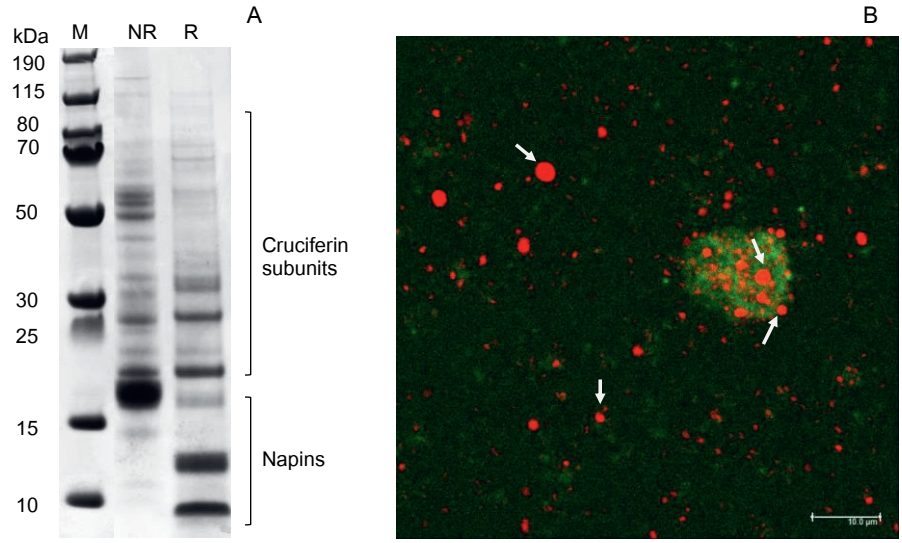

Figure 3.1 A) Electrophoregram (SDS-PAGE) of the protein mixture under non-reducing (NR) and reducing (R) conditions. M: protein molecular weight marker, B) CLSM images of the protein mixture dispersion (0.1 wt%) at pH 7.0. Proteins are shown with green color (stained with Fast green) and oil with red color (stained with Nile red). Oleosomes are indicated with white arrows. Scale bar: 10 μm.

3.3.2 Emulsions with the protein mixture

To evaluate the emulsifying properties of the protein mixture, different protein concentrations were used (standardized on protein content) to stabilize a 10.0 wt% oil-in-water emulsion at pH 7.0. Figure 3.2A presents the individual droplet size ($d_{4,3}$) of the emulsions after the addition of SDS, as a function of protein concentration at time zero and after storage for 7 days. The droplet size decreased with increasing protein concentration and reached a plateau (1.0-1.5 μm) at protein concentrations above 0.7 wt% (protein-rich regime). When the protein concentration was below 0.7 wt%, bigger droplets were formed (2.0-5.0 μm) with higher size variations between samples. In the protein-poor regime (< 0.5 wt%) the lower amount of protein, in combination with the weak electrostatic repulsion at pH 7 (the ζ-potential of the droplets equals -5 mV) (Figure 3.2B), led to more re-coalescence during homogenization, and hence larger droplet sizes[115]. The values for the size of the individual oil droplets reported here at 0.7 wt% protein, were similar to the ones reported when dairy proteins (i.e. sodium caseinate) were used at similar protein to oil ratio[116].

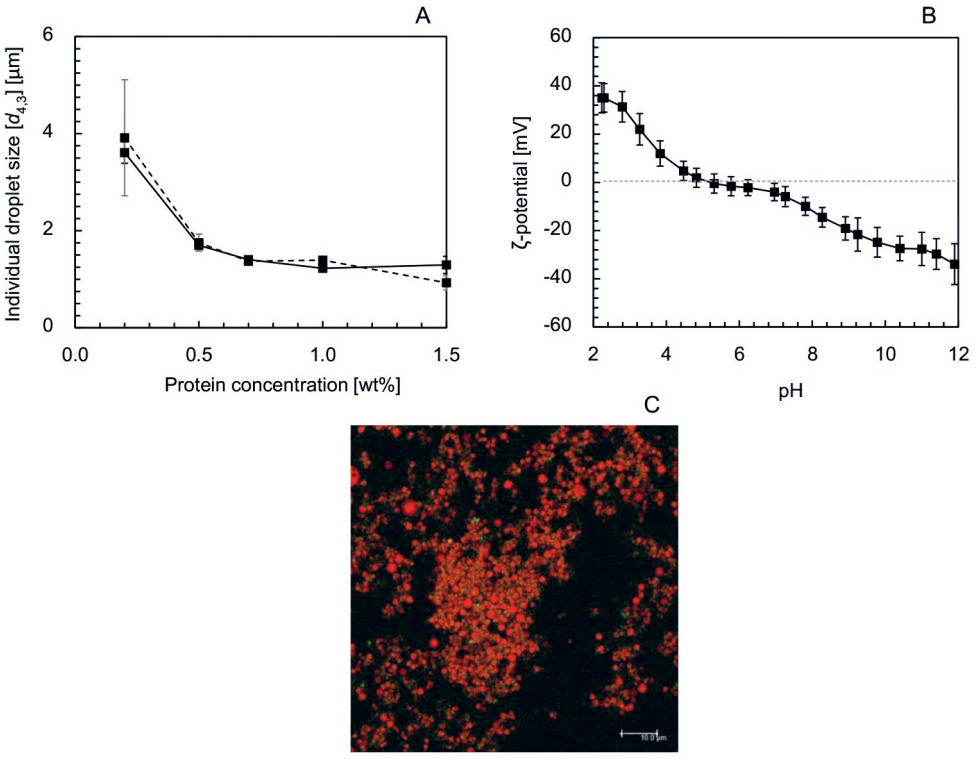

Figure 3.2 A) Individual droplet size ($d_{4,3}$) (measured after the addition of SDS) of 10.0 wt% oil-in-water emulsions stabilized with the protein mixture at different protein concentrations (0.2–1.5 wt%) at pH 7.0 and at t0 (continuous line) and 7 days (dotted line, B) ζ-potential of the emulsion (10.0 wt% oil, 0.7 wt% protein) at a range of pH, C) CLSM image of 10.0 wt% oil-in-water emulsion at t0 stabilized with the protein mixture (0.70 wt% protein) at pH 7.0. The emulsion was stained using Nile red for the oil and Fast Green for the proteins.

To further investigate the microscopic picture of the emulsions we used confocal microscopy. Figure 3.2C displays the CLSM image of the 10.0 wt% oil emulsion at the protein-rich regime (0.7 wt%) stained for the oil (red color) and the proteins (green color). The image shows clusters of aggregated oil droplets (shown as red) of 20-30 µm size with small protein clusters (shown as green) between the oil droplets. The presence of aggregated oil droplets is due to weak repulsive electrostatic forces present at pH 7 (ζ-potential of emulsion equals to -5 mV) (Figure 3.2B) that cannot overcome the attractive Van der Waals interactions. Despite the emulsion droplet aggregation, which induces more droplet-droplet interactions, no coalescence of the individual oil droplets was observed over time (Figure 3.2A).

Inspite of the complexity in composition the “impurities” present in the protein extract, like phenols and oleosomes, did not affect the emulsifying ability of the proteins. In our previous study we

showed that the phenolic compounds present do not interact with the proteins and therefore they do not influence their functional properties[111]. Additionally, the oleosomes and their associated membrane components (i.e. proteins and phospholipids) are not expected to have a notable impact on the interfacial[34] and emulsifying properties of proteins[86,117] especially since they are present in very low concentration in the amount of extract used for the emulsions.

As the protein mixture contained initially two types of proteins, cruciferins and napins in a 1:1 mass ratio, we investigated whether both types of proteins were absorbed at the oil/water interface of the emulsions using electrophoresis (SDS-PAGE). For this analysis we chose the emulsion in the protein-rich regime (at 0.7 wt% protein) where the droplet size is mainly determined by the settings of the homogenizer and not by the amount of proteins present. The electophoregram (Figure 3.3) shows the protein profile of the interface and the continuous phase of the 10.0 wt% oil emulsion stabilized with 0.7 wt% protein. The results showed that at the oil/water interface almost exclusively napins were present, while excess of napins and cruciferins were present at the continuous phase. In a different study when separated napins and cruciferins were used to stabilize oil/water emulsions, it was reported that napins were more efficient emulsifiers than cruciferins[56]. However, it is the first time that a mixture of napins and cruciferins is used and solely napins were identified at the interface.

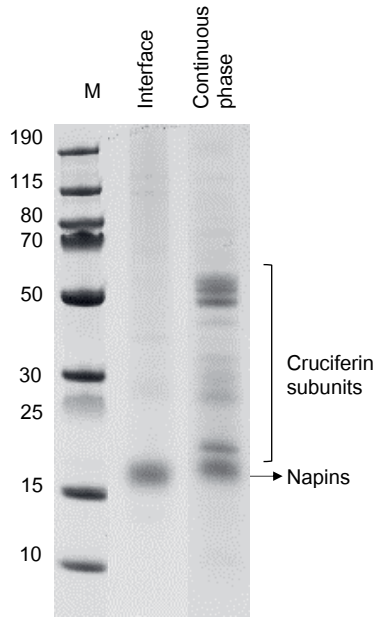

Figure 3.3 Electrophoregram (SDS-PAGE) of the interface and continuous phase of the 10.0 wt% oil emulsion at 0.7 wt% protein at t0 under non-reducing conditions. M: protein molecular weight marker.

The fact that only one type of protein is adsorbed at the interface when a protein mixture is used is not common. So far studies on mixtures of different types of proteins (i.e. dairy proteins or egg yolk proteins) have mainly reported co-adsorption of the proteins at the interface, although the ratios between proteins at the interface typically differ from their ratio in the bulk[118–120].

To confirm whether napins were efficient emulsifiers in the absence of cruciferins, we isolated the napins (protein content of 84.0 ± 1.0) (Figure A3.1, Appendix) and used them to stabilize a 10.0 wt% oil/water emulsion. For comparison with the protein mixture, the same concentration of napins as present in the protein mixture was used.

Figure 3.4A displays the volume-based droplet size distribution of the emulsion (after the addition of SDS) stabilized by napins at 0.35 wt% protein concentration. For comparison we also included the individual droplet size distribution of the emulsion stabilized by the protein mixture at 0.7 wt% protein (of which 0.35 wt% corresponds to napins). The emulsion stabilized with the protein mixture showed a monomodal droplet size distribution with an average droplet size ($d_{4,3}$) of 1.4 ± 0.1 µm. The droplet size distribution of the emulsions stabilized by napins was also monomodal with an average droplet size ($d_{4,3}$) of 3.4 ± 0.14 µm. The individual droplet size of the emulsion stabilized by napins did not change upon storage over 7 days (data not shown), showing that the concentration of napins at the interface was sufficient to form a dense layer that ensured stability against coalescence.

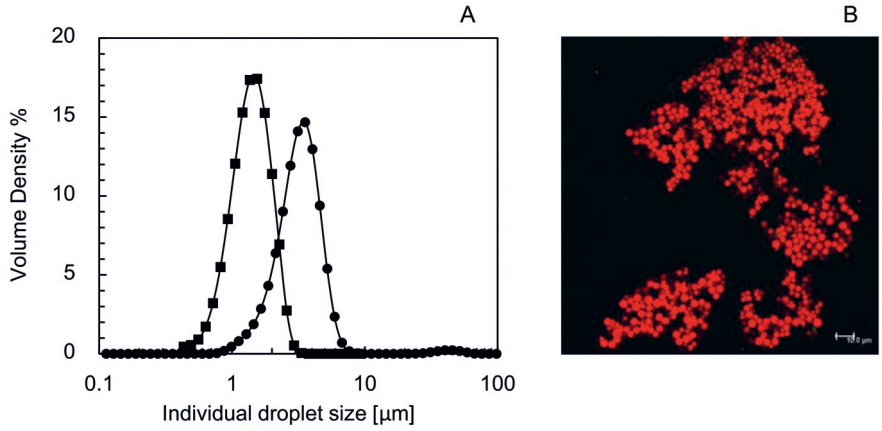

Figure 3.4 A) Individual droplet size distribution as a percentage of volume density after addition of SDS, of 10.0 wt% oil-in-water emulsion, pH 7.0, stabilized with the protein extract (0.7 wt% proteins that contained 0.35 wt% napins) (square symbol) and of 10.0 wt% oil-in-water emulsion, pH 7.0, stabilized with napins (0.35 wt%) (circle symbol), and B) CLSM image of the emulsion stabilized with napins stained with Nile red for the oil and Fast green for the proteins.

Figure 3.4B shows the CLSM image of the emulsions stabilized by napins stained for the oil (red color) and the proteins (green color). Droplets aggregates were present (aggregate size of around 30-50 µm) in the emulsion. The droplet aggregation was assigned to the low charge of the napin molecules adsorbed at the interface (-10.7 ± 1.3 mV), which led to weak electrostatic repulsion between the oil droplets. No protein clusters were present between the oil droplets, in contrast to the emulsions stabilized with the protein mixture (Figure 3.2B). Napins were present as single molecules at pH 7.0 (hydrodynamic diameter of 4.7 ± 0.6 nm), thus no napin aggregates were formed.

The individual droplet size as well as the aggregate size of the emulsions stabilized by napins was bigger than in the emulsions stabilized with the protein mixture where cruciferins were also present. This led to the hypothesis that cruciferins present in the protein mixture had an indirect role in the formation of the droplets. Since we observed protein clusters in between the oil droplets in the emulsion stabilized with the protein mixture but not in the emulsion stabilized with napins, we hypothesized that these protein clusters were cruciferins, that form aggregates due to their hydrophobic character. When these cruciferin aggregates are present in the intervening continuous phase between the oil droplets, they might increase the local viscosity. This higher local viscosity could cause higher shear during homogenization or could impede thin film drainage between the colliding droplets[121,122] which both eventually could lead to smaller droplet sizes.

To understand the arrangement of the proteins at the oil/water interface and continuous phase in the emulsions stabilized by the protein mixture or the napin isolate, we used transmission electron microscopy. The micrograph (Figure 3.5) shows the emulsion droplets stabilized by RPM (Figure 3.5A-C) or by the napin isolate (Figure 3.5D-E) at different magnifications. The images showed oil droplets with a homogeneous similar interface for both emulsions (Figure 3.5C, F). However, in the emulsions stabilized with the protein mixture, high-density dark areas in between the oil droplets (Figure 3.5A-C) were also present, which probably corresponded to cruciferin aggregates.

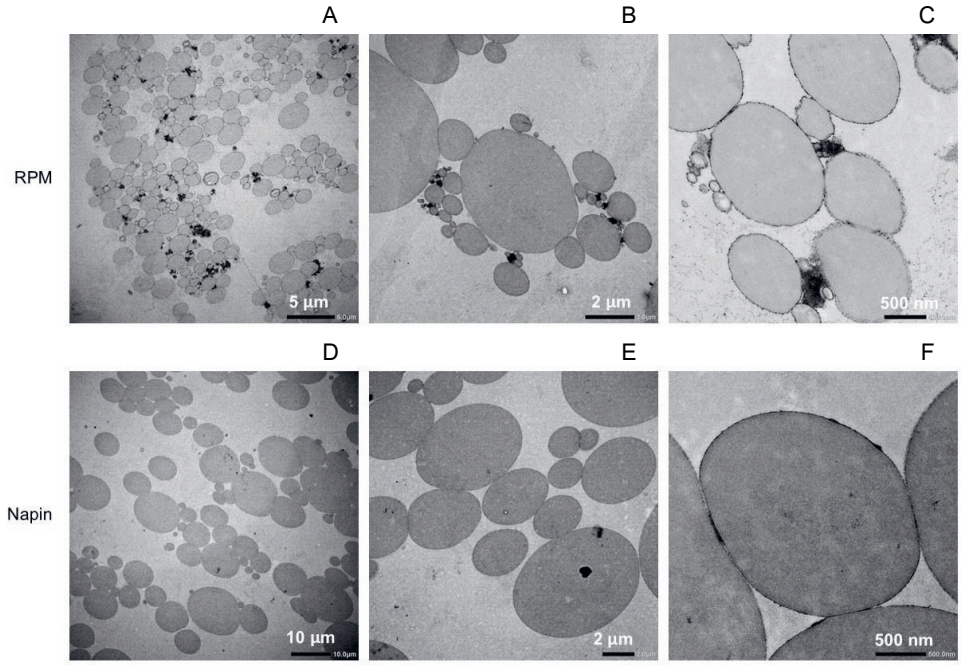

Figure 3.5 TEM images of 10.0 wt% oil-in-water emulsions stabilized with the protein mixture (0.7 wt% proteins) after removal of the unadsorbed proteins (A-C) and of emulsions stabilized with napins (0.35 wt%) (D-F). Magnifications: A) x1200, B) x3000, C) x10000, D) x500, E) x2000, F) x12000.

3.3.3 The interfacial behavior of single napin molecules and the rapeseed protein mixture (RPM)

Interfacial tension

The interfacial behavior of the isolated napin molecules and the protein mixture was further investigated using oscillating drop tensiometry. Figure 3.6 shows the dynamic interfacial tension reduction of the oil/water interface as a function of time for the protein extract (0.01 wt%) or napin isolate dispersions (0.005 wt%). The interfacial tension was reduced from ~25 mN/m to a value of ~9 mN/m in 1.2×10^4 s, for both cases. Both protein systems showed a short lag time of around 1 sec (Figure 3.6, inset) before a further reduction of the tension occurred. The similar behavior of the two protein systems confirmed that cruciferins present in the protein mixture did not co-adsorb at the interface and also, did not displace napins over time. In a previous report, cruciferins were found to have lower surface activity in comparison to napins, leading to a reduction of the interfacial tension only to 15 mN/m[52].

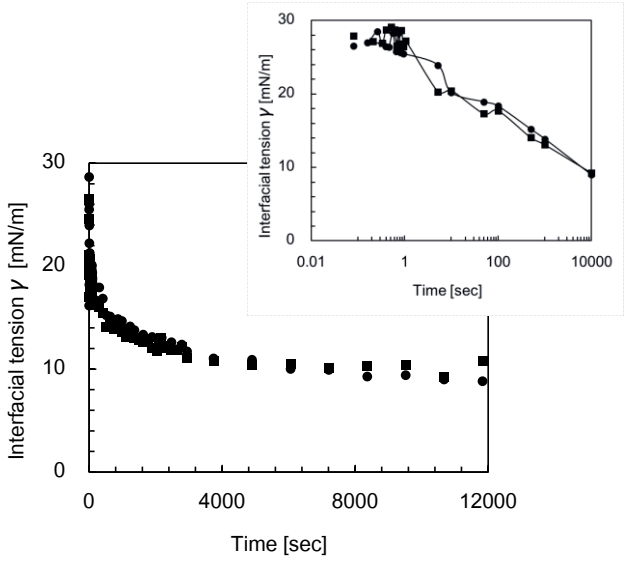

Figure 3.6 Dynamic interfacial tension of protein mixture (squared symbol) and napins (circle symbol) at 0.01 wt% and 0.005 wt% protein concentration respectively (pH 7.0, 20°C). Inset picture: Dynamic interfacial tension reduction in logarithmic scale.

The surface activity of a protein depends on different parameters such as the charge, molecular size and amphiphilicity of a protein, which influence the rate of diffusion towards the interface, and adsorption at the interface[123]. The protein mixture containing both napins and cruciferins, had a low ζ-potential (-15 mV) at the pH value of the emulsions (pH 7.0)[111]. Despite the weak electrostatic

repulsive forces large insoluble clusters were not formed and both proteins were soluble at this pH (Figure A3.1, Appendix), indicating that the attractive forces between the proteins (hydrophobic, dipole) were also weak.

The diffusion of the protein molecules from the bulk to the interface is the first prerequisite for the adsorption of proteins[124]. According to Einstein's equation (Equation 3.6), the diffusion coefficient of the proteins (D) is proportional to Boltzman's constant (k_b) and temperature (T), while it is inversely proportional to the viscosity (η) and the particle radius. Since T and η are constant, the difference in diffusion rate of napins and cruciferins was determined only by the difference in radii of the molecules[125].

$$D = \frac{k_b T}{6\pi\eta r} \tag{3.6}$$

According to Equation 3.3 (Methods), napins have an estimated radius of r_{estim} = 1.7 nm while cruciferins in their hexameric form have a radius of r_{estim} = 4.4 nm. Therefore, the diffusion coefficient of napins is three times larger than that of cruciferins, which allowed them to diffuse faster towards the interface.

After diffusion, the proteins may have to overcome an energy barrier to adsorb[126,127]. The height of the energy barrier and thus the probability to adsorb is related to the structure of the protein and the arrangement of the apolar domains at the oil/water interface[124,127,128]. By looking at the molecular structure of napins and cruciferins one can observe significant differences in structure and distribution of the hydrophobic domains. Napins are albumins with a molecular weight of around 15-17 kDa, having a spherical particle shape while cruciferins are hexameric globulins of around 300 kDa[29]. Cruciferins, in their hexameric form, have the hydrophobic amino acids broadly distributed amongst their peptide chains and as is the case with most proteins, are buried inside the core[35]. The intramolecular hydrophobic attractive interactions contribute to a compact protein structure by holding two trimers together to form the hexamer structure[124]. Cruciferins are considered to have a three-fold higher surface-exposed hydrophobicity than napins ($(S_0)^2$ 347 vs 104)[29]. However, 45% of the amino acids of the peptide chain of napins are hydrophobic, and more importantly, they are concentrated mostly on one exposed side of the protein[36]. The structures of napins and cruciferins are sketched in Figure 3.7.

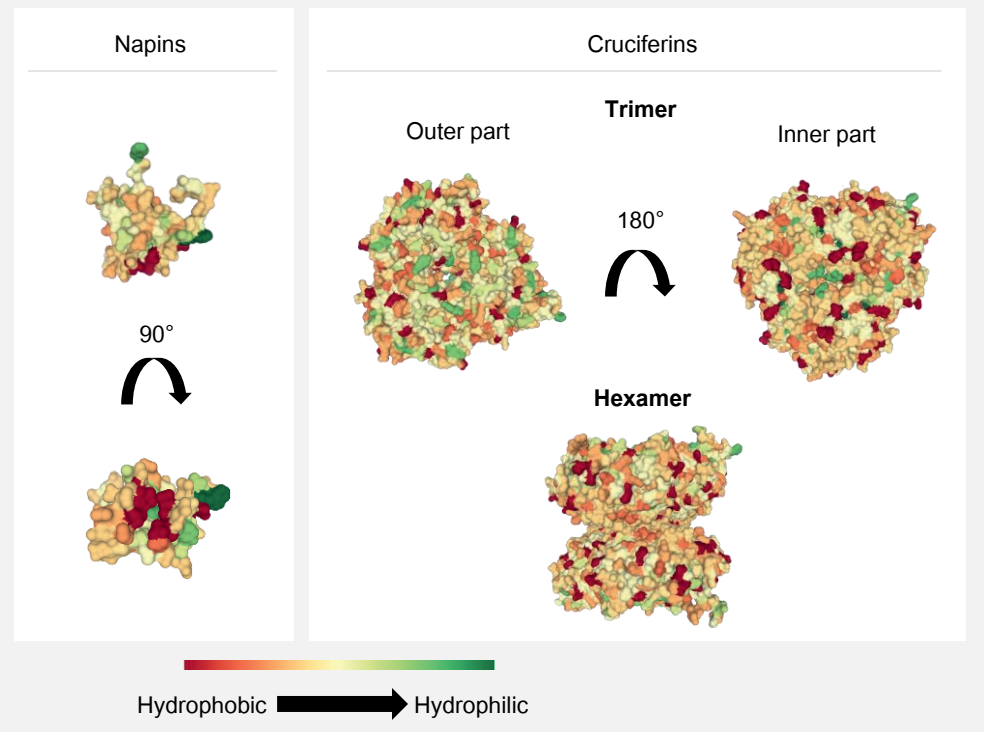

Figure 3.7 Sketch of napins and cruciferins (trimer and hexamer) structure represented as molecular surface, showing the distribution of hydrophobic (red) and hydrophilic (green) domains. (Images retrieved from the RCSB PDB[35,36]).

The fact that there are such distinct domains on the protein, one hydrophobic and one hydrophilic, make napins resemble amphiphilic Janus particles[129]. Janus particles possess two distinct surface regions with each region having a different affinity for the solvents (i.e. water and oil)[130]. These two distinct surface regions have different wettability[129], and as it has been shown previously, lead to a higher surface activity than a homogeneous particle[130,131].

Thus, the higher interfacial activity of napins compared to cruciferins could be attributed to two main reasons; i) their smaller size which allowed faster diffusion towards the interface and ii) their large exposed hydrophobic domain which permitted them to overcome the energy barrier and adsorb at the interface. For the above reasons, cruciferins were prevented from co-adsorbing at the interface and also, could not displace napins over time.

Dilatational interfacial rheology

To gain a further insight into the rheological properties of the oil/water interface after adsorption of napins, and the possible effect of cruciferins on these properties, we employed interfacial dilatational rheology. In Figure 3.8A the dilatational moduli (E_d', E_d'') of the interface stabilized by either the protein mixture or the napin isolate are plotted as a function of increasing oscillation frequencies (ω) on a double logarithmic scale. The results showed a higher elastic (E_d') than viscous modulus (E_d'') in both samples. In both interfaces, the elastic modulus (E_d') showed a minor increase upon increasing frequency while the viscous modulus displayed the contrary behavior (minor decrease). This behavior suggests a very minor dependency of the interparticle interactions at the interface upon oscillatory frequencies. By fitting a power law model through the data of E_d', an exponent of around 0.1 was found. This, together with the low value for the loss tangent (E_d'/ E_d') for both interfaces, indicate a soft solid-like behavior[132].

The moduli were slightly higher for the interface stabilized by the protein mixture compared to the one stabilized by napins. This result points out that the main response at the interface stabilized by the protein extract comes from napins, while there is a minor effect of the cruciferins present in the bulk which appear to interact with the adsorbed layer of napins.

To further investigate if any structure that is present at the interface will be affected when the amplitude of deformation is increased, we studied the dependency of the moduli on deformation amplitude in amplitude sweeps. Figure 3.8B shows the dilatational moduli (E_d', E_d'') of the interface stabilized by the protein mixture or the napin isolate as a function of amplitude. The elastic modulus (E_d') was higher compared to the viscous (E_d'') modulus in both samples. Overall, the elastic moduli were relatively low compared to interfaces stabilized by other commonly used proteins, like whey protein isolate (WPI) (~30 mN/m vs > 40 mN/m)[133,134], which implied that the in-plane interactions between the adsorbed napin molecules were relatively weak. This response indicates that mainly attractive interactions, like van der Waals and hydrogen bonds took place after adsorption. Although sulfur-containing amino acids are involved in the structure of napins, the weak in-plane interactions at the interface show that it is unlikely that a significant amount of covalent sulfur bonds is formed after adsorption. If these bonds were important, a much stiffer response and a stronger dependence on strain amplitude would be observed (i.e. a more profound decrease in E_d' as amplitude increases), a common phenomenon for interfaces stabilized by WPI.

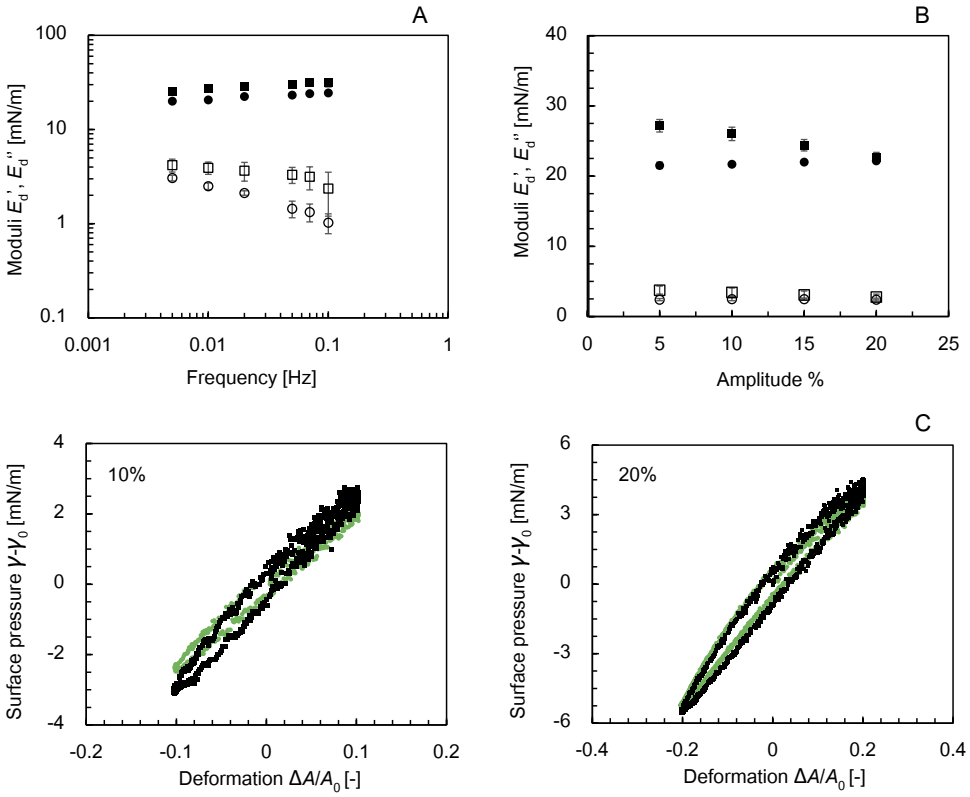

Figure 3.8 A) Dilatational elastic modulus (E_d': filled symbol) and viscous modulus (E_d'': hollow symbol) of protein mixture (square symbol) and napin isolate (circle symbol) upon frequency sweeps at constant dilatational deformation 5%, B) amplitude sweeps at constant oscillatory frequency 0.01 Hz, C) Lissajous plots of interface stabilized by the protein mixture (square symbol, black) and by napin isolate (circle symbol, green) at 10 and 20% dilatational deformation and oscillation frequency at 0.01 Hz.

It is important to emphasize that at the interface stabilized by the napin isolate the moduli were independent of the amplitude of deformation. On the other hand, when the interface was stabilized by the protein mixture, the elastic modulus was somewhat higher at low amplitude and showed a minor decrease upon increasing the amplitude of deformation. When the amplitude reached 20%, both systems had the same elastic and viscous moduli. The higher modulus at low amplitude implies that cruciferins are most likely interacting with the primary layer of napins. The decrease of the modulus upon increasing the amplitude shows that this interaction must be weak and is completely overcome at larger deformations (20%). Thus, the interactions at interface were dominated by napins. This observation, in combination with the fact that we did not see adsorption of cruciferins at the interface, allows us to conclude that cruciferins remain in the bulk and most likely, they just weakly bind to the napin primary layer.

To understand these interactions in more detail, Lissajous plots were used which provide information about the behavior of the interfacial network upon extension and compression. Figure 8C shows the Lissajous plots of the interface stabilized by the protein mixture or napin isolate where the surface pressure is plotted against deformation (Figure 3.8C). At low amplitude (10%) the plots for both interfaces had a narrow ellipse shape. This shape indicates an almost linear, predominantly elastic response of the interface, without noticeable asymmetries, pointing out a weak solid structure[135]. The interface stabilized by the protein mixture showed slightly higher surface pressure upon compression (bottom left quadrant of the plot, at $\Delta A/A_0 = -0.1$) compared to the interface stabilized only by napins (3.1 vs 2.4 mN/m). We assign this difference to the additional weak interactions of cruciferins with the adsorbed napins at the interface. At 20% amplitude of deformation the response of both the interfaces was similar and showed that the surface pressure increased from around 3 mN/m at 10% amplitude to 6 mN/m at 20% amplitude upon compression (bottom left quadrant of the plot, at $\Delta A/A_0 = -0.2$), showing a minor strain hardening behavior. The bottom left part of the ellipse had a pointy tip, indicating that upon compression of the proteins the system was jammed. This behavior suggests weak in-plane attractive interactions at the interface[133]. As napins had low charge at pH 7.0 (-10.7 ± 1.3mV), strong electrostatic repulsion was prevented and thus, weak in-plane attractive forces occurred. Therefore, the main rheological response came from the interactions of napins with the oil phase through its distinct hydrophobic domain[132]. As a result of all the above interactions, a soft-solid like structure of the interface was formed. By comparing our Lissajous plots with the ones recently reported for WPI at similar amplitude (20%) one can clearly observe that WPI-stabilized interfaces give a plot of wider shape at the lower left part[133,134]. This is a result of yielding of the surface microstructure upon compression and the start of the extension, which shows a much stronger structure[133,134] than the one we report here for the napin-stabilized interface.

A schematic representation of the interactions occurring at the interface upon increasing the amplitude of deformation when RPM is used, is given in Figure 3.9. At low amplitude cruciferins interact with the napins at the interface, whereas at higher amplitude these interactions are weakened and only in-plane interactions between napins dominate.

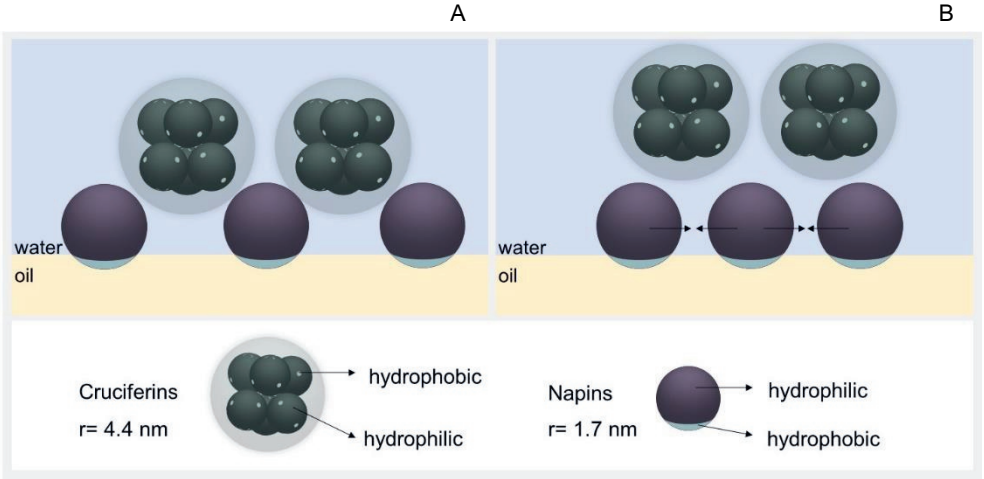

Figure 3.9 Schematic representation of dynamic interactions of cruciferins with the adsorbed napins A) before and B) after compression, when the protein mixture is used to stabilize the interface, showing expel of cruciferins at the continuous phase.

3.4 Conclusions

In this research we investigated the stabilization mechanism of oil/water interfaces when using a rapeseed protein mixture, in which napins and cruciferins co-exist in a 1:1 mass ratio. Our findings suggest that when making oil/water emulsions with the protein mixture, competitive adsorption of napins occurred at the interface. The higher interfacial activity of napins was attributed to their small size (r =1.7 nm) which allowed them to diffuse fast towards the interface. Thereafter, adsorption occurred due to their unique Janus-like structure, as 45% of its amino acids are hydrophobic and primarily located on the one side of the protein as a distinct domain. Cruciferins with bigger size (r = 4.4 nm) and a wider distribution of the hydrophobic amino acids over the structure, did not co-adsorb or displace napins from the interface, but they were suggested to be present in the continuous phase and interact weakly with the primary layer of adsorbed napins. Our results demonstrate the role of individual proteins in complex plant protein extracts that could help utilizing rapeseeds or defatted rapeseeds, optimizing their functionality and establish the optimal composition with respect to sustainability gains.

3.5 Appendix

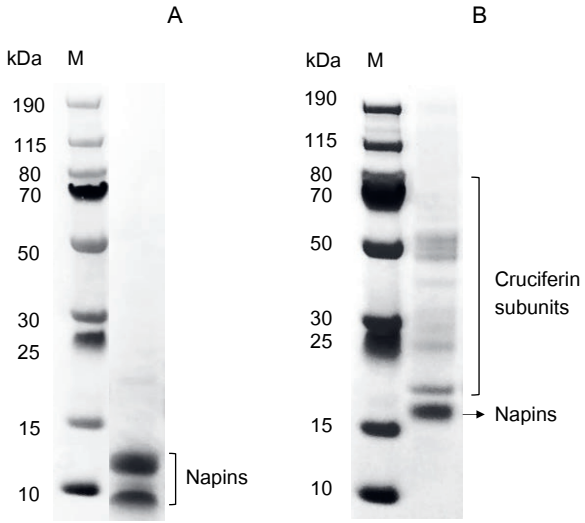

Figure A3.1 A) Electrophoregram of napin isolate under reducing conditions, B) Electrophoregram of the soluble fraction of the rapeseed protein mixture at pH 7 under non-reducing conditions. M: protein molecular weight marker.

Chapter 4

Effect of purification on the emulsifying and interfacial properties of rapeseed extracts of different protein purities at acidic pH (pH 3.8)

This chapter has been submitted as: Ntone, E., Qu, Q., Pyta-Gani., K., Meinders, M., Sagis, L.M.C., Bitter, J.H., & Nikiforidis, C.V. (2021). Sinapic acid impacts the emulsifying properties of rapeseed proteins at acidic pH.

Abstract

Extensive purification of plant proteins is probably not a prerequisite for their emulsifying properties, however, details of the interfacial stabilization mechanism of less purified protein extracts are not sufficiently known. The less purified plant protein extracts contain non-protein compounds, such as phenolic compounds, which can potentially interact with proteins and affect their interfacial properties. Here, we show that when oil-in-water emulsions (10.0 wt% oil) at pH 3.8 are stabilised with a rapeseed protein mixture (RPM) (40 wt% proteins, 6 wt% sinapic acid) at different protein concentrations (0.2-1.5 wt%), emulsion droplets of 2.0-0.6 μm are formed and large protein aggregates are randomly attached to the droplet interface. By removing sinapic acid to produce a rapeseed protein concentrate (RPC) (65 wt% proteins) and use RPC to stabilize emulsions, smaller droplets are formed (0.4-0.5 μm) and no large proteins aggregates are present. According to our findings, sinapic acid does not impact the interfacial composition of the emulsion droplets, as in both RPM- and RPC-stabilized emulsions, primarily napins adsorb at the interface. However, sinapic acid affects the secondary interfacial layer formed by cruciferins, by inducing cruciferin aggregation, which in turn affects droplet formation and stability. Our findings show that sinapic acid affects the emulsification mechanism of rapeseed proteins at acidic pH and recommend that plant protein purification might be necessary for the application of plant proteins in emulsion food products.

4.1 Introduction

The effect of protein purification on the functionality of plant proteins is currently a topic of intense research in food science, both in academia and in industry. To date, several studies using various plant protein sources[30,34,86,108,109,136–138] have shown that extensive purification of plant proteins is not a prerequisite for functionality, such as interfacial and emulsifying properties. Most of these studies have postulated that the functionality of less purified protein extracts is linked to the avoidance of extensive process-induced alterations in the physicochemical properties of the proteins.

Although the results of the above studies are promising for the use of less purified plant protein extracts as emulsifiers in food systems, there is a lack of understanding on the exact emulsification mechanism. The multicomponent nature of the less purified protein extracts includes various types of proteins co-existing with other non-protein molecules, which under various system conditions (e.g. pH) can impact the interactions between the molecules, the adsorption of proteins and the interfacial stabilization.

In our previous research on rapeseed proteins, we showed that at pH 7, a less purified rapeseed protein extract (40 wt% protein), containing both storage proteins (napins and cruciferins) and non-protein molecules (i.e. sinapic acid) can form stable oil-in-water emulsions[30]. At this pH, napins dominate the oil/water interface, due to their small size (r = 1.7 nm) and their concentrated hydrophobic domains on one side of the protein structure, resembling ampliphilic Janus particles. Cruciferins due to their larger size (r = 4.4 nm) and the wide distribution of their hydrophobic domains over their hexameric structure, form a secondary interfacial layer, providing stabilty to the emulsion droplets against coalescence[30]. Under these pH conditions, the free sinapic acid present in the protein extracts does not impact the interfacial properties of the proteins[30,34].

However, at pH 3.8, in which emulsion food products like mayonnaise are produced[139], the emulsification mechanism of the less purified rapeseed protein extracts might differ, as pH can affect the interactions between proteins with sinapic acid, and subsequently the interfacial properties of the proteins[15,37]. At acidic pH conditions, the free sinapic acid present in the less purified rapeseed protein extracts can bind to proteins through non-covalent bonds[37,48,49]. The protein-phenol interactions can alter protein hydrophobicity, structure and size[15,37,140] affecting the protein interfacial properties[48,141]. Hence, it can be suggested that potential interactions of proteins with sinapic acid as affected by pH can impact the emulsification mechanism of less purified rapeseed protein extracts.

This paper aims to establish the emulsifying mechanism of rapeseed protein extracts at pH 3.8. A less purified rapeseed protein mixture (RPM) containing 40 wt% proteins and 6 wt% free sinapic acid and a rapeseed protein concentrate (RPC) containing 65 wt% proteins, where sinapic acid is removed, were used as emulsifiers at pH 3.8. Identifying the potential effect of non-protein compounds, such as phenols, on the interfacial stabilization mechanism of proteins at acidic pH, is essential to evaluate the necessity of protein purification for structuring plant-based food emulsions.

4.2 Materials and methods

4.2.1 Materials

Untreated Alize rapeseeds were used as raw material to extract the rapeseed protein extracts. The seeds were stored at -18°C until use. All chemical reagents were analytical grade and purchased from Sigma Aldrich (Zwijndrecht, Netherlands).

4.2.2 Extraction of rapeseed proteins

The rapeseed protein extracts with a different degree of protein purity -rapeseed protein mixture (RPM) and rapeseed protein concentrate (RPC)- were extracted using our previously developed extraction process[111]. Briefly, dehulled rapeseed particles were dispersed in deionized water (1:8 w/w) and kept at room temperature (around 20°C) for 4 h under continuous stirring using a head stirrer (EUROSTAR 60 digital, IKA, Staufen, Germany). The pH of the dispersion was maintained at 9.0 during the soaking time by adding NaOH (0.5 M). Afterwards, the dispersion was blended with a kitchen blender (HR2093, Philips, Netherlands) at maximum speed for 2 min. To separate the solids from the liquid phase, the slurry was filtered by using a twin-screw press (Angelia 7500, Angel Juicer, Naarden, The Netherlands). The filtrate was filtrated, the pH was re-adjusted to pH 9.0, and centrifuged (10000 g, 30 min, 4°C) (Sorvall Legend XFR, ThermoFisher Scientific, Waltham, MA, USA). A cream layer (oleosome-rich), a serum (rapeseed protein mixture (RPM)) and a pellet (fiber-rich) were collected. The cream layer was carefully removed with a spatula, and the liquid phase (RPM) was filtered through a sieve to remove any floating cream pieces while the pellet was discarded. To obtain the rapeseed protein concentrate (RPC), RPM was first concentrated by ultrafiltration and then diluted 1:1 (v/v) with NaCl (0.08 M) to avoid protein precipitation. Thereafter, it was pumped through two coupled diafiltration cassettes (cut-off 5 kDa; membrane area 0.2 m^2) (Hydrosart, Sartorius, Göttingen, Germany) for 6 cycles until a transparent filtrate was obtained. The inlet and outlet pressure were adjusted to 1.4 and 0.6 bar, respectively. The conversion ratio (CR) was set at 35% (below 40%) to minimize membrane blocking. In the last cycle, we used deionized water to remove any remaining salt. Finally, RPM and RPC were

freeze-dried (Alpha 2-4 LD plus, Martin Christ Gefriertrocknungsanlagen GmbH, Osterode am Harz, Germany) and stored at -18°C until further use.

4.2.3 Isolation of napins

Napins were isolated using a previously reported the method[30]. RPM was first diafiltrated through two coupled 100 kDa cut-off diafiltration cassettes (Hydrosart, Sartorius, Göttingen, Germany) to separate cruciferins (300 kDa) and other high molecular weight non-protein compounds. The filtrate (< 100 kDa) containing napins was collected and concentrated by ultrafiltation and then diluted with NaCl (0.08 M) at a ratio 1:1 to avoid protein precipitation. The diluted filtrate was pumped through another diafiltration system (two coupled diafiltration cassettes; 5 kDa cut-off; membrane area 0.2 m^2) (Hydrosart, Sartorius, Göttingen, Germany) for 6 cycles to remove small molecular weight compounds. In the last cycle we used deionized water to remove the remaining salt. The retentate (> 5 kDa) containing napins was freeze-dried (Alpha 2-4 LD plus, Martin Christ Gefriertrocknungsanlagen GmbH, Osterode am Harz, Germany) and stored at -18°C until further use.

4.2.4 Protein content analysis

The protein content of all the protein extracts was determined on dry-matter weight basis using the Dumas method (FlashEA 1112 Series, Thermo Scientific, Waltham, Massachusetts, US). We used d-methionine (≥ 98%, Sigma Aldrich, Darmstadt, Germany) as a standard and as a control. Cellulose (Sigma Aldrich, Darmstadt, Germany) served as blank. A nitrogen–protein conversion factor of 5.7 (calculated based on amino acid sequence) was chosen.

4.2.5 Emulsion preparation

RPM and RPC were used to stabilize 10.0 wt% oil-in-water emulsions. The protein extracts were dispersed in deionized water, standardized at different protein concentrations (0.2–1.5 wt%). The pH was adjusted to 3.8 and the dispersions were stirred for 2 h at room temperature (around 20° C) with a magnetic stirrer at 300 rpm (2mag magnetic e motion, 2mag AG, Munich, Germany) to ensure hydration and solubilization of the proteins. Subsequently, we applied a pre-homogenization step, where the dispersions were sheared using a disperser (Ultra-Turrax, IKA®, Staufen, Germany) at 8000 rpm for 30 s. Next, 10.0 wt% rapeseed oil was slowly added to the dispersion and sheared for 1 min at 10000 rpm. The formed coarse emulsions were further processed with high-pressure homogenizer (GEA®, Niro Soavi NS 1001 L, Parma, Italy) 5 times at 250 bars.

4.2.6 Emulsion characterization

Particle size distribution

The particle size distribution of the emulsions was measured with laser light scattering using a Mastersizer-2000 (Malvern Panalytical, Malvern, UK). The emulsions were diluted 10x before measurement. To determine the individual droplet size 1.0 wt% SDS solution was added to the emulsions (1:1 v/v) prior to the measurements. The refractive index was set at 1.47 for rapeseed oil and the density at 0.97 g/cc. Measurements are reported as the surface ($d_{3,2} = \Sigma nidi^3/\Sigma nidi^2$) and volume ($d_{4,3} = \Sigma n_i di^4/\Sigma nidi^3$) mean diameter where n_i is the number of droplets with a diameter of di.

Confocal laser scanning microscopy (CLSM)

The microstructure of the emulsions stabilized by RPM and RPC was visualized using Confocal laser Scanning Microscopy (CLSM) (Leica TCS CP5 X, Leica Microsystems, Wetzlar, Germany). Nile red (1 mg/mL in ethanol) and Fast green (1 mg/mL in deionized water) were used to stain the oil and protein respectively, at a sample to dye ratio of 1:200. Nile red was excited at 488 nm and the emission was captured between 500 and 600 nm and Fast green was excited at 633 nm and the emission was captured between 650-750 nm. The dyes were excited and emitted in a sequential mode using white light laser.

Interfacial protein composition

To qualitatively determine the type of proteins adsorbed at the interface sodium dodecyl sulphate–polyacrylamide gel electrophoresis (SDS-PAGE) was used. The emulsions (10 g) were centrifuged (10000 g, 30 min, 4°C) in 15 mL tubes to remove the unadsrorbed proteins. To eliminate any interactions of the non-adsorbed proteins with the interface that could interfere with the results, the emulsions were centrifuged at two pH conditions; 1) at pH 3.8 (control) and 2) at pH 9, where the repulsive electrostatic forces between protein molecules become larger than at pH 3.8, which could eliminate possible interactions of the unadsorbed proteins with the primary layer.

After centrifugation a cream layer (interface) and a serum phase (continuous phase) were obtained. The serum was drained by making holes at the bottom of the tube. The cream was collected with a spatula and resuspended (1:10 w/w) in deionized water and stirred (200 rpm, 1h, room temperature (around 20°C)) (2mag magnetic e motion, 2mag AG, Munich, Germany). The centrifugation step was repeated one more time under the same conditions and the cream was collected and further analyzed with SDS-PAGE.

The resulting samples (interface) were mixed with sample buffer (NuPAGE LDS, ThermoFisher, Landsmeer, the Netherlands) and deionized water to achieve a final protein concentration of 1.0 mg/ml. The prepared samples (1 mL) were further heated for 15 min at 70°C in a heating block and centrifuged (1 min, 2000 g, 20°C) to remove any insoluble material. Next, the gel (NuPAGE Novex 4-12% Bis-Tris Gel, ThermoFisher, Landsmeer, the Netherlands) was assembled and MES running buffer (NuPAGE MES SDS Running Buffer, ThermoFisher, Landsmeer, the Netherlands) was added into the chamber. Ten (10) µl of protein marker (PageRulerTM Prestained Protein Ladder, 10-180 kDa, ThermoFisher, Landsmeer, the Netherlands) and 10 µl of samples were loaded onto the gel. The electrophoresis was carried out at 200 V for 30min. The gel was subsequently washed with distilled water and stained using Coomassie Brilliant Blue R-250 Staining Solution (Bio-Rad Laboratories B.V., Lunteren, the Netherlands) for 1 day under a mild shaking. Afterwards, the staining solution was discarded, and the gel was washed with distilled water and immersed in the destaining solution for 2 days under a mild shaking.

4.2.7 Interfacial properties

Interfacial tension

The interfacial tension of the oil/water interface at pH 3.8 was measured with an automated drop tensiometer (ADT, Tracker, Teclis-instruments, Tassin, France). An oil droplet with a surface area of 15.0 mm2 was created at the tip of a rising-drop capillary. Stripped rapeseed oil was used. The droplet was immersed in the protein dispersion standardized at 0.01 wt% protein content for RPM and RPC. As napins composed 50% of the total proteins in the extracts[30], the dispersion of the napin isolate was standardized at 0.005 wt% proteins. The protein dispersions were filtrated with a 0.2 µm filter before measurement to remove any insoluble material which could disturb the measurements. The interfacial tension γ was monitored for 2 h at 20°C.

Dilatational interfacial rheology

At the end of the interfacial tension measurements, oscillatory interfacial dilatational deformations was applied to determine the dilatational elastic moduli (E_d') and viscous (E_d'') moduli as a function of deformation amplitude. The oil droplet was subjected to sinusoidal deformations at amplitudes of 5–30% of its original surface area at a constant frequency (0.01 Hz). Each amplitude consisted of a series of 5 cycles followed by 5 cycles of resting period. The changes in area and interfacial tension were recorded during the oscillations, and the dilatational elastic (E_d') and viscous (E_d'') moduli were obtained using:

$$E'_d = \Delta\gamma \left(\frac{A_0}{\Delta A}\right) \cos\delta \tag{4.1}$$

$$E''_d = \Delta\gamma \left(\frac{A_0}{\Delta A}\right) \sin\delta \tag{4.2}$$

Where $\Delta\gamma$ is the change of interfacial tension at each deformation, A_0 is the initial droplet surface area (15.0 mm^2), ΔA is the change in droplet surface area and δ is the phase shift of the oscillatory interfacial tension signal with respect to the oscillating area signal.

4.3 Results and discussion

4.3.1 Emulsifying properties of the rapeseed protein extracts

The two rapeseed protein extracts with a different degree of protein purity were extracted using a previously developed protocol[111]. The rapeseed protein mixture (RPM) -recovered as a serum after centrifugation-, composed of 39.4 ± 0.4 wt% proteins (on dry matter, as determined from different batches extracted for this study). The approximate composition of the non-protein compounds as determined from previous studies was 12 wt% oleosomes, 6 wt% phenolic compounds (i.e. sinapic acid), 8 wt% ash and 34 wt% carbohydrates. After we diafiltrated RPM and removed the low molecular weight compounds, the protein content of the rapeseed protein concentrate (RPC) increased to 66.0 ± 3.5 wt%. The oleosome content also increased to 15 wt%, while the phenolic compound, ash and carbohydrate content reduced to 2.5 wt%, 2.5 wt% and 14 wt% respectively[111]. Both RPM and RPC contained napins and cruciferins in a mass ratio of approximately 1:1. The sinapic acid content in RPM and RPC could probably have been overestimated, as the Folin-ciocalteau reagent used for the determination of phenols can also interact with aromatic amino acids containing phenol rings (i.e. phenylalanine, tryptophan, tyrosine) that both napins and cruciferins contain. Using size exclusion chromatography, we previously showed that the phenolic compounds in RPM were completely removed after diafiltration[111]. Thus, we consider that RPC contains almost no sinapic acid.

Next, to assess the impact of composition on the emulsifying properties of the rapeseed protein extracts (RPM, RPC) at pH 3.8, 10.0 wt% oil-in-water emulsions were prepared, standardized at different protein concentrations (0.2-1.5 wt%) and the droplet size and microstructure were characterized. Droplet size is an important emulsion attribute that reflects 1) the ability of proteins to adsorb and stabilize the interface and 2) the impact of the non-protein compounds on the interfacial stabilization mechanism and droplet formation.

Figure 4.1A shows the individual droplet size, measured after the addition of 1.0 wt% SDS, of 10.0 wt% oil-in-water emulsions stabilized with RPM or RPC as a function of protein concentration. The droplet size of the emulsions stabilized with RPM decreased with increasing protein concentration, from 2.0 µm at 0.2 wt% protein concentration to 0.6 µm at 1.5 wt% protein concentration. The droplet size of the emulsions stabilized with RPC showed almost no dependency on the protein concentration with $d_{3,2}$ values around 0.4-0.5 µm.

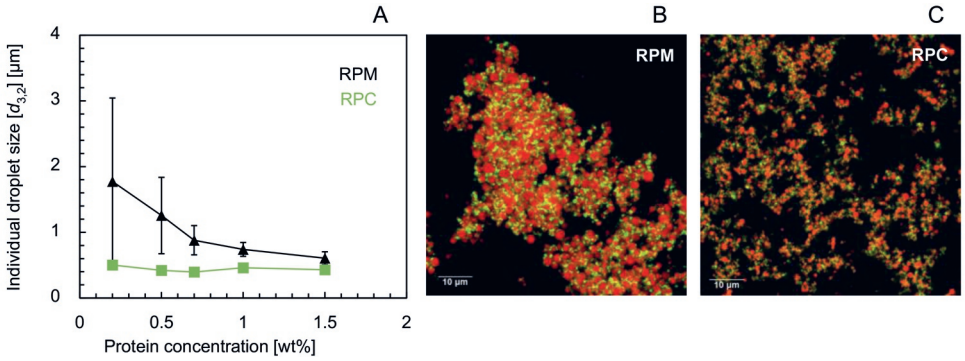

Figure 4.1 A) Individual droplet size measured after the addition of 1.0 % SDS of 10.0 wt% oil-in-water emulsions at pH 3.8 stabilized with RPM (black triangle) or RPC (green square) at different protein concentrations (0.2-1.5 wt%), B-C) CLSM images of 10.0 wt% oil-in-water emulsions stabilized with RPM (B) or RPC (C) at 0.7 wt% protein concentration. The emulsions are stained with Nile red (shown as red) for the oil and Fast green (shown as green) for the proteins, Scale bar: 10 µm.

To visualize the differences in the microstructure of the emulsions stabilized by RPM and RPC, we used confocal microscopy. Figure 4.1B-C shows the CLSM images of 10.0 wt% oil-in-water emulsions stabilized by RPM or RPC at 0.7 wt% protein concentration, where the oil is presented by red and the proteins by green. The images showed the presence of larger and aggregated emulsion droplets in RPM-stabilized emulsions compared to the RPC-stabilized emulsions where smaller and less aggregated droplets were present. Protein aggregates were present in both emulsions, however, in the RPM-stabilized emulsions, we also observed larger protein aggregates that were randomly attached to the oil droplets interface, bridging the droplets. Indeed, the average droplet aggregate sizes ($d_{4,3}$) in RPM-stabilized emulsions ranged from 60-40 µm at 0.2-1.5 wt% protein concentrations while in RPC-stabilized emulsions the average droplet aggregate sizes ($d_{4,3}$) ranged from 2.5-1.5 µm at the same protein concentrations (data not shown).

The protein aggregates present in both RPM and RPC-stabilized emulsions could be related to the low solubility of the proteins in both extracts at pH < 5 (protein solubility < 50 %)[111]. The additional larger protein aggregates in RPM-stabilized emulsions could be correlated with the free sinapic acid (s.a.) present in RPM. Prior studies have shown that at low pH values, the phenolic

hydroxyl groups of phenolic compounds are protonated and non-covalent hydrophobic interactions with proteins may occur and be stabilized by hydrogen bonds[141,142]. Such interactions can potentially cause protein structural changes[142] and protein cross-linking[37] promoting protein aggregation[140,141,143].

We, therefore, hypothesized that the sinapic acid present in RPM affects the emulsifying properties of the proteins by inducing further protein aggregation. To validate our hypothesis, sinapic acid was added to RPC prior to emulsification to reach the same content as present in RPM and made emulsions (standardized at 0.7 wt% protein, 10.0 wt% oil). Figure 4.2 shows the CLSM images of the emulsions stabilized with RPC before (A) and after (B) the addition of sinapic acid. The CLSM images showed that in RPC-stabilized emulsions where sinapic acid was added, larger and aggregated oil droplets with larger droplet aggregates in between the droplets appeared. The above result confirmed that sinapic acid present in rapeseed extracts can impact the emulsifying properties of rapeseed proteins at pH 3.8.

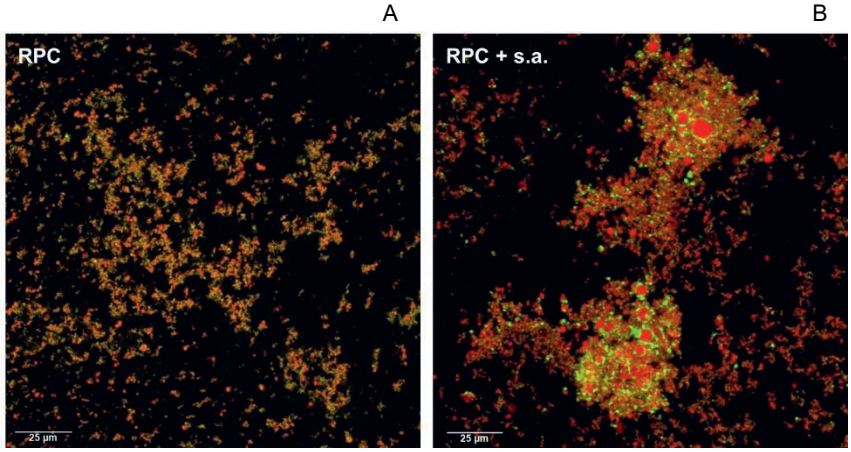

Figure 4.2 CLSM images of 10.0 wt% oil-in-water emulsions stabilized with A) RPC and B) RPC after the addition of sinapic acid (s.a), at 0.7 wt% protein concentration at pH 3.8. The emulsions were stained with Nile red (shown as red) for the oil and Fast green (shown as green) for the proteins, Scale bar: 25 µm.

To further understand the impact of sinapic acid on droplet formation, we investigated in detail the mechanism of droplet stabilization. Our first hypothesis was that sinapic acid affects the ability of proteins to adsorb at the oil droplet interface in RPM-stabilized emulsions. To test this hypothesis, the protein profile at the droplet interface of the RPM- and RPC-stabilized emulsions was analyzed using electrophoresis (SDS-PAGE). For this analysis, the emulsions were centrifuged twice to remove the non-adsorbed proteins. At pH 3.8 in both RPM and RPC dispersions the repulsive electrostatic forces between proteins are weak (ζ-potential around 5 mV)[111] and attractive forces (i.e. hydrophobic and van der Waals forces) between the adsorbed and non-adsorbed proteins

could become dominant[144], preventing the washing of the interface. Thus, the emulsions were also washed at pH 9 where the repulsive electrostatic forces between proteins is three times larger than at pH 3.8 (ζ-potential around –15 mV)[111].

Figure 4.3 shows the electrophoregram of the interface of the RPM and RPC-stabilized emulsions washed at pH 3.8 and at pH 9. At pH 3.8 at both RPM and RPC-stabilized interface a protein band around 17 kDa associated with napins and protein bands of 30-70 kDa which associate with cruciferins[13,29] were observed. However, when the interface was washed at pH 9, at both RPM- and RPC-stabilized interfaces only napins were present while cruciferins were washed out. This outcome shows that the interface stabilized by both RPM and RPC is dominated by napins, while cruciferins probably form an additional secondary layer which interacts with napins through non-covalent bonds. The above stabilization mechanism of the interface is similar to what we observed when we used RPM as an emulsifier at pH 7[30]. This result highlights that independent of the pH conditions the free sinapic acid present in RPM does not affect the ability of napins to adsorb at the interface. The fact that napins dominated the interface can be explained by their small molecular size and amphiphilic properties, which contribute to their higher surface activity than cruciferins[30].

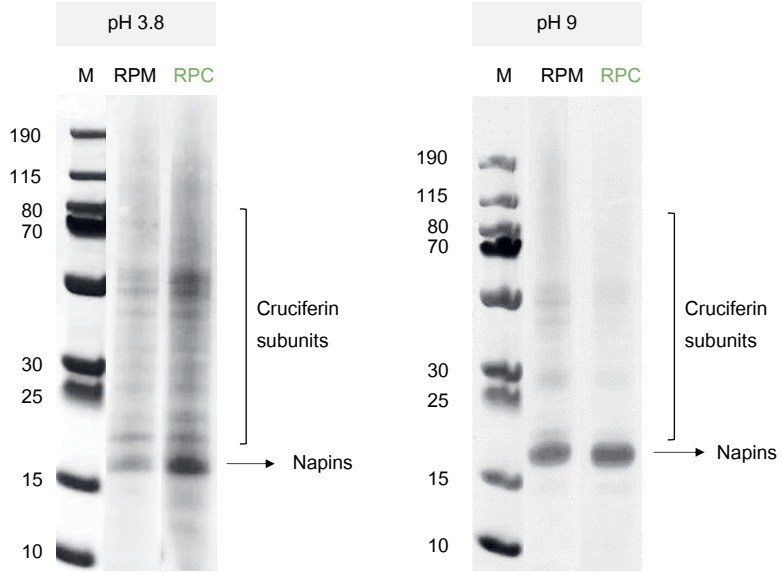

Figure 4.3 Electrophoregram (SDS-PAGE) of the interface of the 10.0 wt% oil and 0.7 wt% protein RPM- and RPC- stabilized emulsions washed with deionized water at A) pH 3.8 and B) pH 9. M: protein molecular weight markers.

As the free sinapic acid in RPM did not affect the ability of napins to adsorb at the interface at pH 3.8, we suggest that the larger oil droplets in RPM-stabilized emulsions emerge from the impact of sinapic acid on the secondary layer formed by cruciferins. Cruciferins at low pH are reported to dissociate from hexamers into trimers[29,145,146]. Although cruciferin dissociation can also induce further protein self-assembly and aggregation[29] (as also observed in the emulsions stabilized by both RPM and RPC), an equilibrium between trimers and aggregates is probably reached[147]. This partial dissociation into trimers results in exposure of the buried hydrophobic residues of the inner face of the cruciferin trimers increasing the surface hydrophobicity of the protein[29,145]. Due to the exposure of hydrophobic residues at low pH, sinapic acid possibly has more binding sites at cruciferins[37]. Additionally, the slightly positive charge of cruciferins at this pH also encourages electrostatic interactions with the negatively-charged sinapic acid[42]. As plant phenols are generally small molecules (180-700 Da) and proteins are comparatively very large (14000-350000 Da), it is likely that more than one phenol molecule can bind to one protein molecule[66]. Moreover, the sinapic acid molecules can bridge different cruciferin molecules together resulting to further protein aggregation. As a result of the sinapic acid-cruciferin interactions, the cruciferin aggregates cannot probably form a homogeneous secondary layer around napins and prevent droplet re-coalescence during turbulence and shear in the homogenizer[122].

4.3.2 Interfacial properties of the rapeseed protein extracts

To further study the interfacial properties and lateral interactions on the interfaces stabilized by RPM or RPC, we applied interfacial dilatational rheology. To understand the impact of cruciferins on the interactions occurring at the interface, pure napins were included in the measurements as they were the primary proteins adsorbed at the interface.

Figure 4.4 displays the interfacial tension reduction using the RPM, RPC and napin isolate after 12000 seconds. Both RPM and RPC reduced the interfacial tension similarly, from 25 mN/m to around 9 mN/m. The interfacial tension decreased only to 13 mN/m when pure napins were used. The lower interfacial tension observed in RPM and RPC samples compared to single napins is possibly the result of the interaction of napins with the cruciferins present in the bulk in RPM and RPC dispersions.

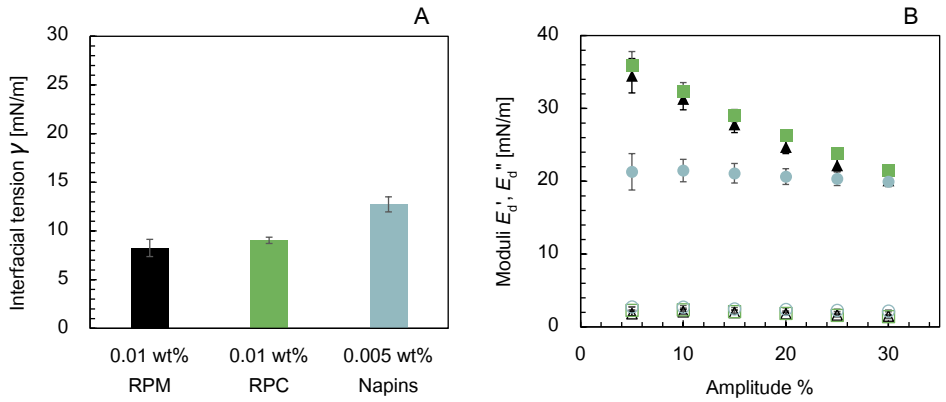

Figure 4.4 A) Interfacial tension (γ) after 12000 s of RPM (black) and RPC (green) dispersions at 0.01 wt% protein concentration and napins (light blue) dispersion at 0.005 wt% protein concentration at pH 3.8 (20°C). The dispersions were filtered with a 0.2 μm syringe filter prior to measurements, B) Dilatational elastic modulus (E_d': filled symbol) and viscous modulus (E_d'': hollow symbol) as a function of amplitude of deformation at constant oscillatory frequency 0.01 Hz. The colors representing RPM, RPC and napins are the same in both panels.

To gain more insights into the interactions between protein molecules at the oil/water interface, we employed interfacial dilatational rheology. In Figure 4.4B we plotted the dilatational moduli of the interfaces stabilized by the protein extracts (RPM, RPC and napins) as a function of amplitude of deformation. The elastic modulus (E_d') was much higher than the viscous modulus (E_d'') in all protein samples, which implies solid-like viscoelastic behavior. The elastic moduli of napins were around 20 mN/m and independent on the amplitude of deformation, which indicates that the interfacial microstructure did not change significantly during deformation. This response implies weak lateral interactions between napin molecules mainly driven by attractive interactions, such as van der Waals and hydrogen bonds after adsorption and no significant formation of covalent sulfur bonds. The result was similar to our previous research at pH 7[30], highlighting that the interactions between napins are not strongly influenced by pH changes.

The elastic moduli (E_d') of RPM and RPC stabilized interfaces were similar and higher than the single napin interface at small amplitudes (E_d' around 36 mN/m). This outcome suggests that cruciferins present in the bulk in RPM and RPC dispersions enhance the lateral interactions of napin molecules and result in a stronger viscoelastic interface than a single layer of napins. The moduli of the interface at pH 3.8 were higher compared to pH 7 (E_d' around 36 at pH 3.8 vs E_d' around 28 mN/m at pH 7 at 5% amplitude)[30]. The differences in the moduli between pH 3.8 and pH 7, suggest that at low pH, the dissociation of cruciferin into trimers with increased hydrophobicity may allow stronger interactions of cruciferins with the adsorbed layer of napins compared to cruciferin hexamers. However, when the amplitude of deformation was increased,

the moduli decreased from around 36 mN/m at 5% amplitude to 20 mN/m at 30% amplitude both in RPM- and RPC-stabilized interfaces, showing that the interfacial microstructure was weakened.

To further understand the behavior of the interfacial network upon extension and compression, we used Lissajous plots, where the surface pressure is plotted against the area deformation. Figure 4.5 shows the Lissajous plots of the interface stabilized by the protein extracts (RPM, RPC, napins). The Lissajous plots of RPM and RPC-stabilized interfaces were similar and displayed an asymmetrically narrow ellipse shape at all amplitudes. At 10% amplitude, upon extension (top right part) the ellipse was slightly wide but becomes very narrow -almost a line- upon compression (bottom left part). By increasing the amplitude to 20% and 30% the curves start to level off on compression as the surface pressure almost does not change by increasing the amplitude (from -5mN/m to -6 mN/m respectively). This levelling off shows a strain softening behavior which suggests that upon compression the interfacial network is jammed, and most-likely the interacting cruciferin molecules forming the secondary layer are expelled to the bulk[148]. A schematic representation of the interactions occurring at the interface upon increasing the amplitude of deformation when RPM or RPC is used is given in Figure 4.6.

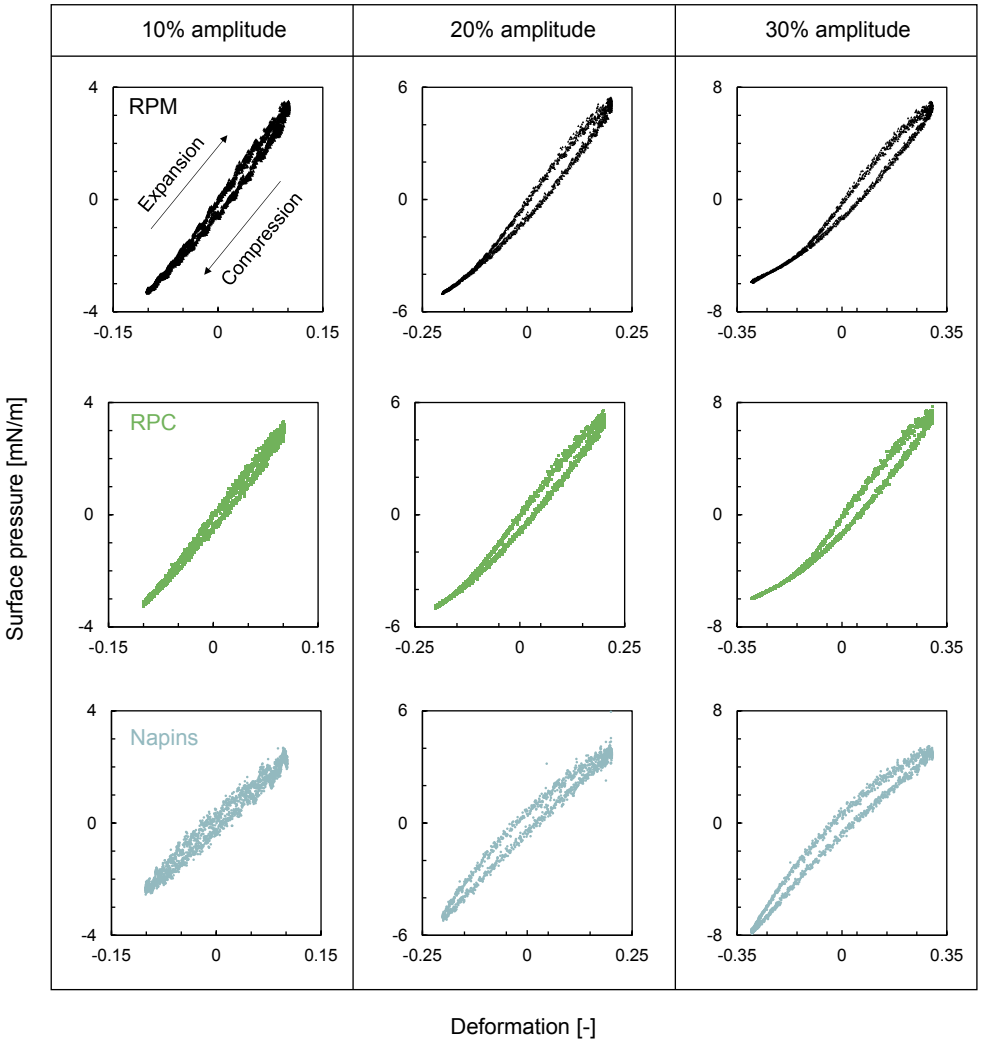

Figure 4.5 Lissajous plots of the interface stabilized by RPM (black), RPC (green), Napins (light blue) at 10%, 20% and 30% amplitude of area deformation.

In comparison, the Lissajous plots of the interface stabilized napins at 10% amplitude showed a narrow ellipse shape without noticeable asymmetries. This shape indicates an almost linear, predominantly elastic response of the interface, indicating a weak solid structure[135]. By increasing the amplitude of deformation to 20% and 30%, the surface pressure increased from -3 mN/m at 10% to -8 mN/m at 30%, at maximum compression (lower left corner of the plot). This increase in surface pressure can be explained by the increased density of napins on compression (increase in protein molecules/area). Additionally, upon compression the slope of the curve increase slightly which indicates a weak strain hardening behavior[132,133,148]. Towards maximum expansion (top right

part), the slope of the curve slightly levels off, showing a strain-softening tendency. This behavior upon expansion and compression implies an interface with weak in-plane interactions with nonlinearities in the response, primarily related to changes in surface density[135,148].

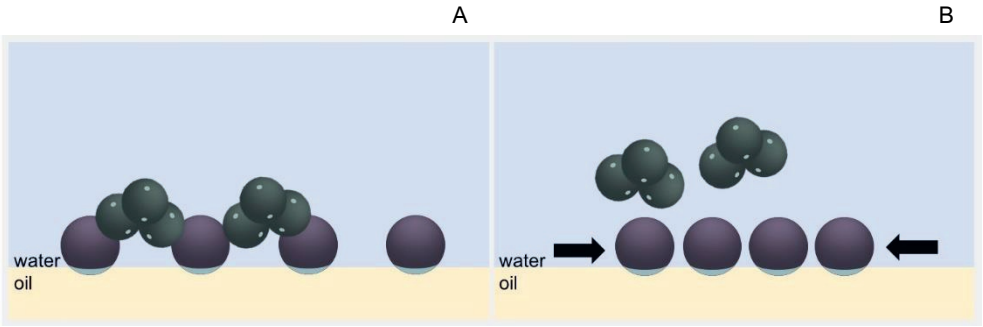

Figure 4.6 Schematic representation of dynamic interactions of cruciferins with the adsorbed napins A) before and B) after compression, when the RPM or RPC is used to stabilize the interface, showing expelling of cruciferins into the continuous phase.

The fact that there are no significant differences observed in the interfacial properties of RPM and RPC determined by the ADT, in contrast to the emulsion properties can be a result of the 1) limited diffusion of large protein aggregates to the interface or even their precipitation during the interfacial measurements, 2) the absence of large aggregates in the system due to the necessary filtration step taken before the interfacial measurements, 3) the higher surface area created during emulsification, where the large cruciferin aggregates possibly have a more drastic effect on droplet formation; at these significantly higher surface areas the number of large cruciferin aggregates is probably insufficient to form a homogeneous secondary layer which strongly interacts with the primary layer of napins and sufficiently cover the created interface. Moreover, as a result of turbulence and high shear forces in the homogenizer these weakly bound aggregates could be expelled from the interface. As a result, during emulsification, the colliding oil droplets recoalesce, and larger emulsion droplets are formed when RPM is used as an emulsifier.

All the above results from the emulsion and interfacial measurements combined, show that the presence of sinapic acid present in RPM does not affect the ability of napins to adsorb at the interface, but suggest that sinapic acid affects the secondary layer formation by cruciferins by inducing aggregation. A schematic representation of the suggested emulsification mechanism of RPM and RPC-stabilized interface is illustrated in Figure 4.7.

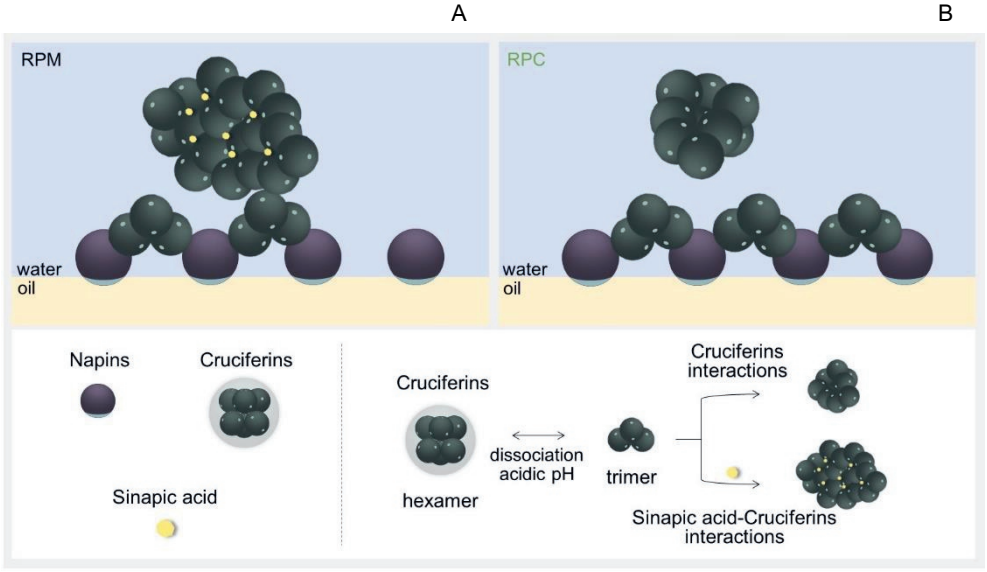

Figure 4.7 Schematic representation of the suggested stabilization mechanism of A) RPM and B) RPC-stabilized interface at acidic pH. The size of molecules and the number of cruciferin trimers and sinapic acid in each protein aggregate are not to scale.

4.4 Conclusions

In this research, we investigated the mechanism of interface stabilization when a rapeseed protein mixture (RPM) containing 40 wt% proteins and 6 wt% free sinapic acid and a rapeseed protein concentrate (RPC) containing 65 wt% proteins in which sinapic acid is removed are used as emulsifiers at pH 3.8. The two extracts showed different emulsification properties; Larger emulsion droplets and larger protein aggregates randomly attached at the interface of the droplets were found in RPM-stabilized emulsions compared to RPC-stabilized emulsions. The presence of sinapic acid in RPM does not impact the interfacial composition, with napins being adsorbed at the interface. However, sinapic acid in RPM affects the secondary layer formed by cruciferins by inducing cruciferin aggregates. This aggregation probably results in a less homogenous second ary layer that cannot strongly interact with the primary adsorbed layer of napins and prevent recoalescence of the colliding oil droplets during homogenization. Thus, larger oil droplets are formed when RPM is used as an emulsifier. We anticipate that our insights into the effect of sinapic acid on the emulsification mechanism of less purified rapeseed protein extracts can be used to evaluate the need for protein purification for the application of these extracts in emulsion food products.

Chapter 5

The complementary functionalities of rapeseeds proteins in structuring emulsion-filled gels

This chapter has been submitted as: Ntone, E.*, Kornet, R.*, Venema, P., Meinders, M.B.J., van der Linden, E., Bitter, J.H., Sagis, L.M.C., Nikiforidis, C.V. (2021) Napins and cruciferins in rapeseed protein extracts have complementary roles in structuring emulsion-filled gels.

*The authors have contributed equally to this work and share first authorship

Abstract

We investigated the complementary roles of napins and cruciferins present in a rapeseed protein mixture (RPM) in structuring emulsion-filled gels (EFGs). The role of napins is to stabilize the emulsion droplets, while cruciferins, which were previously found to interact with the adsorbed napin interfacial layer, can build the protein gel network around the droplets. The effects of oil concentration (0-30 wt%) and pH (5 and 7) on the rheological and microstructural properties of EFGs were investigated. In the absence of oil, at pH 5, due to low protein solubility, RPM formed a heterogeneous network built of protein aggregates. At pH 7, RPM was more soluble and formed a homogeneous network built of strand-like protein structures with higher gel firmness. In the presence of emulsion droplets, the gel firmness increased, with a more pronounced reinforcement at pH 5 compared to pH 7. The type of gel network did not change by the presence of emulsion droplets neither at pH 5 nor at pH 7, as suggested from confocal microscopy and the unchanged response to large deformation. This implies that the protein backbone dictated the network structure. The higher gel firmness in presence of emulsion droplets, is explained by the fact that the emulsion droplets are stiffer than the protein matrix, and interact with the protein matrix, acting as protein particles that expand the protein network. This research shows that the presence of two different proteins with complementary roles in a less purified protein extract, provides a single protein ingredient suitable for structuring food emulsion-filled gels.

5.1 Introduction

Traditionally, plant protein extraction processes focus on high protein purity and yield[9], although often there is a trade-off between purity and yield[14,149]. In recent years, more attention has been paid to the environmental impact of plant protein extraction -such as energy and water usage- and to the effect of protein extraction and purity on functionality[8,10,150,151]. It has been reported that less purified plant protein extracts yield equal or better foaming, emulsifying, and gelling properties compared to highly purified plant protein extracts for a variety of plant sources. Examples of such plant sources include soy[137], peas[136,138], chickpeas[152], sunflower seeds[86] and rapeseeds[34]. The functionality of the less purified plant protein extracts can be ascribed to the different functionalities of the proteins in the mixture and the prevention of process-induced protein interactions (e.g., leading to aggregation).

Rapeseeds are a potential source of functional proteins, containing two types of storage proteins, named napins and cruciferins. Napins are small molecular weight albumins (15-17 kDa), which are soluble in a wide pH range and show high heat stability (with a denaturation temperature $T_d \geq 100°C$)[33]. The hydrophobic domains of napins are concentrated on one side of the protein, reminiscent of a Janus particle[30]. Cruciferins, are globulins with a high molecular weight (300 kDa) and an hexamer structure consisting of two trimers[29]. The hydrophobic domains of cruciferins are widely distributed over the surface, and also buried within the cruciferin trimers[29]. The hexamer structure of cruciferins is more susceptible to structural changes and unfolding upon heating and pH changes compared to napins[31,33].

In a previous work, we showed that a less purified rapeseed protein mixture (RPM) with 40 wt% protein content and all storage proteins present (napins and cruciferins) -obtained from non-defatted seeds after aqueous alkaline extraction and subsequent separation of proteins from oil- can form stable emulsions at pH 7. Napins were found to govern the interface of the emulsion droplets, while cruciferins weakly interacted with the primary adsorbed layer[30]. Napins exhibit higher interfacial activity than cruciferins[56], probably due to their architecture[30]. However, it has been reported that cruciferins have better gelling properties, as they form firmer gels than napins upon heat-induced gelation[55,57,58].

Considering the emulsifying properties of napins and gelling properties of cruciferins, we anticipate the two proteins present in RPM can have complementary functionalities in structuring emulsion-filled gels (EFGs). Such EFG's are protein gels with embedded emulsion droplets[153]. Different kinds of food products such as set yoghurt, fresh cheese, puddings, dairy desserts and sausages can be categorized as protein emulsion-filled gels[154]. When RPM is used to structure EFGs, napins can stabilize the emulsion droplets, and cruciferins which weakly interact with napins at the

interface[30], can build the protein gel network, and both proteins interacting at the droplet-matrix contact sites.

Depending on the interactions on the two proteins on droplet-matrix contact sites, EFGs can show different rheological characteristics[155,156]; When the droplet interface interacts with the matrix, as in the case of napins with cruciferins[30], the droplets can act as active fillers, and potentially reinforce the gel structure. Such interactions are often seen in case the droplets are stabilized by proteins[153,157], whereas surfactant-coated oil droplets usually do not or only weakly interact with the protein matrix[158–160]. Apart from the droplet-matrix interactions, the rheological characteristics of EFGs depend on the protein and oil content, and the stiffness of the droplets and the matrix[155,156].

In this work we used the less purified rapeseed protein mixture (RPM) containing napins and cruciferins to structure EFGs, which were studied using bulk rheology and confocal microscopy. The effect of oil concentration and pH on the rheological properties and microstructure of the EFGs was investigated. Exploiting the potential complementary roles of the different proteins present in plant extracts, may lead to the employment of protein mixtures with multiple-functions, increasing the overall sustainability of plant-based foods.

5.2 Material and methods

5.2.1 Materials

Untreated Alize rapeseeds (stored at -18°C) were used for the extraction of the protein mixture. Rapeseed oil was kindly provided by Nutricia Research B.V. All other chemicals were of analytical grade and obtained from Sigma Aldrich (Steinheim, Germany). All samples were prepared with demineralised water. All samples and subsequent analyses were performed in duplicates.

5.2.2 Extraction of the rapeseed protein mixture

The rapeseed protein mixture (RPM) was extracted as described before[111]. Dehulled rapeseeds were soaked in deionized water at a ratio of 1:8 (w/w) at pH 9.0 (adjusted with 0.5 M NaOH solution) under continuous stirring with a head stirrer (EUROSTAR 60 digital, IKA, Staufen, Germany) at room temperature (~20°C) for 4 h. Afterwards, the dispersion was blended with a kitchen blender (HR2093, Philips, Netherlands) for 2 min at maximum speed. To separate the solids from the liquid phase, the resulting slurry was filtered using a twin-screw press (Angelia 7500, Angel Juicer, Naarden, The Netherlands). The filtrate was collected, the pH was adjusted to pH 9.0, and centrifuged (10000 g, 30 min, 4°C) (Sorvall Legend XFR, ThermoFisher Scientific, Waltham, MA, USA). A cream layer (oleosome-rich), a serum (protein mixture (RPM)) and a pellet (fibre-rich) were obtained. The serum was freeze-dried (Alpha 2–4 LD plus, Martin Christ

Gefriertrocknungsanlagen GmbH, Osterode am Harz, Germany) to obtain an RPM powder, which was stored at -18°C until further use.

5.2.3 Characterization of the rapeseed protein mixture

Protein content

The protein content of the freeze-dried RPM was determined with the Dumas method (FlashEA 1112 Series, Thermo Scientific, Waltham, Massachusetts, US); d-methionine (≥ 98%, Sigma Aldrich, Darmstadt, Germany) was used as a standard and as a control. Cellulose (Sigma Aldrich, Darmstadt, Germany) was used as blank. A nitrogen-protein conversion factor of 5.7 -calculated based on amino acid sequence –was used.

Protein profile of supernatant after centrifugation

The qualitative analysis of the proteins present in the supernatant after removal of large aggregates from RPM dispersions at pH 5 or pH 7 was carried out using sodium dodecyl sulphate–polyacrylamide gel electrophoresis (SDS-PAGE), to provide a protein profile. First, the RPM was dispersed in deionized water (standardized at 0.5 wt% protein content), the pH was adjusted to pH 5 or pH 7 using 0.5 M NaOH or HCl and the dispersions were stirred at room temperature for 2 h with a magnetic stirrer at 300 rpm (2mag magnetic e motion, 2mag AG, Munich, Germany), followed by centrifugation (10000 g, 30 min, 20°C) (Sorvall Legend XFR, ThermoFisher Scientific, Waltham, MA, USA). A pellet, a clear serum and a thin cream layer of oleosomes at the surface were obtained. The clear serum was carefully separated and mixed with a sample buffer (NuPAGE® LDS, Thermo- Fisher, Landsmeer, the Netherlands) to achieve a final protein concentration of 1.0 mg/mL. Then, 10.0 µL of a protein marker (PageRuler™ Prestained Protein Ladder, 10–180 kDa, ThermoFisher, Landsmeer, the Netherlands) and 15 µL of the sample were loaded onto the gel (NuPAGE® Novex® 4–12% Bis-Tris Gel, ThermoFisher, Landsmeer, the Netherlands). MES running buffer (NuPAGE® MES SDS Running Buffer, ThermoFisher, Landsmeer, the Netherlands) was used. The gel was washed with water and stained (Coomassie Brilliant Blue R-250 Staining Solution, Bio-Rad Laboratories B.V., Lunteren, the Netherlands) overnight under gentle shaking. Thereafter, the gel was washed with demineralized water and destained (destaining solution of 10% ethanol and 7.5% acetic acid in deionized water) overnight under gentle shaking. Images of the gels were taken using a camera.

5.2.4 Preparation of emulsions used in emulsion-filled gels

To obtain emulsion-filled gels with final concentrations of 10.0, 20.0 and 30.0 wt% oil, emulsions of 11.6, 22.7 and 33.5 wt% oil (of total mass) were prepared using RPM. To ensure a similar individual droplet size of the emulsion droplets at different oil concentrations, the protein to oil ratio was kept at 1:14.3 (w/w) (based on protein content of RPM) as well as the number of passes through the homogenizer (N = 5), and the homogenization pressure was adjusted. In Table 5.1 the homogenization pressures and the protein concentrations used for the different emulsions are summarized. The emulsions were prepared as previously reported[30]. First, RPM was dispersed in deionized water (aqueous phase) at the corresponding protein concentration, the pH was adjusted to 7.0 and the dispersions were stirred for 2 h at room temperature (~20° C) with a magnetic stirrer at 300 rpm (2mag magnetic e motion, 2mag AG, Munich, Germany) to allow hydration and solubilization of the proteins. Thereafter, a pre-homogenization step was applied using a shear homogenizer (Ultra-Turrax, IKA®, Staufen, Germany) set to 8000 rpm for 30 s. Next, the rapeseed oil was slowly added to the dispersion and sheared for 1 min at 10000 rpm. The coarse emulsion was further processed with a high-pressure homogenizer (GEA®, Niro Soavi NS 1001 L, Parma, Italy) for 5 passes.

After the addition of 1.0 wt% SDS solution to the emulsions at a ratio of 1:1 (v/v), the individual droplet size of the emulsions was measured using a Bettersizer S3 Plus (3P Instruments GmbH & Co. KG, Odelzhausen I Germany). The individual droplet size expressed as volume ($d_{4,3} = \Sigma n_i d_i^4 / \Sigma n_i d_i^3$) and surface ($d_{3,2} = \Sigma n_i d_i^3 / \Sigma n_i d_i^2$) mean diameter (where n_i is the number of droplets with a diameter of d_i) is also given in Table 5.1.

Table 5.1 Oil concentration, protein concentration, homogenization pressure (bar) and individual droplet size of the emulsions prepared at pH 7 in deionized water, used for the preparation of the emulsion-filled gels (±standard deviation).

Oil (wt% of total)	Protein concentration (wt% of total)	Homogenization pressure (bar)	$d_{4,3}$ (μm)	$d_{3,2}$ (μm)
11.6	0.8	250	1.7 ± 0.0	1.5 ± 0.0
22.7	1.6	300	1.9 ± 0.5	1.4 ± 0.2
33.5	2.3	350	2.2 ± 0.5	1.6 ± 0.1

5.2.5 Preparation of emulsion-filled gels

The emulsion-filled gels (EFGs) containing different oil concentrations (10.0, 20.0 and 30.0 wt% of total mass) were prepared by dispersing RPM powder in the emulsions of different oil concentrations (prepared as described in section 5.2.4), resulting in protein-enriched emulsions. RPM was added to the emulsions to achieve a concentration of 15.0 wt% in the aqueous phase of each emulsion system. A reference sample (gel matrix) in which RPM was dispersed in water at the same concentration was also prepared. The pH of the systems was adjusted to pH 5 or pH 7 and the samples were left for 2 h under continuous stirring using a magnetic stirrer at 200 rpm (2mag magnetic e motion, 2mag AG, Munich, Germany) to allow hydration and solubilization of the added proteins. Thereafter, the samples were stored at 4°C until the next day when the rheological tests were performed.

5.2.6 Microstructural visualization

To visualize the microstructure of the emulsion-filled gels (EFGs), the protein-enriched emulsions were stained with Nile red (1 mg/mL dissolved in ethanol) and Fast green (1 mg/mL dissolved in deionized water) at a sample to dye ratio of 1:200 for the oil and protein, respectively. The stained samples were transferred to sealed glass chambers (Gene frame 65 µl adhesives, Thermo Fisher Scientific, United Kingdom). The frames were placed in a water bath (100°C, 15 min). Afterwards, the samples were cooled immediately with water to room temperature. The samples were visualized using a Confocal Laser Scanning Microscope with a water immersion objective at 63x magnification (Leica SP8-SMD microscope, Leica Microsystems, Wetzlar, Germany). Nile red was excited at 488 nm and the emission was measured between 500 and 600 nm and Fast green was excited at 633 nm and the emission was measured between 650-750 nm. The dyes were excited and emitted in a sequential mode using a white light laser.

5.2.7 Shear viscosity measurements

The shear viscosity of the protein dispersions (15.0 wt% RPM) was measured with an MCR302 rheometer (Anton Paar, Graz, Austria). The samples were transferred to a double-gap geometry (DG 26.7) The steady-shear viscosities were measured for 2 min, with incrementing shear rates of 0.1, 0.5, 1, 5, 10, 50, 100 s^{-1} followed by decrementing shear rates of 50, 10, 5, 1, 0.5 and 0.1 s^{-1}. The temperature was kept constant at 20°C. The experiment was set up in this way to determine the shear dependency (e.g. shear-thinning behavior) and to determine whether the dispersions showed thixotropy and/or hysteresis.

Small Amplitude Oscillatory Shear (SAOS) rheology

The samples were studied on their gelling behavior with an MCR302 rheometer (Anton Paar, Graz, Austria). The protein-enriched emulsions were transferred to a concentric cylinder (CC-17). A sand-blasted geometry was used, to reduce the chance of wall-slip. A solvent-trap was placed on top of the cylinder, to prevent solvent evaporation upon heating. The sample was heated from 20°C to 100°C with a rate of 3°C / min, kept at 100°C for 10 min, and cooled to 20°C with a rate of 3°C / min. To make sure that no gel maturation took place, the sample was kept at 20°C for another 5 min. Throughout this temperature sweep, an oscillatory deformation was imposed at a constant frequency of 1 Hz and a strain of 1%, which fell within the linear viscoelastic (LVE) regime of the gel. The response was recorded and the resulting *G'* and *G"* were determined by the Rheocompass Software (Anton Paar, Graz, Austria). All samples were measured in duplicate.

Large Amplitude Oscillatory Shear (LAOS) rheology

After the temperature sweep, the emulsion-filled gels were characterized for their non-linear rheological behavior, using the same rheometer and geometry as for the SAOS measurements. The strain was increased logarithmically from 0.1-1,000% at a constant frequency of 1 Hz and a temperature of 20°C. The end of the LVE regime was defined as the strain at which the *G'* had decreased to 90% of its original value, which was expressed as the critical strain.

For each imposed strain amplitude, the oscillating strain, stress and shear rate signals were recorded. This data was normalized, and elastic and viscous Lissajous plots were constructed. The elastic and viscous contributions at each strain amplitude were calculated by the Rheocompass Software (Anton Paar, Graz, Austria), and plotted in the Lissajous figures.

The area enclosed within the Lissajous curves represents the energy dissipated (E_d) per unit volume during one oscillatory cycle. This information can be summarized by plotting the energy dissipation ratio as a function of strain amplitude. The energy dissipation ratio (ϕ) is the ratio of the dissipated energy at a certain strain amplitude (E_d) over the energy dissipated by a perfect plastic material (E_d (pp))[161]. The energy dissipation ratio is related to the loss modulus (*G"*) and the maximum stress (σ_{max}) at a given strain amplitude γ_0 by Equation 5.1[162]:

$$\Phi = \frac{E_d}{(E_d)_{pp}} = \frac{\pi G'' \gamma_0}{4\sigma_{max}} \tag{5.1}$$

5.2.8 Statistical Analysis

All measurements were performed at least in duplicate. The standard deviations of the mean values were calculated and used to express the variability. Claims regarding statistical differences were supported by one-way ANOVA analysis. Significance was defined as $P < 0.05$.

5.3 Results and discussion

Rapeseed protein mixtures (RPM) were extracted from non-defatted and dehulled rapeseeds following our previously reported aqueous extraction process[111], and used as starting material to prepare the emulsion-filled gels. The followed extraction protocol aimed to simultaneously extract napins and cruciferins, and the oleosomes present in the seeds, and to maintain protein and oleosome natural physicochemical properties, eliminating process-induced interactions of proteins with co-extracted phenols.

The resulting rapeseed protein mixture (RPM) had an average protein content of 39.4 ± 0.4 wt% (as determined from different batches extracted for this study), and consisted of napins and cruciferins in a mass ratio of 1:1. The approximate composition of the remaining non-protein molecules, based on previous studies, were 12.0 wt% intact oleosomes, 6.0 wt% free phenolic compounds, 8.0 wt% ash and 35.0 wt% polysaccharides[30,111].

5.3.1 Physicochemical properties of RPM dispersions

For the use of RPM as a dual-purpose ingredient in emulsion-filled gels, it was needed to understand the physicochemical properties of the protein network (matrix) and the embedded emulsion droplets. To understand the matrix properties, we first studied RPM in dispersions at pH 5 and pH 7. A concentration of 15.0 wt% RPM (which corresponds to 5.9 wt% protein) in EFGs was chosen, as from preliminary data (not shown here) this concentration was found to be sufficient for gel formation. Thereafter, the emulsion droplets stabilized with RPM were characterized.

First the effect of the solubility of rapeseed proteins on the shear viscosity of RPM aqueous dispersions (15.0 wt% RPM) as a function of pH was studied. Figure 5.1 shows the viscosity of RPM dispersions as a function of shear rate at pH 5 and pH 7. The viscosity of the protein dispersion at pH 7 hardly changed as a function of shear rate, closely resembling Newtonian behavior. At pH 5 the viscosity was higher and showed a decrease with increasing shear, indicating shear thinning behavior. Both at pH 5 and pH 7 the backward loop showed the same shear-dependency of viscosity as the forward loop, indicating that there was no hysteresis in the dispersions. Newtonian-like behavior is typically seen for water and oil[163] and may indicate the absence of large or interacting molecules. The absence of hysteresis at pH 7 implies the absence of larger particles and is consistent with the higher solubility of RPM at pH 7[111]. The higher viscosity at pH 5 compared to pH 7 indicates an increased effective protein volume fraction. This is supported by the observed shear-thinning behavior, which implies that larger -and possibly interacting- particles are present at rest. These protein particles or aggregates either align with the flow or break down with increasing shear. In the latter case, the particles must recover in timescales shorter than in which the viscosity is measured at a specific shear rate, as no hysteresis was observed.

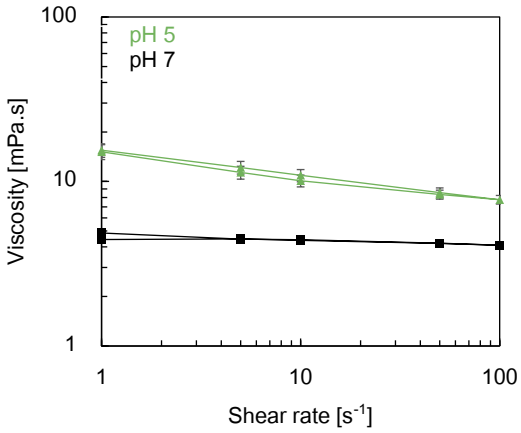

Figure 5.1 Shear viscosities in forward and backward loop of 15.0 wt% rapeseed protein mixture (RPM) dispersions at pH 5 and 7. The shear rate was increased (and decreased) stepwise. All samples were measured in duplicate and the standard deviations are represented by the error bars (with some of them smaller than the data points).

The presence of larger protein aggregates at pH 5 compared to pH 7 is in line with our previous findings and can probably be related to the lower electrostatic repulsion between proteins at pH 5 (ζ-potential around -5 mV) compared to pH 7 (ζ-potential around -15 mV)[111]. Previously it has been shown that the solubility of rapeseed proteins is lower at pH 5 compared to pH 7 (i.e. 40 vs 70

wt%)[30,33,68]. The different solubility of proteins at these pH values is also linked with different gelling behavior of rapeseed proteins[31].

It has been previously reported that napins are soluble at a broader pH range compared to cruciferins, for which solubility increases by increasing pH[29], and with minimal solubility reported close to pH 4-5[52,164]. Therefore, to determine the type of proteins present in the aggregates at each pH, the larger insoluble protein aggregates were removed using centrifugation, and the protein composition of the supernatant was determined using electrophoresis. Figure 5.2 shows the electrophoregram (SDS-PAGE) of the proteins present in the supernatant of centrifuged RPM dispersions prepared at pH 5 and pH 7. Both at pH 5 and pH 7, we identified a band around 17 kDa, which is related to napins[97]. At pH 7 several bands in the range of 20-70 kDa were also present, corresponding to cruciferins[96]. The band representing napins shows a similar intensity at pH 5 and 7, indicating that the solubility of napins is not affected in this pH range. The cruciferin bands were more pronounced at pH 7 than at pH 5, indicating that cruciferins formed larger insoluble aggregates at pH 5, which were centrifuged out and resulted in a lower band intensity. The lower solubility of cruciferins at this pH could be a result of the nearly zero net charge of cruciferins close to pH 5[55], which probably cause the formation of cruciferin aggregates[29]. In addition, the phenolic compounds (i.e. sinapic acid) present in RPM can induce aggregation, particularly close to the isoelectric point, leading to further protein aggregation[37,42].

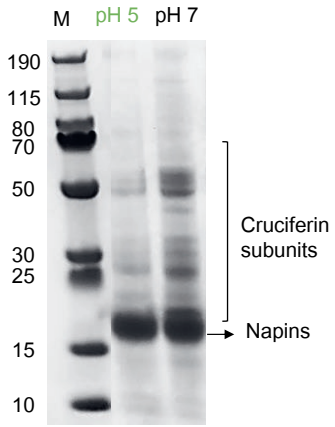

Figure 5.2 Electrophoregram (SDS-PAGE) under non-reducing conditions of the proteins present at supernatant of RPM dispersions (0.5 wt% protein) prepared at pH 5 and pH 7, obtained after centrifugation.

5.3.2 Properties of emulsion droplets used in EFGs

The emulsion droplet size is one important parameter that influences the rheological and mechanical properties of EFGs[165–167]. To exclude any effect of droplet size, we standardized the mean emulsion droplet size independently of the oil concentration, by keeping the same protein to oil ratio and adjusting the homogenization pressure as summarized earlier in Table 5.1. The droplet size distribution of the emulsions was similar for all the emulsions independent of the oil concentration, with a mean individual droplet size ($d_{4,3}$) around 2.0 μm (Table 5.1) (size not significantly different between samples as $P > 0.05$).

Another important parameter that affects the rheological properties of EFGs is the interaction between the emulsion droplets and the protein matrix, which is influenced by the interfacial composition of the droplets[165,167,168]. All the emulsions were prepared (prior to the addition of 15.0 wt% RPM) at pH 7, as from our previous research we know that when using RPM as an emulsifier at pH 7, the interface of the droplets is dominated by napins, while cruciferins weakly interact with the primary adsorbed layer[30]. This interfacial composition results in a viscoelastic interface, with an elastic modulus (E_d') of approximately 25 mN/m (at 5% amplitude).

5.3.3 Rheological behavior of the emulsion-filled gels

Small Amplitude Oscillatory Shear (SAOS)

To determine the effect of pH and oil concentration on the gelling properties of EFGs, the protein-enriched emulsions were subjected to a temperature sweep and the rheological behavior was studied. Figure 5.3 shows the storage modulus (G') of the protein-enriched emulsions at different oil concentrations (10.0-30.0 wt%) and pH conditions (pH 5 and 7) as a function of time and temperature increase. It shows that even before heating, an increased oil content leads to an increased G' at both pH 5 and 7. At pH 5, the tan δ decreases with increasing oil content and approaches a value of 1 at 30.0 wt% oil content (not shown in figure). Upon heating an initial gradual increase in G' was observed in the first 20 min and $T < 60°C$, followed by a steeper increase at 80°C and a second slope at 100°C. The denaturation temperatures of cruciferins and napins have been reported as 80-90 and 100-110°C respectively at pH 7[34,164,169] and decrease with decreasing pH[29,170]. Considering the decreased denaturation onset at pH 5, it is expected that the two slopes in the heating stage (at 80° and 100°C) correspond to the onset of denaturation of cruciferins and napins, respectively. From Figure 5.3 it is also observed that upon cooling there is only a subtle increase in G', and no gel maturation occurs during the final 5 min holding time at 20°C. At pH 5 there is also a pronounced G' increase of the heat-set gels when the oil content increases, which implies that the emulsion droplets reinforce the gel.

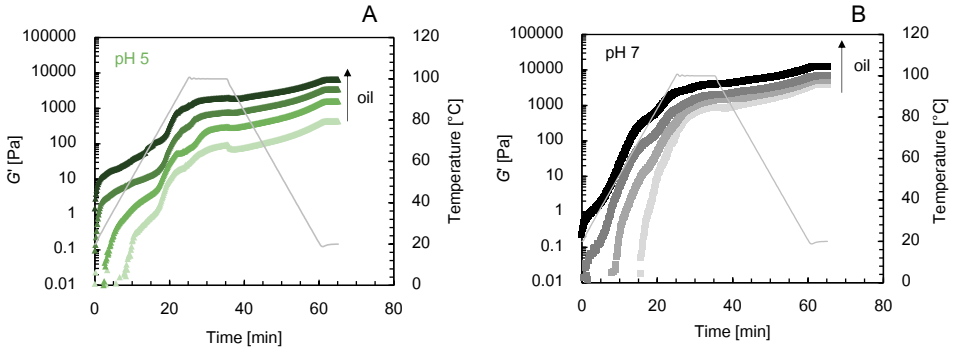

Figure 5.3 Temperature sweeps of the matrix (no oil) and emulsion-filled gels with 0.1 to 0.3 oil mass fraction at A) pH 5 and B) pH 7, containing 15.0 wt% rapeseed protein mixture (RPM) in the aqueous phase. A darker color represents more oil. All samples were measured in duplicate and a representative curve is shown.

The situation at pH 7 is different; there is a much steeper increase in *G*' at the heating stage and a less pronounced slope deflection at higher temperatures. Also here the *G*' increases to a limited extent upon cooling, and no gel maturation occurs during the 5 min holding time at 20°C. Figure 5.3 shows that the RPM forms a firmer gel (i.e. higher *G*') without oil at pH 7, compared with pH 5. This is consistent with what has been reported elsewhere for a rapeseed protein isolate[55]. However, in our study we see that with increasing oil fraction there is less reinforcement, eventually leading to a similar *G*' at 30.0% oil for pH 5 and 7.

At both pH 5 and pH 7, an initial *G*' increase at 20-70°C was observed, which is below the denaturation onset temperatures of cruciferins and napins. It appears that a network already starts to form at these temperatures. This observation is consistent with another study on the gelling properties of rapeseed proteins, where a similar early increase of the *G*' was observed at pH 4 and 7[55]. We also noticed that this increase started earlier by increasing the oil concentration in the EFGs. Therefore, we hypothesize that the increase in *G*' at low temperatures could be caused by emulsion droplet-droplet interactions or interactions with the forming protein matrix.

To understand the differences in the degree of gel reinforcement in the EFGs at pH 5 and pH upon oil addition, in Figure 5.4A we plotted the ratio between the *G*' of each EGF (G'_{EFG}) relative to the *G'* of the protein gel matrix where no oil was present (G'_{matrix}), as proposed by[171] (G'_{EFG}/G'_{matrix}). At pH 5 the G'_{EFG} / G'_{matrix} shows a steep increase with increasing oil, whereas at pH 7 the increase is more subtle. In both cases the increase effect becomes more pronounced with an increasing oil content. Similar observations were seen for casein emulsion-filled gels (acidified), polyvinyl alcohol-congo red gels, and whey protein isolate gels, in case the macromolecule covering the particles was selected on its ability to interact with the matrix[171,172]. To further understand the

reasoning behind the higher reinforcement observed at pH 5 compared to pH 7, additional analyses were necessary and are discussed in the following parts, where after a mechanism is proposed in section 5.3.5.

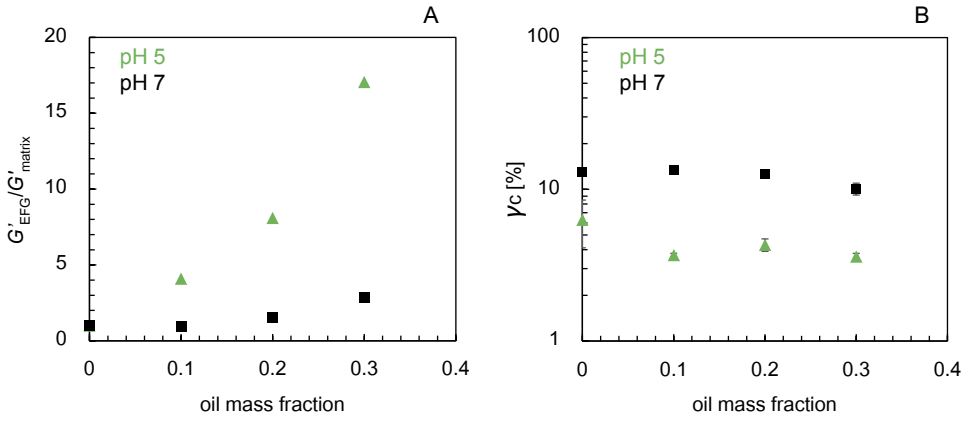

Figure 5.4 A) Degree of reinforcement expressed as G'_{EFG} / G'_{matrix} as function of oil mass fraction and B) critical strain as function of oil mass fraction (right panel). pH 5 is represented by green triangles and pH 7 by black squares. The critical strains are averages from duplicate measurements and the error bars represent the standard deviations.

Apart from the effect of emulsion droplets on gel firmness, another rheological property of the gels that can be influenced by the presence of emulsion droplets is the resistance against deformation. Aiming to assess how the increase in oil concentration affects the end of the linear viscoelastic (LVE) regime of the EFGs, we determined the critical strain of the different EFGs as shown in Figure 5.4. In Figure 5.4B the end of the LVE regime, expressed as a critical strain of EFGs at pH 5 and pH 7, is presented as a function of oil concentration. The critical strain was higher at pH 7 than pH 5 but remained quite constant with increasing oil concentration for both pH values, with critical strain values around 10% and 8%, respectively. In contrast to the increase in G' by oil addition as shown in Figure 5.3, the extent of the LVE regime was much less affected by an increased oil content. This result shows that the structural properties of the gel protein matrix were not affected by the addition of emulsion droplets, indicating that the structural properties are mostly determined by the proteins in the gel matrix. However, this figure only provides limited information about the material's response to deformation and no information about its response beyond the LVE regime. To study the emulsion-filled gels response to large deformation, large amplitude oscillatory shear (LAOS) rheology was used.

Large Amplitude Oscillatory Shear (LAOS)

The response of the emulsion-filled gels to non-linear deformation was studied by applying a strain sweep. At each strain amplitude the oscillatory waveform data was collected and Lissajous plots were constructed for an RPM heat-set gel (matrix) and RPM emulsion-filled gels (EFGs) with varying oil concentrations, at pH 5 and 7 at five strain amplitudes. Figure 5.5 shows the elastic Lissajous plots where the normalized stress versus strain is plotted and Figure 5.6 shows the viscous Lissajous plots, where the normalized stress as a function of normalized shear rate are shown. In the elastic Lissajous plots (Figure 5.5) and 1% strain deformation, the gels are still within their LVE regime and show a narrow elliptical shape, indicating predominant elastic behavior. For the viscous Lissajous plots (Figure 5.6) the elastic response corresponds with a nearly circular shape. When the strain deformation increases to 50%, the elliptical shapes deflect and an overshoot of the stress at maximum strain is observed, indicating intracycle strain stiffening behavior. At pH 5 the curves are slightly wider, which indicates that the viscous response at pH 5 becomes more dominant. This is also seen from the viscous Lissajous plots in Figure 5.6, where the shapes change from circular to rhomboidal. At 100% strain deformation the curves widen further, and the viscous response becomes more dominant at both pH 5 and 7. At 500% strain deformation the behavior at pH 5 and 7 start to diverge. The gels at pH 5 now show a nearly rectangular shape, implying a plastic response -an initially elastic response at maximum strain, followed by yielding and flow at nearly constant stress- while the gels at pH 7 persist in their strain stiffening behavior. The wiggles observed at pH 5, and the bowtie-like shape at pH 7 for $EFG_{0.3}$, probably result from sample or tool inertia effects coupling to the elasticity of the sample.

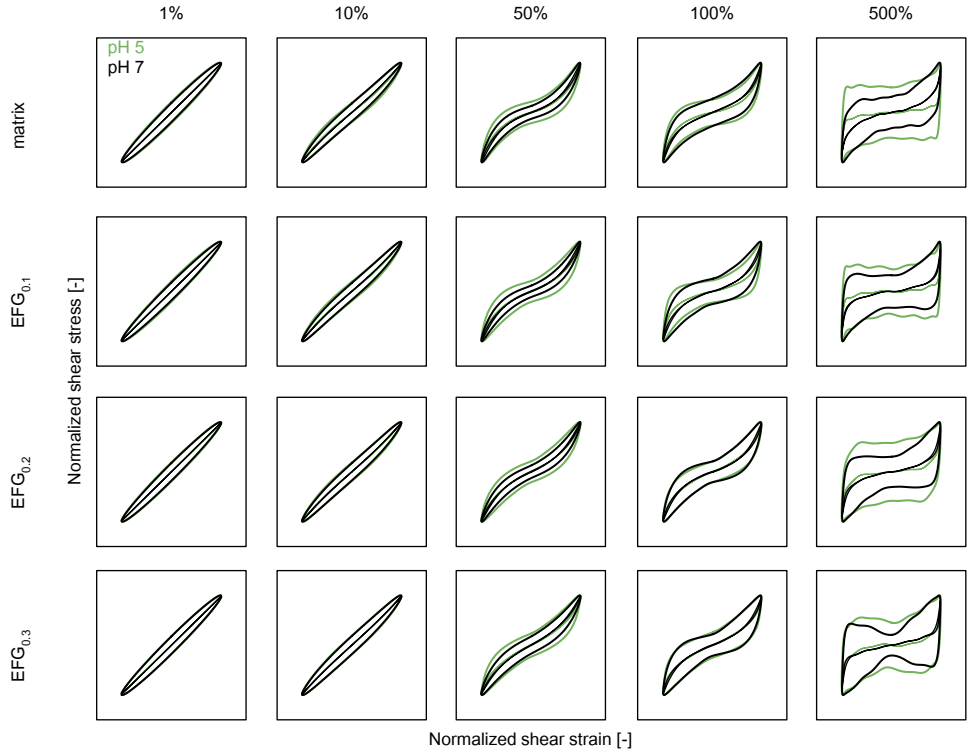

Figure 5.5 Elastic Lissajous plots of normalized stress versus strain, at strain amplitudes of 1, 10, 50, 100 and 500%. The strain amplitudes were applied on the gelled matrix and emulsion-filled gels with 15.0 wt% rapeseed protein mixture (RPM) in the water phase and oil mass fractions ranging between 0.1 and 0.3. pH 5 is represented as green and pH 7 as black. The grey lines within the curves represent the elastic stress contribution.

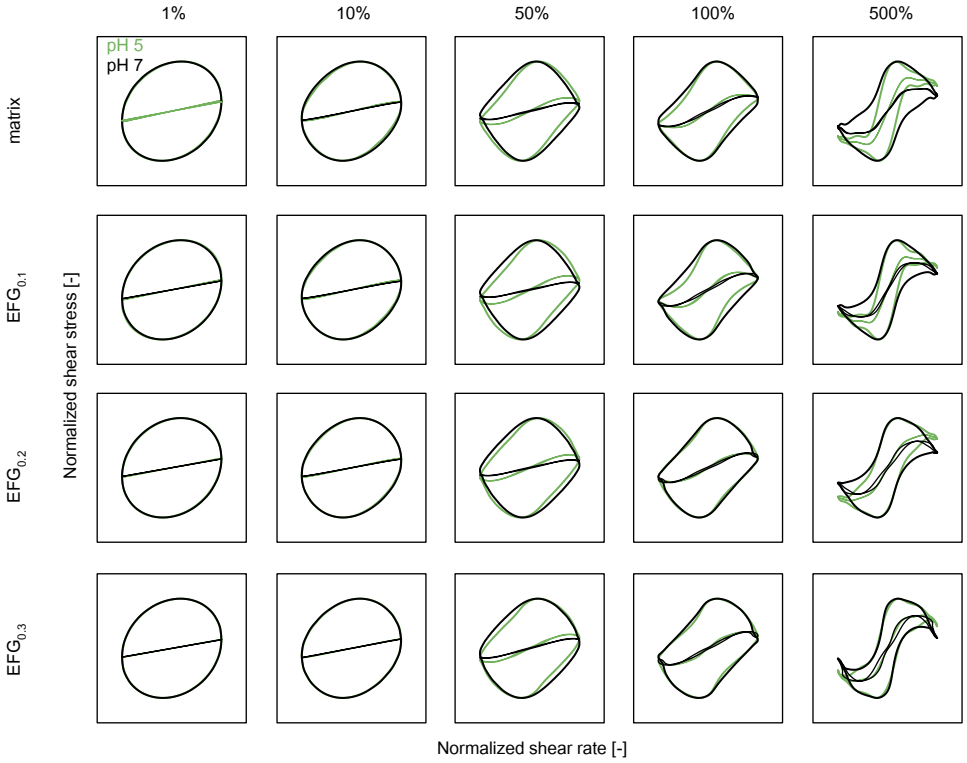

Figure 5.6 Viscous Lissajous plots of normalized stress versus strain rate, at strain amplitudes of 1, 10, 50, 100 and 500%. The strain amplitudes were applied on the gelled matrix and emulsion-filled gels with 15.0 wt% rapeseed protein mixture (RPM) in the water phase and oil mass fractions ranging between 0.1 and 0.3. pH 5 is represented as green and pH 7 as black. The grey lines within the curves represent the viscous stress contribution.

For a more quantitative analysis of the elastic and viscous dominated stages in the response to strain deformation, as well as the transition between them, we plotted the energy dissipation ratio as a function of strain, at a fixed frequency of 1 Hz (Figure 5.7). This is the ratio of the dissipated energy within one cycle divided by the dissipation in a material displaying ideal plastic behavior. As we already saw in the Lissajous plots, oil has little effect on the overall non-linear behavior of the emulsion-filled gels. The results confirm that oil has hardly any effect on the breakdown behavior of EFGs, and that the protein network structure dictates the linear and nonlinear behavior. The above outcome also implies that the connections between emulsion droplets and the proteins are weaker than the connections between proteins, as the emulsion droplets do not lead to an increased deformability of the gel. The pH, on the other hand, affects the non-linear behavior of the gels. Figure 5.7 shows an increase in the energy dissipation ratio already at 20% strain at pH 5, while at pH 7 the increase starts at 70% strain, which indicates that at pH 5 the EFGs are more

brittle than at pH 7. The difference between pH 5 and 7 is probably related to the presence of protein aggregates initially in the system at pH 5, resulting in a weaker (lower *G'*) and more brittle gelled protein structure.

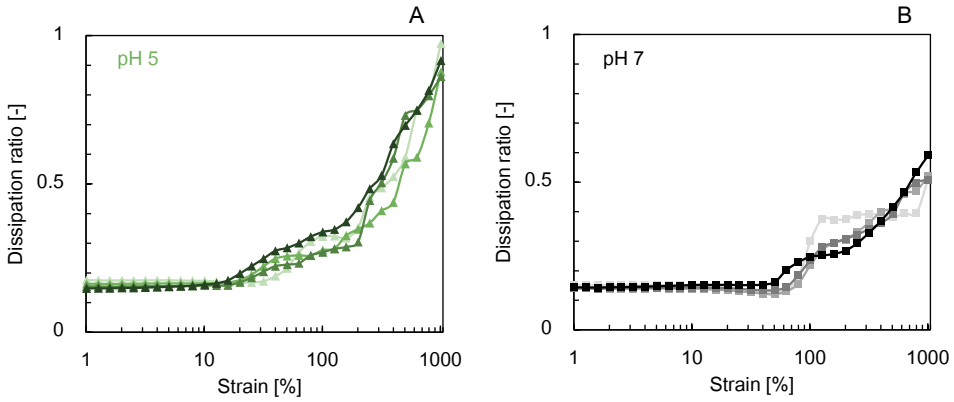

Figure 5.7 Energy dissipation ratios of the gelled matrix and the emulsion-filled gels at A) pH 5 and B) pH 7, with a constant RPM concentration of 15.0 wt% in the water phase and oil mass fractions ranging between 0.1 and 0.3. A darker color represents more oil. All samples were measured in duplicate and a representative curve is shown.

5.3.4 Microstructure of the emulsion-filled gels

Aiming to identify whether the differences observed in the rheological properties between the EFGs at different pH relate to differences in the microstructure of the EFGs, we used confocal laser scanning microscopy (CLSM). In Figure 5.8 the CLSM images of the protein matrices (top row) and EFGs with 10.0 wt% oil (bottom row) at pH 5 (A) and pH 7 (B) are displayed. At pH 5, we observed a heterogeneous protein matrix that consisted of randomly associated large protein aggregates. At pH 7, the protein matrix was more homogeneous with proteins arranged in elongated stranded-like structures. Both protein gel matrices also contained oleosomes (around 1.8 wt% of total mass), shown as spherical droplets, as RPM was extracted from non-defatted rapeseeds. Upon addition of emulsion droplets in the protein matrix, the droplets appeared as part of the protein matrix both at pH 5 and pH 7, without affecting the way the matrix was structured. Here, we present the CLSM images of only the EFGs of 10.0 wt% oil, as the higher opacity of the EFGs at higher oil concentrations did not allow us to get high resolution images.

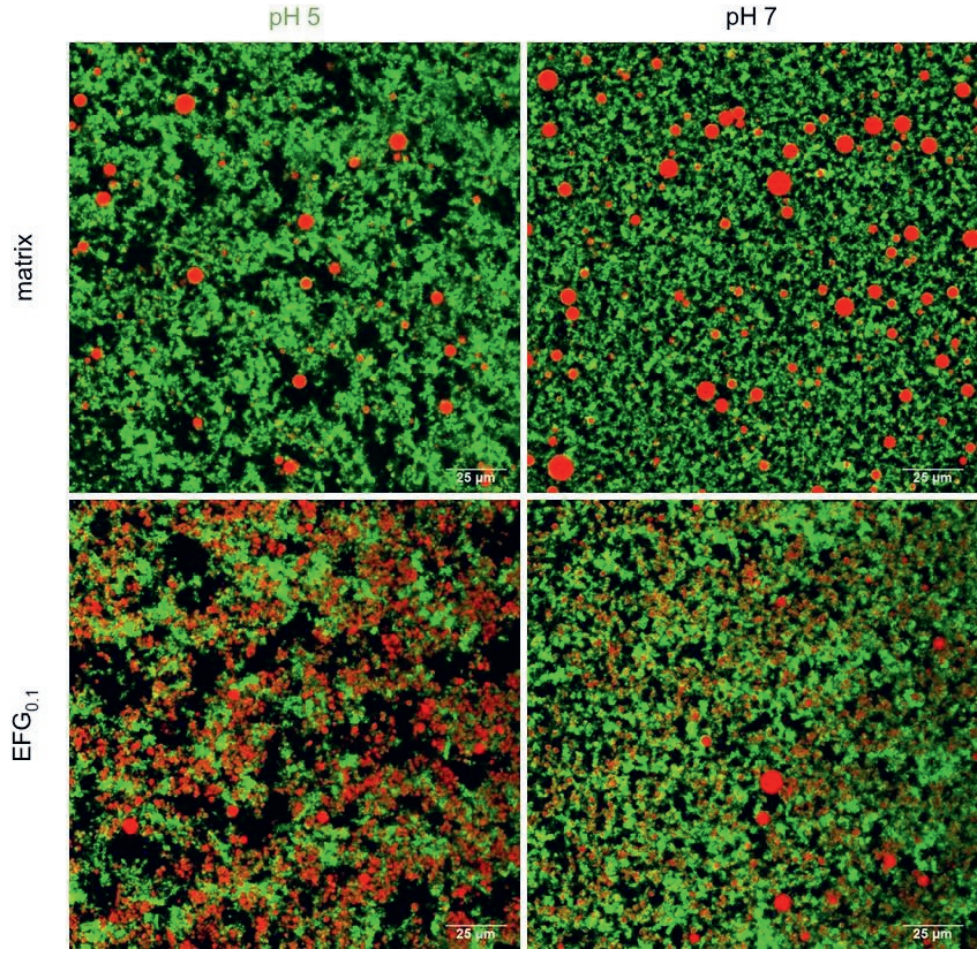

Figure 5.8 CLSM images of; Top row: gelled protein matrix at pH 5 and pH 7, containing 15.0 wt% RPM where the proteins and oleosomes present are visualized, and bottom row: EFGs containing 15.0 wt% RPM and 10.0 wt% oil at pH 5 and pH 7, where the proteins and emulsion droplets are visualized. Proteins and oil are stained with Fast green and Nile red respectively.

Matrix heterogeneity has been previously highlighted as an important parameter for the rheological properties of gels[136], while the formation of particulate-like or strand-like protein gels is pH dependent[173]. At pH 5 the proteins in RPM were less soluble and pre-aggregated before heating, compared to pH 7. This pre-aggregated state resulted in a lower number of connections per unit volume of proteins[136] and possibly partial unfolding of the proteins upon heating[173], leading to a weaker and more heterogeneous protein network. The formation of protein strand-like structures at pH 7 could be attributed to the relatively stronger electrostatic repulsive forces between the proteins at this pH (ζ-potential around -15 mV[111]) which could lead to a parallel arrangement of the

protein polypeptide chains upon unfolding, with increased intermolecular interactions[173]. This arrangement in turn resulted in a more homogeneous and firmer protein network (higher *G'*).

5.3.5 Mechanistic understanding for gel reinforcement by the presence of emulsion droplets

It was found that the presence of emulsion droplets reinforces the gel firmness of rapeseed protein mixture (RPM) gels and that the reinforcement was more pronounced at pH 5 than pH 7. For a better understanding of the mechanism behind this reinforcement, there are three factors to consider.

The first factor is whether the interface of the emulsion droplets interact with the matrix, which determines whether a filler is active or inactive[165]. Earlier research showed that napins dominate the oil droplet interface in emulsions stabilized by RPM, as a result of their small size and Janus-like conformation. Furthermore, cruciferins appeared to weakly interact with the interfacial layer of napins[30]. The napin-cruciferin interactions at the emulsion droplet-matrix interface suggest that the napin-stabilized emulsion droplets can be present as active fillers in a protein network built by cruciferins.

The second factor to consider is the stiffness of the droplets relative to the matrix, which can be expressed by the M ratio:

$$M = \frac{G'_{filler}}{G'_{matrix}} \tag{5.2}$$

When M < 1 the matrix is stiffer than the filler, and when M > 1 the emulsion droplets (fillers) are stiffer than the matrix. Given that stiffer droplets can interact with the matrix (active fillers), they gel structure can be reinforced[167,171,174]. The *G'* of the matrix was measured, and the G' of the filler can be estimated using:

$$G'_{filler} = \frac{2E'_d}{r} \tag{5.3}$$

which is an expression based on van Vliet (1988)[171]. In its original form, this expression is based on the surface tension of the oil-water interface, which is appropriate for interfaces stabilized by low molecular weight surfactants. Here, as the interface was stabilized by proteins -which form interfaces with a predominantly viscoelastic solid-like behavior- the interfacial tension was replaced by the dilatational elastic modulus (E_d').

In earlier research[30] the dilatational elastic modulus was found to be around 25 mN/m, and the average droplet size of the emulsions ($d_{4,3}$) was around 2 µm as shown in Table 5.1. Taking into account these values the estimated G'_{filler}, and the measured G' values for the RPM matrix at pH 5 and 7 were used to determine the M ratio. The M ratios were 126 and 12 at pH 5 and 7, respectively. This indicates that the emulsion droplets were stiffer than the matrix, and thus would have the potential to reinforce emulsion-filled gels. Considering that the stiffer napin-stabilized droplets interact with the protein matrix as suggested earlier, they can reinforce the gel firmness by increasing the number of connections per unit volume of the protein network. The 10-fold higher M ratio at pH 5 compared to pH 7 (126 vs 12) also indicates that the emulsion droplets are significantly much stiffer (higher G'_{filler}) than the protein matrix at pH 5 compared to pH 7. This difference can also justify the higher degree of reinforcement observed at pH 5 after the addition of emulsion droplets.

The third factor to consider is the matrix microstructure. In the CLSM images (Figure 5.8), we showed that at pH 5 gels with higher heterogeneity built of protein aggregates were formed, whereas at pH 7 the gels had a more homogeneous structure built of protein strands. The same microstructure was observed upon addition of emulsion droplets. It has been previously reported that in EFGs, a higher degree of matrix heterogeneity results in a larger gel reinforcement effect by addition of oil, compared to more homogeneous gels[175]. The suggested explanation for this increase is the accumulation of the dispersed droplets in the protein-poor regions of heterogeneous protein matrices, increasing the effective volume fraction of the droplets[175].

The higher degree of gel heterogeneity observed here at pH 5 can also justify the higher reinforcement of the gel firmness observed at pH 5 compared to pH 7. However, in contrast to the suggested changes in the gel structure by oil addition in the aforementioned study (i.e. accumulation of droplets)[175], in the CLSM images (Figure 5.8) we did not observe any changes in the type of protein gel network (i.e. aggregates or strands) or changes in the heterogeneity or homogeneity of the structure upon addition of emulsion droplets, neither at pH 5 nor pH 7. The unchanged microstructure of EFGs in addition to the unchanged critical strain or response of the gel structure to large deformations upon addition of emulsion droplets, suggests that the microstructure of the protein matrix and the EFGs is dictated by protein-protein interactions.

Therefore, the added emulsion droplets, being stiffer than the protein matrix and interacting with the protein matrix, act like protein particles that increase the number of connections between the proteins. Thus, the size and effective volume fraction of the protein aggregates or strands is increased, resulting in higher gel firmness (i.e. higher G').

The rheological data, combined with CLSM images, also give some insight into how the gel network is built on a microscale. According to the scaling model developed by Shih et al. (1990), the gel structure can be classified by two regimes, in which either the inter- or intra-floc links are stronger[176]. In a weak-link regime, the inter-floc links are weaker than the intra-floc links, whereas in a strong-link regime the inter-floc links are stronger than the intra-floc links[176]. To quantify this accurately, one needs to determine the dependence of G' and γ_0 on matrix protein concentration, which was out of scope for this study. This is typically quantified for protein gels, without the added complexity of incorporated oil (i.e. emulsion-filled gels). The CLSM images suggested that emulsion droplets were incorporated within protein network, and that the protein aggregates (pH 5) or strands (pH 7) increased in size with increased oil content. Rheological data showed that the γ_0 was hardly affected by an increased oil content. If the gels were in a strong-link regime it would be expected that an increased oil content would affect the breakdown behavior, as new type of interactions between the matrix and droplet interface are formed. We did not observe an effect of oil on the $\gamma_{0,}$ which is why it is hypothesized that RPM forms weak-link gels.

5.4 Conclusions

We showed that when napins and cruciferins are both present in a less purified rapeseed protein mixture, can have complementary roles in structuring EFGs, with napins stabilizing the emulsion droplets and cruciferins building the protein network. In the emulsion-filled gels, pH played an important role in the type of protein network formed upon gelation; at pH 5 a more heterogeneous protein network and less firm emulsion-filled gels were formed compared to pH 7, possibly due to the higher pre-aggregated state of cruciferins at pH 5. Independent of pH, the presence of emulsion droplets led to increase of the gel firmness with more pronounced effects at low pH. The mechanism of reinforcement of EFGs by the presence of emulsion droplets is attributed to the fact that the added emulsion droplets were stiffer than the protein matrix, and interacted with the protein matrix, acting as “effective” protein particles that increase the number of connection points in the protein network. Our results can inspire food manufacturers and scientists to exploit the potential complementary functionalities of various extracted plant proteins to create multi-functional ingredients that can enhance the performance of plant-based foods.

Chapter 6

Linking oleosome monolayer properties with oleosome functionality

This chapter has been submitted as: Ntone, E., Rosenbaum, B., Sridharan, S., Willems, S.B.J., Moultos, O., Vlugt, T.J.H., Meinders, M., Sagis, L.M.C., Bitter, J.H., & Nikiforidis, C.V. (2021). Smart lipid balloons: Stimuli-responsive natural lipid droplets for selective lipid trafficking

Abstract

Oleosomes or as called lipid droplets, play a crucial role in the biological function of cells, due to their ability to traffic lipids through their triacylglycerol core. In this work, by combining experimental techniques with molecular dynamics simulations, we show the molecular mechanism behind the ability of these natural carriers to traffic lipids and any hydrophobic molecules (absorption or release), which is controlled by the oleosome phospholipid monolayer. Through hydrophobic forces, lipids can permeate the oleosome monolayer and rest in their core, leading to an oleosome volume expansion and decrease of the monolayer density. Similarly, the release of lipids from the oleosome core leads to oleosome deflation, like a balloon losing its air content, proving a release mechanism through a channel. The ability of the oleosomes to expand in volume or shrink is assigned to the weak lateral molecular interactions in the phospholipid monolayer which sits on the liquid triacylglycerol core, permitting a reversible dilation. The mechanistic understanding of lipid trafficking by oleosomes is ameliorating the understanding the oleosome functions, which can lead to delicate and targeted carrying and delivery of therapeutics for disease treatments.

6.1 Introduction

Oleosomes, also known as oil bodies or lipid droplets, are ubiquitous cell organelles increasingly acknowledged in cell biology as dynamic molecular machinery, heavily contributing to cell homeostasis[177]. A major contribution of oleosomes to cell homeostasis is by realizing lipid trafficking; Oleosomes absorb free lipids to prevent lipotoxicity and regulate lipid supply[178], act as hubs of lipid synthesis and accumulation[19,179–182], or supply lipids to other cell organelles[180–182] and even invasive microorganisms[183].

During triacylglycerol biogenesis from the endoplasmic reticulum (ER)[184], oleosomes are formed by coating the triacyclglycerols with a monolayer of phospholipids (PL) decorated with enzymatic or structural proteins[185–187]. Many studies have reported that located enzymes[188] and proteins[189–192] in the monolayer mediate the production of lipids or their lipolysis in oleosomes and also the interaction of oleosomes with surrounded organelles[180–182].

However, it is possible that the phospholipid monolayer of oleosomes provides the necessary mechanical properties that make oleosomes capable to absorb free lipids in the cell or to supply lipids to other cell organelles. Similar to membrane bilayers, lateral packing, expandability, or compressibility of the phospholipids should be very important to oleosome functions[193]. Diffusion of apolar lipids through the phospholipid monolayer into the oleosome core and the supply of lipids from oleosomes to neighboring organelles require oleosomes with the ability to deform, by expanding in volume or shrink[180,181,194]. Both phospholipid monolayer density (number of phospholipids per surface area) and lateral phospholipid interactions should be pivotal to this capability of oleosomes, as they define the resistance of oleosomes to deformation[195]. The oleosome monolayer density also designates the direction of molecular diffusion in or out of oleosomes[19].

The exact mechanism and correlation between the phospholipid monolayer properties and lipid trafficking by oleosomes is not yet comprehended, mostly due to limitations of the analytical techniques being used. In this work, to identify the molecular mechanism behind the ability of oleosomes to traffic lipids, we employed experimental soft matter science combined with molecular dynamics simulations. The synergy of experimental techniques with simulations helps to bypass the limitations of each methodology and suggest on a molecular level the mechanism behind the main oleosome regulatory function.

With this knowledge we are aiming to understand the mechanism that these natural carriers are using for lipid trafficking, and use them in turn for selective trafficking of hydrophobic therapeutic molecules[20,196,197]. A schematic overview of lipid trafficking realized by oleosomes resulting to

oleosome volume expansion or shrinkage, and the approach used in this work to identify the underlying mechanism behind the main oleosome function is given in Figure 6.1.

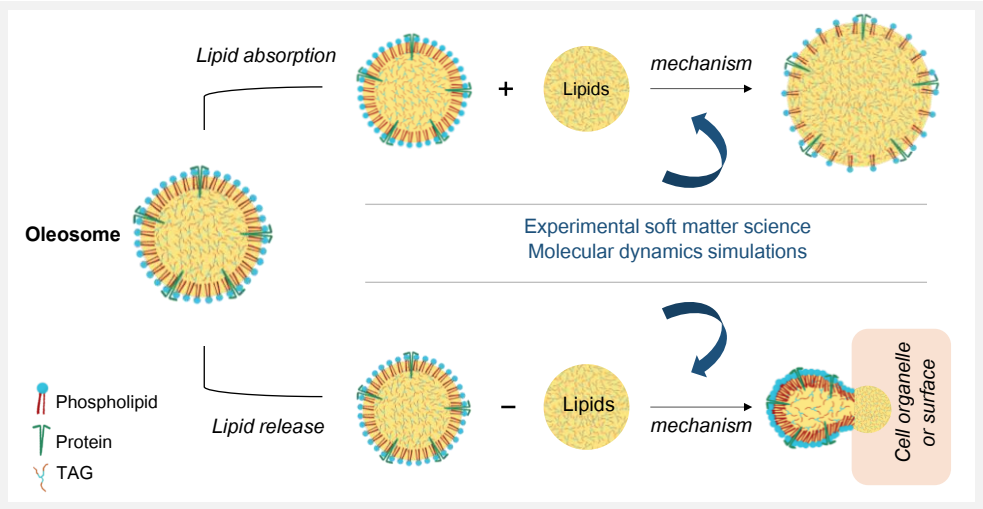

Figure 6.1 Schematic overview of lipid trafficking realized by oleosomes resulting to oleosome volume expansion or shrinkage, and the approach used in this work to identify the underlying mechanism behind the oleosome function. Size of molecules not to scale.

6.2 Materials and methods

6.2.1 Materials

The oleosomes were extracted from untreated Alize rapeseeds stored at -18°C. All chemicals used were of analytical grade and were purchased from Sigma Aldrich (St Louis, MO, USA).

6.2.2 Purification of rapeseed oleosomes

Pure oleosomes were extracted using the protocol as described by de Chirico et al. 2018[60] with the following modifications: 100 g of dehulled rapeseeds were soaked in sodium bicarbonate pH 9.5 (0.1 M) in seeds to buffer ratio of 1:7 w/w for 4 hrs under continuous stirring (RW 20 digital stirrer, IKA ®, Staufen, Germany) to ensure proper mixing. After soaking, the seeds were blended at maximum speed for 90 seconds (Philips Avance HR2093, Eindhoven, the Netherlands). As a first step to remove the solids, the mixture was passed through a cheesecloth. The filtrate was centrifuged (30 min.; 10000 g; 4°C; SORVALL Legend XFR centrifuge by Thermo Fischer SCIENTIFIC, Waltham, USA) in 250 mL centrifuge tubes to remove extraneous proteins and fibers. After centrifugation, the top layer (cream) was collected. The cream layer was spread over a filter paper (Whatman ®, grade 4) to absorb most of the remaining liquid. The cream was resuspended in new extraction medium (1:4 w/w) and centrifuged under the same conditions. After

the second centrifugation, the cream layer was collected in the same manner and resuspended in deionized water (1:4 w/w). A third and final centrifugation followed, and the cream layer containing purified oleosomes was again collected and stored at 4°C until further use.

6.2.3 Homogenization of purified oleosomes with free lipids

The purified oleosomes were dispersed in deionized water to a final concentration of 10.0 wt% oleosomes. 70g of oleosome dispersion was first sheared using a disperser (Ultra-Turrax, IKA®, Staufen, Germany) at 8000 rpm for 30 s. Next, rapeseed oil was slowly added to the dispersion in a mass ratio of 1:1 or 1:3 of LDs in the dispersion (i.e. 7 g) to rapeseed oil (7 and 21 respectively) and sheared for 1 min at 10000 rpm. The formed coarse emulsion was further processed with high-pressure homogenizer (GEA®, Niro Soavi NS 1001 L, Parma, Italy) for 5 cycles at 300 bars. The number of experiments and additional analyses was at least n ≥ 3 of independent experiments.

6.2.4 Particle size distribution of oleosomes before and after free lipid absorption

The particle size distribution of the oleosomes after treatment was determined by laser diffraction using a Bettersizer S3 Plus (3P Instruments GmbH & Co. KG, Odelzhausen,Germany). The measurement settings were adjusted to a refractive index 1.46-1.47 and a density 0.91 g/cc for rapeseed LDs. 1.0 wt% Sodium Dodecyl Sulfate (SDS) was added to the samples in a ratio of 1:1 (v/v) to disrupt possible aggregates and determine the individual particle size. The stirring speed of the small volume sample dispersion unit was set to 1,600 rpm.

The measurements were reported as volume ($d_{4,3} = \Sigma n_i d_i^4 / \Sigma n_i d_i^3$) and surface ($d_{3,2} = \Sigma n_i d_i^3 / \Sigma n_i d_i^2$) mean diameter where n_i is the number of droplets with a diameter of d_i. The average values are a result of measurements of at least three individual samples (n ≥ 3) and the ± symbol represents the standard deviation.

6.2.5 Calculation of surface area and estimation of molecules per surface area before and after free lipid absorption by oleosomes

The total area (A_T) of the oleosomes before and after contact with the clustered hydrophobic molecules (TAGs) was calculated using equation:

$$A_{\mathrm{T}} = A_{\mathrm{d}} \times N_{\mathrm{d}} \tag{6.1}$$

where A_d is the area of one droplet and equals to $A_{\mathrm{d}} = 4\pi(\frac{1}{2} d_{3,2})^2$, N_d is the number of droplets, equal to $N_{\mathrm{d}} = \frac{V_{oil}}{V_{\mathrm{d}}}$, V_d is the volume of one droplet, equal to $V_{\mathrm{d}} = \frac{4}{3}\pi(\frac{1}{2} d_{3,2})^3$.

The number of phospholipids (N_{PL}) per area was estimated using equation:

$$N_{PL} = \frac{\frac{M_T}{M_w}}{A_T} \times N_A \quad (6.2)$$

M_T equals the total mass of phospholipids in the reference oleosome dispersion, assuming that this is 0.6 wt% of the total oleosome mass[198]. PL in seed oleosomes composes around 0.6-2 wt%[90,198,199] while proteins are 0.4-1.4 wt% of the total oleosome mass[26,90]. We used PL for exemplification, but the same trend is expected for proteins associated with oleosomes.

M_w is the molecular weight of the phospholipids. Assuming that these are all phosphatidylcholine,

M_w equals 786.1 g/mol, N_A is Avogadro's number ($6.02214*10^{23}$ mol^{-1}). The inverse quantity ($1/N_{PL}$) gives the Area per PL.

6.2.6 Confocal Laser Scanning Microscopy (CLSM)

The structure of oleosomes before and after free lipid absorption was studied using a Confocal Laser Scanning Microscope (Leica SP8-SMD microscope, Leica Microsystems, Wetzlar, Germany) with a 63x magnification water immersion lens. The samples were diluted 100x in deionized water. Nile Red (0.01 wt% in ethanol) was used to stain the lipids in a ratio of 1:200 (v/v) dye solution to sample. Nile red was excited at 488 nm and the emission was measured between 500 and 600 nm. The images were analyzed using the Leica Application Suite X software.

6.2.7 Dilatational interfacial rheology

To apply dilatational interfacial rheology, the oleosome monolayer was reconstructed in a drop tensiometer using the isolated molecules present in the oleosome monolayer of the purified rapeseed oleosomes. First, the purified oleosomes were dried in the oven at 45°C for 2 days. The dried oleosomes were defatted using Soxhlet extraction with petroleum ether for 7h. The remaining solids (molecules from monolayer) were left under the fume hood for solvent evaporation for 2 days. The solids were ground to a fine powder using a mortar and stored at -18°C until further use. Dispersions containing 0.05-0.001 wt% of the isolated monolayer molecules were prepared in deionized water in a conical glass flask. To ensure solubilization each dispersion was subjected to an ultrasonication bath for 1h prior to the measurements.

Oscillatory dilatational interfacial rheology was applied to characterize the interfacial elastic (E_d') and viscous (E_d'') moduli as a function deformation amplitude using an automated drop tensiometer (ADT, Tracker, Teclis-instruments, Tassin, France). The oleosome monolayer

dispersions were transferred into the cuvette, the syringe was immersed and 15 mins of waiting time was applied for any insoluble material to settle down and any air bubbles created from the sonication to reach the surface. Thereafter, the first oil droplet was expelled and a new oil droplet with a surface area of 20.0 mm^2 was created at the tip of a rising-drop capillary needle (gauge 20). Stripped rapeseed oil was used. The interfacial tension γ was calculated from the shape of the droplet using the Laplace equation and monitored for 2 h (7200 s) at 20°C. After, the droplet was subjected to sinusoidal deformations with an amplitude of 5-50% of its original surface area at a constant frequency (0.02 Hz). Each amplitude consisted of a series of 5 cycles followed by a period of 5 blank cycles. The interfacial tension and area changes were recorded during oscillations, and the dilatational elastic (E_d') and viscous (E_d'') moduli were obtained according to equations:

$$E_d' = \Delta\gamma \left(\frac{A_0}{\Delta A}\right) \cos\delta \tag{6.3}$$

$$E_d'' = \Delta\gamma \left(\frac{A_0}{\Delta A}\right) \sin\delta \tag{6.4}$$

where $\Delta\gamma$ is the change of interfacial tension at each deformation, A_0 is the initial droplet surface area (20.0 mm^2), ΔA is the change in droplet surface area and δ is the phase shift oscillatory interfacial tension signal. The results are an average of two individual samples (n = 2).

6.2.8 Contact of purified oleosomes with hydrophobic surfaces

Fluorescent microscope imaging was employed to study the contact establishment of oleosomes with surfaces of different hydrophobicities. A patterned surface consisting of hydrophobic and hydrophilic lanes was prepared according to ref.[200]. The surface was modified with 1H, 1H, 2H, 2H-perfluorooctyl trichlorosilane (PFOTS), which is hydrophobic. First, microscope coverslips were cleaned in ethanol and water then dried. Coverslips were then placed in a plasma oven for 5 minutes at high energy to 'activate' the surface and generate free silanol groups (this allows for the trichlorosilane part to form an assembled monolayer on the glass surface). The coverslips were then placed in a glass petri dish in a desiccator along with a glass vial containing 100 µL of pure PFOTS (the PFOTS is therefore not directly in contact with coverslips). The desiccator was then pumped down to high vacuum, the pump was switched off and the desiccator was left overnight for chemical vapor deposition (CVD) of PFOTS on the coverslips (general method for creating coatings on (glass) surfaces). The next day the slides were removed from the desiccator, washed with isopropanol, dried, and left in the oven at 70°C for at least 30 minutes. For creating patterns, PDMS stamps with line features were cut to an appropriate size (around 0.75 cm^2), sonicated in ethanol, and then placed on the PFOTS glass surface. Plasma treatment for 4 cycles of 1 minute

each was then applied to etch away unprotected areas of the surface. A schematic representation of the preparation process of the surfaces is given in Figure 6.2. As a reference complete hydrophilic surface, plain microscope cover slips were used which were plasma treated accordingly to remove any impurities.

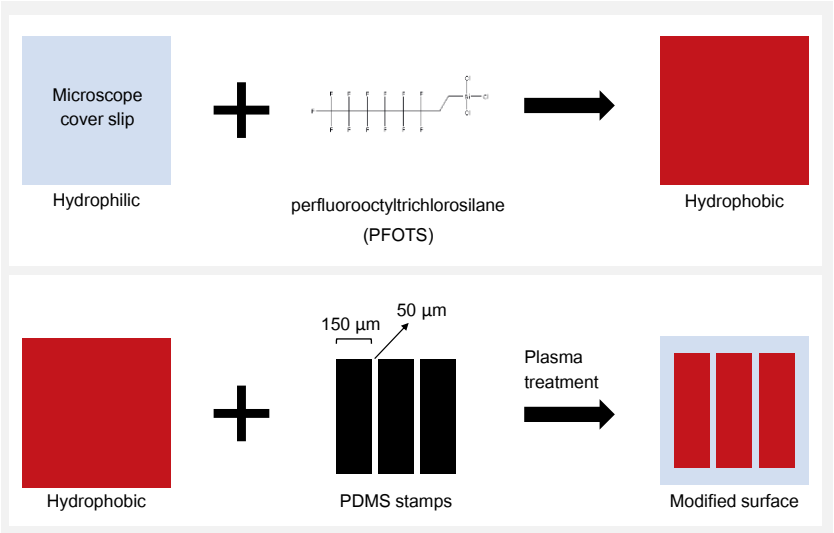

Figure 6.2 Flow diagram of preparation of surfaces with alternating hydrophobic and hydrophilic lanes.

The dispersions of 10.0 wt% oleosomes were diluted 100 times in deionized water and Nile red was added to stain the lipid phase. The functionalized surfaces were fully covered with the oleosome dispersions for 10 mins. Thereafter, the surfaces were gently rinsed with deionized water to remove the excess oleosomes and dried under nitrogen at very mild flow rates. The surfaces were then visualized under a fluorescent light microscope (Leica DMi8, Leica Microsystems, Wetzlar, Germany). To exclude any effect of the added fluorescent dye on oleosome contact establishment with the surfaces, samples without the addition of dye were also prepared and studied under the light microscope.

Pure hydrophobic (non-patterned) and hydrophilic surfaces were used to determine their contact angles (drop tensiometer). A drop of 5 µl deionized water was placed on the corresponding surface and the contact angle was measured using the one measurement option for a rising drop in a drop tensiometer (ADT, Tracker, Teclis-instruments, Tassin, France). The values were found to be 102° and 60° for the hydrophobic and the hydrophilic surface respectively.

6.2.9 Atomic force microscopy (AFM)

For simplicity in the analysis, non-patterned modified hydrophobic surfaces were used to study the outcome of oleosome contact with hydrophobic surfaces with atomic force microscopy. Oleosome dispersions were prepared as mentioned before without the addition of Nile red and the same procedure of incubation and rinsing was followed.

The surfaces were imaged using an atomic force microscope (AFM, MultiMode 8-HR, Bruker, USA). A scanasyst(R) air probe was used with a tip diameter of 2 nm. The bruker scanasyst tapping mode was used and an image with a scan size of 12.5 x 12.5 µm, scan rate of 0.977 Hz and 256 lines was used. The images were analysed using Nanoscope Analysis 1.5 software (Bruker, USA).

6.2.10 Molecular dynamics simulations

The open-source MD simulation package GROMACS 2020.2[201] was used for all simulations. Newton's equations of motion were integrated using the leap-frog algorithm with a timestep of 20 fs. The coarse-grained Martini 3 force field[202] was used to model all components. Most simulations were conducted on 28 cores achieving simulation speeds of ca. 300 ns/day. The cutoff for the van der Waals and electrostatic interactions was set to 1.1 nm. VMD 1.9.3[203] was used for all visualizations. Our initial system consisted of an oleosome droplet made of a triolein core and DPPC as the single PL in the monolayer, and a similar size droplet of assembled triolein molecules. Triolein was chosen as it is the major cellular neutral lipid[204], and DPPC as the most commonly used PL in molecular simulations[202]. Both the oleosome and the assembled triolein droplet contained 2560 triolein molecules, and had radii of approximately 11 nm (Table A6.1, Appendix). The PL density of the oleosome monolayer was varied by using 1200, 1600, and 2000 DPPC molecules, corresponding to PL densities of 0.7, 0.9, and 1.1 PL/nm^2, respectively. These densities correspond to the mass range of PL in seed LDs (0.6-2.0 wt%)[90,198,199]. Radii and PL densities of all droplets can be found in Table A6.1 (Appendix). The simulation box dimensions were set equal to 52 x 32 x 32 nm. Periodic boundary conditions were imposed in all directions. The molecules from the Martini representation comprising the system were water (WN) as the solvent, DPPC as the single PL covering oleosomes, and triolein as the lipid inside the oleosome and the free triolein droplet, shown in Figure 6.3. The triolein molecule for Martini was constructed based on ref.[205], while the force field details for the rest of the molecules are taken from ref.[202]. Figure 6.3 shows the Martini representation of the simulated molecules and the group (bead) names.

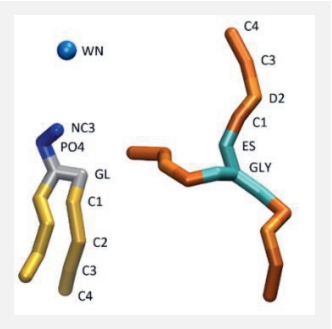

Figure 6.3 The molecules simulated in this study using the coarse-grained Martini force field[201]. Left: water and DPPC, right: triolein. In this study, the number of water, DPPC and triolein molecules used was equal to 350,000, 1,200 and 2,560, respectively. The coloring scheme for all molecules is consistent with the one used in the main manuscript.

The initial configurations comprised two subsystems, each one containing a simulation box with a hydrated TAG and oleosome droplet, respectively. These two boxes were positioned next to each other along the x axis, separated by 0.47 nm. 400 ps runs at 305 K and 1 bar in the isothermal isobaric ensemble (*NpT*) were carried out to homogenize the two subsystems and equilibrate the final system. Production runs of 50 ns at 305 K and 1 bar in the *NpT* ensemble were performed for simulating the fusion of the droplets. The Berendsen[206] and Parrinello-Rahman[207] barostats with coupling constants of 12 ps were used for the equilibration and production runs, respectively. The velocity rescale thermostat[208] implemented in GROMACS with a coupling constant of 1 ps was used in all runs. In order to obtain statistics for the fusion phenomena, ten independent production runs were performed, each one starting from a different initial configuration.

For the computation of radial component densities (RCDs), 200 concentric bins were used. The RCDs are averaged over the number of beads and timeframes, where timeframes were sampled every 10 ps, and divided by the number of frames and the volume of the bin to obtain the component density with a unit of nm^{-3}. At least 10 ns of simulation time were carried out for the computation of RCDs.

The standard deviation of a binomial sampling distribution $\hat{p}$ can be calculated from:

$$\sigma_{\hat{p}} = \sqrt{\frac{p(p-1)}{n}} \tag{6.5}$$

Where p is the population proportion and n is the sample size.

6.3 Results and discussion

In this work, we investigated the correlation of the molecular properties of the oleosome monolayer with lipid trafficking, and the underlying mechanism behind this relation. To suggest the mechanism behind lipid trafficking by oleosomes on a molecular level, we combined experimental soft matter science, including light scattering, advanced microscopy, surface functionalization and interfacial dilatational rheology, with coarse-grained molecular dynamics (MD) simulations.

6.3.1 Oleosomes dispersed in aqueous systems can absorb free lipids and fuse to maintain the molecular density at their monolayer

To investigate the ability of oleosomes to absorb free lipids, expand in volume, and adjust the density of their monolayer, we first purified oleosomes from rapeseeds (*Brassica napus*). We chose rapeseeds as a model system since they are eukaryotic organisms with a plethora of oleosomes. The purified oleosomes were recovered as a concentrated cream which contained 24.2 ± 2.8 wt% moisture. Lipids consisted 95.8 ± 0.9 wt% of the total dry weight while proteins accounted for 2.0 ± 0.1 wt% of the total dry weight. The protein profile of oleosomes showed the presence of mainly oleosins at the interface (Figure A6.1, Appendix), which are the main structural proteins related to rapeseed oleosomes[209,210]. We thereafter dispersed the oleosomes in deionized water at a final oleosome concentration of 10.0 wt% and vigorously mixed them with free triacylglycerols (TAGs) at different oleosome to TAGs ratios.

To investigate the response of oleosomes upon contact with free TAGs, we first determined the particle size distribution of oleosomes before and after lipid absorption (Figure 6.4A). The initial size distribution of oleosomes ranged from 0.5 to 10.0 μm with an average individual particle size ($d_{4,3}$) of 1.7 ± 0.1 μm, which is within the size range generally reported for cytoplasmic oleosomes[20,187]. By adding free TAGs in the oleosome dispersion in a 1:1 Oleosome:TAGs mass ratio and after a homogenization step, we observed that there was almost no change in the size distribution ($d_{4,3}$ = 1.7 ± 0.4 μm), suggesting that the number of droplets was doubled. This result shows that the number of monolayer molecules initially present in oleosomes were adequate to stabilize the additionally created surface. Further increase in the mass of added free TAGs (1:3 Oleosome:TAGs) led to a shift of the size distribution to higher values and a significant increase of the oleosome size, with the $d_{4,3}$ value increasing from 1.7 ± 0.1 to 3.3 ± 0.5 μm. This increase in size suggests droplet coalescence, possibly due to the inability of the molecules present to stabilize the significantly higher amount of TAGs and surface area.

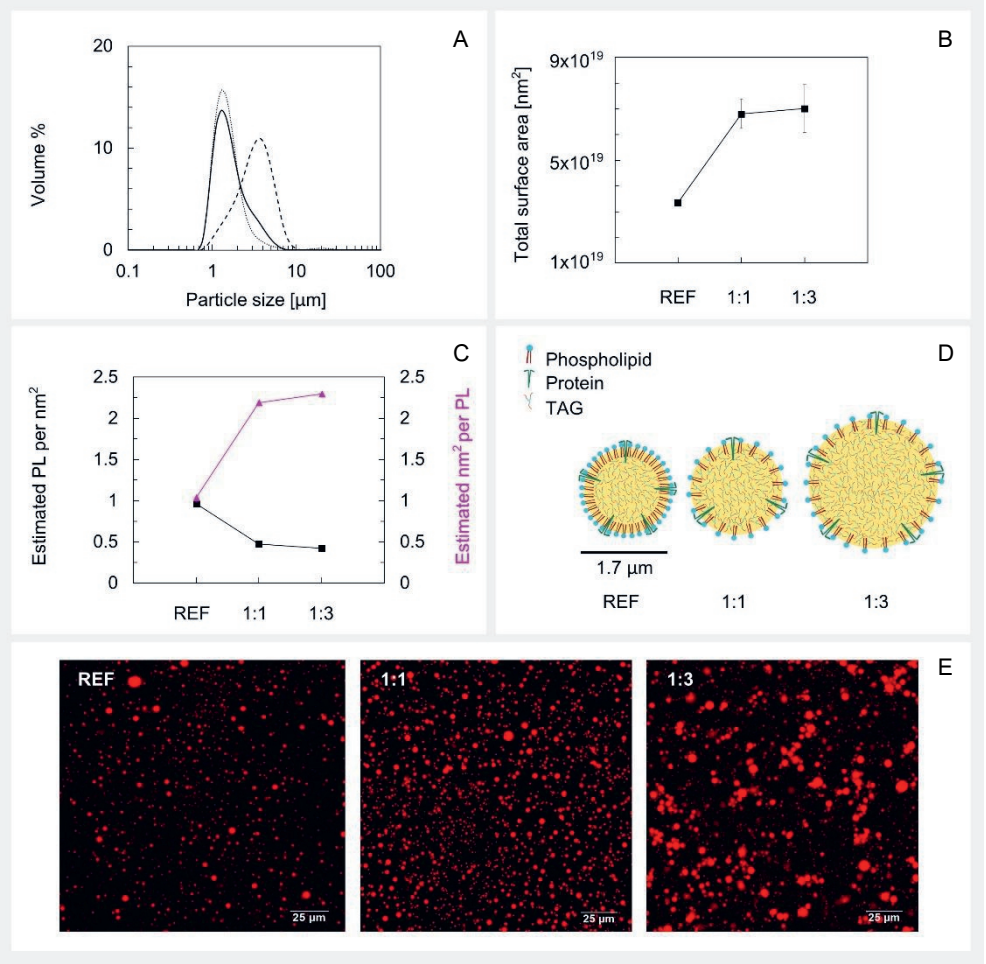

Figure 6.4 A) Individual droplet size distribution of oleosomes as a volume% at reference state (continuous line) and after TAGs addition in the oleosome dispersion at a ratio of 1:1 (dotted line), 1:3 (dashed line), B) Total surface area of oleosomes as a function of increasing TAG mass, C) Estimated number of PL per surface area (black square symbol) and estimated area per PL (magenta triangle symbol) as a function of increasing TAG mass, D) Schematic representation of the oleosome monolayer after free TAGs absorption showing changes in the molecular density in the monolayer (size of molecules not to scale), E) CLSM images of oleosomes at reference state (REF) and after TAGs addition in a mass ratio of 1:1 and 1:3 stained with Nile Red. Scale bar: 25 µm.

To assess the changes in monolayer density upon TAGs absorption by oleosomes, we estimated the number of molecules per area of oleosomes before and after the addition of free TAGs. For this calculation, we first determined the total oleosome surface area before and after fusion using Equation 6.1 (Methods), as illustrated in Figure 6.4B. Secondly, we presented the changes in monolayer density as changes in the number of PL per Area or Area per PL using Equation 6.2 (Methods), as shown in Figure 6.4C. For simplicity, we focused the discussion of this manuscript on PL, however, since proteins (i.e. oleosins) are also present in the oleosome monolayer we expect a similar trend.

The initial aqueous dispersion of 10.0 wt% oleosomes resulted in an initial total surface area of ca. $3x10^{19}$ nm^2 (Figure 6.4B). Taking into account that a minimum of 0.6 wt% of oleosomes are PL[198], we estimated that the oleosome monolayer surface had an initial density of 1 PL per nm^2 (or a corresponding area of 1 nm^2 per PL) (Figure 6.4C). After mixing with free TAGs in 1:1 mass ratio, since the particle size distribution and average oleosome size hardly changed ($d_{4,3}$ = 1.7 ± 0.4 µm), whereas the number of lipid droplets was doubled, the surface area is doubled ($7x10^{19}$ nm^2). As the number of PL present in the dispersion was constant, the monolayer density of the newly formed oleosomes is now half of that of the reference system (0.5 PL/nm^2 vs 1 PL/nm^2). This monolayer density corresponds to 2 nm^2 available per PL instead of 1 nm^2 per PL in the reference system, suggesting the formation of LDs with surface voids. At the lowest Oleosome:TAGs ratio (1:3), the resulted particle size ($d_{4,3}$ = 3.3 ± 0.5 µm) led to a similar total surface area ($7x10^{19}$ nm^2) with a similar PL density (0.4 PL/nm^2), corresponding to an available area of approximately 2 nm^2 per PL (Figure 6.4B,C). A schematic representation of the estimated oleosome monolayer molecular density after free TAGs absorption is given in Figure 6.4D. The fact that at this LD:TAGs ratio (1:3) the surface area and PL density remained almost constant at the expense of an increase in oleosome size, indicates that the number of PL molecules present was not adequate to sufficiently cover the additional interface to prevent coalescence and create stable droplets[211]. The droplets coalesced (fused) to maintain the PL monolayer density constant and minimize the Gibbs free energy. In cells, fusion between oleosomes has also been related to the shortage of molecules in the monolayer[212–216].

Given that oleosomes could incorporate even 3 times their initial lipid mass, fuse, and form stable droplets with lower monolayer density, is an indication that the intermolecular interactions in the monolayer are weak and can be disrupted. The weak lateral interactions in the monolayer are probably the reason behind the ability of oleosomes to absorb free lipids in cells at the expense of volume expansion. The capability of oleosomes to absorb free lipids is one of the crucial biological functions of oleosomes, since it is the mechanism that prevents lipotoxicity caused by the presence of free lipids.

When investigating the changes in oleosome size upon the incorporation of free TAGs, as shown in Figure 6.4A, we noticed that regardless of the increase in $d_{4,3}$ at 1:3 Oleosome:TAGs ratio, there was an overlap of the size distribution curves at the range of 1.0-2.0 μm. This overlap possibly indicates that although the average size of the droplets was significantly increased, there might be a subset of droplets which retained their initial size. The coexistence of smaller droplets with the bigger ones at the 1:3 Oleosome: TAGs was also confirmed with the use of confocal microscopy. In the CLSM images (Figure 6.4E) it can be observed that a big share of oleosomes appears as spherical droplets with sizes larger than 5.0 μm, but there are also droplets with a diameter below 2.0 μm. The coexistence of smaller droplets with the larger ones as a result of fusion suggests that not all contacts during mixing led to fusion. We hypothesize that a heterogeneous change of the droplet size relates to the initial oleosome monolayer density. As it has been previously reported, during biogenesis from the ER, oleosomes may acquire a different number of molecules in their monolayer, which in turn is connected to the different roles of oleosome[21,217]. A lower surface density of structural proteins[212–214] or PL[215,216] can facilitate fusion. Therefore, a higher monolayer density could significantly increase the stability of oleosomes and decrease their likelihood to disrupt and fuse.

These experiments ratify the potential interdependence between oleosome monolayer density and the outcome upon contact with other (hydrophobic) molecules. A direct quantification of the monolayer density and the molecular details behind lipid uptake and fusion is further elucidated using molecular dynamics (MD) simulations.

6.3.2 Monolayer density regulates molecular orientation and interactions which determine the lipid fusion mechanism in oleosomes: An *in-silico* investigation

Molecular Dynamics (MD) simulations are a powerful tool that provides access to the inter- and intra-molecular interactions within the oleosome monolayer[218,219]. Performing MD simulations enables us to suggest and elaborate on the possible physical mechanisms governing the fusion of free TAGs into oleosomes that we observed in the experimental data discussed earlier, and the effect of the monolayer density on lipid uptake. In this work, we carried out simulations using the coarse grained Martini force field[202] of an oleosome droplet with a triolein core and a dipalmitoylphosphatidylcholine (DPPC) as a single PL in the monolayer. The Martini force field is the natural choice here since a fully atomistic representation of the molecules would limit the MD simulations to timescales at which fusion would not occur (i.e. a few ns). Martini is proven to be an indispensable tool for simulating lipid bilayers, polymers and biomolecules[220,221]. To simulate the mass range of PL molecules in the oleosome monolayer that has been reported[90,198,199] we varied the PL density from 0.7-1.1 PL/nm^2 (Table A6.1, Appendix). We created configurations of

assembled triolein molecules next to the oleosome in water and investigated the mechanism of the diffusion into oleosomes (Figure 6.5). For consistency throughout the text, we will refer to the DPPC molecules as PL, and the free assembled triolein molecules as free TAGs.

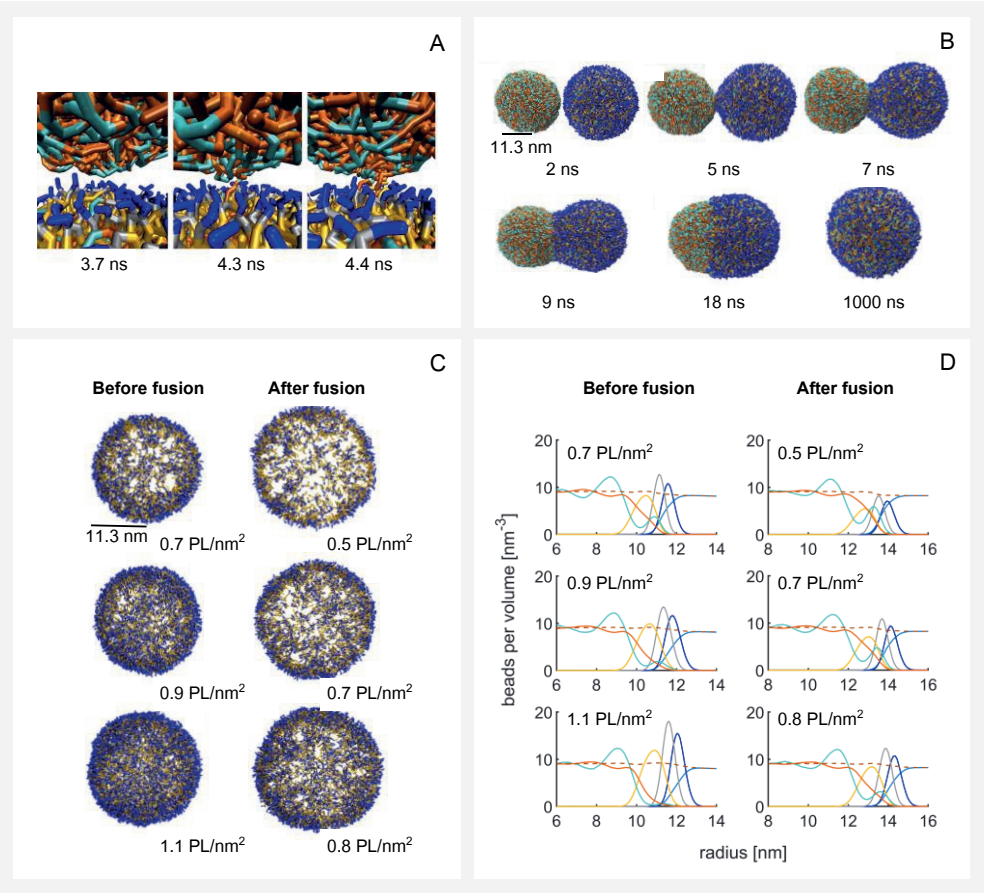

Figure 6.5 A) Snapshots of MD simulations showing the initial contact of oleosome having 0.9 PL/nm^2 with the free lipid assembly. The slightly hydrophilic heads of the TAG molecules are shown in cyan color, while the hydrophobic tails are shown in orange color. The color code used for the DPPC molecules is as follows: blue color for the head groups, grey color for the glycerol sections and yellow color for the tails. Water molecules are omitted for clarity, B) Simulation snapshots showing the time evolution of the fusion process, C) Oleosomes of different PL densities showing the PL distribution before and after fusion, and the increase in oleosome size after fusion. (only DPPC molecules are shown), D) Radial component density graphs of oleosomes (left) and oleosomes fused with the TAG assemblies (right). The bead positions used to construct the radial component density are sampled computed from 1000 simulation frames sampled every 10 ps. Simulations details can be found in the Methods section.

In Figure 6.5 (A-B) we outline in detail an example of the molecular mechanism behind the fusion of the free TAGs into oleosomes. Initially, to come into close proximity, the neighboring droplets should overcome the energy barrier associated with the hydration repulsion[222], i.e. the force acting between the two solvated droplets keeping them apart. As time evolves, the TAGs of the assembly create a contact site with the surface of the oleosomes through the interstitial water film[223] (Figure 6.5A). This contact is initially triggered by the attractive hydrophobic forces between the TAGs of the assembly and the oleosome lipid core and PL hydrophobic tails. Lasting contact between one or a few TAGs of the assembly with the oleosome surface develops to a stalk[223] (Figure 6.5B). The stalk formation entails oleosome monolayer deformations[222] and specifically requires the protrusion of the hydrophobic PL tail of oleosomes towards the free TAGs assembly. The stalk in turn expands to create a fusion pore and subsequently a channel. Ultimately, the oleosome monolayer opens to absorb the free TAGs.

Figure 6.5C shows the surface of oleosomes with different PL densities that we used in our simulations to study the effect of PL density on the likelihood of fusion. From the droplets shown in Figure 6.5C (left column), it is clear that at 0.7 PL/nm^2 there is more void space at the surface of oleosomes which reduces by increasing the number of PL to 0.9 and 1.1 PL/nm^2. Statistical analysis of our simulations showed that the likelihood of fusion of free TAGs with oleosomes decreased as the number of PL per monolayer area increased. In particular, for oleosomes with 0.7 PL/nm^2 the probability of fusion was found to be 0.7 ± 0.1 (i.e., 7 out of 10 simulations resulted in fused systems) while for oleosomes with 0.9 and 1.1 PL/nm^2, the probability of fusion was 0.5 ± 0.2 and 0.3 ± 0.1, respectively. The standard deviations were calculated based on the assumption that the fusion process can be approximated by a binomial distribution[224]. The size of oleosomes increased after absorbing the free TAGs (Table A6.1, Appendix), leading to a less dense monolayer compared to the initial system (Figure 6.5C right column). It is important to mention that before, but also after fusion, as shown in Figure 6.5C, the PLs in the monolayer were not homogeneously distributed over the surface within their designated space, but were present as detectable molecular clusters, leading to irregular gaps in the monolayer surface free of PL. Phase separation and arrangement of PL into random clusters is typically attributed to excluded volume and to van der Waals interactions[225], and the balance between loss of conformational entropy and gain in attractive forces. This cluster arrangement is another indication of weak lateral interactions and the absence of strong network formation in the monolayer, which in turn allows the volume expansion of oleosomes for absorption of free TAGs.

To better understand and quantify the effect of oleosome monolayer density on the molecular arrangement and likelihood of fusion, we computed the respective radial component densities (RCDs). Figure 6.5D shows the RCDs where the distribution of the PL and lipid molecules over

the radius of an oleosome droplet before and after fusion is plotted. The graph shows that before fusion (Figure 6.5D left column), in oleosomes with low monolayer density (0.7 PL/nm^2) the TAGs glycerol group (cyan line) is placed towards the surface and overlaps with the PL glycerol (grey line) and head groups (blue line). This orientation is imposed by the voids at the LD interface, causing the more hydrophilic part of the TAG molecule (glycerol) to move forward in order to limit the unfavorable interaction of the TAG hydrophobic tails with water. With increasing monolayer density (i.e. decreasing the surface voids), the molecular orientation of the TAG changes in such a way that their hydrophobic tails (orange line) move towards the surface to interact with the PL glycerol (grey line) and lipid groups (yellow line). As a result of this orientation and interactions at increasing oleosome monolayer densities, fewer PL tails are available to protrude towards the surface to connect with the free TAGs assembly. Additionally, with increasing the monolayer density, the limited surface voids also hinder the hydrophobic interactions of the oleosome TAG hydrophobic tails with the free TAGs. For these reasons, we can conclude that increasing PL monolayer density results in a decreased likelihood of fusion.

After fusion is achieved, as the oleosome size increased the area per PL is also increased (Table A6.1, Appendix), indicating the creation of new gaps at the interface (Figure 6.5C right column). After fusion the molecular orientation changes; In all systems the TAG glycerol group (cyan line) moves forward and overlaps with the PL glycerol (grey line) and head groups (blue line), while the relatively more hydrophobic TAG tails (orange line) extend to the PL glycerol (grey line) and lipid groups (yellow line) (Figure 6.5D right column). This molecular orientation occurs due to the presence of new surface voids at the oleosome interface after fusion, imposing the relatively more hydrophilic part of TAGs (glycerol) to orient towards water.

6.3.3 Oleosomes channel lipids and deflate upon contact with hydrophobic surfaces

Apart from lipid absorption, the second major role of oleosomes is managing cellular stress through channeling lipids to other cell organelles[226]. Studying the mechanism of lipid release from oleosomes would allow us to understand the channeling of molecules from oleosomes to other cell organelles in order to achieve targeted and controlled release of hydrophobic molecules carried by LDs.

Aiming to reveal the mechanism of oleosome lipid release and the nature of forces behind lipid channeling, we deposited purified rapeseed oleosomes onto 1H, 1H, 2H, 2H-perfluorooctyl trichlorosilane (PFOTS) patterned functionalized glass surfaces. Due to the plasma induced patterning using PDMS stamps with line features (Methods), the surface is designed to have alternating hydrophobic and hydrophilic lanes. To visualize the oleosomes on these surfaces we stained oleosomes with Nile red and used fluorescent light microscopy. Figure 6.6A shows the

fluorescent microscopy images of oleosomes on the functionalized surface where oleosomes appear in red. We show that after gently rinsing the surfaces with water, the oleosomes were mostly present on the hydrophobic lanes, while almost none of them were on the hydrophilic lanes. Oleosomes are suggested to have a hydrophilic surface which is negatively charged at pH values above 5. Therefore, it is expected that they will not adhere to the hydrophilic lanes which are also negatively charged due to the hydroxyl groups. As a result, oleosomes were washed out from the hydrophilic lanes.

In addition, many oleosomes present on the hydrophobic surface were not spherical but had an irregular shape showing as free oil. The fact that many oleosomes remained attached to the hydrophobic surface indicates strong attractive hydrophobic forces which resulted in the channeling of the oleosome lipid core towards the hydrophobic surface and subsequent disruption of the oleosome spherical shape.

To analyze the system using a higher resolution, and confirm the release of the oleosome lipid core, we used atomic force microscopy (AFM) which allows the study of the oleosomes on a nanoscale level. Figure 6.6B shows the 3D AFM images of oleosomes on a fully functionalized PFOTS hydrophobic surface. The analysis revealed the presence of clustered oleosomes with a retained spherical periphery (greater height) and a sunken hub (lower height), surrounded by bulk material, probably free lipids (greater height).

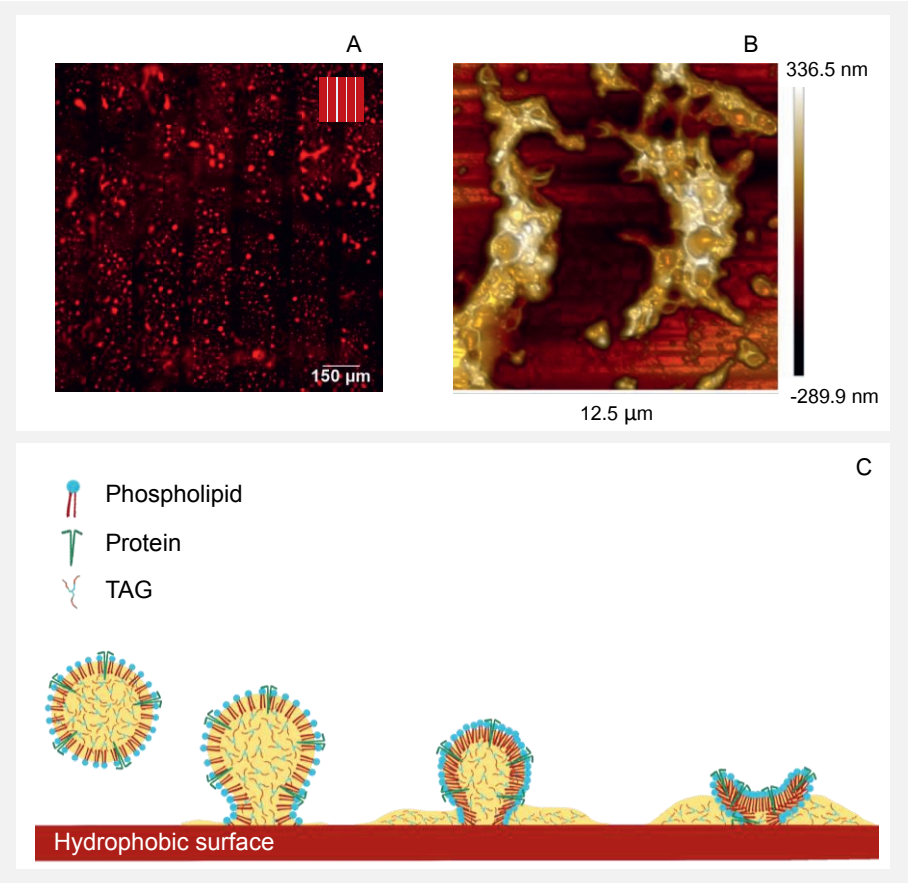

Figure 6.6 A) Fluorescent LM images of purified oleosomes stained with Nile Red on a surface of alternating hydrophobic (150 µm broad) and hydrophilic (50 µm broad) lanes. Scale bar: 150 µm. In the schematic representation of the surfaces red and light blue represent the hydrophobic and hydrophilic part, respectively, B) 3D AFM images of oleosomes on modified hydrophobic surface, C) Graphical visualization of the hypothetical mechanism of oleosome lipid release on the hydrophobic surface (size of molecules not to scale).

All the above findings strongly indicate that the mechanism behind contact establishment and lipid release on the hydrophobic surface is associated with hydrophobic interactions. These interactions can be initiated by contact of the oleosome lipid core with the hydrophobic surface through the monolayer voids and realized through PL protrusion, similar to what we demonstrated with MD simulations. As oleosomes did not rupture and only deflated upon this contact, we suggest that the release of lipids was realized through the creation of a channel/bridge between the oleosome monolayer and the hydrophobic surface. As the lipid core was released through this channel, oleosomes shrink, and to reduce the membrane tension arising from the very high molecular density (crowding) in the monolayer, they finally buckle and deflate. A schematic representation of

the proposed lipid release mechanism is shown in Figure 6.6C. This outcome also suggests that oleosomes are surrounded by an elastic monolayer that enables oleosomes to deflate and not rupture while releasing their core lipids.

It is important to note that the mechanism of lipid release and oleosome shrinkage upon contact with the hydrophobic surface, resembles the channeling of oleosome lipids to other organelles inside cells[226–228]. It has been shown that oleosome contacts with other cell organelles are very dynamic, and coupled to growth and shrinkage cycles of oleosomes[180]. Based on our findings, we suggest that when oleosomes come in contact with the membrane of other organelles or microorganisms, which also contain lipids and hydrophobic domains, protrusion of the PL hydrophobic tails from both sites is taking place and lipid channels are formed. As a result, molecules can be transferred in both directions. When oleosomes provide the lipids, they shrink and deflate. Deflated oleosomes have also been observed under other cell biological processes, (e.g., seed germination), as a result of oleosomes providing "fuels" to the seed[180,211,229].

6.3.4 Oleosomes have a dilatable monolayer which can reversibly expand and shrink

To investigate the lateral molecular interactions in the oleosome monolayer and its viscoelastic properties during expansion and shrinkage, we used interfacial dilatational rheology. Aiming to re-create the oleosome monolayer we isolated the molecules (i.e. PL and proteins) present in the oleosome monolayer surface of purified rapeseed oleosomes and used them to stabilize an oil/water interface. For simplicity, we will refer to the isolated monolayer molecules as monolayer. First, we measured the interfacial tension γ as a function of bulk concentration of monolayer material (Figure 6.7A). The analysis showed that by increasing the concentration in the bulk phase, the interfacial tension was decreased, indicating that a higher number of molecules was adsorbed at the interface (higher surface density). Even higher concentrations (0.05 wt%), led to a rapid decrease of the interfacial tension (γ < 3 mN/m) and spontaneous expelling of the droplet (data not shown here). The droplet expelling from the syringe upon interfacial tension reduction could be compared with the expelling of oleosomes from ER to the cytosol, which is known as budding process[230]. Budding of oleosomes from the ER is a tension-driven process as it is thermodynamically favored when the surface tension of the monolayer and the ER bilayer are lowered[19]. The type and number of molecules in the oleosome monolayer surface determine the surface tension and whether or not budding of oleosomes from the ER to the cytosol will occur[177,231].

To study the molecular lateral interactions in relation to the molecular density at the interface, we further applied dilatational interfacial rheology, where we determined the elastic (E_d') and viscous (E_d'') moduli of the interface as a function of the amplitude of deformation as presented in Figure

6.7B. The E_d' was higher than the E_d'' and ranged between 18-20 mN/m in all concentrations tested. These E_d' values are relatively low compared to, for example, interfaces stabilized by proteins which interact at the interface (i.e., whey protein isolate E_d' > 40 mN/m)[134], suggesting the absence of strong network formation at the interface. At low bulk concentrations (0.001 wt%), we noted a slight decrease of E_d' for increasing amplitude of deformation.

At the highest concentration (0.01 wt%) we could not apply amplitudes above 15%, as upon compression, the increase in molecular density and crowding of molecules led to the expelling of the droplet from the syringe. However, by lowering the concentration to 0.005 wt% or 0.001 wt%, we could compress the interface to up to 30% and 50% respectively, before expelling of the droplet.

Aiming to dive deeper into the molecular lateral interactions at the interface we used Lissajous curves where we plotted the surface pressure (γ-γ_0) against the area deformation ($\Delta A/A_0$) at the highest amplitude that we could achieve at each concentration (Figure 6.7C). At the highest concentration (0.01 wt%) and 15% amplitude, the curve had a narrow elliptical shape, implying a primarily elastic response of the interface[135]. Upon maximum compression (lower left part) and subsequent expansion the curve has a pointy tip, meaning a similar response in surface pressure upon compression and subsequent expansion, indicating weak lateral interactions[134]. Lateral interactions may originate: 1) from PL polar head groups or from the hydrophilic domain of the oleosome associated proteins, through electrostatic and/or van der Waals forces, and 2) from PL tail groups or the hydrophobic parts of the proteins. However, the main type of PL in oleosomes is, phosphatidylcholine[232], which is zwitterionic and limits the interactions between polar heads while PL tail-tail interactions are counteracted by PL tail-TAG interactions[233]. In addition, the main oleosome associated proteins found in the purified oleosomes were oleosins, which have a very small hydrophilic part and an extended hydrophobic domain with more than 70% of the amino acids being hydrophobic[234]. This hydrophobic domain in turn would strongly interact with the lipids on the droplet, hampering further protein-PL interactions. Previous study on interfacial properties of oleosins has also demonstrated that oleosins do not extensively interact at the interface, forming a weak network that can be disrupted upon oscillations[235].

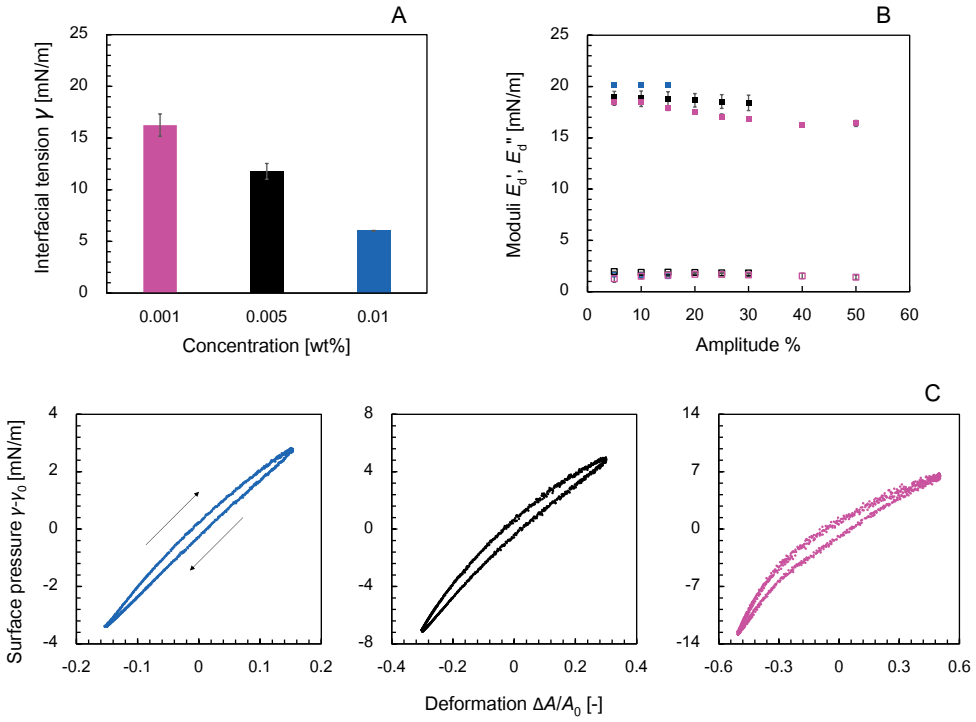

Figure 6.7 A) Dynamic interfacial tension γ of an oil/water interface measured after 2 h as a function of oleosome monolayer concentration in the aqueous phase [in wt%], B) dilatational elastic modulus (E_d': filled symbol) and viscous modulus (E_d": hollow symbol) as a function of deformation amplitude (10-50%) at constant oscillatory frequency 0.02 Hz, C) Lissajous plots showing changes in the surface pressure (γ-γ_0) upon area deformation ($\Delta A/A_0$) at the highest amplitude reached at each membrane concentration. The curves include the 3 middle cycles of each oscillation. The arrow pointing to the right indicates expansion and the arrow pointing to the left designates compression. Color of the curves correspond to the colors used for the concentrations in A).

By lowering the bulk concentration (0.005 wt%) and reaching 30% amplitude, the shape of the plot remained elliptical but slightly wider (more viscous) while we observed non-linearities; Upon expansion (upper right part) the curve started to slightly bend horizontally, showing interfacial strain softening. This softening behavior eventuates from disruption (weakening) of the molecular network at the interface upon higher expansion of the droplet surface area. As more interface was created, fewer molecules per area were present (increase in surface gaps) leading to an increase in the surface pressure. Unlike lipid bilayers, monolayers can cope with extensive stretching (with major variations in area per lipid) at the cost of increasing surface tension[236]. The results are also in line with the changes in PL interactions, clustering, and increase in area per PL that we observed in MD simulations upon fusion and volume expansion of oleosomes.

At the same concentration (0.005 wt%) upon compression (lower left part) the curve was slightly bent vertically. This result suggests strain stiffening behavior on compression, probably due to formation of densely clustered regions[148] (highly packed interface). PL monolayers have been found to form a tangential lattice at close packing and become oriented more normal to the interface at lower concentrations[233] (e.g., extension). The strain hardening due to increased molecular density per interfacial area might also explain the reorganization of the single oleosome monolayer into a liquid-crystalline shell that has been reported during consumption of oleosome lipids and oleosome shrinkage for metabolic needs[182]. Both strain softening on expansion and strain hardening on compression were even more apparent in the Lissajous curve of the lowest concentration tested (0.001 wt%), as the lower molecular density at the interface allowed even higher deformations (50% amplitude). Overall, this behavior upon expansion (softening) and compression (hardening) indicate the formation of a 2d soft glass phase at the interface[135] and shows weak lateral interactions which can be disrupted, facilitating the dilation of the oleosome monolayer surface.

The molecular arrangement was restored upon expansion in all concentrations tested, showing that all changes were reversible. Oleosomes were proved to be soft droplets that do not rupture on compression and can fully recover upon stress release, while monolayer density is also related to the mechanical properties[237]. PL monolayer structures are reversible not only during isothermal compression and expansion steps but also during isobaric heating and cooling steps[238]. This unique monolayer property allows oleosomes to deliberately grow and shrink in order to mediate lipid trafficking. This oleosome monolayer elasticity could have been already inherited during biogenesis of oleosomes, as oleosome formation from the ER requires the deformation of the ER monolayer[230]. Thus, oleosomes acquire a monolayer that is now proven to be significantly and reversibly deformable.

6.4 Conclusions

In this work we investigated on a molecular level the mechanism behind the ability of oleosomes to traffic lipids and hydrophobic molecules. Using experimental soft matter science combined with coarse grained molecular dynamics simulations we studied lipid trafficking by oleosomes in relation to the oleosome monolayer molecular density, lateral interactions and dilatability. When purified oleosomes meet excess free lipids, they absorb the free lipids and expand in volume, while adjusting their monolayer molecular density. The number of phospholipids initial present on the oleosome monolayer determine the likelihood of free lipid absorption. Higher number of phospholipids in the monolayer leads to lower likelihood of fusion between the oleosomes and free lipids. The mechanism behind free lipid absorption involves hydrophobic interactions between the

oleosome lipid core and PL hydrophobic tails with the free lipids. Lipid release from oleosomes is also initiated by hydrophobic interactions and results to oleosome deflation, showing a release mechanism through channel formation. The ability of oleosomes to deflate, like balloons when losing the air, and not rupture upon lipid release shows a monolayer with high elasticity allowing oleosomes to channel lipids. The weak lateral molecular interactions occurring in the oleosome monolayer support oleosome volume expansion and compression, while the molecular density in the monolayer determines the extent of monolayer dilatability. We anticipate that our findings could contribute to a more inclusive discussion on the underlying mechanism of oleosome molecular trafficking *in vivo* and will lead to the utilization of oleosomes as carriers with tailored properties for selective absorption and release of hydrophobic molecule.

6.5 Appendix

6.5.1 Methods

Composition analysis

To determine the moisture content of the recovered purified oleosomes, samples (~1 g) were dried at 60°C until reaching a stable weight (24 hrs). The samples cooled down to room temperature in a glass desiccator (Duran, Wertheim/Main, Germany) for 30 min. The moisture content (wt%) was calculated based on the weight loss after drying.

The oil content (OC) of the oleosomes was calculated on a dry-matter weight basis using Soxhlet extraction. The lipids were extracted for 7 hrs with petroleum ether (40-60°C) as a solvent. The lipid content after extraction was calculated using:

$$OC\ (wt\%) = 100 \times \left(\frac{M_o}{M}\right) \tag{A6.1}$$

where M_o [g] is the mass of the extracted oil and M [g] the initial sample mass.

The protein content (PC) of the recovered purified oleosomes on dry-matter weight basis was determined using the dumas method (FlashEA 1112 Series, Thermo Scientific, Waltham, Massachusetts, US); d-methionine (≥ 98%, Sigma Aldrich, Darmstadt, Germany) was used as a standard and as a control. Cellulose (Sigma Aldrich, Darmstadt, Germany) served as blank. A nitrogen-protein conversion factor of 5.7 was used and the protein content was calculated using:

$$PC\ (wt\%) = 100 \times \left(\frac{NC * 5.7}{M}\right) \tag{A6.2}$$

where PC is the protein content, NC is the nitrogen content, and M is the mass of the dry sample.

Electrophoresis (SDS-PAGE)

The protein profile of the proteins in purified oleosomes was determined with sodium dodecyl sulphate-polyacrylamide gel electrophoresis (SDS-PAGE). The samples were analyzed under non-reducing and reducing conditions. Reducing agent (NuPAGE ® Sample Reducing Agent) was added to break disulphide bonds in napin and cruciferin chains, enabling the detection of their presence. The samples were prepared as follows:

- 100 µL sample with a protein concentration of 3.3 mg/mL on average.
- 250 µL NuPAGE ® LDS sample buffer
- 100 µL NuPAGE ® Sample Reducing Agent or deionized water
- 550 µL deionized water

The samples were vortexed and then centrifuged for one minute at 2000 rpm to eliminate undissolved material. Subsequently, samples were heated in a heating block (Eppendorf Thermomixer C, Eppendorf Nederland B.V., Nijmegen, the Netherlands) for 10 minutes at 70°C to denature the proteins. Samples were centrifuged at the same settings again. 18 µL of sample were loaded in a NuPAGE Novex® (by Thermo Fischer SCIENTIFIC, Walham, USA) gel (4-12% Bis-Tris, 1.0 mm, 12 wells), submersed in a NuPAGE® MES SDS running buffer. Ten (10) µL of a PageRuler™ Plus prestained protein ladder (10-250 kDa) was loaded. The gels ran for a minimum of 35 minutes at a constant 200 V in a Mini Gel Tank (Invitrogen by Fischer Scientific, Waltham, USA). Subsequently, the gels were rinsed three times with demi-water and stained with Coomassie Brilliant Blue R-250 staining solution for 50 minutes while gently shaking at room temperature. The gels were rinsed three times with demi-water and destained with washing buffer (10.0 wt% ethanol and 7.5 wt% acetic acid in deionized water) for a minimum of two hours at room temperature. Afterwards, the gels were stored at room temperature in demi-water filled plastic boxes. The lids were covered with aluminum foil to prevent light degradation of the bands.

6.5.2 Results on characterization of purified rapeseed oleosomes

Protein profile

To evaluate the purity of the obtained oleosomes the protein profile was analyzed using electrophoresis (SDS-PAGE). The electophoregram (Figure A6.1) shows the protein profile of the oleosomes under non-reducing conditions. The oleosins (15-17 kDa), caleosins (20-27 kDa) and steroleosins (40-55 kDa) appeared to constitute the majority of proteins present. Above 115 kDa some undefined bands were present, which may have been a slight carry-over of enzymes[60]. Almost no bands related to storage rapeseed proteins (napins and cruciferins) were present, indicating a relatively pure system.

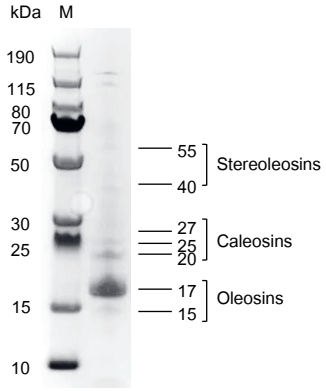

Figure A6.1 Electrophoregram (SDS-PAGE) of purified oleosomes under non-reducing conditions. M: protein molecular weight marker.

Molecular dynamic simulations

Table A6.1 Measured radii (r) PL per Area (nm^2) of oleosome droplets and Area (nm^2) per PL of LD droplets of 1200-2000 DPPC molecules per LD before and after fusion.

Droplet	r [nm]	PL/nm^2	nm^2/PL
Triolein assembly	10.3	-	-
LD-1200	11.3	0.7	1.34
LD-1600	11.6	0.9	1.06
LD-2000	12.0	1.1	0.90
LD-1200 fused	13.6	0.52	1.93
LD-1600 fused	13.8	0.67	1.50
LD-2000 fused	14.2	0.79	1.27

Chapter 7

General discussion

7.1. Overview

The aim of this thesis was to provide a mechanistic understanding of the relation between the extraction process and the functionality of less purified rapeseed ingredients (proteins and oleosomes) for food applications. In this section, the thesis outline and the main findings of each chapter are first summarized. Thereafter, the findings of each chapter are put into perspective with the challenges and main considerations in the extraction processes of oilseed proteins with respect to protein functionality. Finally, an outlook is given on the potential changes that need to be considered in the current oilseed valorization process to promote the exploitation of oilseed proteins in foods.

7.2. Thesis outline and main findings

The research described in the chapters of this thesis was divided into **three main objectives** as described in **Chapter 1**; the **first** research objective was to understand the effect of the **extraction process** on the **physicochemical properties of rapeseed proteins and oleosomes**. The **second** research objective was to investigate the **emulsifying properties** of **rapeseed proteins** when present in mixtures with other non-protein molecules. The **third** research objective was to characterize the **interfacial properties** of **rapeseed oleosomes** and investigate their **functionality** potential.

In **Chapter 2**, the decisions prior to the design of an alternative extraction process were first explained. Considering the impact of the current oilseed valorization process on the physicochemical and functional properties of proteins, we decided to omit the defatting process and use an aqueous extraction to simultaneously obtain the proteins and the oil in the form of oleosomes. The intact rapeseeds were first dehulled to eliminate part of the phenolic compounds present in the hulls and facilitate the soaking of the seeds. Aiming to extract both storage proteins (napins and cruciferins) and oleosomes and to prevent the irreversible complexation between proteins and coextracted phenolic compounds (i.e. sinapic acid) the pH of the extraction was maintained at pH 9. The soaked seeds were mechanically treated with a screw press to break the seed structure and the released proteins and oleosomes were further separated by centrifugation. This separation resulted in 1) an **oleosome-rich extract**, in which around 60% of the lipids initially present in the seed were recovered in their natural lipid structure, as a dense oil-in-water emulsion (40 wt% oil) and 2) a protein-rich extract containing around 40 wt% of the proteins initially present in the seed, with a protein content of about 40 wt% on dry matter. In this protein-rich extract (referred to in this thesis as **rapeseed protein mixture (RPM)**), both storage proteins, intact oleosomes and free phenols were present. By applying a diafiltration step, the free phenols and

other low molecular weight compounds were removed, resulting in a concentrate (**rapeseed protein concentrate (RPC)**) with about 65 wt% protein content on dry matter. As confirmed by the different analyses performed in this study, following this extraction protocol, the physicochemical properties of the proteins were preserved, and no complexation with phenolic compounds took place, which was also reflected in the bright colors of the protein extracts.

The second research objective was to assess the functionality of less purified protein extracts. To realize this assessment, a mechanistic understanding on the interfacial stabilization mechanism was necessary. As described in **Chapter 3,** first RPM, containing 40 wt% proteins and both storage proteins, and non-protein compounds such as oleosomes and phenolic compounds present, was used as an emulsifier at pH 7. When oil-in-water emulsions were prepared, we found that only napins were adsorbed at the interface, resulting in a soft solid-like interface. Cruciferins appeared to weakly interact with the adsorbed layer of napins, forming a secondary layer that provides stability to the emulsion droplets against coalescence during emulsification. The oleosomes and free phenols present, did not hinder the ability of proteins to stabilize the interface.

In **Chapter 4**, the effect of purification (i.e. diafiltration) on the interfacial stabilization mechanism when RPM and RPC are used as emulsifiers at pH 3.8 was investigated. In this research, we found that the emulsion properties (i.e. droplet size) were different between the two protein extracts, with larger emulsion droplets present in RPM-stabilized emulsions compared to RPC-stabilized emulsions. The interfacial composition was similar in both systems and with pH 7, with napins being adsorbed at the interface and cruciferins forming a secondary layer, preventing droplet coalescence during emulsification. The difference observed in emulsion droplet size between RPM- and RPC-stabilized emulsions were assigned to the presence of sinapic acid in RPM, which interacted with cruciferins inducing their aggregation, and affecting droplet formation and stability during emulsification.

The findings on the interfacial stabilization mechanism when RPM is used as an emulsifier, with napins being adsorbed at the interface and cruciferins weakly interacting, guided us to the research described in **Chapter 5.** In this research, the emulsifying properties of napins and the gelling properties of cruciferins were combined to created emulsion-filled gels. For this purpose, RPM containing both napins and cruciferins was used both as an emulsifier and gelling agent. The effect of pH (pH 5 and 7) and oil concentration (0-30 wt%) on the rheological and microstructural properties of the emulsion-filled gels was investigated. At pH 5 and in the absence of oil, RPM formed a heterogeneous network built of protein aggregates, whereas at pH 7, RPM formed a homogeneous network built of strand-like protein structures with higher gel firmness (i.e. higher *G*'). The rheological and microstructural differences observed in the protein gel matrices were

assigned to the lower protein solubility and larger protein aggregates at pH 5 compared to pH 7. With the addition of emulsion droplets in the protein gel matrix the firmness of the EFGs was increased (increase in *G'*), with a more pronounced reinforcement of the gel firmness at pH 5 compared to pH 7. The type of gel network did not change by the addition of oil droplets neither at pH 5 nor at pH 7, evidenced by confocal microscopy and an unchanged response to large deformation. These findings show that the protein backbone dictated the network structure. The incorporated emulsion droplets acted as protein particles that increased the size of protein aggregates and strands, which led to more connections, reinforcing the gel firmness.

In **Chapter 6**, the relation between oleosome phospholipid monolayer properties, such as molecular density (number of molecules per area), lateral interactions and dilatability, and the ability of oleosomes to traffic lipids was investigated. In this work, experimental techniques were combined with coarse-grained molecular dynamics simulations to provide a mechanistic understanding of the relation of monolayer physical properties and lipid trafficking (absorption and release). From this research it was found that the ability of oleosomes to traffic lipids is regulated by the molecular density and lateral molecular interactions in their monolayer. Through hydrophobic forces free lipids can permeate the oleosome monolayer and be stored in the oleosome core. By increasing the monolayer molecular density, the adsorption of free lipid by oleosomes is limited. Free lipid absorption by oleosomes results in an oleosome volume expansion and adjustment of the monolayer molecular density. With a similar mechanism initiated by hydrophobic forces, oleosomes can release the lipids from their core. The lipid release in turn leads to oleosome deflation, indicating a release mechanism through a channel. The ability of the oleosomes to expand in volume or shrink upon absorption or release of lipids respectively is assigned to the weak lateral interactions in the monolayer, which allow a reversible dilation.

An overview of all the chapters found in this thesis and the main findings is given in Figure 7.1.

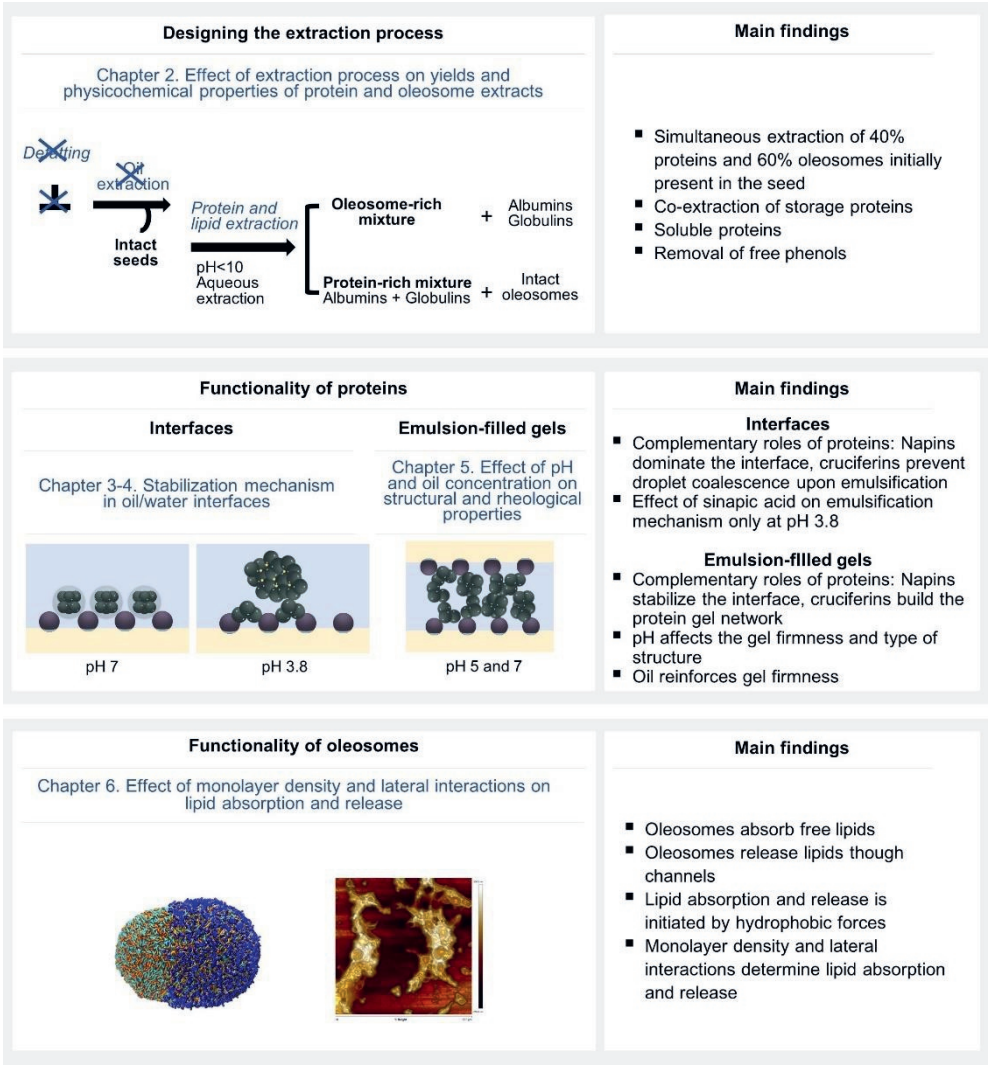

Figure 7.1 Overview of thesis outline and main findings

7.3. (Re) Designing the oilseed valorization

Oilseeds, due to their high protein content (20-30 wt%), are a good source of new protein ingredients for food applications. As discussed in **Chapter 1**, one of the roles of proteins in food systems is to stabilize oil-in-water emulsions. The main oilseed proteins that are currently being exploited as emulsifiers in foods derive from soybeans[12]. In this thesis, we showed that also rapeseeds (*Brassica napus*) are a promising source of sustainable proteins that can serve as emulsifiers in foods. However, due to the sustainability demand for new plant proteins, more oilseed protein sources should be explored[7].

In oilseeds, such as in rapeseeds, typically two types of proteins -albumins and globulins- are present, which have different physicochemical and functional properties. In the oilseed cell matrix, the proteins coexist with high amounts of lipids (40-50 wt%) and with phenolic compounds. The presence of two types of proteins in combination with the molecular complexity in the seed matrix makes the extraction of oilseed proteins a cumbersome process. As a result, oilseed proteins are not widely explored as functional ingredients in foods (i.e. as emulsifiers).

To understand how oilseeds can be utilized to extract proteins and how oilseed proteins can be used as emulsifiers, as shown in this thesis, a mechanistic understanding is imperative. Understanding the relationship between the extraction process and the emulsifying properties of the protein extracts will aid to formulate design guidelines on how to obtain highly functional proteins from oilseeds.

7.3.1. Understanding the protein extraction process

The first parameter which affects the functional properties of proteins is the extraction process. Oilseed proteins are currently extracted from the seeds after lipid extraction. As described in **Chapter 1**, the lipid extraction process starts with the flaking of the seeds to rupture the seed coat and the cells and subsequent heating (77°-100°C). Thereafter the seeds are mechanically pressed to extract most of the lipids (60-70%). To maximize the lipid extraction yields the remaining lipids in the residual pressed cake are further extracted with organic solvents (i.e. with hexane). The residual defatted product after lipid extraction, known as cake or meal, is processed in a desolventizer-toaster with steam (100°-130°C) to remove the solvent and to improve the nutritional quality by removing volatile glucosinolates[43,44]. The resulting protein-rich meal contains around 35-40 wt% proteins on dry matter[45], and serves as the starting material to extract the proteins.

The current extraction process has a tremendous impact on the yield and functionality of the proteins. Due to the heating steps and the use of organic solvents, the proteins remaining in the residual cake lose their natural physicochemical properties, such as solubility[44,239]. To increase solubility and protein extraction yields, the proteins are extracted in high amounts of water and high alkaline pH conditions (pH > 10) are applied[68,69,240]. The high alkaline pH results in irreversible complexation of the proteins with the coextracted phenolic compounds. Under alkaline pH, the coextracted phenolic acids are oxidized to more reactive products like quinones[41]. The protein-phenol interactions in turn can alter the protein structure[15]. For instance, in sunflower seeds, covalent bonding between proteins and the main phenolic compound, chlorogenic acid, occurs at pH 8, with an impact on the secondary and tertiary structure of the proteins[81]. The structural changes of proteins can result in a decreased capability of proteins to adsorb at an interface and decrease the surface tension[15,37]. Covalent bonding between globular proteins and phenolic compounds has also been reported to negatively affect the interfacial layer strength and foam stability[48].

To further purify the alkali-extracted proteins, acid precipitation is commonly applied[47,65], in which albumins are separated from the globulins[241]. The albumin-rich fraction is usually discarded, resulting in the loss of a valuable ingredient in this process. Besides, acid precipitation of proteins often results in irreversible aggregation of proteins with a negative impact on their functional properties. Protein aggregation has been previously shown to result in the formation of less stable emulsions against coalescence upon large deformations compared to non-aggregated proteins[50]. Apart from the impact on emulsifying properties, aggregation of proteins has been reported to negatively affect the gelling properties of proteins by reducing the gel firmness (*G*') upon heat-induced gelation of proteins[136,152].

7.3.2 Points of attention in oilseed protein extraction

In this thesis, to avoid the implications of the current protein extraction process and maintain the physicochemical and functional properties of the proteins, it is suggested to reconsider several steps and factors in the current oilseed valorization process. Depending on the oilseed source the optimal extraction conditions might differ.

The first step to be reconsidered is the removal of lipids before protein extraction using pressing, heating, and organic solvents. In **Chapter 2** of this thesis, it was shown that the simultaneous extraction of proteins and lipids where no pressing, heating or organic solvents is involved, is beneficial for protein solubility, extraction yields, and color of the protein extracts. The negative impact of heating on protein solubility, extraction yields, and color has been previously highlighted,

with non-pressed or cold-pressed rapeseed meals providing more soluble, light-colored protein extracts compared to heat-treated (toasted) meals[46].

Secondly, to prevent the irreversible protein-phenol interactions during extraction, the type of phenolic compounds present in each oilseed source should be examined. In rapeseeds, sinapic acid is the main phenolic compound, mainly present in the hulls. At pH values above pH 9.5, ionic bonding between proteins and sinapine (the choline ester of sinapic acid) occurs, leading to coextraction of phenolic compounds[40]. Further increase of pH above pH 10, accelerates the oxidation of sinapic acid to thomasidioic acid and further to quinones which are more reactive[41,42]. In this thesis we showed that dehulling of the seeds before the extraction and maintaining the pH of the extraction at pH 9, limits the coextraction of sinapic acid and prevents the irreversible complexation of proteins with sinapic acid. Following this approach, the secondary structure of proteins and protein solubility was not significantly affected by the presence of free sinapic acid. The avoidance of protein-phenol complexations was also reflected in the bright color of the protein extracts that we obtained by this process. The coextracted free sinapic acid in turn can easily be removed from the protein extract by a simple diafiltration step. Depending on the type of phenols present, the optimal extraction pH value might differ. For instance, in the case of sunflower seeds, to avoid the irreversible complexation of the proteins with the chlorogenic acid present, the pH of the extraction should be lower than pH 8[81].

The third factor to consider is the structural and physicochemical properties of each protein species present in oilseeds. In rapeseeds, both albumins and globulins -napins and cruciferins- are present. The two proteins have different physicochemical properties that can affect their extraction, such as isoelectric point and subsequent solubility[13,29]. Napins and cruciferins have been reported to have an isoelectric point at pH 11 and pH 7 respectively[13]. By adjusting the pH of the solvent far from the isoelectric point of both proteins (i.e. pH 9 for rapeseed proteins) and omit the precipitation step that separates albumins from globulins, we achieved the coextraction of both proteins in the protein extracts. Thus, by studying the physicochemical properties of the protein species in each seed before the extraction, a protein extract with a representative seed protein composition can be achieved. An overview of the factors to consider for the extraction of proteins from oilseeds is given in Figure 7.2.

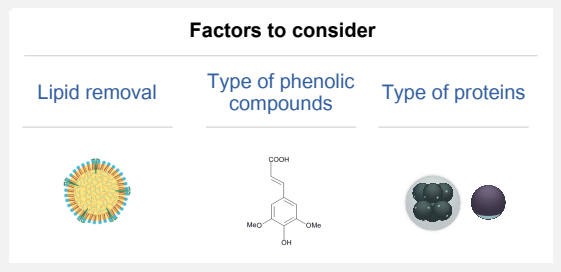

Figure 7.2 Factors to consider for the extraction of proteins from oilseeds

7.4 The underlying mechanism behind protein emulsifying properties

An important parameter which affects the emulsifying properties of the proteins is the composition of the protein extracts. Depending on the extraction process, the composition of the protein extracts can differ. The protein extraction process discussed in this thesis, results to less purified protein extracts (40-65 wt% protein purity), containing both storage proteins, and non-protein compounds, such as oleosomes and phenols. Several studies on other plant sources, such as sunflower seeds[86] or peas[108,109], have shown that less purified protein extracts have emulsifying properties similar to those of highly purified protein extracts.

As described in **Chapters 3-5**, under specific conditions (i.e. pH) the different molecules present in a less purified extract can compete for the interface, but also show synergistic effects, and hence either impair or enhance the interfacial properties of the proteins. Therefore, a mechanistic understanding of the interfacial properties of the protein extracts as a function of composition and pH is essential. In this thesis, we provided a methodology to gain a mechanistic understanding behind the functionality of complex plant-protein extracts. This methodology included 1) the composition analysis of the extracts (i.e. protein content, non-protein molecules, protein species present), 2) the physicochemical properties of the molecules present in the extracts (i.e. size, structure), and 3) the role of each molecule in the functionality of the extract (i.e. the stabilization of the oil/water interface).

7.4.1 Role of protein species in the interfacial stabilization mechanism

As it was showcased in this thesis, it is necessary to understand the role of each protein species on the interfacial stabilization mechanism. Different types of plant proteins result in the formation of interfaces with diverse rheological properties[11,103], which is very relevant for the targeted application. Second, the effect of non-protein molecules on the interfacial stabilization mechanism should be examined, as it allows to determine the optimal level of purification needed for the desired functionality.

In the case of rapeseeds, when less purified protein extracts, containing both albumins and globulins, are used as emulsifiers, independent of the pH conditions tested in this thesis (pH 3.8 and 7), it was shown that the albumins (i.e. napins) predominantly adsorb at the interface. The reason behind this stabilization mechanism, is that napins have smaller size than cruciferins (r = 1.7 vs 4.4 nm) and their hydrophobic domains are concentrated on one size of the protein, resembling amphiphilic Janus particles. Therefore, napins can diffuse faster than cruciferins and anchor easily at the oil/water interface. The lateral interactions between the adsorbed napins was similar at pH 3.8 and 7, forming a soft-solid structure at the interface which was not affected by the deformation of the interface (constant elastic (E_d') and viscous (E_d") moduli over a deformation range from 5 to 20%.

By combining the results of the protein profile at the oil/water interface with the dilatational interfacial rheology, it was also shown that the non-adsorbed proteins can also play a role in the interfacial stabilization mechanism. The findings of this thesis showed that the cruciferins present in the extracts interacted with the adsorbed napins and enhanced the interactions between napins. These interactions provided additional stability to the emulsions against coalescence during droplet formation in the homogenizer. In contrast to napin-napin interactions, the magnitude of the cruciferin-napin interactions was dependent on pH. At pH 3.8 the interactions between cruciferins with the adsorbed napins were stronger compared to pH 7 (higher elastic modulus) as shown in Figure 7.3, possibly due to the dissociation of cruciferins into trimers with increased hydrophobicity.

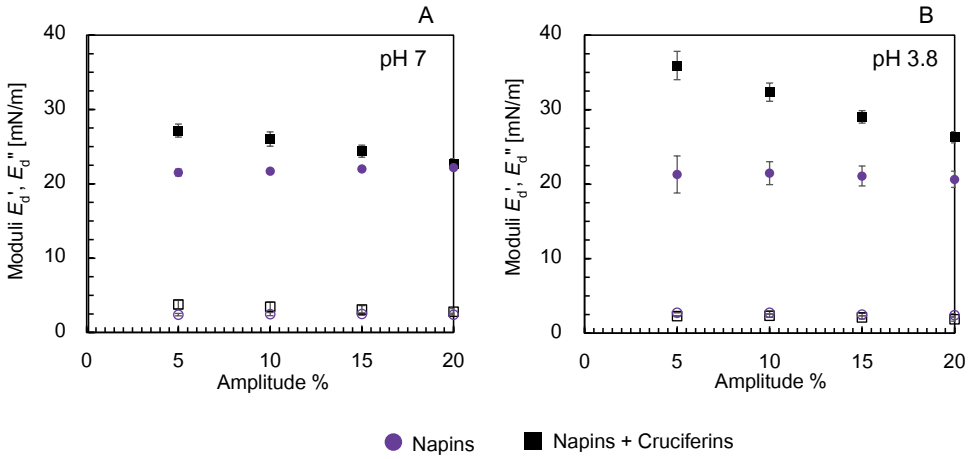

Figure 7.3 Dilatational elastic modulus (E_d': filled symbol) and viscous modulus (E_d": hollow symbol) of napins (purple circle symbol) and napins and cruciferins (black square symbol) upon amplitude sweeps.

Moreover, in **Chapter 5** it was discussed that the co-existence of the two protein species in a protein extract can be beneficial. In this chapter it was suggested that the interfacial properties of napins as shown in this thesis and the gelling properties of cruciferins as they have been previously reported[55,57,58], can be combined to structure emulsion-filled gels. In emulsion-filled gels napins can stabilize the emulsion droplets and cruciferins build the protein gel network. By combining two analytical tools such as confocal microscopy and bulk rheology, it was shown that pH affects the type of gel structure, the gel firmness, and the degree of reinforcement by oil addition; Aggregation of proteins at pH 5 resulted in less firm gels (i.e. lower *G*') with a heterogeneous structure built of protein aggregates, whereas less aggregated proteins at pH 7 formed a homogeneous network built of strand-like protein structures with higher gel firmness (i.e. higher *G*'). The microstructure of the emulsion-filled gels with 10.0 wt% oil as affected by pH is shown in Figure 7.4.

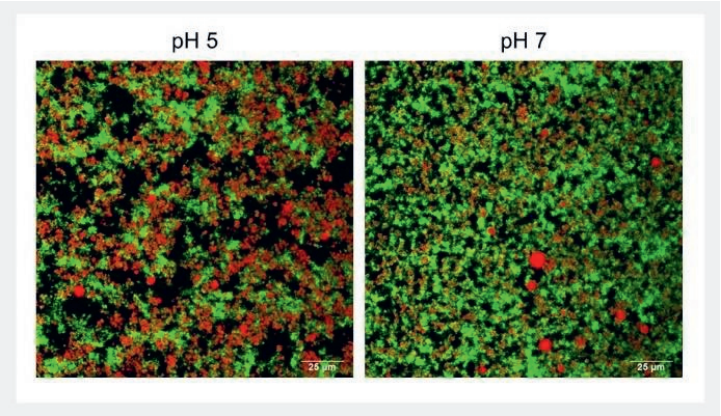

Figure 7.4. CLSM images showing the microstructure of emulsion-filled gels with 10.0 wt% oil at pH 5 (left) and pH 7 (right). Green: proteins, Red: oil.

In this thesis, by achieving a mechanistic understanding, a link between the composition of the protein extracts with the molecular properties and functionality was established, and several guidelines for the extraction and functionality of proteins were provided; 1) albumins have good emulsifying properties and should not be discarded during the protein extraction process, 2) the coexistence of both types of proteins (napins and cruciferins) in the protein extracts is advantageous in stabilizing oil/water interfaces and in structuring emulsion-filled gels, 3) the aggregated status of proteins can impact the structural and rheological properties of emulsion-filled gels. Therefore, the current applied separation process of the two proteins during extraction by the means of acid precipitation, which affects both protein composition and aggregation status, should be avoided in the process design for the application of proteins in emulsions and emulsion-filled gels.

Although the above findings suggest that coexistence of the two proteins can be advantageous for some food applications and their separation is redundant, for some other applications the presence of both proteins might not be favorable; For instance, the use of rapeseed proteins as ingredients in high-protein drinks, where high amounts of proteins (around 10%) are heated and must remain in a liquid structure, would benefit from the absence of cruciferins and the presence of only napins are more heat-stable than cruciferins. Similarly, cruciferins have been suggested as more suitable proteins than napins for the creation of nanoparticles via cold-induced gelation for the delivery of bioactive compounds[242]. Hence, it is recommended that the extraction process of proteins should be tailored accordingly to obtained protein extracts with the optimal composition for the targeted functionality.

7.4.2 Role of non-protein compounds on the interfacial stabilization mechanism

The presence of non-protein molecules in less purified protein extracts, such as oleosomes or phenolic compounds can also impact the interfacial stabilization mechanism of the proteins. Understanding the effect of non-protein compounds on protein functionality can aid to suggest the necessary level of purification during the extraction process for the desired functionality.

In **Chapter 3-5**, it was shown that lipids, when present in their natural structures as oleosomes, do not influence the interfacial stabilization mechanism of proteins in oil/water interfaces. Similar observations were made in less purified protein extracts from sunflower seeds[86].

Regarding the presence of phenolic compounds, in this thesis it was highlighted that pH is an important parameter that can affect the interactions of proteins with phenolic compounds. In **Chapter 3** we showed that the presence of free phenolic compounds did not impact the interfacial properties of the proteins at pH 7. However, in **Chapter 4** it was shown that at acidic pH conditions (pH 3.8) phenolic compounds can interact with proteins and induce protein aggregation. The aggregation of proteins reduces the ability of the proteins to protect the emulsion droplets against coalescence during emulsification. The effect of sinapic acid on the interfacial stabilization mechanism of rapeseed proteins as a function of pH is illustrated in Figure 7.5.

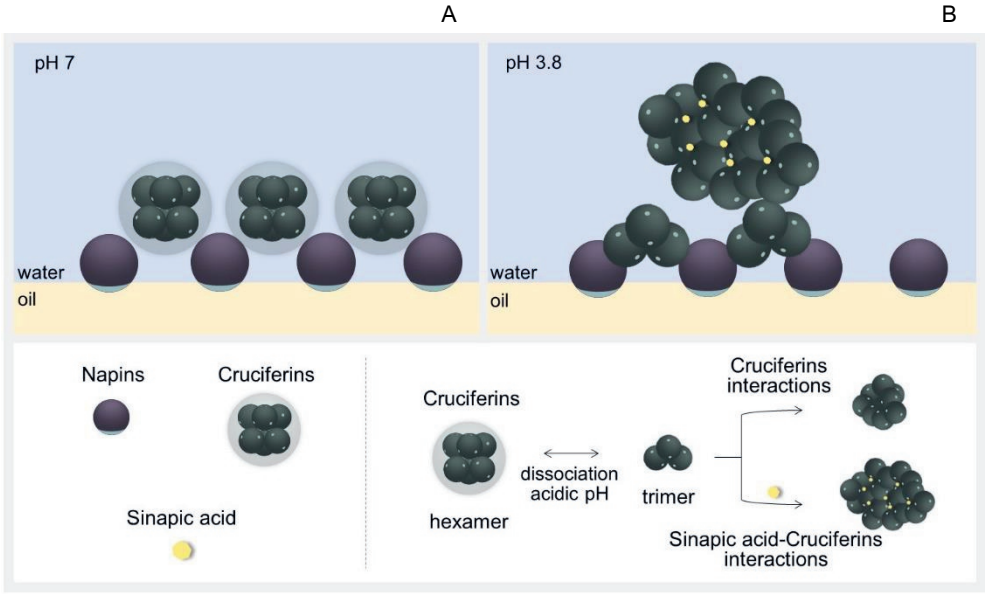

Figure 7.5. Effect of sinapic acid on the interfacial stabilization mechanism of rapeseed proteins at A) pH 7 and B) pH 3.8. The size of molecules and the number of cruciferin trimers and sinapic acid in each protein aggregate are not to scale.

Nevertheless, studies have shown that protein aggregation is not always undesired but can be advantageous or even necessary in structuring plant-based emulsion products. For instance, Sridharan et al. (2021) showed that protein aggregates formed under acidic pH conditions are essential for 3-D printing jammed emulsion systems, as they enhance the interactions between the emulsion droplets, providing the necessary plasticity to the system[243]. In some other cases, for example in sunflower seeds, physical bonding of protein with phenolic compounds have shown to even be advantageous for the long term stability of emulsions against coalescence[140]. However, as highlighted in **Chapter 1**, if during the extraction process complexation of phenolic compounds with proteins is prevented, the free phenolic compounds can be easily removed via diafiltration, when it is considered necessary for the targeted application.

7.5. Relation of lipid extraction with lipid functionality

Although oilseeds can be a valuable source of proteins for structuring food emulsions, we should realize that the main purpose of oilseeds is to provide oil in the food industry. Oilseed oils are used for different food purposes, for instance as bulk cooking oil or as structuring ingredient in food applications. In emulsion-type food applications, as studied in this thesis, the oil serves as an ingredient to create oil-in-water emulsions.

Inside the oilseeds the lipids are organized structures called oleosomes or lipid droplets[19]. In the natural oleosome structure, a monolayer of structural proteins and phospholipids surrounds the lipids, to provide protection against physical and chemical stresses[20]. This structure results to naturally emulsified droplets in the cells which are stable against coalescence and oxidation.

During the conventional extraction process of lipids from oilseeds, as mentioned earlier, the seeds are first flaked, heated (77°-100°C) and pressed to extract the majority of lipids (60-70%). The remaining oil in the pressed cake is further extracted with solvent (i.e. with hexane) to maximize the oil yield (> 90%)[43,44]. One of the purposes of heating is to decrease the oil viscosity and increase oil droplet coalescence, to facilitate the oil extraction during the following pressing steps. Organic solvents are also used to dissolve the residual oil present in the cake[43,44]. As a result of the heating, pressing and solvent extraction steps, the natural structure of lipids is disrupted.

However, if the current oilseed processing is redesigned and the defatting step is omitted as suggested in this thesis, the lipid structure can be maintained, and the lipids can be recovered in their natural structure. Although the lipid extraction yields are lower than the conventional lipid extraction process (60% vs > 90%), in this thesis it was shown that preserving the natural structures of lipids can provide several advantages; The first advantage of extracting the lipids as a natural oil-in-water emulsion, is that the oil does not need to be extracted and re-processed to form

emulsion-type products, but can be used as such in these food products. Additionally, by understanding the physicochemical properties of the natural emulsion droplets as discussed in **Chapter 2** (i.e. the charge over a pH range), the interactions between the oleosome droplets can be tuned to tailor the rheological properties of the emulsion. The tuning step can be applied during the oleosome extraction and recovery; In particular, after the aqueous extraction of lipids and proteins, the lipids are separated from the proteins using centrifugation. As shown in Figure 7.6, at pH conditions close to pH 4-5, the repulsive forces between the oleosome droplets are weak (ζ-potential around 0 mV), whereas at pH above pH 6, higher repulsive forces occur (ζ-potential around -30 mV). Tuning the pH before the centrifugation step can result in repulsion or attraction of the oleosome droplets resulting in oil-in-water emulsions with liquid to soft-solid structures respectively. Thus, depending on the targeted application, the optimal separation conditions can be chosen.

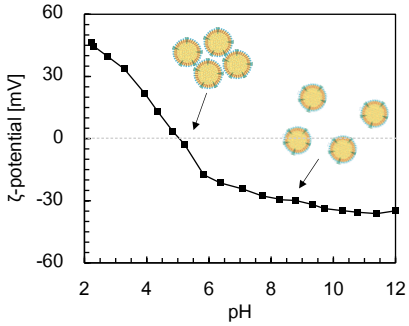

Figure 7.6. Charge of aqueous extracted oleosomes as a function of pH.

In summary, the extraction of lipids in the natural structure of oleosomes, allows 1) the obtaining of a natural oil-in-water emulsion with stability against coalescene and oxidation, and 2) the ability to tune the rheological structure of the emulsion with simple steps. These properties can lead to the exploitation of oleosomes as substitutes of engineered emulsions in a range of oil-in-water (food) emulsions.

Moreover, as highlighted in **Chapter 6**, oleosomes in cells play a crucial biological role in cell homeostasis by realizing lipid trafficking. Driven by the knowledge on the biological functions of oleosomes and by implementing experimental soft matter techniques combined with molecular dynamics simulations, in **Chapter 6** it was shown that oleosomes can absorb and release lipids. Therefore, oleosomes have also a high potential to serve as emulsifiers or carriers of hydrophobics with controlled absorption and release. The functionality potential of oleosomes, can be exploited not only by the food industry but also by the pharmaceutical industry, for controlled trafficking of bioactives or therapeutics[20].

By gaining a mechanistic understanding on lipid trafficking realized by oleosomes as described in **Chapter 6** and summarized in Figure 7.7**,** several parameters that affect the ability of oleosomes to traffic lipids can be suggested. First, the number of molecules present in the oleosome monolayer (i.e. phospholipids) are important in this mechanism, with less molecules in the monolayer facilitating lipid absorption. Secondly, it was shown that lipid absorption by oleosomes is initiated by hydrophobic interactions between the free lipids and the oleosome lipid core and phospholipid tails. Thirdly, it was revealed that oleosomes release lipids from their core, and do not rupture but deflate, showing that the release possibly occurs through channels. In the lipid release mechanism hydrophobic interactions are also pivotal. Lastly, it was suggested that the ability of oleosomes to traffic lipids is related to the weak lateral interactions of the molecules in the monolayer that allow the deformation of the monolayer. Similarly, the number of molecules in the monolayer are important in this mechanism, with less molecules allowing a higher degree of deformation.

With this knowledge on the mechanism behind lipid trafficking by oleosomes, different points of consideration in the use of oleosomes as carriers or for the design of oleosome-inspired carriers can be issued; 1) the number of molecules at the interface which will ensure lipid absorption, 2) the involvement of stimuli necessary to achieve lipid release from oleosomes (i.e. hydrophobic interactions), 3) the selection of interacting molecules that will assure the necessary degree of deformability upon lipid absorption and release.

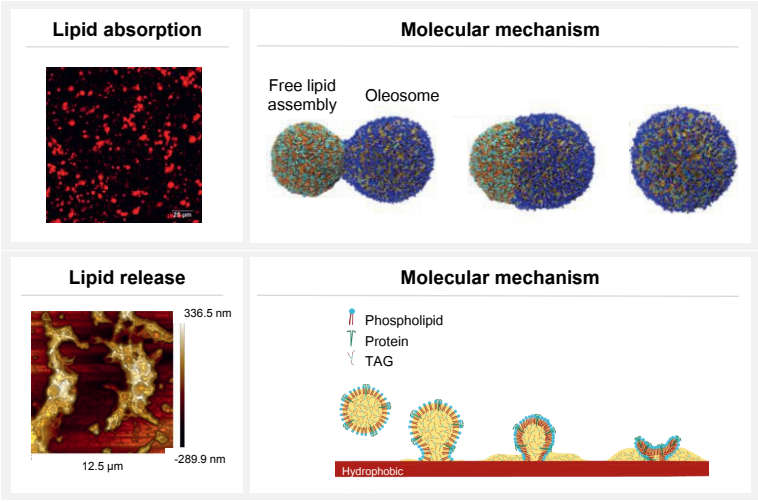

Figure 7.7. Summary of the mechanism on lipid absorption and release from oleosomes.

7.6 Outlook and future perspective on oilseed valorization

The findings of this thesis highlight that the selection of the extraction processing conditions is crucial in obtaining functional oilseed proteins that can serve as building blocks in emulsions and emulsion-filled gels in foods. The findings of this thesis recommend that for the extraction of highly functional protein ingredients for food applications, several steps in the current oilseed valorization process should be reconsidered.

7.6.1 Proteins

Ingredient companies should realize that a universal process protocol for oilseed protein extraction might not be ideal for bringing the new plant proteins that the food market demands. The findings of this thesis showed the significance of studying in depth the molecules present in each oilseed and following the appropriate guidelines during protein extraction in order to explore new plant protein sources. In this approach, the collaboration of different scientific disciplines is recommended; Plant scientists, knowing the structure and physicochemical properties of oilseed molecules, such as type of proteins or phenols, and physical chemists, predicting the interactions between molecules at different conditions (i.e. pH or heat), should provide insights to food engineers on how the protein extraction process should be adapted and optimized for each oilseed. Since the protein extracts are intended for foods, nutritionists should also be part of these discussions, to provide input on which proteins are of nutritional interest and on which molecules are considered anti-nutritional factors that should be limited during the extraction. In this way, next to soybean proteins that are currently used in foods, other oilseed proteins such as rapeseed or sunflower proteins can be introduced. This approach can broaden the portfolio of plant proteins that can compete dairy proteins, increasing the sustainability gain of foods.

In this thesis a direct link between the extraction process and functionality of the protein extracts is provided, necessary to promote the use of oilseed proteins in foods. Depending on the oilseed source and the applied extraction process, extracts with different molecular composition and subsequent functionality are obtained. In **Chapters 2-5**, the necessary methodology to determine the role of each molecule on the functionality of these complex protein extracts is provided. Quantitative and qualitative compositional analysis of the extracts are the first loops in the link between extraction and functionality. Moreover, the combination of different analytical techniques is crucial to provide a mechanistic understanding behind the function of these extracts. For instance, in the study of emulsion-filled gels, the coupling of interfacial and bulk rheology with confocal microscopy was necessary to evaluate the effect of emulsion droplets on the rheological and microstructural properties of the gels. Additionally, it was shown that to evaluate the necessity

of purification on functionality and design accordingly the protein extraction process, the functionality of the extract should be determined under various system conditions (i.e. pH).

In this thesis it was shown that less purified protein extracts from rapeseeds have a composition that is suitable to stabilize both emulsions and emulsion-filled gels. The different proteins present in these extracts have complementary functionalities, while the presence of non-protein compounds (i.e. phenolic compounds), is not always a hurdle for protein functionality. The outcome of this research suggests that a less purified protein extract can function as a multi-purpose ingredient.

From an oilseed protein ingredient manufacturing point of view, the outcome of this thesis can be used to reduce the extraction steps to only soaking, blending, screw-pressing and centrifuging (as explained in **Chapter 2**). With the methodology used in this thesis and the mechanistic understanding we provided for complex plant-protein extracts, we showed that a proper understanding of the role of each protein and non-protein compound in the functionality of the extract can lead to the reduction of the extraction steps, bringing a positive environmental impact. In addition, reducing the extraction steps lowers the production costs of the ingredients, bringing more cost-effective plant proteins to the market. As the cost of the dominant plant proteins, such as pea proteins, is constantly increasing due to the high demand of plant-based foods, the production of more cost-effective ingredients will motivate the use of other plant proteins as well.

From a food product manufacturing point of view, the findings of this thesis recommend that a less purified protein extract can serve as an ingredient with multiple functionalities (i.e. both as emulsifier and as structuring ingredient in emulsion-filled gels). Using one multi-functional protein ingredient instead of many single-function ingredients, reduces the food production steps, for instance by omitting the pre-mixing steps of several ingredients needed to achieve a combined functionality. Thus, the food industry can reduce the food production steps, increasing the overall environmental benefit and reducing the production costs. Moreover, the use of cost-effective ingredients in combination with cost-effective production, will also result in more affordable plant-based products, promoting their consumption, and contributing in this way to the overall protein transition.

However, the complete shift of the current oilseed ingredient industry towards new processes (i.e aqueous extraction) and products (i.e. proteins) might not be realistic, due to the fact that the main targeted ingredient from oilseeds is the oil. The global oil consumption has raised by 209% between 2001 and 2019, up to 200 million tones/year[244].

We believe that a hybrid process between the conventional oil extraction currently used and the aqueous extraction suggested in this thesis, might provide the optimal solution for obtaining functional oilseed food ingredients. The hybrid process can include the partial removal of most lipids from the seeds as liquid oil, without preheating of the seeds and by using only pressing that does not reach elevated temperatures (< 50°C). Pressing at low temperatures ensure the preservation of the protein physicochemical properties and enhances protein solubility and extraction yields[46]. This approach is also beneficial for the functional properties of the proteins, such as emulsifying properties[86]. At the same time, previous research has shown that the residual oil present in the cake after pressing of seeds at temperatures below 45°C, is in the form of oleosomes[86]. From the residual gentle-pressed cake, highly functional proteins and intact oleosomes can be extracted using the aqueous extraction process and guidelines as suggested in this thesis.

7.6.2 Oleosomes

Except from the highly functional oilseed proteins that can expand the portfolio of plant proteins in foods, obtaining intact oleosomes can advance the applications of oilseed oil as we discussed earlier. Currently, industry develops technologies aiming to efficiently extract and use plant lipids in their natural structures (oleosomes or lipid droplets) rather than liquid oil.

The first step in exploiting the functionality potential of the natural lipid structures is to understand which disciplines have been studying them and what knowledge each discipline can provide. Different science fields have given different names to the natural lipid structures; Food scientists commonly call them oleosomes, while plant and biology scientists call them lipid droplets. However, it is important to understand that all disciplines refer to the same structure, as inside all eukaryotic organisms, such as plants, lipids are organized and stored in these naturally emulsified oil droplets[19].

In food science, aqueous extracted oleosomes have been mainly studied as natural oil-in-water emulsions or as carriers of hydrophobic molecules, such as flavors or colors. However, in plant biology and human nutrition and physiology, the same structures are being studied in parallel *in-vivo* about their natural structure and stability, and their ability to carry hydrophobic molecules inside cells. Thus, there is a lot of common interest and knowledge to be shared between the different disciplines about these organelles.

From the food science approach, as discussed in this thesis, the benefit of using the oleosome structures as substitutes of engineered (food) emulsions is that the oil does not need to be extracted and re-processed. This approach automatically reduces many processing steps both in

the ingredient but also in the food manufacturing industry, increasing the environmental gain of plant-based foods. In parallel, the oleosome structure 1) provides the ability to tune the rheological properties of the food system and 2) protects naturally the lipids from oxidation and coalescence. From a food manufacturing perspective, it means that fewer ingredients such as emulsifiers, stabilizers, thickeners, and antioxidants are needed, which could result to "greener" and "cleaner" labels in the food products.

From the biology science approach, as highlighted in **Chapter 6**, the natural biological mechanism of oleosomes is to traffic lipids to other cell organelles. This function of oleosomes can inspire food scientists to use oleosomes not only as substitutes of engineered emulsions but also as carriers to entrap and deliver sensitive hydrophobic compounds such as bioactives or drugs through foods. Moreover, the ability of oleosomes to absorb and release hydrophobic molecules can find applications further than foods, like in medical or in environmental sciences[20]. In medical applications, oleosomes can be used to deliver hydrophobic drugs at designated targets (i.e. specific human cells). In environmental sciences, oleosomes with modified surfaces have been researched for their ability to decontaminate environmental samples[245]. The latter paves the path for medical sciences as well, to possibly use oleosomes not only as tools to deliver desired compounds but inversely, as tools to remove undesired toxic hydrophobic compounds from the human body.

But, to explore all the application potentials of oleosomes in different scientific disciplines, an in depth understanding of the structure of these organelles and the cause behind the function is crucial. How oleosomes can be beneficial for science, what else is there to explore about these structures? In this thesis by using a multi-disciplinary methodology, combining soft matter with computational science, it was shown that the oleosome monolayer is a very important structural element that dictates the function of oleosomes. In **Chapter 6** the significance of the number of molecules in the monolayer and their interactions on the lipid absorption and release mechanism of oleosomes was proved.

With this knowledge, we can further explore how the increase or decrease in the number of molecules in the monolayer affects this mechanism, by adding or removing molecules from the monolayer. Moreover, we can further research, how altering of molecules in the monolayer (i.e. different phospholipid or protein composition) affects the lateral interactions and subsequently the permeability and dilatability of oleosomes. For instance, the phospholipid composition in lipid bilayers determines the permeability and dilatability of the bilayer, with unsaturated phospholipids giving more permeable and less stable bilayers, compared to saturated phospholipids which form

more rigid and impermeable bilayer structures[246]. This knowledge allows us to modify or design oleosomes with specific permeability and dilatability based on the targeted application.

Additionally, the phospholipid and protein number and composition and the interplay between them also determines the curvature of biological membranes, which in turn can influence their size and geometry[21,247–249]. Depending on the relative sizes of the lipid head group to the lateral extent of the hydrophobic chains, phospholipids can be represented as inverse cones, cylinders, or cones[248]. Phospholipids with an overall inverted conical shape build structures with positive curvature like micelles, cylindrical-shaped phospholipids preferably form zero curvature structures like lamellar phase, and conical-shaped phospholipids form structures with negative curvature like hexagonal phase[250]. Proteins, also induce curvature in biological membranes, but, to create shapes, membranes must be able to deform[230,248]. Using a similar methodology as in this thesis, which involves both experimental soft matter (e.g. dilatational interfacial rheology) and computational science (molecular dynamics simulations), we can further explore the impact of different monolayer compositions and lateral interactions on the structure-function relationship of oleosomes. The size of oleosomes can also be altered by implementing mechanical treatment to the extracted oleosome dispersions. Homogenization can be used to narrow the oleosome size distribution, while microfluidics can possibly offer the possibility to create single-sized designer oleosomes, using the natural monolayer molecules or other desired molecules. Tuning the molecular composition in the oleosome monolayer and the size or geometry of oleosomes, for example from µm to nm or from spheres to cylinders respectively, might advance or broaden the applications for oleosomes.

In this thesis, using molecular dynamics simulations, surface modification techniques and advanced microscopy, it was also shown that the absorption and release of lipids by oleosomes is driven by hydrophobic forces. This finding is very important in understanding the conditions under which oleosomes are able to function as carriers, and which stimuli we need to involve in order to release the carried molecules in the sites of action. In nature, possibly other stimuli, such as specific molecules (i.e. proteins), or environmental stimuli (i.e. heat or light) might also be driving forces for oleosome function, and/or affect the tethering mechanism of oleosomes with other cell organelles. For example, specific proteins have shown to mediate contact and lipid transfer from oleosomes to other cell organelles and vice versa[189,251,252]. Therefore, more stimuli should be explored for their ability to tune the oleosome function. Plant and human biologists should provide knowledge on what type of molecules in the oleosome monolayer (i.e. proteins) and what type of stimuli (i.e. solvents, heat, light) have been observed in nature to influence the structure and function of oleosomes.

Combining the knowledge from this thesis with other studies from various disciplines we can suggest 1) which molecules on the oleosome monolayer are important in the absorption of hydrophobic compounds from oleosomes, 2) which molecules are needed for the interaction of oleosomes with cells, 3) how these molecules are influenced by different stimuli, 4) which stimuli result in absorption and/or release of the encapsulated molecules. By deciphering the engineering principles of nature we can either 1) use natural oleosomes with certain characteristics (i.e. specific molecules and structure) as carriers that can target specific cells, 2) modify oleosomes by removing or adding molecules to alter the absorption and release mechanism, the shape and/or the interactions with specific cells or 3) design oleosome-inspired carriers based on the compound we want to encapsulate or the cell we want to target. In this way we can pave the path to expand the use oleosomes from substitutes of engineered emulsions in foods to carriers of bioactives or drugs for treating various health conditions.

As the use of oleosomes as carriers of bioactives or drugs targets the human body, human biologists, nutritionists and physiologists should collaborate with food and/or medical scientists in these studies. The biocompatibility, biodegradability and stability of oleosomes or designer oleosomes within the human body, and the conditions and stimuli needed for oleosomes to remain stable and selectively deliver the compounds at the desired points of action, should be extensively first explored using *in-vitro* studies.

Exploring oilseeds as sources of sustainable functional ingredients requires the engagement of both academic and industrial worlds, from extraction to application. The collaboration of food, soft matter, biologists, human nutrition and physiology and plant science is necessary to understand what kind of molecules oilseeds contain, why, what is their role in nature and how the knowledge in *in-vivo* functions can be translated in *ex-vivo* applications. Ingredient and food production companies in turn, should collaborate with scientists to discuss how the single-molecule function can be translated into a factory-scale ingredient and product manufacturing. The collaboration between all these disciplines will increase the prospect of oilseed proteins and lipids to be used in foods or other niche applications (i.e. pharmaceutics), and can enhance the overall valorization of oilseeds.

References

(1) Poore, J.; Nemecek, T. Reducing Food's Environmental Impacts through Producers and Consumers. *Science (80-.).* **2018**, *360* (6392), 987–992. https://doi.org/10.1126/science.aaq0216.

(2) Ritchie, H.; Reay, D. S.; Higgins, P. The Impact of Global Dietary Guidelines on Climate Change. *Glob. Environ. Chang.* **2018**, *49* (June 2017), 46–55. https://doi.org/10.1016/j.gloenvcha.2018.02.005.

(3) Springmann, M.; Wiebe, K.; Mason-D'Croz, D.; Sulser, T. B.; Rayner, M.; Scarborough, P. Health and Nutritional Aspects of Sustainable Diet Strategies and Their Association with Environmental Impacts: A Global Modelling Analysis with Country-Level Detail. *Lancet Planet. Heal.* **2018**, *2* (10), e451–e461. https://doi.org/10.1016/S2542-5196(18)30206-7.

(4) McMichael, A. J.; Powles, J. W.; Butler, C. D.; Uauy, R. Food, Livestock Production, Energy, Climate Change, and Health. *Lancet* **2007**, *370* (9594), 1253–1263. https://doi.org/10.1016/S0140-6736(07)61256-2.

(5) Springmann, M.; Clark, M.; Mason-D'Croz, D.; Wiebe, K.; Bodirsky, B. L.; Lassaletta, L.; de Vries, W.; Vermeulen, S. J.; Herrero, M.; Carlson, K. M.; Jonell, M.; Troell, M.; DeClerck, F.; Gordon, L. J.; Zurayk, R.; Scarborough, P.; Rayner, M.; Loken, B.; Fanzo, J.; Godfray, H. C. J.; Tilman, D.; Rockström, J.; Willett, W. Options for Keeping the Food System within Environmental Limits. *Nature* **2018**, *562* (7728), 519–525. https://doi.org/10.1038/s41586-018-0594-0.

(6) Alzagtat, A. A.; Alli, I. Protein-Lipid Interactions in Food Systems: A Review. *Int. J. Food Sci. Nutr.* **2002**, *53* (3), 249–260. https://doi.org/10.1080/09637480220132850.

(7) Kotecka-Majchrzak, K.; Sumara, A.; Fornal, E.; Montowska, M. Oilseed Proteins – Properties and Application as a Food Ingredient. *Trends Food Sci. Technol.* **2020**, *106* (October), 160–170. https://doi.org/10.1016/j.tifs.2020.10.004.

(8) Schutyser, M. A. I.; van der Goot, A. J. The Potential of Dry Fractionation Processes for Sustainable Plant Protein Production. *Trends Food Sci. Technol.* **2011**, *22* (4), 154–164. https://doi.org/10.1016/j.tifs.2010.11.006.

(9) Berghout, J. A. M.; Pelgrom, P. J. M.; Schutyser, M. A. I.; Boom, R. M.; Van Der Goot, A. J. Sustainability Assessment of Oilseed Fractionation Processes: A Case Study on Lupin Seeds. *J. Food Eng.* **2015**, *150*, 117–124. https://doi.org/10.1016/j.jfoodeng.2014.11.005.

(10) Lie-Piang, A.; Braconi, N.; Boom, R. M.; van der Padt, A. Less Refined Ingredients Have Lower Environmental Impact – A Life Cycle Assessment of Protein-Rich Ingredients from Oil- and Starch-Bearing Crops. *J. Clean. Prod.* **2021**, *292*. https://doi.org/10.1016/j.jclepro.2021.126046.

(11) McClements, D. J.; Bai, L.; Chung, C. Recent Advances in the Utilization of Natural Emulsifiers to Form and Stabilize Emulsions. *Annu. Rev. Food Sci. Technol.* **2017**, *8* (1), 205–236. https://doi.org/10.1146/annurev-food-030216-030154.

(12) Day, L. Proteins from Land Plants - Potential Resources for Human Nutrition and Food Security. *Trends Food Sci. Technol.* **2013**, *32* (1), 25–42. https://doi.org/10.1016/j.tifs.2013.05.005.

(13) Wanasundara, J. P. D. Proteins of Brassicaceae Oilseeds and Their Potential as a Plant Protein Source. *Crit. Rev. Food Sci. Nutr.* **2011**, *51* (7), 635–677. https://doi.org/10.1080/10408391003749942.

(14) Tamayo Tenorio, A.; Kyriakopoulou, K. E.; Suarez-Garcia, E.; van den Berg, C.; van der Goot, A. J. Understanding Differences in Protein Fractionation from Conventional Crops, and Herbaceous and Aquatic Biomass - Consequences for Industrial Use. *Trends Food Sci. Technol.* **2018**, *71* (December 2017), 235–245. https://doi.org/10.1016/j.tifs.2017.11.010.

(15) Rawel, H. M.; Meidtner, K.; Kroll, J. Binding of Selected Phenolic Compounds to Proteins. *J. Agric. Food Chem.* **2005**, *53* (10), 4228–4235. https://doi.org/10.1021/jf0480290.

(16) Murphy, D. J.; Cummins, I. Biosynthesis of Seed Storage Products during Embryogenesis in Rapeseed, Brassica Napus. *J. Plant Physiol.* **1989**, *135* (1), 63–69. https://doi.org/10.1016/S0176-1617(89)80225-1.

(17) Höglund, A. S.; Rödin, J.; Larsson, E.; Rask, L. Distribution of Napin and Cruciferin in Developing Rape Seed Embryos. *Plant Physiol.* **1992**, *98* (2), 509–515. https://doi.org/10.1104/pp.98.2.509.

(18) Boulard, C.; Bardet, M.; Chardot, T.; Dubreucq, B.; Gromova, M.; Guillermo, A.; Miquel, M.; Nesi, N.; Yen-Nicolaÿ, S.; Jolivet, P. The Structural Organization of Seed Oil Bodies Could Explain the Contrasted Oil Extractability Observed in Two Rapeseed Genotypes. *Planta* **2015**, *242* (1), 53–68. https://doi.org/10.1007/s00425-015-2286-4.

(19) Thiam, A. R.; Farese, R. V.; Walther, T. C. The Biophysics and Cell Biology of Lipid Droplets. *Nat. Rev. Mol. Cell Biol.* **2013**, *14* (12), 775–786. https://doi.org/10.1038/nrm3699.

(20) Nikiforidis, C. V. Structure and Functions of Oleosomes (Oil Bodies). *Adv. Colloid Interface Sci.* **2019**, *274*, 102039. https://doi.org/10.1016/j.cis.2019.102039.

(21) Thiam, A. R.; Beller, M. The Why, When and How of Lipid Droplet Diversity. *J. Cell Sci.* **2017**, *130* (2), 315–324. https://doi.org/10.1242/jcs.192021.

(22) Beyzi, E.; Gunes, A.; Buyukkilic Beyzi, S.; Konca, Y. Changes in Fatty Acid and Mineral Composition of Rapeseed (Brassica Napus Ssp. Oleifera L.) Oil with Seed Sizes. *Ind. Crops Prod.* **2019**, *129* (November 2018), 10–14. https://doi.org/10.1016/j.indcrop.2018.11.064.

(23) Farag, R. S.; Hallabo, S. A. S.; Hewedi, F. M.; Basyony, A. E. Chemical Evaluation of Rapeseed. *Fette, Seifen, Anstrichm.* **1986**, *88* (10), 391–397. https://doi.org/10.1002/lipi.19860881006.

(24) Jolivet, P.; Boulard, C.; Bellamy, A.; Larré, C.; Barre, M.; Rogniaux, H.; D'Andréa, S.; Chardot, T.; Nesi, N. Protein Composition of Oil Bodies from Mature Brassica Napus Seeds. *Proteomics* **2009**, *9* (12), 3268–3284. https://doi.org/10.1002/pmic.200800449.

(25) Lin, L. J.; Liao, P. C.; Yang, H. H.; Tzen, J. T. C. Determination and Analyses of the N-Termini of Oil-Body Proteins, Steroleosin, Caleosin and Oleosin. *Plant Physiol. Biochem.* **2005**, *43* (8), 770–776. https://doi.org/10.1016/j.plaphy.2005.07.008.

(26) Purkrtova, Z.; Jolivet, P.; Miquel, M.; Chardot, T. Structure and Function of Seed Lipid Body-Associated Proteins. *Comptes Rendus - Biol.* **2008**, *331* (10), 746–754. https://doi.org/10.1016/j.crvi.2008.07.016.

(27) Chéreau, D.; Videcoq, P.; Ruffieux, C.; Pichon, L.; Motte, J.-C.; Belaid, S.; Ventureira, J.; Lopez, M. Combination of Existing and Alternative Technologies to Promote Oilseeds and Pulses Proteins in Food Applications. *OCL - Oilseeds fats, Crop. Lipids* **2016**, *23* (4), 11. https://doi.org/https://doi.org/10.1051/ocl/2016020.

(28) Chmielewska, A.; Kozłowska, M.; Rachwał, D.; Wnukowski, P.; Amarowicz, R.; Nebesny, E.; Rosicka-Kaczmarek, J. Canola/Rapeseed Protein–Nutritional Value, Functionality and Food Application: A Review. *Crit. Rev. Food Sci. Nutr.* **2020**, *0* (0), 1–21. https://doi.org/10.1080/10408398.2020.1809342.

(29) Perera, S.; McIntosh, T.; Wanasundara, J. P. D. Structural Properties of Cruciferin and Napin of Brassica Napus (Canola) Show Distinct Responses to Changes in PH and Temperature. *Plants* **2016**, *5* (3), 36. https://doi.org/10.3390/plants5030036.

(30) Ntone, E.; van Wesel, T.; Sagis, L. M. C.; Meinders, M.; Bitter, J. H.; Nikiforidis, C. V. Adsorption of Rapeseed Proteins at Oil/Water Interfaces. Janus-like Napins Dominate the Interface. *J. Colloid Interface Sci.* **2021**, *583*, 459–469. https://doi.org/10.1016/j.jcis.2020.09.039.

(31) Wanasundara, J. P. D.; McIntosh, T. C.; Perera, S. P.; Withana-Gamage, T. S.; Mitra, P. Canola/Rapeseed Protein-Functionality and Nutrition. *Ocl* **2016**, *23* (4), D407. https://doi.org/10.1051/ocl/2016028.

(32) Schwenke, K. D. Structural Studies on Native and Chemically Modified Storage Proteins from Rapeseed (Brassica Napus L.) and Related Plant Proteins. *Nahrung* **1990**, *34* (3), 225–240. https://doi.org/10.1002/food.19900340307.

(33) Wanasundara, J. P. D.; Abeysekara, S. J.; McIntosh, T. C.; Falk, K. C. Solubility Differences of Major Storage Proteins of Brassicaceae Oilseeds. *J. Am. Oil Chem. Soc.* **2012**, *89* (5), 869–881. https://doi.org/10.1007/s11746-011-1975-9.

(34) Yang, J.; Faber, I.; Berton-Carabin, C. C.; Nikiforidis, C. V.; van der Linden, E.; Sagis, L. M. C. Foams and Air-Water Interfaces Stabilised by Mildly Purified Rapeseed Proteins after Defatting. *Food Hydrocoll.* **2021**, *112*, 106270. https://doi.org/10.1016/j.foodhyd.2020.106270.

(35) Image from the RCSB PDB (rcsb.org) of PDB ID 3KGL; Tandang-Silvas, M. R. G.; Fukuda, T.; Fukuda, C.; Prak, K.; Cabanos, C.; Kimura, A.; Itoh, T.; Mikami, B.; Utsumi, S.; Maruyama, N. Crystal Structure of Procruciferin, 11S Globulin from Brassica Napus. *Biochim Biophys Acta* **2010**, *1804*, 1432–1442. https://doi.org/10.2210/pdb3KGL/pdb.

(36) Image from the RCSB PDB (rcsb.org) of PDB ID 1PNB; Rico, M.; Bruix, M.; Gonzalez, C.; Monsalve, R.; Rodriguez, R. 1H NMR Assignment and Global Fold of Napin BnIb, a Representative 2S Albumin Seed Protein. *Biochemistry* **1996**, *35* (49), 15672–15682. https://doi.org/10.2210/pdb1PNB/pdb.

(37) Ozdal, T.; Capanoglu, E.; Altay, F. A Review on Protein-Phenolic Interactions and Associated Changes. *Food Res. Int.* **2013**, *51* (2), 954–970. https://doi.org/10.1016/j.foodres.2013.02.009.

(38) SzydłOwska-Czerniak, A. Rapeseed and Its Products-Sources of Bioactive Compounds: A Review of Their Characteristics and Analysis. *Crit. Rev. Food Sci. Nutr.* **2013**, *53* (4), 307–330. https://doi.org/10.1080/10408398.2010.529959.

(39) Arntfield, S. D. *Proteins from Oil-Producing Plants*; Woodhead Publishing Limited, 2004. https://doi.org/10.1533/9781855738379.1.146.

(40) Xu, L.; Diosady, L. L. Interactions between Canola Proteins and Phenolic Compounds in Aqueous Media. *Food Res. Int.* **2000**, *33* (9), 725–731. https://doi.org/10.1016/S0963-9969(00)00062-4.

(41) Cai, R. C.; Arntfield, S. D.; Charlton, J. L. Structural Changes of Sinapic Acid during Alkali-Induced Air Oxidation and the Development of Colored Substances. *J. Am. Oil Chem. Soc.* **1999**, *76* (6), 757–764. https://doi.org/10.1007/s11746-999-0172-6.

(42) Rubino, M. I.; Arntfield, S. D.; Nadon, C. A.; Bernatsky, A. Phenolic Protein Interactions in Relation to the Gelation Properties of Canola Protein. *Food Res. Int.* **1996**, *29* (7), 653–659. https://doi.org/10.1016/S0963-9969(97)89643-3.

(43) Mosenthin, R.; Messerschmidt, U.; Sauer, N.; Carré, P.; Quinsac, A.; Schöne, F. Effect of the Desolventizing / Toasting Process on Chemical Composition and Protein Quality of Rapeseed Meal. *J. Anim. Sci. Biotechnol.* **2016**, *7* (1), 1–12. https://doi.org/10.1186/s40104-016-0095-7.

(44) McCurdy, S. M. Effects of Processing on the Functional Properties of Canola/Rapeseed Protein. *J. Am. Oil Chem. Soc.* **1990**, *67* (5), 281–284. https://doi.org/10.1007/BF02539677.

(45) Arntfield, S.; Hickling, D. Meal Nutrition and Utilization. *Canola Chem. Prod. Process. Util.* **2011**, 281–312. https://doi.org/10.1016/B978-0-9818936-5-5.50014-0.

(46) Fetzer, A.; Herfellner, T.; Stäbler, A.; Menner, M.; Eisner, P. Influence of Process Conditions during Aqueous Protein Extraction upon Yield from Pre-Pressed and Cold-Pressed Rapeseed Press Cake. *Ind. Crops Prod.* **2018**, *112*, 236–246. https://doi.org/10.1016/j.indcrop.2017.12.011.

(47) Manamperi, W. A. R.; Wiesenborn, D. P.; Chang, S. K. C.; Pryor, S. W. Effects of Protein Separation Conditions on the Functional and Thermal Properties of Canola Protein Isolates. *J. Food Sci.* **2011**, *76* (3), 266–273. https://doi.org/10.1111/j.1750-3841.2011.02087.x.

(48) Yang, J.; Lamochi Roozalipour, S. P.; Berton-Carabin, C. C.; Nikiforidis, C. V.; van der Linden, E.; Sagis, L. M. C. Air-Water Interfacial and Foaming Properties of Whey Protein - Sinapic Acid Mixtures. *Food Hydrocoll.* **2021**, *112*, 106467. https://doi.org/10.1016/j.foodhyd.2020.106467.

(49) Cao, Y.; Xiong, Y. L. Interaction of Whey Proteins with Phenolic Derivatives Under Neutral and Acidic PH Conditions. *J. Food Sci.* **2017**, *82* (2), 409–419. https://doi.org/10.1111/1750-3841.13607.

(50) Zhou, X.; Sala, G.; Sagis, L. M. C. Bulk and Interfacial Properties of Milk Fat Emulsions Stabilized by Whey Protein Isolate and Whey Protein Aggregates. *Food Hydrocoll.* **2020**, *109* (May), 106100. https://doi.org/10.1016/j.foodhyd.2020.106100.

(51) Carre, P.; Citeau, M.; Robin, G.; Estorges, M. Hull Content and Chemical Composition of Whole Seeds, Hulls and Germs in Cultivars of Rapeseed (Brassica Napus). *OCL - Oilseeds fats, Crop. Lipids* **2016**, *23* (3). https://doi.org/10.1051/ocl/2016013.

(52) Cheung, L.; Wanasundara, J. P. D.; Nickerson, M. T. The Effect of PH and NaCl Levels on the Physicochemical and Emulsifying Properties of a Cruciferin Protein Isolate. *Food*

Biophys. **2014**, *9* (2), 105–113. https://doi.org/10.1007/s11483-013-9323-2.

(53) Cheung, L.; Wanasundara, J. P. D.; Nickerson, M. T. Effect of PH and NaCl on the Emulsifying Properties of a Napin Protein Isolate. *Food Biophys.* **2014**, *10* (1), 30–38. https://doi.org/10.1007/s11483-014-9350-7.

(54) Malabat, C.; nchez-Vioque, R. I. S.; Rabiller, C.; Gu guen, J. Emulsifying and Foaming Properties of Native and Chemically Modified Peptides from the 2S and 12S Proteins of Rapeseed (Brassica Napus L.). *J. Am. Oil Chem. Soc.* **2001**, *78* (3), 235–242. https://doi.org/10.1007/s11746-001-0251-x.

(55) Tan, S. H.; Mailer, R. J.; Blanchard, C. L.; Agboola, S. O.; Day, L. Gelling Properties of Protein Fractions and Protein Isolate Extracted from Australian Canola Meal. *Food Res. Int.* **2014**, *62*, 819–828. https://doi.org/10.1016/j.foodres.2014.04.055.

(56) Krause, J. P.; Schwenke, K. D. Behaviour of a Protein Isolate from Rapeseed (Brassica Napus) and Its Main Protein Components - Globulin and Albumin - At Air/Solution and Solid Interfaces, and in Emulsions. *Colloids Surfaces B Biointerfaces* **2001**, *21* (1–3), 29–36. https://doi.org/10.1016/S0927-7765(01)00181-3.

(57) Schwenke, K. D.; Dahme, A.; Wolter, T. Heat-Induced Gelation of Rapeseed Proteins: Effect of Protein Interaction and Acetylation. *J. Am. Oil Chem. Soc.* **1998**, *75* (1), 83–87. https://doi.org/10.1007/s11746-998-0015-x.

(58) Yang, C.; Wang, Y.; Vasanthan, T.; Chen, L. Impacts of PH and Heating Temperature on Formation Mechanisms and Properties of Thermally Induced Canola Protein Gels. *Food Hydrocoll.* **2014**, *40*, 225–236. https://doi.org/10.1016/j.foodhyd.2014.03.011.

(59) Iwanaga, D.; Gray, D. A.; Fisk, I. D.; Decker, E. A.; Weiss, J.; McClements, D. J. Extraction and Characterization of Oil Bodies from Soy Beans: A Natural Source of Pre-Emulsified Soybean Oil. *J. Agric. Food Chem.* **2007**, *55* (21), 8711–8716. https://doi.org/10.1021/jf071008w.

(60) De Chirico, S.; di Bari, V.; Foster, T.; Gray, D. Enhancing the Recovery of Oilseed Rape Seed Oil Bodies (Oleosomes) Using Bicarbonate-Based Soaking and Grinding Media. *Food Chem.* **2018**, *241*, 419–426. https://doi.org/10.1016/j.foodchem.2017.09.008.

(61) Nikiforidis, C. V.; Karkani, O. A.; Kiosseoglou, V. Exploitation of Maize Germ for the Preparation of a Stable Oil-Body Nanoemulsion Using a Combined Aqueous Extraction-Ultrafiltration Method. *Food Hydrocoll.* **2011**, *25* (5), 1122–1127. https://doi.org/10.1016/j.foodhyd.2010.10.009.

(62) Shen, Z.; Wijesundra, C.; Ye, J.-H. Effect of Seed Heat-Treatment on the Oxidative Stability of Canola Oil Body Emulsions. *Food Nutr. Sci.* **2012**, *3* (7), 981–990. https://doi.org/10.4236/fns.2012.37130.

(63) Chen, B.; McClements, D. J.; Gray, D. A.; Decker, E. A. Physical and Oxidative Stability of Pre-Emulsified Oil Bodies Extracted from Soybeans. *Food Chem.* **2012**, *132* (3), 1514–1520. https://doi.org/10.1016/j.foodchem.2011.11.144.

(64) Wanasundara, J. P. D.; Tan, S.; Alashi, A. M.; Pudel, F.; Blanchard, C. Proteins from Canola/Rapeseed: Current Status. In *Sustainable Protein Sources*; Academic Press, 2016; pp 285–304. https://doi.org/10.1016/B978-0-12-802778-3.00018-4.

(65) Tzeng, Y. M.; Diosady, L. L.; Rubin, L. J. Production of Canola Protein Materials by Alkaline Extraction, Precipitation, and Membrane Processing. *J. Food Sci.* **1990**, *55* (4), 1147–1151. https://doi.org/10.1111/j.1365-2621.1990.tb01619.x.

(66) Rawel, H. M.; Meidtner, K.; Kroll, J. Binding of Selected Phenolic Compounds to Proteins. *J. Agric. Food Chem.* **2005**, *53* (10), 4228–4235. https://doi.org/10.1021/jf0480290.

(67) Campbell, L.; Rempel, C.; Wanasundara, J. P. D. Canola/Rapeseed Protein: Future Opportunities and Directions—Workshop Proceedings of IRC 2015. *Plants* **2016**, *5* (2), 17. https://doi.org/10.3390/plants5020017.

(68) Gerzhova, A.; Mondor, M.; Benali, M.; Aider, M. Study of Total Dry Matter and Protein Extraction from Canola Meal as Affected by the PH, Salt Addition and Use of Zeta-Potential/Turbidimetry Analysis to Optimize the Extraction Conditions. *Food Chem.* **2016**, *201*, 243–252. https://doi.org/10.1016/j.foodchem.2016.01.074.

(69) Manamperi, W. A. R.; Chang, S. K. C.; Wiesenborn, D. P.; Pryor, S. W. Impact of Meal Preparation Method and Extraction Procedure on Canola Protein Yield and Properties. *Biol. Eng. Trans.* **2012**, *5* (4), 191–200. https://doi.org/10.13031/2013.42456.

(70) Rawel, H. M.; Meidtner, K.; Kroll, J. Binding of Selected Phenolic Compounds to Proteins. *J. Agric. Food Chem.* **2005**, *53* (10), 4228–4235. https://doi.org/10.1021/jf0480290.

(71) Rosenthal, A.; Pyle, D. L.; Niranjan, K. Simultaneous Aqueous Extraction of Oil and Protein from Soybean: Mechanisms for Process Design. *Food Bioprod. Process.* **1998**, *76* (4), 224–230. https://doi.org/10.1205/096030898532124.

(72) Aider, M.; Barbana, C. Canola Proteins: Composition, Extraction, Functional Properties, Bioactivity, Applications as a Food Ingredient and Allergenicity - A Practical and Critical Review. *Trends Food Sci. Technol.* **2011**, *22* (1), 21–39. https://doi.org/10.1016/j.tifs.2010.11.002.

(73) Ghodsvali, A.; Khodaparast, M. H. H.; Vosoughi, M.; Diosady, L. L. Preparation of Canola Protein Materials Using Membrane Technology and Evaluation of Meals Functional Properties. *Food Res. Int.* **2005**, *38* (2), 223–231.

https://doi.org/10.1016/j.foodres.2004.10.007.

(74) Alu'datt, M. H.; Rababah, T.; Ereifej, K.; Brewer, S.; Alli, I. Phenolic-Protein Interactions in Oilseed Protein Isolates. *Food Res. Int.* **2013**, *52* (1), 178–184. https://doi.org/10.1016/j.foodres.2013.03.010.

(75) Willardsen, R.; Schweizer, M.; Segall, K. I. Canola Protein Production with Low Phytic Acid Content. US 2016/0205968A1, 2016.

(76) Das Purkayastha, M.; Gogoi, J.; Kalita, D.; Chattopadhyay, P.; Nakhuru, K. S.; Goyary, D.; Mahanta, C. L. Physicochemical and Functional Properties of Rapeseed Protein Isolate: Influence of Antinutrient Removal with Acidified Organic Solvents from Rapeseed Meal. *J. Agric. Food Chem.* **2014**, *62* (31), 7903–7914. https://doi.org/10.1021/jf5023803.

(77) Micsonai, A.; Wien, F.; Kernya, L.; Lee, Y. H.; Goto, Y.; Réfrégiers, M.; Kardos, J. Accurate Secondary Structure Prediction and Fold Recognition for Circular Dichroism Spectroscopy. *Proc. Natl. Acad. Sci. U. S. A.* **2015**, *112* (24), E3095–E3103. https://doi.org/10.1073/pnas.1500851112.

(78) Eriksson, I.; Westerlund, E.; Aman, P. Chemical Composition in Varieties of Rapeseed and Turnip Rapeseed , Including Several Samples of Hull and Dehulled Seed. *J. Sci. Food Agric.* **1994**, *66* (2), 233–240. https://doi.org/10.1002/jsfa.2740660219.

(79) Nioi, C.; Kapel, R.; Rondags, E.; Marc, I. Selective Extraction, Structural Characterisation and Antifungal Activity Assessment of Napins from an Industrial Rapeseed Meal. *Food Chem.* **2012**, *134* (4), 2149–2155. https://doi.org/10.1016/j.foodchem.2012.04.017.

(80) Nikiforidis, C. V.; Kiosseoglou, V. Physicochemical Stability of Maize Germ Oil Body Emulsions as Influenced by Oil Body Surface-Xanthan Gum Interactions. *J. Agric. Food Chem.* **2010**, *58* (1), 527–532. https://doi.org/10.1021/jf902544j.

(81) Karefyllakis, D.; Salakou, S.; Bitter, J. H.; van der Goot, A. J.; Nikiforidis, C. V. Covalent Bonding of Chlorogenic Acid Induces Structural Modifications on Sunflower Proteins. *ChemPhysChem* **2018**, *19* (4), 459–468. https://doi.org/10.1002/cphc.201701054.

(82) Klockeman, D. M.; Toledo, R.; Sims, K. A. Isolation and Characterization of Defatted Canola Meal Protein. *J. Agric. Food Chem.* **1997**, *45* (10), 3867–3870. https://doi.org/10.1021/jf970026i.

(83) Capuano, E.; Pellegrini, N.; Ntone, E.; Nikiforidis, C. V. *In Vitro* Lipid Digestion in Raw and Roasted Hazelnut Particles and Oil Bodies. *Food Funct.* **2018**, *9* (4), 2508–2516. https://doi.org/10.1039/C8FO00389K.

(84) Nikiforidis, C. V.; Kiosseoglou, V. Aqueous Extraction of Oil Bodies from Maize Germ

(Zea Mays) and Characterization of the Resulting Natural Oil-in-Water Emulsion. *J. Agric. Food Chem.* **2009**, *57* (12), 5591–5596. https://doi.org/10.1021/jf900771v.

(85) Yoshie-Stark, Y.; Wada, Y.; Wäsche, A. Chemical Composition, Functional Properties, and Bioactivities of Rapeseed Protein Isolates. *Food Chem.* **2008**, *107* (1), 32–39. https://doi.org/10.1016/j.foodchem.2007.07.061.

(86) Karefyllakis, D.; Octaviana, H.; van der Goot, A. J.; Nikiforidis, C. V. The Emulsifying Performance of Mildly Derived Mixtures from Sunflower Seeds. *Food Hydrocoll.* **2019**, *88*, 75–85. https://doi.org/10.1016/j.foodhyd.2018.09.037.

(87) Tzen, J. T. C.; Peng, C. C.; Cheng, D. J.; Chen, E. C. F.; Chiu, J. M. H. A New Method for Seed Oil Body Purification and Examination of Oil Body Integrity Following Germination. *J. Biochem.* **1997**, *121* (4), 762–768. https://doi.org/10.1093/oxfordjournals.jbchem.a021651.

(88) Kapchie, V. N.; Towa, L. T.; Hauck, C.; Murphy, P. A. Evaluation of Enzyme Efficiency for Soy Oleosome Isolation and Ultrastructural Aspects. *Food Res. Int.* **2010**, *43* (1), 241–247. https://doi.org/10.1016/j.foodres.2009.09.019.

(89) Campbell, K. A.; Glatz, C. E.; Johnson, L. A.; Jung, S.; De Moura, J. M. N.; Kapchie, V.; Murphy, P. Advances in Aqueous Extraction Processing of Soybeans. *JAOCS, J. Am. Oil Chem. Soc.* **2011**, *88* (4), 449–465. https://doi.org/10.1007/s11746-010-1724-5.

(90) Tzen, J. T. C.; Huang, A. H. C. Surface Structure and Properties of Plant Seed Oil Bodies. *J. Cell Biol.* **1992**, *117* (2), 327–335. https://doi.org/10.1083/jcb.117.2.327.

(91) Dong, X. Y.; Guo, L. L.; Wei, F.; Li, J. F.; Jiang, M. L.; Li, G. M.; Zhao, Y. Di; Chen, H. Some Characteristics and Functional Properties of Rapeseed Protein Prepared by Ultrasonication, Ultrafiltration and Isoelectric Precipitation. *J. Sci. Food Agric.* **2011**, *91* (8), 1488–1498. https://doi.org/10.1002/jsfa.4339.

(92) Khattab, R. Y.; Arntfield, S. D. Functional Properties of Raw and Processed Canola Meal. *LWT - Food Sci. Technol.* **2009**, *42* (6), 1119–1124. https://doi.org/10.1016/j.lwt.2009.02.009.

(93) Anderson-Hafermann, J. C.; Zhang, Y.; Parsons, C. M. Effects of Processing on the Nutritional Quality of Canola Meal. *Poult. Sci.* **1993**, *72* (2), 326–333. https://doi.org/10.3382/ps.0720326.

(94) Anwar, A.; Clandinin, D. R. Nitrogen Solubility as a Means of Estimating the Gross Protein Value of Rapeseed Meal. *Poult. Sci.* **1970**, *50* (1), 135–136. https://doi.org/10.3382/ps.0500135.

(95) Salazar-Villanea, S.; Bruininx, E. M. A. M.; Gruppen, H.; Hendriks, W. H.; Carré, P.; Quinsac, A.; Poel, A. F. B. Van Der. Physical and Chemical Changes of Rapeseed Meal

Proteins during Toasting and Their Effects on in Vitro Digestibility. *J. Anim. Sci. Biotechnol.* **2016**, *7* (1), 1–11. https://doi.org/10.1186/s40104-016-0120-x.

(96) Dalgalarrondo, M.; Robin, J. M.; Azanza, J. L. Subunit Composition of the Globulin Fraction of Rapeseed (Brassica Napus L.). *Plant Sci.* **1986**, *43*, 115–124. https://doi.org/https://doi.org/10.1016/0168-9452(86)90151-2.

(97) Monsalve, R. I.; Lopez-otin, C.; Villalba, M.; Rodriguez, R. A New Distinct Group of 2 S Albumins from Rapeseed: Amino Acid Sequence of Two Low Molecular Weight Napins. *FEBS Lett.* **1991**, *295* (1), 207–210.

(98) Rawel, H. M.; Czajka, D.; Rohn, S.; Kroll, J. Interactions of Different Phenolic Acids and Flavonoids with Soy Proteins. *Int. J. Biol. Macromol.* **2002**, *30* (3–4), 137–150. https://doi.org/10.1016/S0141-8130(02)00016-8.

(99) Beychok, S. Circular Dichroism of Biological Macromolecules. *Science (80-.).* **1966**, *154* (3754), 1288–1299. https://doi.org/10.1126/science.154.3754.1288.

(100) Nikiforidis, C. V.; Donsouzi, S.; Kiosseoglou, V. The Interplay between Diverse Oil Body Extracts and Exogenous Biopolymers or Surfactants. *Food Res. Int.* **2016**, *83*, 14–24. https://doi.org/10.1016/j.foodres.2016.02.007.

(101) Reynoldst, J. A.; Tanford, C. Binding of Dodecyl Sulfate to Proteins at High Binding Ratios. Possible Implications for the State of Proteins in Biological Membranes. *Proc. Natl. Acad. Sci. U. S. A.* **1970**, *66* (3), 1002–1003. https://doi.org/https://doi.org/10.1073/pnas.66.3.1002.

(102) Burguera, J. L.; Burguera, M. Analytical Applications of Emulsions and Microemulsions. *Talanta* **2012**, *96*, 11–20. https://doi.org/10.1016/j.talanta.2012.01.030.

(103) McClements, D. J.; Gumus, C. E. Natural Emulsifiers — Biosurfactants, Phospholipids, Biopolymers, and Colloidal Particles: Molecular and Physicochemical Basis of Functional Performance. *Adv. Colloid Interface Sci.* **2016**, *234*, 3–26. https://doi.org/10.1016/j.cis.2016.03.002.

(104) Dickinson, E. Adsorbed Protein Layers at Fluid Interfaces: Interactions, Structure and Surface Rheology. *Colloids Surfaces B Biointerfaces* **1999**, *15* (2), 161–176. https://doi.org/10.1016/S0927-7765(99)00042-9.

(105) Hayes, D. G.; Smith, G. A. Biobased Surfactants: Overview and Industrial State of the Art. In *Biobased Surfactants*; Hayes, D. G., Solaiman, D. K. ., Ashby, R. D., Eds.; Elsevier Inc., 2019; pp 3–38. https://doi.org/10.1016/b978-0-12-812705-6.00001-0.

(106) Campbell, K. A.; Glatz, C. E.; Johnson, L. A.; Jung, S.; De Moura, J. M. N.; Kapchie, V.; Murphy, P. Advances in Aqueous Extraction Processing of Soybeans. *J. Am. Oil Chem. Soc.* **2011**, *88* (4), 449–465. https://doi.org/10.1007/s11746-010-1724-5.

(107) Apaiah, R. K.; Linnemann, A. R.; Van Der Kooi, H. J. Exergy Analysis: A Tool to Study the Sustainability of Food Supply Chains. *Food Res. Int.* **2006**, *39* (1), 1–11. https://doi.org/10.1016/j.foodres.2005.04.006.

(108) Geerts, M. E. J.; Nikiforidis, C. V.; van der Goot, A. J.; van der Padt, A. Protein Nativity Explains Emulsifying Properties of Aqueous Extracted Protein Components from Yellow Pea. *Food Struct.* **2017**, *14*, 104–111. https://doi.org/10.1016/j.foostr.2017.09.001.

(109) Sridharan, S.; Meinders, M. B. J.; Bitter, J. H.; Nikiforidis, C. V. Native Pea Flour as Stabilizer of Oil-in-Water Emulsions: No Protein Purification Necessary. *Food Hydrocoll.* **2020**, *101*, 105533. https://doi.org/10.1016/j.foodhyd.2019.105533.

(110) Tamayo Tenorio, A.; Gieteling, J.; Nikiforidis, C. V.; Boom, R. M.; van der Goot, A. J. Interfacial Properties of Green Leaf Cellulosic Particles. *Food Hydrocoll.* **2017**, *71*, 8–16. https://doi.org/10.1016/j.foodhyd.2017.04.030.

(111) Ntone, E.; Bitter, J. H.; Nikiforidis, C. V. Not Sequentially but Simultaneously: Facile Extraction of Proteins and Oleosomes from Oilseeds. *Food Hydrocoll.* **2020**, *102*, 105598. https://doi.org/10.1016/j.foodhyd.2019.105598.

(112) Erickson, H. P. Size and Shape of Protein Molecules at the Nanometer Level Determined by Sedimentation, Gel Filtration, and Electron Microscopy. *Biol. Proced. Online* **2009**, *11* (1), 32–51. https://doi.org/10.1007/s12575-009-9008-x.

(113) Hu, Z.; Wang, X.; Zhan, G.; Liu, G.; Hua, W.; Wang, H. Unusually Large Oilbodies Are Highly Correlated with Lower Oil Content in Brassica Napus. *Plant Cell Rep.* **2009**, *28* (4), 541–549. https://doi.org/10.1007/s00299-008-0654-2.

(114) Nikiforidis, C. V.; Donsouzi, S.; Kiosseoglou, V. The Interplay between Diverse Oil Body Extracts and Exogenous Biopolymers or Surfactants. *Food Res. Int.* **2016**, *83*, 14–24. https://doi.org/10.1016/j.foodres.2016.02.007.

(115) Tcholakova, S.; Denkov, N. D.; Ivanov, I. B.; Campbell, B. Coalescence Stability of Emulsions Containing Globular Milk Proteins. *Adv. Colloid Interface Sci.* **2006**, *123–126* (SPEC. ISS.), 259–293. https://doi.org/10.1016/j.cis.2006.05.021.

(116) de Figueiredo Furtado, G.; Michelon, M.; de Oliveira, D. R. B.; da Cunha, R. L. Heteroaggregation of Lipid Droplets Coated with Sodium Caseinate and Lactoferrin. *Food Res. Int.* **2016**, *89*, 309–319. https://doi.org/10.1016/j.foodres.2016.08.024.

(117) Karefyllakis, D.; Jan Van Der Goot, A.; Nikiforidis, C. V. The Behaviour of Sunflower Oleosomes at the Interfaces. *Soft Matter* **2019**, *15* (23), 4639–4646. https://doi.org/10.1039/c9sm00352e.

(118) Dickinson, E.; Rolfe, S. E.; Dalgleish, D. G. Competitive Adsorption of As1-Casein and

β-Casein in Oil-in-Water Emulsions. *Food Hydrocoll.* **1988**, *2* (5), 397–405. https://doi.org/10.1016/S0268-005X(88)80004-3.

(119) Robson, E. W.; Dalgleish, G. Interfacial Composition of Sodium Caseinate Emulsions. *J. Food Sci.* **1987**, *52* (6), 1694–1698. https://doi.org/https://doi.org/10.1111/j.1365-2621.1987.tb05908.x.

(120) Anton, M.; Gandemer, G. Effect of PH on Interface Composition and on Quality of Oil-in-Water Emulsions Made with Hen Egg Yolk. *Colloids Surfaces B Biointerfaces* **1999**, *12* (3–6), 351–358. https://doi.org/10.1016/S0927-7765(98)00089-7.

(121) Van Aken, G. A.; Zoet, F. D.; Diederen, J. Composition of Thin Films between Emulsion Droplets Stabilized by Protein, as Measured in Highly Concentrated Emulsions. *Colloids Surfaces B Biointerfaces* **2002**, *26* (3), 269–279. https://doi.org/10.1016/S0927-7765(02)00010-3.

(122) Mohan, S.; Narsimhan, G. Coalescence of Protein-Stabilized Emulsions in a High-Pressure Homogenizer. *J. Colloid Interface Sci.* **1997**, *192* (1), 1–15. https://doi.org/10.1006/jcis.1997.5012.

(123) Mitropoulos, V.; Mütze, A.; Fischer, P. Mechanical Properties of Protein Adsorption Layers at the Air/Water and Oil/Water Interface: A Comparison in Light of the Thermodynamical Stability of Proteins. *Adv. Colloid Interface Sci.* **2014**, *206*, 195–206. https://doi.org/10.1016/j.cis.2013.11.004.

(124) Norde, W. Adsorption of Proteins from Solution at the Solid-Liquid Interface. *Adv. Colloid Interface Sci.* **1986**, *25*, 267–340. https://doi.org/10.1016/0001-8686(86)80012-4.

(125) Tambe, D. E.; Sharma, M. M. The Effect of Colloidal Particles on Fluid-Fluid Interfacial Properties and Emulsion Stability. *Adv. Colloid Interface Sci.* **1994**, *52*, 1–63. https://doi.org/10.1016/0001-8686(94)80039-1.

(126) Narsimhan, G.; Uraizee, F. Kinetics of Adsorption of Globular Proteins at an Air-Water Interface. *Biotechnol. Prog.* **1992**, *8* (3), 187–196. https://doi.org/10.1021/bp00015a003.

(127) Damodaran, S. Adsorbed Layers Formed from Mixtures of Proteins. *Curr. Opin. Colloid Interface Sci.* **2004**, *9* (5), 328–339. https://doi.org/10.1016/j.cocis.2004.09.008.

(128) Wierenga, P. A.; Meinders, M. B. J.; Egmond, M. R.; Voragen, F. A. G. J.; De Jongh, H. H. J. Protein Exposed Hydrophobicity Reduces the Kinetic Barrier for Adsorption of Ovalbumin to the Air-Water Interface. *Langmuir*. 2003, pp 8964–8970. https://doi.org/10.1021/la034868p.

(129) Kumar, A.; Park, B. J.; Tu, F.; Lee, D. Amphiphilic Janus Particles at Fluid Interfaces. *Soft Matter* **2013**, *9* (29), 6604–6617. https://doi.org/10.1039/c3sm50239b.

(130) Binks, B. P.; Fletcher, P. D. I. Particles Adsorbed at the Oil-Water Interface: A Theoretical Comparison between Spheres of Uniform Wettability and “Janus” Particles. *Langmuir* **2001**, *17* (16), 4708–4710. https://doi.org/10.1021/la0103315.

(131) Glaser, N.; Adams, D. J.; Böker, A.; Krausch, G. Janus Particles at Liquid-Liquid Interfaces. *Langmuir* **2006**, *22* (12), 5227–5229. https://doi.org/10.1021/la060693i.

(132) Van Kempen, S. E. H. J.; Schols, H. A.; Van Der Linden, E.; Sagis, L. M. C. Non-Linear Surface Dilatational Rheology as a Tool for Understanding Microstructures of Air/Water Interfaces Stabilized by Oligofructose Fatty Acid Esters. *Soft Matter* **2013**, *9* (40), 9579–9592. https://doi.org/10.1039/c3sm51770e.

(133) Hinderink, E. B. A.; Sagis, L.; Schroën, K.; Berton-Carabin, C. C. Behavior of Plant-Dairy Protein Blends at Air-Water and Oil-Water Interfaces. *Colloids Surfaces B Biointerfaces* **2020**, *192*, 111015. https://doi.org/10.1016/j.colsurfb.2020.111015.

(134) Yang, J.; Thielen, I.; Berton-Carabin, C. C.; van der Linden, E.; Sagis, L. M. C. Nonlinear Interfacial Rheology and Atomic Force Microscopy of Air-Water Interfaces Stabilized by Whey Protein Beads and Their Constituents. *Food Hydrocoll.* **2020**, *101* (September 2019), 105466. https://doi.org/10.1016/j.foodhyd.2019.105466.

(135) Sagis, L. M. C.; Scholten, E. Complex Interfaces in Food: Structure and Mechanical Properties. *Trends Food Sci. Technol.* **2014**, *37* (1), 59–71. https://doi.org/10.1016/j.tifs.2014.02.009.

(136) Kornet, R.; Veenemans, J.; Venema, P.; Jan, A.; Goot, V. Der; Meinders, M.; Sagis, L.; Linden, E. Van Der. Less Is More : Limited Fractionation Yields Stronger Gels for Pea Proteins. *Food Hydrocoll.* **2021**, *112*, 106285. https://doi.org/10.1016/j.foodhyd.2020.106285.

(137) Peng, Y.; Kersten, N.; Kyriakopoulou, K.; van der Goot, A. J. Functional Properties of Mildly Fractionated Soy Protein as Influenced by the Processing PH. *J. Food Eng.* **2020**, *275*, 109875. https://doi.org/10.1016/j.jfoodeng.2019.109875.

(138) Fuhrmeister, H.; Meuser, F. Impact of Processing on Functional Properties of Protein Products from Wrinkled Peas. *J. Food Eng.* **2003**, *56* (2–3), 119–129. https://doi.org/10.1016/S0260-8774(02)00241-8.

(139) Depree, J. A.; Savage, G. P. Physical and Flavour Stability of Mayonnaise. *Trends Food Sci. Technol.* **2001**, *12* (5–6), 157–163. https://doi.org/10.1016/S0924-2244(01)00079-6.

(140) Karefyllakis, D.; Altunkaya, S.; Berton-Carabin, C. C.; van der Goot, A. J.; Nikiforidis, C. V. Physical Bonding between Sunflower Proteins and Phenols: Impact on Interfacial Properties. *Food Hydrocoll.* **2017**, *73*, 326–334. https://doi.org/10.1016/j.foodhyd.2017.07.018.

(141) Bock, A.; Steinhäuser, U.; Drusch, S. Partitioning Behavior and Interfacial Activity of Phenolic Acid Derivatives and Their Impact on β-Lactoglobulin at the Oil-Water Interface. *Food Biophysics*. 2021. https://doi.org/10.1007/s11483-020-09663-7.

(142) Jakobek, L. Interactions of Polyphenols with Carbohydrates, Lipids and Proteins. *Food Chem.* **2015**, *175*, 556–567. https://doi.org/10.1016/j.foodchem.2014.12.013.

(143) Czubinski, J.; Dwiecki, K. A Review of Methods Used for Investigation of Protein–Phenolic Compound Interactions. *Int. J. Food Sci. Technol.* **2017**, *52* (3), 573–585. https://doi.org/10.1111/ijfs.13339.

(144) Roth, C. M.; Neal, B. L.; Lenhoff, A. M. Van Der Waals Interactions Involving Proteins. *Biophys. J.* **1996**, *70* (2 I), 977–987. https://doi.org/10.1016/S0006-3495(96)79641-8.

(145) Withana-Gamage, T. S.; Hegedus, D. D.; Qiu, X.; Wanasundara, J. P. D. In Silico Homology Modeling to Predict Functional Properties of Cruciferin. *J. Agric. Food Chem.* **2011**, *59* (24), 12925–12938. https://doi.org/10.1021/jf201979a.

(146) Folawiyo, Y. L.; Apenten, R. K. O. Effect of PH and Ionic Strength on the Heat Stability of Rapeseed 12S Globulin (Cruciferin) by the ANS Fluorescence Method. *J. Sci. Food Agric.* **1996**, 241–246.

(147) Sridharan, S.; Meinders, M. B. J.; Bitter, J. H.; Nikiforidis, C. V. On the Emulsifying Properties of Self-Assembled Pea Protein Particles. *Langmuir* **2020**, *36* (41), 12221–12229. https://doi.org/10.1021/acs.langmuir.0c01955.

(148) Sagis, L. M. C.; Fischer, P. Nonlinear Rheology of Complex Fluid-Fluid Interfaces. *Curr. Opin. Colloid Interface Sci.* **2014**, *19* (6), 520–529. https://doi.org/10.1016/j.cocis.2014.09.003.

(149) Loveday, S. M. Plant Protein Ingredients with Food Functionality Potential. *Nutr. Bull.* **2020**, *45* (3), 321–327. https://doi.org/10.1111/nbu.12450.

(150) Assatory, A.; Vitelli, M.; Rajabzadeh, A. R.; Legge, R. L. Dry Fractionation Methods for Plant Protein, Starch and Fiber Enrichment: A Review. *Trends Food Sci. Technol.* **2019**, *86* (November 2018), 340–351. https://doi.org/10.1016/j.tifs.2019.02.006.

(151) Van Der Goot, A. J.; Pelgrom, P. J. M.; Berghout, J. A. M.; Geerts, M. E. J.; Jankowiak, L.; Hardt, N. A.; Keijer, J.; Schutyser, M. A. I.; Nikiforidis, C. V.; Boom, R. M. Concepts for Further Sustainable Production of Foods. *J. Food Eng.* **2016**, *168*, 42–51. https://doi.org/10.1016/j.jfoodeng.2015.07.010.

(152) Papalamprou, E. M.; Doxastakis, G. I.; Biliaderis, C. G.; Kiosseoglou, V. Influence of Preparation Methods on Physicochemical and Gelation Properties of Chickpea Protein Isolates. *Food Hydrocoll.* **2009**, *23* (2), 337–343. https://doi.org/10.1016/j.foodhyd.2008.03.006.

(153) Dickinson, E. Emulsion Gels: The Structuring of Soft Solids with Protein-Stabilized Oil Droplets. *Food Hydrocoll.* **2012**, *28* (1), 224–241. https://doi.org/10.1016/j.foodhyd.2011.12.017.

(154) Sala, G.; van Vliet, T.; Cohen Stuart, M. A.; Aken, G. A. va.; van de Velde, F. Deformation and Fracture of Emulsion-Filled Gels: Effect of Oil Content and Deformation Speed. *Food Hydrocoll.* **2009**, *23* (5), 1381–1393. https://doi.org/10.1016/j.foodhyd.2008.11.016.

(155) Dickinson, E. *Understanding Food Structures: The Colloid Science Approach*; Elsevier Inc., 2014. https://doi.org/10.1016/B978-0-12-404610-8.00001-3.

(156) Genovese, D. B. Shear Rheology of Hard-Sphere, Dispersed, and Aggregated Suspensions, and Filler-Matrix Composites. *Adv. Colloid Interface Sci.* **2012**, *171–172*, 1–16. https://doi.org/10.1016/j.cis.2011.12.005.

(157) Chen, J.; Dickinson, E.; Edwards, M. Rheology of Acid-Induced Sodium Caseinate Stabilized Emulsion Gels. *Journal of Texture Studies*. 1999, pp 377–396. https://doi.org/10.1111/j.1745-4603.1999.tb00226.x.

(158) Chen, J.; Dickinson, E. Viscoelastic Properties of Heat-Set Whey Protein Emulsion Gels. *J. Texture Stud.* **1998**, *29* (3), 285–304. https://doi.org/10.1111/j.1745-4603.1998.tb00171.x.

(159) Dickinson, E.; Hong, S. T. Influence of Water-Soluble Nonionic Emulsifier on the Rheology of Heat-Set Protein-Stabilized Emulsion Gels. *J. Agric. Food Chem.* **1995**, *43* (10), 2560–2566. https://doi.org/10.1021/jf00058a002.

(160) McClements, D. J.; Monahan, F. J.; Kinsella, J. E. Effect of Emulsion Droplets on the Rheology of Whey Protein Isolate Gels. *J. Texture Stud.* **1993**, *24* (4), 411–422. https://doi.org/10.1111/j.1745-4603.1993.tb00051.x.

(161) Schreuders, F. K. G.; Sagis, L. M. C.; Bodnár, I.; Erni, P.; Boom, R. M.; van der Goot, A. J. Small and Large Oscillatory Shear Properties of Concentrated Proteins. *Food Hydrocoll.* **2021**, *110*, 106172. https://doi.org/10.1016/j.foodhyd.2020.106172.

(162) Ewoldt, R. H.; Winter, P.; Maxey, J.; McKinley, G. H. Large Amplitude Oscillatory Shear of Pseudoplastic and Elastoviscoplastic Materials. *Rheol. Acta* **2010**, *49* (2), 191–212. https://doi.org/10.1007/s00397-009-0403-7.

(163) Yahia, A.; Mantellato, S.; Flatt, R. J. *Concrete Rheology: A Basis for Understanding Chemical Admixtures*; Elsevier Ltd, 2016. https://doi.org/10.1016/B978-0-08-100693-1.00007-2.

(164) Withana-Gamage, T. S.; Hegedus, D. D.; Qiu, X.; Wanasundara, J. P. D. Solubility, Heat-Induced Gelation and Pepsin Susceptibility of Cruciferin Protein as Affected by

Subunit Composition. *Food Biophys.* **2015**, *10* (2), 103–115. https://doi.org/10.1007/s11483-014-9370-3.

(165) Farjami, T.; Madadlou, A. An Overview on Preparation of Emulsion-Filled Gels and Emulsion Particulate Gels. *Trends Food Sci. Technol.* **2019**, *86* (April 2018), 85–94. https://doi.org/10.1016/j.tifs.2019.02.043.

(166) Sala, G.; van Vliet, T.; Cohen Stuart, M.; van de Velde, F.; van Aken, G. A. Deformation and Fracture of Emulsion-Filled Gels: Effect of Gelling Agent Concentration and Oil Droplet Size. *Food Hydrocoll.* **2009**, *23* (7), 1853–1863. https://doi.org/10.1016/j.foodhyd.2009.03.002.

(167) Geremias-Andrade, I.; Souki, N.; Moraes, I.; Pinho, S. Rheology of Emulsion-Filled Gels Applied to the Development of Food Materials. *Gels* **2016**, *2* (3), 22. https://doi.org/10.3390/gels2030022.

(168) Chen, J.; Dickinson, E. Effect of Surface Character of Filler Particles on Rheology of Heat-Set Whey Protein Emulsion Gels. *Colloids Surfaces B Biointerfaces* **1999**, *12* (3–6), 373–381. https://doi.org/10.1016/S0927-7765(98)00091-5.

(169) Wu, J.; Muir, A. D. Comparative Structural, Emulsifying, and Biological Properties of 2 Major Canola Proteins, Cruciferin and Napin. *J. Food Sci.* **2008**, *73* (3). https://doi.org/10.1111/j.1750-3841.2008.00675.x.

(170) Krzyzaniak, A.; Burova, T.; Haertlé, T.; Barciszewski, J. The Structure and Properties of Napin-Seed Storage Protein from Rape (Brassica Napus L.). *Nahrung - Food*. 1998, pp 201–204. https://doi.org/10.1002/(sici)1521-3803(199808)42:03/04<201::aid-food201>3.3.co;2-l.

(171) van Vliet, T. Rheological Properties of Filled Gels. Influence of Filler Matrix Interaction. *Colloid Polym. Sci.* **1988**, *266* (6), 518–524. https://doi.org/10.1007/BF01420762.

(172) Dickinson, E.; Chen, J. Heat-Set Whey Protein Emulsion Gels: Role of Active and Inactive Filler Particles. *J. Dispers. Sci. Technol.* **1999**, *20* (1–2), 197–213. https://doi.org/10.1080/01932699908943787.

(173) Lefevre, T.; Subirade, M. Molecular Differences in the Formation and Structure of Fine-Stranded and Particulate β-Lactoglobulin Gels. *Biopolymers* **2000**, *54*, 578–586. https://doi.org/10.1002/1097-0282(200012)54:7<578::AID-BIP100>3.0.CO;2-2.

(174) Sala, G. *Food Gels Filled with Emulsion Droplets Linking Large Deformation Properties to Sensory Perception*, PhD Thesis.; Wageningen University, 2007.

(175) Oliver, L.; Wieck, L.; Scholten, E. Influence of Matrix Inhomogeneity on the Rheological Properties of Emulsion-Filled Gels. *Food Hydrocoll.* **2016**, *52*, 116–125. https://doi.org/10.1016/j.foodhyd.2015.06.003.

(176) Shih, W.; Shih, Y.; Kim, S.; Liu, J.; Aksay, I. A. Scaling Behavior of the Elastic Properties of Colloidal Gels. *Phys. Rev. A* **1990**, *42* (8). https://doi.org/https://doi.org/10.1103/PhysRevA.42.4772.

(177) Morris, S. N. S.; Olzmann, J. A. A Tense Situation: Maintaining ER Homeostasis during Lipid Droplet Budding. *Dev. Cell* **2019**, *50* (1), 1–2. https://doi.org/10.1016/j.devcel.2019.06.005.

(178) Bosch, M.; Parton, R. G.; Pol, A. Lipid Droplets, Bioenergetic Fluxes, and Metabolic Flexibility. *Semin. Cell Dev. Biol.* **2020**, No. November 2019, 0–1. https://doi.org/10.1016/j.semcdb.2020.02.010.

(179) Wilfling, F.; Wang, H.; Haas, J. T.; Krahmer, N.; Gould, T. J.; Cheng, J.; Graham, M.; Christiano, R.; Fröhlich, F.; Buhman, K. K.; Coleman, R. a; Bewersdorf, J.; Farese, R. V; Walther, T. C. Triacylglycerol Synthesis Enzymes Mediate Lipid Droplet Growth by Relocalizing from the ER to Lipid Droplets. *Dev. Cell* **2013**, *24* (4), 384–399. https://doi.org/10.1016/j.devcel.2013.01.013.

(180) Olzmann, J. A.; Carvalho, P. Dynamics and Functions of Lipid Droplets. *Nat. Rev. Mol. Cell Biol.* **2019**, *20* (3), 137–155. https://doi.org/10.1038/s41580-018-0085-z.

(181) Goodman, J. M. The Gregarious Lipid Droplet. *J. Biol. Chem.* **2008**, *283* (42), 28005–28009. https://doi.org/10.1074/jbc.R800042200.

(182) Mahamid, J.; Tegunov, D.; Maiser, A.; Arnold, J.; Leonhardt, H.; Plitzko, J. M.; Baumeister, W. Liquid-Crystalline Phase Transitions in Lipid Droplets Are Related to Cellular States and Specific Organelle Association. *Proc. Natl. Acad. Sci. U. S. A.* **2019**, *116* (34), 16866–16871. https://doi.org/10.1073/pnas.1903642116.

(183) Bosch, M.; Sanchez-Alvarez, M.; Fajardo, A.; Kapetanovic, R.; Steiner, B.; Dutra, F.; Moreira, L.; López, J. A.; Campo, R.; Morales-paytuví, F.; Tort, O.; Gubern, A.; Templin, R. M.; Curson, J. E. B.; Martel, N.; Català, C.; Lozano, F.; Tebar, F.; Enrich, C.; Vázquez, J.; Pozo, M. A. Del; Sweet, M. J.; Bozza, P. T.; Gross, S. P.; Parton, R. G.; Pol, A. Mammalian Lipid Droplets Are Innate Immune Hubs Integrating Cell Metabolism and Host Defense. *Science (80-.).* **2020**, *8085*. https://doi.org/10.1126/science.aay8085.

(184) Ben M'barek, K.; Ajjaji, D.; Chorlay, A.; Vanni, S.; Forêt, L.; Thiam, A. R. ER Membrane Phospholipids and Surface Tension Control Cellular Lipid Droplet Formation. *Dev. Cell* **2017**, *41* (6), 591-604.e7. https://doi.org/10.1016/j.devcel.2017.05.012.

(185) Tauchi-Sato, K.; Ozeki, S.; Houjou, T.; Taguchi, R.; Fujimoto, T. The Surface of Lipid Droplets Is a Phospholipid Monolayer with a Unique Fatty Acid Composition. *J. Biol. Chem.* **2002**, *277* (46), 44507–44512. https://doi.org/10.1074/jbc.M207712200.

(186) Fujimoto, T.; Ohsaki, Y. Cytoplasmic Lipid Droplets: Rediscovery of an Old Structure as a Unique Platform. *Ann. N. Y. Acad. Sci.* **2006**, *1086* (2006), 104–115. https://doi.org/10.1196/annals.1377.010.

(187) Lundquist, P. K.; Shivaiah, K. K.; Espinoza-Corral, R. Lipid Droplets throughout the Evolutionary Tree. *Prog. Lipid Res.* **2020**, *78*, 101029. https://doi.org/10.1016/j.plipres.2020.101029.

(188) Bhatla, S. C.; Vandana, S.; Kaushik, V. Recent Developments in the Localization of Oil Body-Associated Signaling Molecules during Lipolysis in Oilseeds. *Plant Signal. Behav.* **2009**, *4* (3), 176–182. https://doi.org/10.4161/psb.4.3.7799.

(189) Prinz, W. A. Bridging the Gap: Membrane Contact Sites in Signaling, Metabolism, and Organelle Dynamics. *J. Cell Biol.* **2014**, *205* (6), 759–769. https://doi.org/10.1083/jcb.201401126.

(190) Gong, J.; Sun, Z.; Wu, L.; Xu, W.; Schieber, N.; Xu, D.; Shui, G.; Yang, H.; Parton, R. G.; Li, P. Fsp27 Promotes Lipid Droplet Growth by Lipid Exchange and Transfer at Lipid Droplet Contact Sites. *J. Cell Biol.* **2011**, *195* (6), 953–963. https://doi.org/10.1083/jcb.201104142.

(191) Gao, G.; Chen, F. J.; Zhou, L.; Su, L.; Xu, D.; Xu, L.; Li, P. Control of Lipid Droplet Fusion and Growth by CIDE Family Proteins. *Biochim. Biophys. Acta - Mol. Cell Biol. Lipids* **2017**, *1862* (10), 1197–1204. https://doi.org/10.1016/j.bbalip.2017.06.009.

(192) Pyc, M.; Cai, Y.; Greer, M. S.; Yurchenko, O.; Chapman, K. D.; Dyer, J. M.; Mullen, R. T. Turning Over a New Leaf in Lipid Droplet Biology. *Trends Plant Sci.* **2017**, *22* (7), 596–609. https://doi.org/10.1016/j.tplants.2017.03.012.

(193) Lis, L. J.; McAlister, M.; Fuller, N.; Rand, R. P.; Parsegian, V. A. Measurement of the Lateral Compressibility of Several Phospholipid Bilayers. *Biophys. J.* **1982**, *37* (March), 667–672.

(194) Kory, N.; Thiam, A. R.; Farese, R. V.; Walther, T. C. Protein Crowding Is a Determinant of Lipid Droplet Protein Composition. *Dev. Cell* **2015**, *34* (3), 351–363. https://doi.org/10.1016/j.devcel.2015.06.007.

(195) Chernomordik, L. V.; Kozlov, M. M. Protein-Lipid Interplay in Fusion and Fission of Biological Membranes. *Annu. Rev. Biochem.* **2003**, *72*, 175–207. https://doi.org/10.1146/annurev.biochem.72.121801.161504.

(196) Dubey, R.; Stivala, C. E.; Nguyen, H. Q.; Goo, Y. H.; Paul, A.; Carette, J. E.; Trost, B. M.; Rohatgi, R. Lipid Droplets Can Promote Drug Accumulation and Activation. *Nat. Chem. Biol.* **2020**, *16* (2), 206–213. https://doi.org/10.1038/s41589-019-0447-7.

(197) Boucher, J.; Cengelli, F.; Trumbic, D.; Marison, I. W. Sorption of Hydrophobic Organic

Compounds (HOC) in Rapeseed Oil Bodies. *Chemosphere* **2008**, *70*, 1452–1458. https://doi.org/10.1016/j.chemosphere.2007.08.065.

(198) Nikiforidis, C. V.; Matsakidou, A.; Kiosseoglou, V. Composition, Properties and Potential Food Applications of Natural Emulsions and Cream Materials Based on Oil Bodies. *RSC Adv.* **2014**, *4* (48), 25067–25078. https://doi.org/10.1039/C4RA00903G.

(199) Napier, J. A.; Stobart, A. K.; Shewry, P. R. The Structure and Biogenesis of Plant Oil Bodies: The Role of the ER Membrane and the Oleosin Class of Proteins. *Plant Mol. Biol.* **1996**, *31* (5), 945–956. https://doi.org/10.1007/BF00040714.

(200) Willems, S. B. J.; Schijven, L. M. I.; Bunschoten, A.; Van Leeuwen, F. W. B.; Velders, A. H.; Saggiomo, V. Covalently Bound Monolayer Patterns Obtained by Plasma Etching on Glass Surfaces. *Chem. Commun.* **2019**, *55* (53), 7667–7670. https://doi.org/10.1039/c9cc03791h.

(201) Abraham, M. J.; Murtola, T.; Schulz, R.; Páll, S.; Smith, J. C.; Hess, B.; Lindah, E. Gromacs: High Performance Molecular Simulations through Multi-Level Parallelism from Laptops to Supercomputers. *SoftwareX* **2015**, *1–2*, 19–25. https://doi.org/10.1016/j.softx.2015.06.001.

(202) Marrink, S. J.; Risselada, H. J.; Yefimov, S.; Tieleman, D. P.; De Vries, A. H. The MARTINI Force Field: Coarse Grained Model for Biomolecular Simulations. *J. Phys. Chem. B* **2007**, *111* (27), 7812–7824. https://doi.org/10.1021/jp071097f.

(203) Humphrey, W.; Dalke, A.; Schulten, K. VMD: Visual Molecular Dynamics. *J. Mol. Graph.* **1996**, *14*, 33–38. https://doi.org/https://doi.org/10.1016/0263-7855(96)00018-5.

(204) Caillon, L.; Nieto, V.; Gehan, P.; Omrane, M.; Rodriguez, N.; Monticelli, L.; Thiam, A. R. Triacylglycerols Sequester Monotopic Membrane Proteins to Lipid Droplets. *Nat. Commun.* **2020**, *11* (1), 1–12. https://doi.org/10.1038/s41467-020-17585-8.

(205) Vuorela, T.; Catte, A.; Niemelä, P. S.; Hall, A.; Hyvönen, M. T.; Marrink, S. J.; Karttunen, M.; Vattulainen, I. Role of Lipids in Spheroidal High Density Lipoproteins. *PLoS Comput. Biol.* **2010**, *6* (10). https://doi.org/10.1371/journal.pcbi.1000964.

(206) Berendsen, H. J. C.; Postma, J. P. M.; Van Gunsteren, W. F.; Dinola, A.; Haak, J. R. Molecular Dynamics with Coupling to an External Bath. *J. Chem. Phys.* **1984**, *81* (8), 3684–3690. https://doi.org/10.1063/1.448118.

(207) Parrinello, M.; Rahman, A. Polymorphic Transitions in Single Crystals: A New Molecular Dynamics Method. *J. Appl. Phys.* **1981**, *52* (12), 7182–7190. https://doi.org/10.1063/1.328693.

(208) Bussi, G.; Donadio, D.; Parrinello, M. Canonical Sampling through Velocity Rescaling. *J. Chem. Phys.* **2007**, *126* (1). https://doi.org/10.1063/1.2408420.

(209) Yin, Y.; Guo, L.; Chen, K.; Guo, Z.; Chao, H.; Wang, B. 3D Reconstruction of Lipid Droplets in the Seed of Brassica Napus. *Sci. Rep.* **2018**, No. October 2017, 1–9. https://doi.org/10.1038/s41598-018-24812-2.

(210) Huang, a H. C. Oil Bodies and Oleosins in Seeds. *Annu. Rev. Plant Physiol. Plant Mol. Biol.* **1992**, *43* (1), 177–200. https://doi.org/10.1146/annurev.pp.43.060192.001141.

(211) Kory, N.; Farese, R. V.; Walther, T. C. Targeting Fat: Mechanisms of Protein Localization to Lipid Droplets. *Trends Cell Biol.* **2016**, *26* (7), 535–546. https://doi.org/10.1016/j.tcb.2016.02.007.

(212) Farese, R. V.; Walther, T. C. Lipid Droplets Finally Get a Little R-E-S-P-E-C-T. *Cell* **2009**, *139* (5), 855–860. https://doi.org/10.1016/j.cell.2009.11.005.

(213) Siloto, R. M. P.; Findlay, K.; Lopez-Villalobos, A.; Yeung, E. C.; Nykiforuk, C. L.; Moloney, M. M. The Accumulation of Oleosins Determines the Size of Seed Oilbodies in Arabidopsis. *Plant Cell* **2006**, *18* (8), 1961–1974. https://doi.org/10.1105/tpc.106.041269.

(214) Shimada, T. L.; Hayashi, M.; Hara-Nishimura, I. Membrane Dynamics and Multiple Functions of Oil Bodies in Seeds and Leaves. *Plant Physiol.* **2017**, *176*, pp.01522.2017. https://doi.org/10.1104/pp.17.01522.

(215) Krahmer, N.; Guo, Y.; Wilfling, F.; Hilger, M.; Lingrell, S.; Heger, K.; Newman, H. W.; Schmidt-supprian, M.; Vance, D. E.; Jr, R. V. F.; Walther, T. C. Phosphatidylcholine Synthesis for Lipid Droplet Expansion Is Mediated by Localized Activation of CTP:Phosphocholine Cytidylyltransferase. *Cell Metab.* **2011**, *14* (4), 504–515. https://doi.org/10.1016/j.cmet.2011.07.013.

(216) Guo, Y.; Walther, T. C.; Rao, M.; Stuurman, N.; Goshima, G.; Terayama, K.; Wong, J. S.; Vale, R. D.; Walter, P.; Farese, R. V. Functional Genomic Screen Reveals Genes Involved in Lipid-Droplet Formation and Utilization. *Nature* **2008**, *453* (7195), 657–661. https://doi.org/10.1038/nature06928.

(217) Martin, S.; Parton, R. G. Lipid Droplets: A Unified View of a Dynamic Organelle. *Nat. Rev. Mol. Cell Biol.* **2006**, *7* (5), 373–378. https://doi.org/10.1038/nrm1912.

(218) Lee, S. J.; Schlesinger, P. H.; Wickline, S. A.; Lanza, G. M.; Baker, N. A. Simulation of Fusion-Mediated Nanoemulsion Interactions with Model Lipid Bilayers. *Soft Matter* **2012**, *8* (26), 7024–7035. https://doi.org/10.1039/c2sm25847a.

(219) Ollila, O. H. S.; Lamberg, A.; Lehtivaara, M.; Koivuniemi, A.; Vattulainen, I. Interfacial Tension and Surface Pressure of High Density Lipoprotein, Low Density Lipoprotein, and Related Lipid Droplets. *Biophys. J.* **2012**, *103* (6), 1236–1244. https://doi.org/10.1016/j.bpj.2012.08.023.

(220) Souza, P. C. T.; Alessandri, R.; Barnoud, J.; Thallmair, S.; Faustino, I.; Grünewald, F.; Patmanidis, I.; Abdizadeh, H.; Bruininks, B. M. H.; Wassenaar, T. A.; Kroon, P. C.; Melcr, J.; Nieto, V.; Corradi, V.; Khan, H. M.; Domański, J.; Javanainen, M.; Martinez-Seara, H.; Reuter, N.; Best, R. B.; Vattulainen, I.; Monticelli, L.; Periole, X.; Tieleman, D. P.; de Vries, A. H.; Marrink, S. J. Martini 3: A General Purpose Force Field for Coarse-Grained Molecular Dynamics. *Nat. Methods* **2021**, *18* (4), 382–388. https://doi.org/10.1038/s41592-021-01098-3.

(221) Souza, P. C. T.; Thallmair, S.; Conflitti, P.; Ramírez-Palacios, C.; Alessandri, R.; Raniolo, S.; Limongelli, V.; Marrink, S. J. Protein–Ligand Binding with the Coarse-Grained Martini Model. *Nat. Commun.* **2020**, *11* (1), 1–11. https://doi.org/10.1038/s41467-020-17437-5.

(222) Fan, Z. A.; Tsang, K. Y.; Chen, S. H.; Chen, Y. F. Revisit the Correlation between the Elastic Mechanics and Fusion of Lipid Membranes. *Sci. Rep.* **2016**, *6* (300), 1–10. https://doi.org/10.1038/srep31470.

(223) Kasson, P. M.; Lindahl, E.; Pande, V. S. Atomic-Resolution Simulations Predict a Transition State for Vesicle Fusion Defined by Contact of a Few Lipid Tails. *PLoS Comput. Biol.* **2010**, *6* (6), 1–11. https://doi.org/10.1371/journal.pcbi.1000829.

(224) Feller, W. *An Introduction to Probability Theory and Its Applications*, Third.; Wiley: New York, 1968.

(225) Nagle, J. F. Theory of Lipid Monolayer and Bilayer Phase Transitions: Effect of Headgroup Interactions. *J. Membr. Biol.* **1976**, *27* (1), 233–250. https://doi.org/10.1007/BF01869138.

(226) Jarc, E.; Petan, T. Lipid Droplets and the Management of Cellular Stress. *Yale J. Biol. Med.* **2019**, *92* (3), 435–452.

(227) Benador, I. Y.; Veliova, M.; Mahdaviani, K.; Petcherski, A.; Wikstrom, J. D.; Assali, E. A.; Acín-Pérez, R.; Shum, M.; Oliveira, M. F.; Cinti, S.; Sztalryd, C.; Barshop, W. D.; Wohlschlegel, J. A.; Corkey, B. E.; Liesa, M.; Shirihai, O. S. Mitochondria Bound to Lipid Droplets Have Unique Bioenergetics, Composition, and Dynamics That Support Lipid Droplet Expansion. *Cell Metab.* **2018**, *27* (4), 869-885.e6. https://doi.org/10.1016/j.cmet.2018.03.003.

(228) Welte, M. A. Expanding Roles for Lipid Droplets. *Curr. Biol.* **2015**, *25* (11), R470–R481. https://doi.org/10.1016/j.cub.2015.04.004.

(229) van der Schoot, C.; Paul, L. K.; Paul, S. B.; Rinne, P. L. H. Plant Lipid Bodies and Cell-Cell Signaling a New Role for an Old Organelle? *Plant Signal. Behav.* **2011**, *6* (11), 1732–1738. https://doi.org/10.4161/psb.6.11.17639.

(230) Thiam, A. R.; Forêt, L. The Physics of Lipid Droplet Nucleation, Growth and Budding. *Biochim. Biophys. Acta - Mol. Cell Biol. Lipids* **2016**, *1861* (8), 715–722. https://doi.org/10.1016/j.bbalip.2016.04.018.

(231) Chorlay, A.; Thiam, A. R. An Asymmetry in Monolayer Tension Regulates Lipid Droplet Budding Direction. *Biophys. J.* **2018**, *114* (3), 631–640. https://doi.org/10.1016/j.bpj.2017.12.014.

(232) Ischebeck, T.; Krawczyk, H. E.; Mullen, R. T.; Dyer, J. M.; Chapman, K. D. Lipid Droplets in Plants and Algae: Distribution, Formation, Turnover and Function. *Semin. Cell Dev. Biol.* **2020**, No. January. https://doi.org/10.1016/j.semcdb.2020.02.014.

(233) Pethica, B. A.; Mingins, J.; Taylor, J. A. G. Phospholipid Interactions in Monolayers. *J. Colloid Interface Sci.* **1976**, *55* (1), 2–8. https://doi.org/10.1016/0021-9797(76)90002-3.

(234) Huang, C. Y.; Huang, A. H. C. Unique Motifs and Length of Hairpin in Oleosin Target the Cytosolic Side of Endoplasmic Reticulum and Budding Lipid Droplet. *Plant Physiol.* **2017**, *174* (4), 2248–2260. https://doi.org/10.1104/pp.17.00366.

(235) Nikiforidis, C. V.; Ampatzidis, C.; Lalou, S.; Scholten, E.; Karapantsios, T. D.; Kiosseoglou, V. Purified Oleosins at Air-Water Interfaces. *Soft Matter* **2013**, *9* (4), 1354–1363. https://doi.org/10.1039/c2sm27118d.

(236) Bacle, A.; Gautier, R.; Jackson, C. L.; Fuchs, P. F. J.; Vanni, S. Interdigitation between Triglycerides and Lipids Modulates Surface Properties of Lipid Droplets. *Biophys. J.* **2017**, *112* (7), 1417–1430. https://doi.org/10.1016/j.bpj.2017.02.032.

(237) Yang, N.; Su, C.; Zhang, Y.; Jia, J.; Leheny, R. L.; Nishinari, K.; Fang, Y.; Phillips, G. O. In Situ Nanomechanical Properties of Natural Oil Bodies Studied Using Atomic Force Microscopy. *J. Colloid Interface Sci.* **2020**, *570*, 362–374. https://doi.org/10.1016/j.jcis.2020.03.011.

(238) Xu, L.; Zuo, Y. Y. Reversible Phase Transitions in the Phospholipid Monolayer. *Langmuir* **2018**, *34* (29), 8694–8700. https://doi.org/10.1021/acs.langmuir.8b01544.

(239) Sari, Y. W.; Mulder, W. J.; Sanders, J. P. M.; Bruins, M. E. Towards Plant Protein Refinery: Review on Protein Extraction Using Alkali and Potential Enzymatic Assistance. *Biotechnol. J.* **2015**, *10* (8), 1138–1157. https://doi.org/10.1002/biot.201400569.

(240) Moure, A.; Sineiro, J.; Domínguez, H.; Parajó, J. C. Functionality of Oilseed Protein Products: A Review. *Food Res. Int.* **2006**, *39* (9), 945–963. https://doi.org/10.1016/j.foodres.2006.07.002.

(241) Akbari, A.; Wu, J. An Integrated Method of Isolating Napin and Cruciferin from Defatted Canola Meal. *LWT - Food Sci. Technol.* **2015**, *64* (1), 308–315. https://doi.org/10.1016/j.lwt.2015.05.046.

(242) Akbari, A.; Wu, J. Cruciferin Nanoparticles: Preparation, Characterization and Their Potential Application in Delivery of Bioactive Compounds. *Food Hydrocoll.* **2016**, *54*, 107–118. https://doi.org/10.1016/j.foodhyd.2015.09.017.

(243) Sridharan, S.; Meinders, M. B. J.; Sagis, L. M. C.; Bitter, J. H.; Nikiforidis, C. V. Jammed Emulsions with Adhesive Pea Protein Particles for Elastoplastic Edible 3D Printed Materials. *Adv. Funct. Mater.* **2021**, *2101749*, 1–11. https://doi.org/10.1002/adfm.202101749.

(244) Pilorgé, E. Sunflower in the Global Vegetable Oil System: Situation, Specificities and Perspectives. *OCL - Oilseeds fats, Crop. Lipids* **2020**, *27*, 34. https://doi.org/https://doi.org/10.1051/ocl/2020028.

(245) Leng, S. H.; Yang, C. E.; Tsai, S. L. Designer Oleosomes as Efficient Biocatalysts for Enhanced Degradation of Organophosphate Nerve Agents. *Chem. Eng. J.* **2016**, *287*, 568–574. https://doi.org/10.1016/j.cej.2015.11.087.

(246) Akbarzadeh, A.; Rezaei-Sadabady, R.; Davaran, S.; Joo, S. W.; Zarghami, N.; Hanifehpour, Y.; Samiei, M.; Kouhi, M.; Nejati-Koshki, K. Liposome: Classification, Preparation, and Applications. *Nanoscale Res. Lett.* **2013**, *8* (1), 1. https://doi.org/10.1186/1556-276X-8-102.

(247) Zimmerberg, J.; Kozlov, M. M. How Proteins Produce Cellular Membrane Curvature. *Nat. Rev. Mol. Cell Biol.* **2006**, *7* (1), 9–19. https://doi.org/10.1038/nrm1784.

(248) Callan-Jones, A.; Bassereau, P. Curvature-Driven Membrane Lipid and Protein Distribution. *Curr. Opin. Solid State Mater. Sci.* **2013**, *17* (4), 143–150. https://doi.org/10.1016/j.cossms.2013.08.004.

(249) Choudhary, V.; Golani, G.; Joshi, A. S.; Cottier, S.; Schneiter, R.; Prinz, W. A.; Kozlov, M. M. Architecture of Lipid Droplets in Endoplasmic Reticulum Is Determined by Phospholipid Intrinsic Curvature. *Curr. Biol.* **2018**, *28* (6), 915-926.e9. https://doi.org/10.1016/j.cub.2018.02.020.

(250) Van Den Brink-Van Der Laan, E.; Antoinette Killian, J.; De Kruijff, B. Nonbilayer Lipids Affect Peripheral and Integral Membrane Proteins via Changes in the Lateral Pressure Profile. *Biochim. Biophys. Acta - Biomembr.* **2004**, *1666* (1–2), 275–288. https://doi.org/10.1016/j.bbamem.2004.06.010.

(251) Toulmay, A.; Prinz, W. A. Lipid Transfer and Signaling at Organelle Contact Sites: The Tip of the Iceberg. *Curr. Opin. Cell Biol.* **2011**, *23* (4), 458–463. https://doi.org/10.1016/j.ceb.2011.04.006.

(252) Salo, V. T.; Belevich, I.; Li, S.; Karhinen, L.; Vihinen, H.; Vigouroux, C.; Magré, J.; Thiele, C.; Hölttä-Vuori, M.; Jokitalo, E.; Ikonen, E. Seipin Regulates ER –Lipid Droplet

Contacts and Cargo Delivery . *EMBO J.* **2016**, *35* (24), 2699–2716. https://doi.org/10.15252/embj.201695170.

Summary

Oilseeds, containing high amounts of proteins and lipids -essential structuring and nutritional ingredients in foods- are one of the most promising ingredient sources for food applications. An application of oilseed lipids is to serve as raw materials for oil-in-water emulsion-type food products, while proteins can be used in the same type of products to stabilize the free oil in water. The current oilseed ingredient valorization process focuses on lipid extraction, while proteins are extracted from the residual defatted material. However, this process requires multiple energy consuming steps, and the heating and organic solvents applied to the defatted material have a negative impact on protein extractability and functionality. A solution to enhance the potential use and sustainability of oilseed ingredients for foods might be offered from the development or improvement of the current process, by reducing the processing steps. This approach results in less purified plant-based ingredients instead of highly purified ingredients, with potentially different functionality in food systems. Therefore, in this thesis we aim to enhance the potential use of less purified oilseed ingredients for food applications by providing an alternative extraction process and a mechanistic understanding on the relation between extraction and functionality of less purified oilseed proteins and lipids.

In **Chapter 1**, we discuss the motives behind the shift towards plant-based ingredients in foods, and the main challenges in the current extraction process and the functionality of plant-based ingredients. In this chapter we deliberate about the potential of oilseeds as a source of food ingredients, with focus on rapeseeds. An overview of the main compounds present in oilseeds is provided and the link between the structural organization in the cell matrix and the physicochemical properties of each compound of interest with the extraction process is made. The current oilseed valorization process has a tremendous negative impact on protein extractability and functionality, due to protein denaturation and complexation with phenolic compounds present in the seeds. Additionally, the protein purification process results in selective extraction of the different protein species present in the seeds. In this chapter, we highlight the processing steps that need to be reconsidered to increase the potential of oilseed ingredients in food application. As an alternative method, we suggest omitting of the defatting step in the oilseed valorization process. This process results in less purified extracts, in which lipids are extracted in their natural structures, called oleosomes, and the different proteins present in oilseeds are co-extracted in protein-rich extracts. As less purified extracts might possess different functionalities compared to highly purified extracts, a mechanistic understanding on the relation between the extraction process and functionality of the extracts is necessary to determine the optimal level of purification needed for the desired functionality.

The first objective of this thesis was to understand the effect of the extraction process on the physicochemical properties of rapeseed proteins and oleosomes. In **Chapter 2** we describe in detail the alternative extraction process of rapeseed proteins and oleosomes and explain the decisions prior to the design of the process. In this process we omitted the defatting step and use an aqueous extraction to simultaneously extract proteins and lipids (as oleosomes). The seeds were dehulled to eliminate the extraction of phenolic compounds present in the hulls and prevent their complexation with proteins. As pH is an important parameter for the extraction and functionality of proteins and oleosomes, the extraction pH was maintained at pH 9, to prevent the irreversible complexation of proteins with phenolic compounds (i.e. sinapic acid), and to extract both storage rapeseed proteins (napins and cruciferins) and oleosomes. By mechanically breaking the seed structure with a screw-press, the proteins and oleosomes were released and further separated by centrifugation. As a result, 1) 60% of the lipids initially present in the seed were recovered in their natural lipid structure as dense oil-in-water emulsion (40 wt% oil) referred in this thesis as oleosome-rich extract, and 2) 40 wt% of the proteins initially present in the seed were recovered in a protein-rich extract referred to in this thesis as rapeseed protein mixture (RPM). RPM had 40 wt% protein content on dry matter and both storage proteins (napins and cruciferins), intact oleosomes and free phenols were present. Diafiltration of RPM, where free phenols and other low molecular weight compounds were removed, resulted in a protein concentrate (rapeseed protein concentrate (RPC)) with about 65 wt% protein content on dry matter. Performing several analyses in the extracts obtained by this extraction protocol, we confirmed that the physicochemical properties of the proteins were preserved, and no irreversible complexation with phenolic compounds occurred.

The second research objective was to assess the functionality of less purified protein extracts obtained as described in Chapter 2. In **Chapters 3,4** and **5**, we discuss the functional properties of the less purified rapeseed protein extracts and the mechanistic understanding behind the functionality. In **Chapter 3** we investigated the interfacial stabilization mechanism at the oil/water interface when RPM, containing both storage proteins and non-protein compounds was used as an emulsifier at neutral pH conditions (pH 7). When oil-in-water emulsions were prepared, we found that only napins were adsorbed at the interface, resulting in a soft solid-like interface. Cruciferins appeared to weakly interact with the adsorbed layer of napins, forming a secondary layer that provides stability to the emulsion droplets against coalescence during emulsification. The oleosomes and free phenols present, did not hinder the ability of proteins to stabilize the interface.

In **Chapter 4**, we discuss the effect of purification (i.e. diafiltration) on the interfacial stabilization mechanism when RPM and RPC are used as emulsifiers at acidic pH (pH 3.8). The emulsion properties (i.e. droplet size) were different between the two protein extracts, with larger emulsion droplets present in RPM-stabilized emulsions compared to RPC-stabilized emulsions. In both systems, and similar to pH 7, napins were adsorbed at the interface and cruciferins formed a secondary layer, preventing droplet coalescence during emulsification. The differences observed in emulsion droplet size between RPM- and RPC-stabilized emulsions were assigned to the presence of sinapic acid in RPM, which interacted with cruciferins inducing their aggregation, and affecting droplet formation and stability during emulsification.

The outcome on the interfacial stabilization mechanism in Chapters 3 and 4, guided us to the research described in **Chapter 5.** In this research, we showed that the coexistence of napins and cruciferins can be beneficial in structuring emulsion-filled gels, with napins being adsorbed at the interface and cruciferins building the protein network. Thus, RPM containing both napins and cruciferins was used both as an emulsifier and gelling agent. The effect of pH (pH 5 and 7) and oil concentration (0-30 wt%) on the rheological and microstructural properties of the emulsion-filled gels was investigated. By combining analytical tools, such as confocal microscopy and bulk rheology, we showed that pH affects the type of gel structure, the gel firmness, and the degree of reinforcement by oil addition. Aggregation of proteins at pH 5 resulted in less firm gels (i.e. lower *G*') with a heterogeneous structure built of protein aggregates, whereas less aggregated proteins at pH 7 formed a homogeneous network built of strand-like protein structures with higher gel firmness (i.e. higher *G*'). With the addition of emulsion droplets in the protein gel matrix the firmness of the EFGs was increased (increase in *G*'), with a more pronounced reinforcement at pH 5 compared to pH 7. The type of gel network did not change by the addition of oil droplets neither at pH 5 nor at pH 7. It was concluded that the protein backbone dictated the network structure while the incorporated emulsion droplets acted as protein particles reinforcing the gel firmness.

In **Chapter 6**, experimental techniques were combined with coarse-grained molecular dynamics simulations to provide a mechanistic understanding on the relation between oleosome monolayer properties, such as molecular density (number of molecules per area), lateral interactions and dilatability, with the ability of oleosomes to traffic lipids. It appeared that molecular density and lateral molecular interactions in the monolayer regulate lipid trafficking. By increasing the monolayer molecular density, the adsorption of free lipid by oleosomes was limited. Free lipid absorption by oleosomes resulted in oleosome volume expansion and adjustment of the monolayer molecular density. Oleosomes also released lipids from their core and deflated, indicating a release mechanism through a channel. Lipid absorption and release was found to be

initiated by hydrophobic forces. Dilatational interfacial rheology studies showed that the ability of the oleosomes to expand in volume or shrink upon absorption or release of lipids respectively is assigned to the weak lateral interactions in the monolayer, which allow a reversible dilation.

Lastly in **Chapter 7**, we revisited the main findings and conclusions of all the chapters of this thesis. In this chapter we first aimed to suggest several points of attention and guidelines for oilseed valorization. The three key factors to consider during oilseed valorization are 1) the removal of lipids before protein extraction with pressing, heating, and organic solvents, 2) the type of phenolic compounds present in each oilseed source in order to choose extraction conditions that will prevent irreversible protein-phenol complexation and 3) the structural and physicochemical properties of each protein species present in oilseeds in order to coextract both proteins and to preserve their natural physicochemical properties and functionality. To understand the relation between extraction and functionality of less-purified protein extracts, we aimed to provide a mechanistic understanding behind the function of all extracts. With this mechanistic understanding, we were able to link the composition of the protein extracts with the molecular properties and functionality in several systems, and provide several guidelines for the extraction and functionality of proteins; 1) selective extraction of proteins by means of precipitation, which results in globulin-rich extracts and neglects the albumins should be avoided, as albumins (i.e. napins) have good emulsifying properties, 2) the coexistence of both types of proteins (napins and cruciferins) in the protein extracts is advantageous in stabilizing oil/water interfaces and in structuring emulsion-filled gels, 3) the aggregated status of proteins can impact the structural and rheological properties of emulsion-filled gels and 4) the removal of non-protein compounds (i.e. phenolic compounds) might be necessary in specific system conditions (i.e. pH) to achieve the desired functionality. Finally, in this chapter we provide an outlook and future perspective on oilseed valorization. Our findings show the significance of studying in depth the molecules present in each oilseed and of providing a direct link between the extraction process and functionality of the protein extracts, to promote the use of oilseed proteins in foods and bring new plant proteins in the market. In parallel, by providing in this thesis a mechanistic understanding behind the ability of oleosomes to absorb and release lipids, we showed that the oleosome monolayer is a very important structural element that dictates the function of oleosomes. The findings of this thesis on the relation between the number of molecules in the monolayer and their interactions with lipid absorption and release, pave the path to explore further how we can tailor the oleosome monolayer properties in order to expand the use of oleosomes as carriers of sensitive hydrophobic molecules in food and/or medical applications.

Acknowledgments

This journey, to the Ithaca that I decided to travel to, was full of experiences and knowledge. In these years of travelling in the road of science, I learned and achieved many things, not only as a scientist but also as a person. But I was not alone. I was accompanied by many people, who were willing to travel with me, and who made this journey unique.

I would first like to thank my supervisors, who started this journey with me, and believed in me, from the beginning until the end. Costas, I was very lucky to have you as my daily supervisor. You were always there, to guide me with your knowledge, to discuss with me, to support me in my ups and downs, to exchange ideas, to motivate me when needed. Your enthusiasm and passion for science and your perfectionism were catalytic in my development, both as a scientist and as a person. Thank you also for the brainstorming sessions in Biobased Soft Materials group, we built a nice team of PhDs and students. Leonard, thank you for your support and guidance these years. I really appreciate your positive and polite way of explaining science and transferring knowledge. Thank you for your very constructive feedbacks. I learned a lot from you, and I became a more confident scientist. Harry, thank you for believing in me and for welcoming me in the Biobased Chemistry and Technology (BCT) group. Thank you for always bringing the helicopter view on the discussion table. Our discussions and support always helped me to see the broader picture of my research and the broader picture of myself. Thank you for teaching me how to write facts before fiction. I feel grateful and lucky that my Lernaean Hydra had these three heads. With your supervision, you all helped me to become a better scientist, a better person, a better supervisor myself.

In BCT I met many people, who contributed to my good memories and experiences in this journey. I would first like to thank my officemate. Marlene, I am very happy that I shared the igloo with you. Thank you for aaaaall the coffees, the nice discussions, and the laughs. Thank you for listening to me and my complaints, for always bringing a smile in the room. I will miss a lot these moments in our office, and our spontaneous after-work beers. Cynthia and Laura, thank you for all the joyful coffees, discussions, and beers. Lorenz, thank you for the music, the bread, the “animal”, the LC-MS, and all the random discussions. Umay, it was very nice to meet a kind person like you. Matthijs, I was very happy to exchange plants with you. Christos, thank you for the nice collaboration and all the talks and beers. Thanks as well to all my other PhD colleagues and staff members in BCT for the nice coffee and lunch breaks. You all made these breaks unique. As my PhD included a lot of lab work, I want to specially thank Susan, Anne-Marie, and Nadine, for your valuable help in the lab, your excellent organization, and your willingness to solve any problem,

any moment. I hope I will be lucky enough to work with people like you in the future. Gerda and Danielle, I am very grateful for your help from my first until my last day in BCT. Your kindness and care were very important. Last but not least, I want to thank all my BSc and MSc students, that contributed to this work. Kirsten, Tessa, Christian, Kindi, Qiyang, I enjoyed working with you, I learned a lot during this process. I want to thank you all for your effort and contribution to my research and to my personal development.

My PhD project was also part of a bigger project organized by the Top Institute Food and Nutrition (TiFN). I want to thank the TiFN team. I would first like to thank Marcel Meinders and Erik van der Linden, who gave me the chance to work in this project. I still remember my enthusiasm in my first interview with you for the PhD position. Marcel, thank you also for leading this project with respect to everyone's needs, and for listening to my ideas and concerns. Thank you for bringing your ideas and concerns as well in our discussions, it was a very important addition to my development. I want to thank all the PhDs that we built this team together. Emma, Jack, Maud, Remco, Simha, Dana, Marius, thank you all for all the nice discussions, the solidarity, the laughs, the help, the collaboration. I am very happy that I met you all. You are all great scientists. Additional thanks to Remco for the very nice collaboration and paper, I learned a lot from you. Jack, thank you as well for all the help, your enthusiasm and willingness to help are very inspiring. Helene and Irene, your help and support in the lab was very important and valuable, especially in my first steps in the lab. Thank you very much. Jacqueline, thank you for the nice collaboration in my first student supervision, and your nice explanations about sustainability. Thanks to all the TiFN team colleagues for the nice discussions. Finally, I would like to thank all the experts from the industry, for the nice collaboration, the fruitful discussions and ideas, and for bringing the application relevance in my work.

And now it's time to thank my "Thuis", the Guyzzzz that were and are always by my side. Simha, thank you for living up to the expectations of all your roles these years. You are a colleague, a friend, a housemate. Thank you for listening to me, for sharing all the good and bad moments with me, for the endless day and night discussions, for all the reassurance. Thank you for understanding me without even talking. Carlos, we should give you a "patience award" (imagine). You had to cope with not only one but two PhDs in this house, simultaneously. Thank you for tolerating my grumpy moments (many), for listening to my concerns (and my songs), for always taking care of me and my needs, for bringing the home-feeling in the house. Thank you for balancing our non-stop complaining days with Simha. Guyzz, you were my daily support and company, you shared the good times with me, and you supported me and hugged me in my bad moments. I couldn't ask for a better house, for better friends. Thank you for letting me choose movies and for letting me sleep on the couch while I was forcing you to watch them.

Christina, you are my harbor. Thank you for your endless support all these years, from the far past till the end of my PhD. Thank you for always being there, for taking care of me, for hugging me (although you know I don't like it), for advising me to follow my feelings, for sharing our inner thoughts so transparently with each other. Thank you for my room in Utrecht. Looking forward to moving closer to you. Marianna, thank you for bringing joy and care all these years in my life through our friendship. Thank you for building so many relaxing and casual moments when I needed them. Thank you for our nights in Vera, our trips, our non-stop shopping, our coffees in the village, our poetry nights. Looking forward to writing our bipolar poem. Giorgo, you always take care of me. Thank you for tolerating the Elena-Christina combo, for listening or not listening to us, for all the liquors and the cocktails, for not being mad at me when I do not pick up the phone. Maria, you are far but magically you are always there the right moment. You know. Special thanks for my last summer, for bringing carefree moments, for making the days to look easier. Andres and Ale thank you for the Sunday brunches and walks. Thanasaki, Elenitsa is very happy that she met such a caring and silent person like you. Thank you for spoiling me. Dimitri, I appreciate the way you say "Lenio". It reflects your kindness and care. Thank you for all the nice talks we had these years.

But these years, I also had often trips back home. Eleni, Ioanna, Nasia, thank you for always being there. Thank you for welcoming me back home every time with the same enthusiasm, for taking care of me, for always being alert in this WhatsApp group, even if we are very far from each other. You know how to eliminate distance. Dimitri and Giorgo, thank you for the timeless friendship.

Μαμά και μπαμπά, σας ευχαριστώ που είστε πάντα εκεί, που μου δώσατε φτερά και ώθηση γι' αυτό το ταξίδι, που στηρίζετε κάθε μου απόφαση, σας ευχαριστώ για την ανιδιοτέλεια σας σε όλα. Ριχάρδε, σ'ευχαριστώ για την ατελείωτη στήριξη, με συγκινεί που είσαι περήφανος για μένα.

About the author

Eleni (usually called Elena) Ntone was born in Thessaloniki in Greece, on the 15th of October 1991. Eleni did a Bachelor's in Food Science, in the School of Agriculture, in Aristotle University of Thessaloniki, in Greece. During her BSc studies, Eleni also followed an Erasmus program, in the University of Bologna in Italy, mainly to experience living abroad. In 2015, she moved to The Netherlands to start her MSc studies in Food Technology, in Wageningen University. Her first contact with research was in her MSc thesis at the group of Food Quality and Design and Biobased Chemistry and Technology, where she researched the effect of matrix complexity and processing on lipid digestion from nuts, which resulted to her first publication. During her MSc internship in Friesland Campina, she also conducted research on novel protein functional ingredients within the R&D department. Both exciting experiences in the field of research, led to her decision to continue with her studies. In 2017, Eleni was hired as a PhD candidate at the chair group of Biobased Chemistry and Technology. Her PhD focused on the relation between the extraction process and functionality of plant proteins and lipids from oilseeds. Her PhD project was part of a bigger project organized by Top Institute Food and Nutrition (TiFN) and supported by the main food industry leaders.

Email: entone2@gmail.com

List of publications

Ntone, E., Bitter, J. H., & Nikiforidis, C. V. (2020). Not sequentially but simultaneously: Facile extraction of proteins and oleosomes from oilseeds. *Food Hydrocolloids*, 102, 105598.

Ntone, E., van Wesel, T., Sagis, L. M., Meinders, M., Bitter, J. H., & Nikiforidis, C. V. (2021). Adsorption of rapeseed proteins at oil/water interfaces. Janus-like napins dominate the interface. *Journal of Colloid and Interface Science*, 583, 459-469.

Ntone, E., Qu, Q., Pyta-Gani., K., Meinders, M., Sagis, L.M.C., Bitter, J.H., & Nikiforidis, C.V. (2021). Sinapic acid impacts the emulsifying properties of rapeseed proteins at acidic pH. *Submitted*

Ntone, E.*, Kornet, R.*, Venema, P., Meinders, M.B.J., van der Linden, E., Bitter, J.H., Sagis, L.M.C., Nikiforidis, C.V. (2021) Napins and cruciferins in rapeseed protein extracts have complementary roles in structuring emulsion-filled gels. *Submitted*

Ntone, E., Rosenbaum, B., Sridharan, S., Willems, S.B.J., Moultos, O., Vlugt, T.J.H., Meinders, M., Sagis, L.M.C., Bitter, J.H., & Nikiforidis, C.V. (2021). Smart lipid balloons: Stimuli-responsive natural lipid droplets for selective lipid trafficking. *Submitted*

*The authors have contributed equally to this work and share first authorship

Overview of completed training activities

Discipline courses		
Food proteins: functionality, modifications and analysis	Wageningen, The Netherlands	2018
Microscopy and Spectroscopy in Food and Plant Sciences	Wageningen, The Netherlands	2019
Conferences and symposia		
Future Catalysis	Wageningen, The Netherlands	2017
Seminar on the possibilities of surface analysis	Wageningen, The Netherlands	2018
Thermodynamics and Phase Transitions in Food Processing	Wageningen, The Netherlands	2018
Bioderived and Bioinspired Functional Membranes	Wageningen, The Netherlands	2018
Seminar on Fluorescence imaging	Wageningen, The Netherlands	2018
Physical and chemical stability of Pickering emulsions	Wageningen, The Netherlands	2018
32nd EFFoST International Conference[1]	Nantes, France	
Adding Action and Color to Electron Microscopy: New Tools for Correlated Light and Electron Microscopy	Wageningen, The Netherlands	2018 2018
Oil Body Conference[2]	Wageningen, The Netherlands	2018
CHAINS conference[1]	Veldhoven, The Netherlands	2018
15th International Hydrocolloids Conference[2]	Melbourne, Australia	2020
Oleosome/Lipid droplet Young Science event[2]	Online	2021
Research Conference Plant-Based Foods & Proteins, Europe 2021[2]	Online	2021
General courses		
VLAG PhD week	Baarlo, The Netherlands	2018
Start to supervise BSc and MSc students	Wageningen, The Netherlands	2018
Scientific Publishing	Wageningen, The Netherlands	2019
Supervising BSc and MSc thesis students	Wageningen, The Netherlands	2019
Scientific Artwork, Data visualization and Infographics with Adobe Illustrator	Online	2020
Carreer Orientation	Online	2021
Scientific writing	Online	2021
Others		
TiFN A2R workshop[2]	Wageningen, The Netherlands	2017
Preparation of research proposal	Wageningen, The Netherlands	2018
Participation in the organization of Oil body conference	Wageningen, The Netherlands	2018
TiFN retreat[2]	Wageningen, The Netherlands	2018
PhD study trip[2]	Copenhagen, Denmark	2018
TiFN Expert meetings[2]	Wageningen, The Netherlands	2017-2021
Biweekly project meetings	Wageningen, The Netherlands	2017-2021
Biweekly team meetings	Wageningen, The Netherlands	2017-2021
Organisation of PhD trip to France	Wageningen, The Netherlands	2021
Organization of Oleosome/Lipid droplet Young Scientist event	Wageningen, The Netherlands	2021

[1]poster presentation, [2]oral presentation

The research described in this thesis was part of a project that was organized by and executed under the auspices of TiFN, a public-private partnership on precompetitive research in food and nutrition. Funding for this research was obtained from Unilever Research and Development Wageningen, Nutricia Research B·V., Bel group, Pepsico Inc., the Netherlands Organisation for Scientific Research (NWO) and the Top-sector Agri&Food.

Financial support from Wageningen University and TiFN for printing this thesis is gratefully acknowledged.

Cover design: Gizem Üstüner

This thesis was printed by Proefschriftmaken (100 copies)